Investigation into the ion channels and plasma membrane properties of white adipocytes

Donna Cynthia Bentley, BSc.

Thesis submitted to the University of Nottingham for the degree of Doctor of Philosophy

JULY 2013

Abstract

Ca^{2+} is a ubiquitous intracellular signalling molecule that is involved in the regulation of numerous cellular functions. To date Ca^{2+} influx pathways present in white fat adipocytes have not been characterised. Additionally impaired $[Ca^{2+}]_i$ management is implicated in the induction of the insulin resistant state in adipocytes. As adipocytes have a prominent role in the management of energy homeostasis, the presence of Ca^{2+} influx pathways was examined.

Initial $[Ca^{2+}]_i$ measurements confirmed the presence of functional Ca^{2+} influx and efflux pathways in adipocytes. Further $[Ca^{2+}]_i$ measurements identified the $Ca_v1.3$ Voltage-gated Ca^{2+} channel (VGCC). The presence of the α_1 subunit of $Ca_v1.3$ channel protein in adipocytes was confirmed by Western blotting, the expression of which was reduced in adipocyte samples sourced from Zucker obese rats.

Initial $[Ca^{2+}]_i$ imaging experiments utilising conditions of elevated extracellular K^+ (50mM) did not stimulate Ca^{2+} influx. The plasma membrane potential (Vm) regulates many physiological processes, including cellular Ca^{2+} influx by VGCCs, with dysregulations in Vm underlying functional pathologies. K^+ is widely believed to be the predominant ion that controls Vm for many cell types, however, whether K^+ regulates adipocyte Vm is also unknown, prompting, investigation into the ionic species involved in the regulation of Vm in primary and differentiated 3T3-L1 adipocytes. As insulin and β-adrenoceptors regulate adipocyte function, their effect on Vm was also explored.

The Vm of primary and 3T3-L1 adipocytes were -34.14mV (n=68) and -28.5mV (n=88) respectively. Elevation of extracellular K^+ from 5.6mM to 50mM had no significant effect on the Vm of either type of adipocyte. The role of Cl^- on adipocyte Vm was then investigated. Reduction of extracellular Cl^- from 138 to 5mM, by equimolar substitution with Gluconate significantly depolarised the Vm of both primary and 3T3-L1 adipocytes. Patch clamp investigations also revealed a role of Na^+ in adipocyte Vm. Neither insulin (100nM) or the β-adrenocpetor agonist isoprenaline (10μM) significantly changed adipocyte Vm.

The role of Cl^- in adipocyte Vm is indicative of the presence of Cl^- channels, however electrophysiological studies failed to characterise the Cl^- currents underlying adipocyte Vm.

Overall, further investigations are required to characterise not only the Ca^{2+} influx pathways in adipocytes, and the roles thereof, but also the means by which they are regulated.

Acknowledgements

I would like to express my gratitude to my supervisors Dr. Paul.A.Smith and Dr. Sue.L.F.Chan. Thank you for your patience, guidance mentoring and support through good times, and bad. You both helped me to achieve one of my greatest life ambitions, which I will carry with me throughout my career and beyond.

Thank you, Dr. Amanda Wheal of Dr. Michael Randall's laboratory and the technical staff of the FRAME laboratory for the generous provision of tissue throughout the course of my study. Additionally thanks go to Mr. Liaque Latif for helping me with my Western blot experiments.

I want to take the opportunity to thank all of my friends who have been there through my PhD journey. I am lucky in that I feel I don't have the space to name you all one by one, but if you are reading this then you will indeed know who you are. All of you have helped in your own special way and I wouldn't be where I am without you, you are all indeed my extended family. Special thanks go to Kayleigh Wardell, you have flown with me when I was flying high, and picked me up when I was down. I couldn't have asked for a better or more supportive friend to help me get through the rollercoaster ride that has been the last 4 years. Thank you Nazia Maroof and Asma Khan for sharing the after-hours office experience with me, your company kept me motivated and inclined to keep working. Thank you Marie Drouin for recognising when I needed a break and insisting I take one, and to Kieran Desmond for keeping me company during those long nights of writing up at home. Also thank you Michal Ciganek for your constant encouragement, and thank you to Neil Thornton and Ben Lilley for always being there.

Most importantly, extra special thanks go to my family, I know I could not have done this without you. Thank you Mum for being my rock, my inspiration, and a relentless fountain of support. Thank you Dad for always coming to my rescue and for encouraging me to keep going even when I felt I couldn’t go any further. Thank you, Isabeau and Charlotte, my dear sisters and best friends. I know I have not been around much this last few years, but you two have always been there regardless, ready to present me with new opportunities, listen to me, or just be ready at the right time with a massive bar of chocolate or funny story to cheer me up. Lots and lots of love to you both.

Abbreviations

$[Ca^{2+}]_i$	Intracellular calcium concentration
2-DOG	2-Deoxyglucose
AA	Arachadonic acid
AC	Adenylate cyclise
ADRD	Adipocyte differentiation-related protein
AID	Alpha interaction domain
AGTL	Adipose triglyceride lipase
AKAP	A-kinase anchor protein
APS	Ammonium persulfate
ATP	Adenosine triphosphate
BAPTA-AM	1,2-Bis(2-aminophenoxy)ethane-N,N,N',N'-tetraacetic acid
BMI	Body mass index
BSA	Bovine serum albumin
BZP	Benzothiazepine
Ca^{2+}	Calcium
cAMP	Cyclic adenosine monophosphate
$Ca_v1.x$	L-type VGCC where subtype is unknown
CCB	Ca^{2+} channel blocker
CIC	Voltage-dependent chloride channels
CFTR	Cystic fibrosis transmembrane conductance regulator
CsA	Cyclosporine
DCB	3,4-dichlorobenzamil
DHP	Dihydropryidines
DIDs	Diisothiocyano-2,2'-stilbenedisulfonic acid
DMEM	Dulbecco's modified Eagle's medium

DMSO	Dimethyl-sulphoxide
DPBS	Dulbecco's phosphate-buffered saline
DPC	Diphenylcarbonate
DRG	Dorsal root ganglion
EGTA	Ethylene glycol-bis(β-aminoethyl ether)-N,N,N',N'-tetracetic acid
ER	Endoplasmic reticulum
Fluo-4 AM	Glycine, N-[4-[6-[(acetyloxy)methoxyl]-2,7-difluoro-3-oxo-3H-xanthen-9-yl]-2-[2-[2-[bis[2-[(acetyloxy)methoxyl]-2-oxoethyl]amino]-5-methylphenoxy]ethoxy]phenyl]-N-[2-[(acetyloxy)methoxy]-2-oxoethyl]-(acetyloxy)methyl ester
GABA	Gamma-amino butyric acid
GH	Growth hormone
GLUT	Glucose transporter
GPCR	G-protein coupled receptor
HEPES	N-2-Hydroxyethylpiperazine-N'-2-ethanesulfonic acid
HSL	Hormone sensitive lipase
HVA	High voltage activated
IBMX	3-isobutyl-1-methylxanthine
IC_{50}	Concentration at which half maximal inhibition occurs
IL	Interleukin
IP3	Inositol-1,4,5-triphosphate
IRS	Insulin receptor substrate
I-V	Current-Voltage
KBR	(2-[2-[4-(nitrobenxyloxy)phenyl]-ethyl]isothiourea methanesulfonate
LVA	Low voltage activated
MDR	Multiple drug resistant transporter
MGL	Monoglyceride lipase

NaAsp	Sodium aspartate
NaGlu	Sodium Gluconate
NCX	Na^+/Ca^{2+} exchanger
NMG	N-Methyl-D-glucamine
NMDA	N-methyl-D-aspartate
NPPB	5-nitro-2-(3-phenylpropylaminobenzoic acid
NSCC	Non selective cation channel
OAG	1-oleoyl-2-acetyl-sn-glycerol
OKA	Okadaic acid
PAA	Phenylalkylamine
PBS	Phosphate buffered saline
PDE-3	Phosphodiesterase 3
PI3K	Phosphatidylinositol-3-kinase
PIP_2	Phosphatidylinositol 4,5-bisphosphate
PKA	cAMP-dependent protein kinase
PKC	Protein kinase C
PKD	Protein kinase D
PLM	Phospholemman
PMA	Phorbol 12-myristate 13-acetate
PPARγ	Peroxisome proliferator activated receptor-gamma
PTX	Pertussis toxin
RMP	Resting membrane potential
ROI	Region of interest
RT-PCR	Reverse transcription polymerase chain reaction
RVD	Regulatory volume decrease
RVI	Regulatory volume increase
RYR	Ryanodine receptor
SDS-PAGE	Sodium dodecyl sulphate-polyacrilamide gel electrophoresis

SEA400	(2-[4-[2,5-difluoro-phenyl]methoxy]phenoxy)-5-ethoxyaniline
S.E.M	Standard error of the mean
Ser	Serine
SOC	Store-operated calcium channel
SREBP	Sterol regulatory element binding protein
TAG	Triacylglycerol
TBST	Tris buffered saline Tween 20
TEA	Tetraethyl ammonium
TEMED	Tetramethylethylenediamine
TES	[N-Tris(hydroxymethyl) methyl-2-aminoethane sulfonic acid
TG	Triglycerides
TNF	Tumour necrosis factor
TPA	12-O-tetradecanoyl-phorbol-13-acetate
TRPC	Transient receptor potential canonical channel
VDI	Voltage-dependent inactivation
VGCC	Voltage-gated calcium channel
VLDL	Very low density lipoproteins
Vm	Plasma membrane potential
VRAC	Volume-regulated chloride channel
WAT	White adipose tissue

Table of contents

List of figures and tables

Chapter 1

Chapter 2

Chapter 3

Chapter 4

Chapter 5

Chapter 1

General Introduction

1.1 Overview

This introduction aims to present an overview of Ca^{2+} as a signalling molecule, an overview of adipocytes and the biochemical functions thereof and how they are regulated by insulin. The implications of dysregulated $[Ca^{2+}]_i$ on adipocyte function are also discussed.

1.2 Calcium as a signalling molecule

Cytosolic Ca^{2+} is a ubiquitous intracellular signalling molecule. Not only does it play a role in intracellular signalling in virtually all kinds of mammalian cells, but it also regulates numerous cellular processes (Blaustein and Lederer, 1999). Examples of processes where Ca^{2+} signalling is implicated, include fertilisation, cardiac muscle contraction, nervous transmission and apoptotic cell death (Blaustein and Lederer, 1999, Szent-Gyorgyi, 1975, Berridge et al., 2000). Ca^{2+} homeostasis is essential, in order to enable the cell to carry out basic functions including proliferation, differentiation and metabolism (Roderick and Cook, 2008, Berridge et al., 2000). Dysregulated Ca^{2+} signalling is implicated in the pathogenesis of various disease states, including heart failure, Alzheimer's disease, cancer and diabetes (Small, 2009, Roderick and Cook, 2008, Tuomilehto et al., 1999). Each cell expresses a particular complement of Ca^{2+} signalling components, a combination of various Ca^{2+} influx/ efflux pathways and intracellular storage routes. This complement of Ca^{2+} signalling pathways enables the cell to generate $[Ca^{2+}]_i$ signals pertaining to the requirements of both global and microdomains. This allows any particular cell to control $[Ca^{2+}]_i$ in a specific manner in accordance with the cellular function that it regulates (Roderick and Cook, 2008). For example, in neurons, there is spatial variation in $[Ca^{2+}]_i$ signalling (Nakamura et al., 2002). At synaptic junctions Ca^{2+} triggers

exocytosis within a millisecond time period, conversely processes like gene transcription and cell proliferation require Ca^{2+} to operate from a minutes to hours time-scale (Berridge et al., 2003). Resting levels of $[Ca^{2+}]_i$ are maintained at ~100nM. Elevations in $[Ca^{2+}]_i$ through cellular Ca^{2+} signalling arise from either or both external sources of Ca^{2+} through plasma membrane Ca^{2+} channel opening or via release of Ca^{2+} from internal ER or SR stores such that $[Ca^{2+}]_i$ can rise, sometimes as high as ~1μM (Roderick and Cook, 2008, Parekh and Putney, 2005).

A brief summary of extracellular Ca^{2+} influx pathways, intracellular release pathways and Ca^{2+} clearance mechanisms are presented herein.

1.2.1 Pathways of Ca^{2+} influx

Ca^{2+} can act as an intracellular signalling molecule following influx from the extracellular compartment, or following release from the endoplasmic reticulum. Ion channels mediating Ca^{2+} influx which are present on the plasma membrane surface comprise voltage gated Ca^{2+} channels (VGCCs), store operated Ca^{2+} channels (SOCs), second messenger operated channels (SMOC), receptor operated Ca^{2+} channels (ROC) (Barritt, 1999) and, in some instances, the reverse mode of the sodium calcium exchanger (NCX). Through alternative splicing (a process by which the exons of the RNA produced by gene transcription are joined in different ways, resulting in translation into differing protein isoforms), all Ca^{2+} channels and exchangers have numerous isoforms, resulting in a complement of proteins with subtly different properties, thus expanding the versatile nature of Ca^{2+} signalling (Berridge et al., 2003).

VGCCs are activated upon membrane depolarisation (Catterall, 2000) and are discussed in more detail in Chapter 3. SOCS are involved in capacitative Ca^{2+}

entry and are activated by depletion of intracellular stores (Parekh and Putney, 2005). The proposed mechanism is that store depletion activates Ca^{2+} entry via transient receptor potential (TRP) channels which are directly activated by Ins(1,4,5)P_3 receptors (Boulay et al., 1999). SMOC are activated by inositol phosphates, cyclic nucleotides and lipid derived messengers such as diacylglycerol (Tu et al., 2009). ROCs activate following binding of a hormone or neurotransmitter agonist (Parekh and Putney, 2005). An example of an ROC Ca^{2+} channel is the N-methyl-D-aspartate receptor (NMDA) which is activated by glutamate (Nahum-Levy et al., 2001, Berridge et al., 2003). The NCX is a bidirectional exchanger, it is further discussed in Chapter 3.

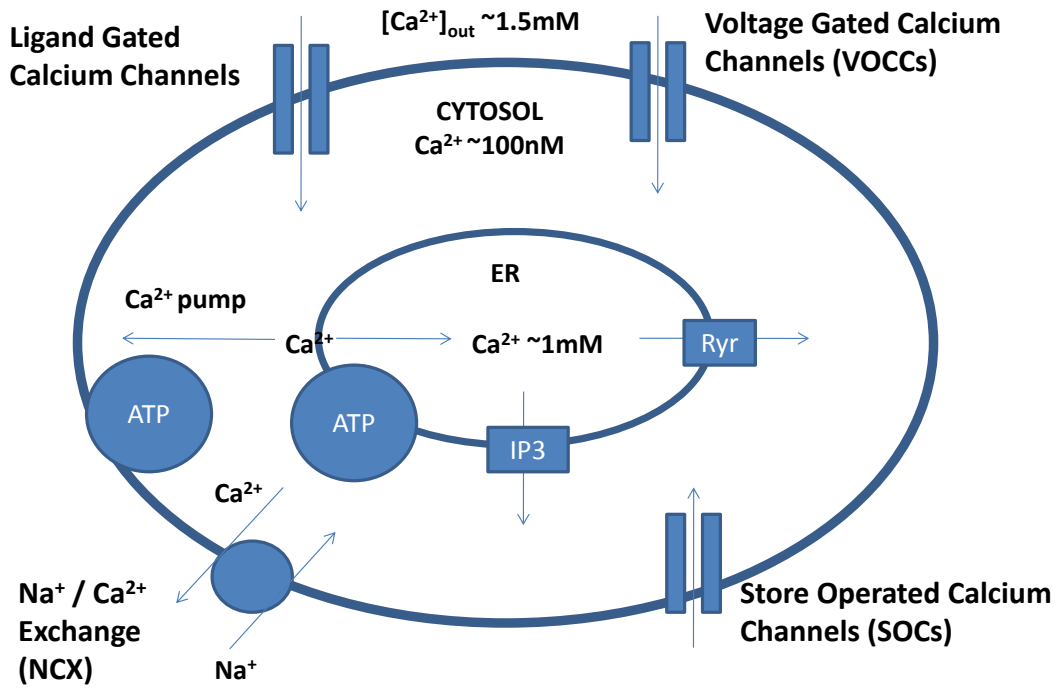

Figure 1.1. A generalised overview of cellular Ca^{2+}influx pathways, adapted from Rang *et al* (2003). Voltage-gated Ca^{2+} channels, VGCCs; Store operated Ca^{2+} channels, SOCs; Na^{+}/Ca^{2+} exchanger, NCX; Adenosine triphosphate, ATP; Endoplasmic reticulum, ER; inositol triphosphate, IP3; Ryanodine receptor, RyRs.

1.2.2 Intracellular Ca^{2+}

In addition to influx from the extracellular mileu, elevations in $[Ca^{2+}]_i$ can also arise through release of Ca^{2+} from the internal stores. Intracellular Ca^{2+} channels are located on the membranes of the endoplasmic and sarcoplasmic reticulum (ER/SR). The release of Ca^{2+} from internal stores is regulated by inositol-1,4,5 triphosphate ($Ins(1,4,5)P_3$) receptors or ryanodine receptors (RYRs) (Berridge et al., 2000). Both $Ins(1,4,5)P_3$ receptors and RYRs are sensitive to Ca^{2+} and, as such, cause calcium-induced calcium release (CICR). $Ins(1,4,5)P_3$ receptors are regulated by numerous substrates, however the most prominent substrates for the $Ins(1,4,5)P_3$ receptors are $Ins(1,4,5)P_3$ and Ca^{2+}. $Ins(1,4,5)P_3$ upon binding to its receptor increases the receptors sensitivity to Ca^{2+}. Ca^{2+} has a biphasic action upon the $Ins(1,4,5)P_3$ receptor. $[Ca^{2+}]_i$ stimulates the receptor at low concentrations (100-300nM), however following Ca^{2+} release into the cytosol, elevated $[Ca^{2+}]_i$ concentrations (>300nM) have an inhibitory action upon the $Ins(1,4,5)P_3$ receptor and inactivate the channel (Berridge et al., 2003). The RYR receptor, like the $Ins(1,4,5)P_3$ receptor, has a varied response to Ca^{2+}. At nM Ca^{2+} concentrations the RYR receptor is inactive, RYR receptors activate at µM Ca^{2+} concentrations and are inactivated by "high" Ca^{2+} concentrations within the mM range (Berridge et al., 2003, Bezprozvanny et al., 1991).

Cytosolic Ca^{2+} binds to its effectors, initiating a cellular response. This accounts for a small proportion of cytosolic Ca^{2+}, the remaining Ca^{2+} is either bound to Ca^{2+} binding proteins designated as "Ca^{2+} buffers", re-sequestered or extruded. Buffers such as calbindin, D-28 and calrectin modulate short-lived intracellular Ca^{2+} signals by altering the amplitude and recovery time of Ca^{2+} transients (Schwaller, Berridge et al., 2003). The mitochondria can also propagate

intracellular Ca^{2+} signals by releasing Ca^{2+}, replenishing intracellular stores (Demaurex et al., 2009).

1.2.3 Cytosolic Ca^{2+} clearance mechanisms

Following a Ca^{2+} signal event, there is a requirement for the $[Ca^{2+}]_i$ to be restored to its resting level. Ca^{2+} clearance mechanisms that function to return $[Ca^{2+}]_i$ to its basal state and/ or replenish the intracellular Ca^{2+} stores comprise of the sodium calcium exchanger, (discussed in more detail in Chapter 3), and the plasma membrane Ca^{2+} ATPase. The plasma membrane Ca^{2+} ATPase functions as a cytosolic Ca^{2+} extrusion mechanism, whereas the SR/ER Ca^{2+} ATPase transports cytosolic Ca^{2+} into the ER/SR stores (Berridge et al., 2000). The mitochondria also sequester Ca^{2+}, by way of proton extrusion, creating an electrochemical gradient that is used to drive Ca^{2+} uptake via the H^+/Ca^{2+} uniporter (Demaurex et al., 2009). Reciprocal interactions are reported between the ER/SR and the mitochondria. The ER/SR is a source of Ca^{2+} for the mitochondria, which in turn modifies the Ca^{2+} feedback mechanisms that regulate Ca^{2+} release from the SR (Berridge et al., 2000). Additionally, the pumps and transporters mentioned above are active in different circumstances. The plasma membrane and SE/ER pumps have a high affinity for Ca^{2+} but a low rate of transport, whereas the NCX and mitochondrial uniporter transport Ca^{2+} quickly and are responsive to Ca^{2+} within the nM to μM range, although for fast mitochondrial Ca^{2+} uptake to be observed, $[Ca^{2+}]_i$ must be higher than 400nM (Collins et al., 2001).

1.3 An overview of adipose tissue

Two types of adipose tissue exist, brown, and white. This thesis is concerned with white adipose tissue. White adipose tissue comprises a variety of cell types including monocytes, stromal vascular cells, endothelial cells, with the major cellular constituent being white fat adipocytes (Kershaw and Flier, 2004). Adipose tissue deposits are classified as either subcutaneous or visceral (Giorgino et al., 2005). The physical functions of adipose tissue are summarised as providing thermal insulation and cushioning as protection against mechanical damage for the internal organs. The biochemical function of adipocytes is the management of the triglyceride energy stores. Adipocytes store energy in the form of triglycerides (TG) within lipid droplets during times of calorific excess (lipogenesis). During fasting or physical exercise free fatty acids (FFAs) are released from the adipocyte triglyceride stores into the circulation by lipolysis, the ester bonds in triglycerides are hydrolysed, releasing fatty acids and glycerol (Fruhbeck et al., 2001). The FFA are oxidised by other tissues such as skeletal muscle, liver, kidney and myocardium, to provide energy (Giorgino et al., 2005, Arner, 2003, Carmen and Victor, 2006). Lipolysis is discussed in more detail in Chapter 3, Section 3.1.

Adipose tissue is a target tissue for the action of insulin, along with skeletal muscle, cardiac muscle (e.g. insulin-stimulated glucose uptake) (Purcell et al.) and liver (Cherrington et al., 2007). The actions of insulin upon adipocytes include stimulation of adipocyte lipogenesis (fatty acid synthesis), glucose uptake, inhibition of lipolysis. Insulin also regulates the synthesis and secretion of adipocyte secreted cytokines (see section 1.6), and stimulates the differentiation of pre-adipocytes into mature adipocytes (Arner, 2003).

1.3.1 Fat storage/utilisation by adipocytes

Adipocytes vary in diameter between 20-200μM, depending on their lipid content, with 95% of adipocyte volume comprising the lipid droplet (Arner, 2005a). Fat accumulation within adipocytes depends on the balance between lipogenesis and lipolysis (Kersten, 2001). Excess fat accumulation results in obesity, which is associated with insulin resistance (IR) and type 2 diabetes (Kahn et al., 2006), indeed the majority of patients with type 2 diabetes are obese (Aulchenko et al., 2007).

Obesity results from a prolonged imbalance between the storage and utilisation of TGs within adipose tissue. Adipose tissue expansion in obesity can arise due to either an expansion of adipocyte size, or an increased differentiation of pre-adipocytes into adipocytes. Impairments of TG mobilisation in obesity could result from genetic variations, abnormal regulation of adrenoceptors or hormone sensitive lipase (HSL), resulting in a reduced lipolytic activity within adipocytes, or reductions in the oxidation of long chain fatty acids (Diraison et al., 2003). Total fat mass has been used as a determinant of obesity-related insulin resistance; however fat distribution is also an important factor which has been shown to influence IR (Aulchenko et al., 2007). It has been suggested that the location and type of adipose deposit (subcutaneous or visceral) influences the adipocytes response to regulatory factors involved in lipogenesis (Roberts et al., 2009). Abdominal, particularly visceral, obesity is linked to insulin resistance, type 2 diabetes, hypertension and dyslipidaemia (Arner, 2003, Giorgino et al., 2005). In humans, it has been shown that visceral adipocyte size was inversely related to insulin responsiveness (Lundgren et al., 2004), whereas, studies in insulin resistant rats demonstrated a significant improvement in glucose uptake following surgical removal of visceral fat (Gabriely et al., 2002). The rate of

lipolysis in visceral compartments is higher, as the visceral fat depot is less responsive to the antilipolytic effects of insulin. Rapid visceral fat metabolism results in high delivery of FFAs to the liver as the visceral fat depot connects to the portal vein. Increased FFA delivery to the liver stimulates gluconeogenesis and increased triglyceride synthesis (Arner, 2003). Additionally the increased levels of circulating FFA in the plasma causes ectopic accumulation of TG in skeletal muscle and liver. Eptopic deposition of triglycerides in skeletal muscle and liver are associated with the development of insulin resistance (Giorgino et al., 2005, Bays et al., 2004). Elevated plasma FFA caused by resistance to the anti-lipolytic properties of insulin in adipocytes can lead to elevated hepatic glucose production, diminished insulin secretion from pancreatic β-cells (Bays et al., 2004) and a reduction in glucose uptake in skeletal muscle and liver (as discussed in section 1.5.2). Additionally in insulin resistant conditions, adipocytes secrete elevated amounts of insulin resistance inducing cytokines such as TNF-α and IL-6. A reduction in secretion of the insulin-sensitizing cytokine adiponectin has also been reported (Bays et al., 2004). Adipose-derived cytokines are discussed in more detail in Section 1.6.

1.3.2 De novo lipogenesis

FFAs in adipocyte lipogenesis can be derived from *de novo* lipogenesis, i.e. the synthesis of fatty acids from glucose or non-lipid precursors. This lipogenic pathway occurs in both the liver and the adipose tissue (Frayn, 2003). Fatty acid synthase (FAS) regulates *de novo* lipogenesis from acetyl-CoA, malonyl-CoA and nicotinamide adenine dinucleotide phosphate oxidase (NADPH). FAS is highly expressed within the adipose tissue and liver (Ranganathan et al., 2006). It has, however, been suggested that *de novo* lipogenesis is not the prominent lipogenic pathway in humans (Diraison et al., 2003, Guo et al., 2000). Conversely, expression of acetyl-CoA, carboxylase A and FAS, which are involved in *de novo* lipogenesis, have all been reported in human adipose tissue (Frayn, 2001). Also the sterol regulatory element binding protein (SREBP) isoform SREBP-1c is a transcription factor which is highly expressed in adipose tissue that functions to regulate the expression of genes involved in *de novo* lipogenesis. Pathways of lipogenesis are summarised in Figure 1.2.

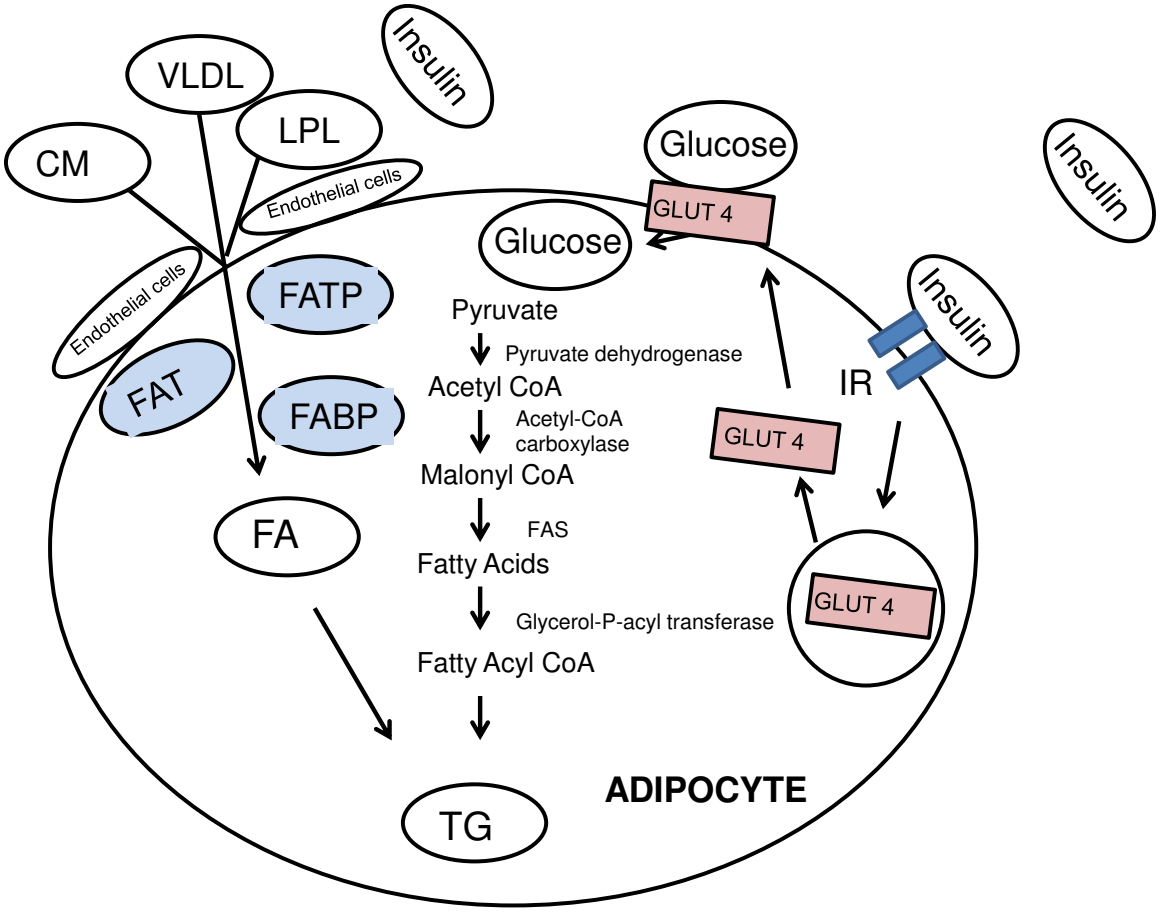

Figure 1.2. **Pathways of lipogenesis in the white fat adipocyte** adapted from Kersten (2000), Roberts (2009) and Vazquez-vela (2008)**.** In lipoprotein lipase (LPL) lipogenesis, Insulin activates LPL on the surface of the vascular endothelium. Activated LPL hydrolyse TGs and release FA from the chylomicrons and VLDL, after which FA's are taken into the adipocytes via FA transporters FABP, FAT and FATP. FA are re-esterified with glycerol-3-phosphate to give rise to triglycerides. In de novo lipogenesis FA's are synthesised from non-lipid precursors. Insulin binds the insulin-receptor on the adipocyte surface and promotes the translocation of GLUT4 to the cell membrane, facilitating cellular glucose uptake. High insulin levels activate pyruvate dehydrogenase, which forms acetyl-CoA. Acetyl-CoA carboxylase froms malonyl-CoA from acetyl CoA. LPL, lipoprotein lipase; FAT fatty acid transferase; FATP, fatty acid transport protein; FABP, fatty acid binding protein; TG, triglyceride; IR, Insulin receptor; FAS, fatty acid synthase; CM, chylomicron.

1.3.3 Uptake of fatty acids from the plasma

Dietary FFA account for 30-40% of energy intake, comprising mostly of long chain fatty acids esterified in TGs; These TGs are too large to transition from the capillaries into the interstitial fluid, and as such they cannot be directly taken up by the adipocytes (Frayn, 2003). Fatty acids used for TG synthesis in adipocytes are derived from the plasma in the form of TG-rich lipoproteins (chylomicrons) and from very low density lipoproteins (VLDL) produced from fatty acids synthesised and secreted from the liver (Glatz et al., 2010). Fatty acids are released from the chylomicrons carrying exogenous lipids and VLDL lipoproteins via the lipoprotein lipase (LPL)-mediated hydrolysis of their TGs at the capillary endothelium (Glatz et al., 2010). This process generates non-esterified fatty acids for uptake by peripheral tissues (Ranganathan et al., 2006), see Figure 1.2.

In the fed state, LPL expression within adipose tissue is elevated. Fatty acid transporters facilitate and regulate FFA transport through the adipocyte plasma membrane. The fatty acid transporters are fatty acid translocase (Hao et al., 2010) (or CD36 in humans) and the fatty acid transport protein (FATP), both of which are integral membrane proteins. FAT/CD36 is highly expressed in adipose tissue (Coburn et al., 2001), and has been shown to be an important mediator of fatty acid uptake. FAT/CD36-null mice exhibited a 50%-80% reduction in CD36 uptake within their adipose tissue (Coburn et al., 2001). FATP1 and FATP4 isoforms of the fatty acid transport protein are highly expressed in adipocytes, and following differentiation of 3T3-L1 fibroblasts to adipocytes (Czech, 2002). The fatty acid binding protein (FABP) is a fatty acid transporter (Large et al., 2004). FABPs expressed in adipose tissue are the adipocyte-lipid-binding-protein (ALBP) and the keratinocyte-lipid-binding-protein (KLBP) (Fisher et al., 2002).

The relative contribution of each of these transporters to fatty acid uptake is still under investigation, however it has been suggested that the relative contribution of each fatty acid transporter to fatty acid uptake may vary depending upon physiological conditions (Czech, 2002). Insulin has been suggested to be involved in the expression of ALBP/KLBP between subcutaneous and visceral fat depots. The protein ratio of each transporter type was related to fasting insulin concentrations in lean subjects but not in obese individuals, of which the latter group were insulin resistant (Fisher et al., 2001). The differences observed between lean and obese subjects are suggestive of adipose tissue ALBP/KLBP involvement in the pathogenesis of insulin resistance (Fisher et al., 2001).

Following FFA entry into the adipocyte, re-esterification is necessary for the storage of TG. Insulin is an important hormonal factor influencing lipogenesis (Kersten, 2001). Insulin causes the translocation of fatty acid transporters from the intracellular stores to the plasma membrane in order to facilitate fatty acid uptake (Glatz et al., 2010); see Figure 1.2. In mature adipocytes and adipose tissue, insulin increases LPL mRNA levels, and also regulates the activity of LPL post-transcriptionally and post-translationally (Wang and Eckel, 2009). Insulin augments the expression of the genes encoding the enzymes involved in fatty acid biosynthesis, including fatty acid synthase and acetyl CoA (Diraison et al., 2003) and, lipogenesis is also subject to regulation by transcription factors, namely the sterol regulatory element binding proteins (SREBPs) and the Peroxisome proliferator activated receptor-gamma (PPARγ).

1.4 Transcription factors involved in lipogenesis

1.4.1 SREBP

The sterol regulatory element binding proteins (SREBPs) are transcription factors involved in lipogenesis. SREBPs are a group of basic helix loop helix (bHLH) leucine zipper transcription factors (Yokoyama et al., 1993), consisting of the two isoforms of SREBP-1; SREBP-1a and SREBP-1c, (Kersten, 2001) and SREBP-2. SREBP-1c is the predominant isoform expressed in liver and adipose tissue (Yahagi et al., 2002). The stimulatory effect of insulin on fatty acid synthesis is mediated by an increase in SREBP-1c. Examples of genes involved adipocyte lipogenesis which are regulated by SREBPs are the low density lipoprotein receptor gene (Yokoyama et al., 1993), fatty acid synthase (Brown and Goldstein, 1997) and lipoprotein lipase genes (Kim and Spiegelman, 1996).

1.4.2 PPARγ

The PPAR family of transcription factors comprise 3 members PPARα, PPARβ/δ and PPARγ (Wahli and Michalik). PPARγ is an important transcription factor in adipose tissue, commonly known to induce differentiation of pre adipocytes into mature fat cells (Kersten, 2001). PPARγ is activated by fatty acids and drugs of the thiazolidine class. To date it is known that PPARγ regulates genes encoding the fatty acid binding protein, lipoprotein lipase (Wang and Eckel, 2009), fatty acid transport protein (FATP), acyl-CoA synthetase, phosphor-enol pyruvate carboxykinase, the phosphor-enol pryuvate carboxykinase and the fasting induced adipose factor FIAF/ PPARγ angiopoietin related fasting induced adipose PGAR (Kersten, 2001). Both insulin and SREBP-1 stimulate PPARγ expression, this in conjunction with the observation that the majority of the known genes encoded by PPARγ are involved in the lipogenic pathway, implicating PPARγ's

involvement in lipogenesis. The involvement of PPARγ in lipogenesis is supported by data from clinical studies, whereby subjects taking thiazolidinedione, PPARγ-activating drugs, gain weight (Fuchtenbusch et al., 2000).

It is reported that adipocytes from obese subjects are enlarged and have elevated basal levels of lipolysis (Large et al., 1999) and elevated levels of $[Ca^{2+}]_i$. It is possible that there are associations between obesity, elevated adipocyte $[Ca^{2+}]_i$, elevated lipolysis and peripheral insulin resistance. It seems reasonable to suggest that elevated levels of FFAs in the circulation would result in increased activation of the PPARs and SREBP transcription factors, therefore increasing transcription of the genes involved in lipogenesis, further exacerbating fat storage within the adipocyte and contributing to the development of insulin resistance. Indeed fatty acids are ligands for PPARs; additionally elevated circulating FFA cause numerous disruptions to the regulation of energy metabolism, examples of FFA disruptions to energy metabolism are presented in section 1.5.2. Contrary to this suggestion, correlations between adipocyte size and lipogenic gene expression (PPARγ-1 PPARγ-2 and the fatty acid synthase gene (FASN)) are inverse, suggestive of a physiological mechanism which downregulates *de novo* lipogenesis as adipocytes expand to prevent uncontrolled expansion to a possibly detrimental phenotype (Roberts et al., 2009).

1.5 Adipocyte function

1.5.1 The role of $[Ca^{2+}]_i$ in dysregulated insulin-stimulated lipogenesis

Food intake is not reported to be elevated in *agouti* mice, suggestive of altered energy homeostasis being accountable for their increased fat mass (Carroll et al., 2004). Studies in obese visible yellow mice (A^{vy}/a) have demonstrated that (A^{vy}/a) mice exhibit both elevated $[Ca^{2+}]_{i,}$ and elevated FAS activity (an enzyme involved in *de novo* lipogenesis) of ~7.2 fold in conjunction with their obesity when compared with lean controls (Kim et al., 1996). Elevations in $[Ca^{2+}]_i$ are correlated with body weight, suggesting a link between $[Ca^{2+}]_i$ and the mechanism of obesity in *agouti* mice (Zemel et al., 1995). Nifedipine is a dihydropryidine (DHP) Ca^{2+} channel blocker, reported to block L-type VGCCs (Lipscombe et al., 2004). (A^{vy}/a) mice fed on a nifedipine diet exhibited reduced epididymal, perirenal and retroperitonal fat pad weights when compared to (A^{vy}/a) mice fed on a nifedipine free diet. Nifedipine had no effect upon fat pad weights of control animals. Additionally, Ca^{2+} channel antagonism by nifedipine ameliorated the ~ 7 fold increase in FAS activity in subcutaneous adipose tissue, but only marginally in visceral adipose tissue of (A^{vy}/a) (Kim et al., 1996). This is suggestive of Ca^{2+} action upon FAS, exacerbating *de novo* lipogenesis, contributing to the induction of the insulin resistant state and that there are variations in Ca^{2+} regulation of lipogenesis pathways between different murine fat depots.

1.5.2 Elevated plasma FFA concentrations in whole body insulin resistance

Elevated plasma FFA are associated with the hepatic and peripheral insulin resistance. The Randle cycle is a model of elevated circulating FFAs in the onset of peripheral insulin resistance. Randle *et al* (1963) proposed a mechanism to explain how elevated plasma fatty acids inhibit glucose uptake. Randle *et al* (1963) demonstrated in both muscle and adipose tissue that FFA competes with glucose as an energy substrate. In response to elevated FFA concentrations, an increase in fatty acid oxidation occurs. In brief, increased levels of fatty acid oxidation results in an increase in cellular acetyl CoA, resulting in the inhibition of pyruvate dehydrogenase. The end-point is an elevation in intracellular glucose and glucose-6-phosphate concentrations, resulting in a reduction in glucose uptake (Randle et al., 1963). Boden *et al* (2002) investigated the mechanisms underlying FFA inhibition of insulin-stimulated glucose uptake in healthy subjects, (Boden et al., 1994) and in patients with type 2 diabetes (Boden and Chen, 1995). With normal subjects, fat infusions inhibited glucose uptake in a dose-dependent manner. Four to six hours post 750μM fat infusion resulted in elevated glucose-6-phosphate concentration. Intermediate 550μM fat infusion resulted in decreased muscle glucose-6-phosphate concentrations, as attributed to reduced glucose transport (Boden et al., 1994). Fat infusion reduced insulin-stimulated glucose uptake in the type 2 diabetic subjects by 40-50%, this was accompanied by inhibition of glycogen synthesis and glycolysis (Boden and Shulman, 2002). Later studies by Roden *et al* (1996) also postulated an inhibitory effect of FFA on insulin-stimulated glucose transport in muscle by way of inhibited glucose transport/phosphorylation (Roden et al., 1996).

There are several suggestions as to how FFA inhibit insulin-stimulated glucose transport, including direct effects upon GLUT-4 transporter activity, or FFA-induced changes in the synthesis and trafficking of GLUT-4. Additionally Dresner *et al* (1999) examined the effect of elevated FFA concentrations on phosphatidylinositol 3-kinase (PI3K) activity (a regulator of GLUT-4 translocation in muscle). In comparison to control subjects, FFA infusion abolished IRS-1 associated PI3K activity in response to insulin stimulation. It is possible that the effect of FFA could occur at the level of PI3K, or via alteration of another step in the insulin signalling pathway (Dresner et al., 1999).

Elevated levels of circulating fatty acids give rise to reduced insulin stimulated glucose uptake in peripheral insulin responsive tissues, thus contributing to the development of insulin resistance. As $[Ca^{2+}]_i$ is important to the biochemical functionality of adipocytes, the consequences of dysregulated $[Ca^{2+}]_i$ in adipocytes could not only disrupt the biochemical functions of adipocytes, but also affect peripheral insulin responsive tissues and potentially be a crucial factor in the development of insulin resistance. Insulin resistance results in elevated levels of circulating insulin, which has also been reported to elevate adipocyte $[Ca^{2+}]_i$ (Draznin et al., 1988). The role of $[Ca^{2+}]_i$ in adipocyte lipolysis is discussed herin.

1.5.3 The role of adipocyte $[Ca^{2+}]_i$ in lipolysis

The role of $[Ca^{2+}]_i$ in adipocyte lipolysis is yet to be fully clarified. There is evidence in support of $[Ca^{2+}]_i$ as both a positive (Allen and Beck, 1986, Katocs et al., 1974) and a negative regulator of lipolysis (Xue et al., 2001, Xue et al., 1998).

Stimulation of lipolysis by catecholamines is reported to be only partially dependent on $[Ca^{2+}]_i$ (Allen and Beck, 1986, Schimmel, 1973). Stimulation of cAMP accumulation, by isoprenaline or forskolin was not affected by the presence or absence of $[Ca^{2+}]_i$, although the rates of lipolysis were reduced by ~40% in the absence of extracellular Ca^{2+}, indicative of a requirement for Ca^{2+} at a step in the lipolytic cascade distal to cAMP (Allen and Beck, 1986). Additionally Izawa and Komabayashi (1994) provided evidence for the requirement of Ca^{2+}-calmodulin for the full activation of lipolysis, as lipolytic responses to noradrenaline and dibutyryl cAMP were blunted in the presence of calmodulin inhibitor W7 (Izawa and Komabayashi, 1994). Both Izawa and Komabayashi (1994) and Kawai (1985) suggest Ca^{2+} calmodulin activates cAMP dependent protein kinase (PKA) in primary adipocytes, and in fat cell extracts. In the lipolytic cascade PKA phosphorylates HSL, activating lipolysis (Kawai, 1985). It has also been suggested that Ca^{2+} action on lipolysis in adipocytes is mediated by Ca^{2+}-calmodulin, by stimulating the ERK/MAPK cascade, which then activates HSL (Della Rocca et al., 1997).

To the contrary, work by Xue *et al* (2001) provided evidence of $[Ca^{2+}]_i$ having an inhibitory effect upon lipolysis in human adipocytes. An increase in $[Ca^{2+}]_i$ was attained by elevating $[K^+]_o$ to 100mM. This treatment was found to inhibit agonist-stimulated lipolysis. Conversely, elevated conditions of $[K^+]_o$ at 40mM to

60mM were shown not to affect basal or isoprenaline-stimulated lipolysis in either rabbit or mouse white fat adipocytes (Garcia-Barrado et al., 2001). This could be indicative of a species difference in the lipolytic responses to $[Ca^{2+}]_i$. In the study by Xue *et al* (2001), it was suggested that the ability of $[Ca^{2+}]_i$ to inhibit lipolysis occurs via activation of phosphodiesterase 3B (PDE3B), the same PDE isoforms that mediates the antilipolytic effects of insulin. However, insulin and $[Ca^{2+}]_i$ were suggested to activate PDE3B by different mechanisms but they both ultimately result in a reduction in cAMP, reducing HSL phosphorylation with subsequent inhibition of lipolysis (Xue et al., 2001).

The recombinant murine *agouti* protein has also been demonstrated to cause elevations in $[Ca^{2+}]_i$ in 3T3-L1 adipocytes (Kim et al., 1997). The recombinant *agouti* protein inhibited basal lipolysis by 60% in comparison to controls, and agonist (ACTH and forskolin) induced lipolysis (Xue et al., 1998). Additionally arginine vasopressin, (which is known to activate Ca^{2+} influx by way of phosphoinositide hydrolysis (Kondo et al., 1989)) and KCl-induced inhibition of forskolin stimulated lipolysis in recombinant *agouti* adipocyte samples by 56% and 50%, respectively. The anti-lipolytic effects of the *agouti* protein were revoked by treatment with nitrendipine (30 μM) (a Ca^{2+} channel blocker) indicative of extracellular Ca^{2+} influx in the involvement of the anti-lipolytic effects of *agouti*.

Taken together, the role of Ca^{2+} on lipolysis and the mechanisms by which Ca^{2+} acts to mediate its effects, be they stimulatory or inhibitory, is not fully understood. It is apparent that there is a requirement for $[Ca^{2+}]_i$ in lipolysis signalling pathway, however the consequences of abnormal $[Ca^{2+}]_i$ and the influx pathway by which this is derived needs further investigation.

1.5.4 Insulin-stimulated glucose uptake

Insulin is secreted from β-cells in the islets of Langerhans of the pancreas, and is released into the circulation in response to elevated levels of plasma glucose. The liver, skeletal muscle and adipose tissue are the primary targets for the actions of insulin (Klip and Ramlal, 1987). The insulin receptor is a transmembrane glycoprotein with intrinsic tyrosine kinase activity (Gammeltoft and Van Obberghen, 1986). The insulin receptor (IR) is an $\alpha_2\beta_2$-tetramer (Ding et al., 2002). The α-subunit pair comprise the insulin binding site, and is situated exterior to the plasma membrane. The β-subunits are transmembrane proteins which contain the tyrosine kinase domains. Upon insulin binding to the α-subunits the tyrosine kinase activity of IR is stimulated. As such, the insulin receptor autophosphorylates tyrosine residues within the β-subunit. (Ding et al., 2002). Initially, insulin receptor substrate (IRS) proteins are phosphorylated on tyrosine residues by the insulin receptor (Whitehead, Molero et al. 2001). The proteins which comprise the IRS family are as follows; IRS-1 and IRS-2 which are ubiquitously expressed IRS-3; which has been demonstrated in adipose tissue; IRS-4, which is so far only reported in cultured embryonic kidney cells; and Gab1, which is widely expressed also (Taha and Klip, 1999). The IRS proteins are not functionally interchangeable; mice deficient in IRS-1 show 50-60% reduction in insulin-stimulated glucose uptake, even though there are other IRS substrate protein substrates for the insulin receptor (Bruning et al., 1997).

Following phosphorylation of IRS-1, IRS-1 is available to bind src-homology-2 domain containing proteins such as phosphatidylinositol 3-kinase (PI3K) (Hering et al., 2008) and growth factor bound protein (GrB2) (Taha and Klip, 1999). PI3K interacts with IRS1/2 via its regulatory subunit P85, this interaction results

in PI3K activation and instigation of the phosphorylation cascade involving downstream effectors, such as protein kinase C (PKC) and protein kinase B (PKB), resulting in insulin-stimulated glucose uptake, glycogen synthesis, lipogenesis and inhibition of lipolysis. Also, interaction of IRS1/2 with Grb-2 activates the mitogen-activated (MAP) protein kinase insulin signalling cascade. The MAP kinase insulin signalling cascade is reported not to be involved in the metabolic responses of insulin (Taha and Klip, 1999).

The consequence of the IRS signalling cascade is the promotion of GLUT-4 translocation from the intracellular stores to the plasma membrane (Giorgino et al., 2005, Taha and Klip, 1999). GLUT-4 transporters are sequestered within storage vesicles in the Golgi apparatus. The transporters are transported across the cytosol following receipt of the downstream signals produced by the insulin receptor (Whitehead et al., 2001). The effect of insulin on vesicle mobilisation is reversible; reductions in the level of circulating insulin results in removal of the plasma GLUT-4 receptors by endocytosis. A summary of the insulin signalling cascade is shown in Figure 1.3.

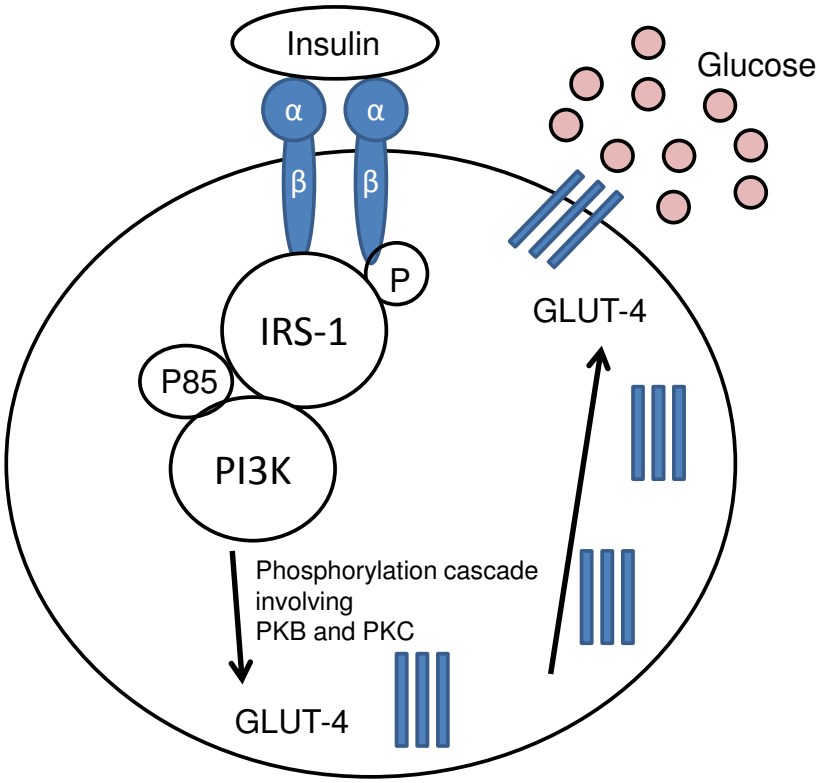

Figure 1.3. Insulin stimulated glucose uptake. Insulin binds to the insulin receptor α subunit stimulating the tyrosine kinase activity of the insulin receptor. The insulin receptor autophosphorylates tyrosine residues within its β-subunit. Insulin receptor substrate proteins (IRS) are phosphorylated. IRS-1 binds to PI3K via its regulatory subunit P85, activating PI3K. The activated PI3K initiates a complex phosphorylation cascade involving protein kinase C (PKC) and protein kinase B (PKB) resulting in GLUT-4 translocation from intracellular GLUT-4 storage vesicles to the adipocyte plasma membrane.

Ca^{2+}-dependent "conventional" PKCs have been implicated in insulin-stimulated glucose transport in 3T3-L1 adipocytes (Tsuru et al., 2002). Ca^{2+} channel opening either by receptor-mediated or voltage-dependent mechanisms is suggested to prolong PKC activation (Nishizuka, 1995), resulting in elevated GLUT-4 translocation to the adipocyte plasma membrane giving rise to elevated glucose uptake (Kohn et al., 1996). This may therefore contribute to the development of obesity by way of increased fat storage within the adipocyte.

1.5.5 The role of Ca^{2+} in adipocyte insulin resistance

It has been suggested that dysregulated Ca^{2+} homeostasis contributes to reduced adipocyte responsiveness to insulin. Both experimental and clinical evidence pertaining to dysregulated Ca^{2+} influx by way of $Ca_v1.2$ / $Ca_v1.3$ VGCCs contributing to diminished insulin responsiveness, as defined by reduced insulin stimulated glucose uptake is reviewed in Chapter 3, Sections 3.7.2 and 3.7.3. Other aspects of $[Ca^{2+}]_i$ involvement in insulin resistance is discussed herin.

1.5.6 The role of Ca^{2+} in dysregulated insulin-stimulated glucose uptake

Relationships between elevated $[Ca^{2+}]_i$ and dysregulated insulin-stimulated glucose transport in adipocytes have been reported (Reusch et al., 1991, McCarty, 2006, Draznin et al., 1989, Begum et al., 1993). Furthermore, it has been suggested that an optimal range of $[Ca^{2+}]_i$ for insulin-stimulated glucose transport in isolated rat adipocytes (Draznin et al., 1987b) of 140-370nM $[Ca^{2+}]_i$ is required for normal adipocyte function, with extremes either side of this range resulting in a diminished response to insulin.

Conversely some studies investigating the link between $[Ca^{2+}]_i$ and insulin-stimulated glucose uptake in primary adipocytes (Kelly et al., 1989) and in 3T3-L1 adipocytes (Klip and Ramlal, 1987) do not describe an association between elevated Ca^{2+} and a reduction in insulin-stimulated glucose uptake. However in the studies that do report an association between $[Ca^{2+}]_i$ and cellular responsiveness to insulin, elevations in $[Ca^{2+}]_i$ have been suggested to cause resistance to insulin by way of reduced glucose uptake, using the 2-deoxyglucose uptake assay (Reusch et al., 1993, Reusch et al., 1991, Begum et al., 1993). The reduction in insulin-stimulated glucose transport by elevated

$[Ca^{2+}]_i$ was shown not to affect insulin binding to the insulin receptor, or the tyrosine kinase activity of the insulin receptor, thus implicating the involvement of elevated $[Ca^{2+}]_i$ at a step in the insulin signalling cascade distal to the insulin receptor (Begum et al., 1992).

Conditions of elevated extracellular K^+ have been used to elevate $[Ca^{2+}]_i$ in numerous cell types, including adipocytes (Pershadsingh et al., 1989, Haspel et al., 2005, Yaguchi and Nishizaki, 2010, Reusch et al., 1991).

Reusch *et al* (1991) demonstrated that the consequences of elevated $[Ca^{2+}]_i$ in adipocytes manifest as an increase in GLUT-4 phosphorylation and a reduction in insulin-stimulated glucose transport. The phosphorylation status of GLUT-4 was shown by way of Western-blotting, not to affect the translocation of the GLUT-4 transporter to the adipocyte plasma membrane. Investigations into the mechanism underlying the elevated $[Ca^{2+}]_i$ disruption to GLUT-4 phosphporylation showed that elevated $[Ca^{2+}]_i$ inhibited PP1 activity. Inhibition of PP1 was suggested to occur by a cAMP dependent mechanism. Adipocytes with elevated $[Ca^{2+}]_i$ demonstrated a 2x elevation in $[cAMP]_i$ in comparison to controls. Later studies by Begum *et al* (1992) show elevated $[Ca^{2+}]_i$ induces cAMP mediated phosphorylation and activation of inhibitor 1, resulting in an inhibition of PP1 activity and subsequent inactivation of GLUT-4. In support of cAMP in the diminished activity of GLUT-4 RPcAMP (a cAMP antagonist) prevented inhibitor-1 activation (Begum et al., 1992). In further support of the role of elevated $[Ca^{2+}]_i$ in the phosphorylation of GLUT-4, treatment of adipocytes with nitrendipine (a Ca^{2+} channel blocker) restored GLUT-4 phosphorylation (Reusch et al., 1993).

The observation that adipocytes from obese individuals exhibit elevated $[Ca^{2+}]_i$ in comparison to gender and age matched lean controls (Byyny et al., 1992), is suggestive of Ca^{2+} involvement in insulin resistance in obese individuals, in part by reduced insulin-stimulated glucose uptake, possibly by way of inhibitor-1 activation.

As previously mentioned deficiencies in $[Ca^{2+}]_i$ are also reported to have adverse effects on insulin signalling. In 3T3-L1 adipocytes chelation $[Ca^{2+}]_i$ by calmodulin agonist W13 and 1,2-bis(2-aminophenoxy)ethane-N,N,N,N-tetraacetic acid acetoxymethylester (BAPTA AM) inhibited insulin-stimulated 2-deoxyglucose uptake by up to ~95%, which was later shown to occur as a result of diminished GLUT-4 translocation to the plasma membrane. BAPTA AM inhibited insulin-stimulated translocation of the GLUT-4 transporter to the plasma membrane by ~50% suggestive of a requirement of Ca^{2+} in the translocation of GLUT-4 from the intracellular vesicles to the plasma membrane (Whitehead et al., 2001). Treatment of BAPTA AM or W13 treated cells with ionophores A23187 or ionomycin prevented the inhibition of AKT (protein kinase B) phosphorylation and subsequent translocation of GLUT-4 by Ca^{2+} chelation, suggestive of a requirement for Ca^{2+} in the activation of protein kinase B (Whitehead et al., 2001).

1.6 Adipokines in insulin sensitivity

Until recently adipocytes were considered a somewhat inert energy store, however, it is now recognised as a major endocrine organ, secreting an expanding plethora of hormones, adipokines and other proteins with the capacity to impact upon energy metabolism (Antuna-Puente et al., 2008) Adiponectin and resistin are factors which are known to be produced only within

adipose tissue (Roth et al., 2004), see Figure 1.4. Other adipocyte secreted hormones are also shown in Figure 1.4.

Among the expanding number of proteins that are secreted by adipocytes, only those that have a key role in energy metabolism and insulin resistance, will be discussed briefly herein, namely TNF-α, IL-6, resistin, and adiponectin. A brief summary of the sources, functions and interactions of these adipokines is shown in Table 1.1.

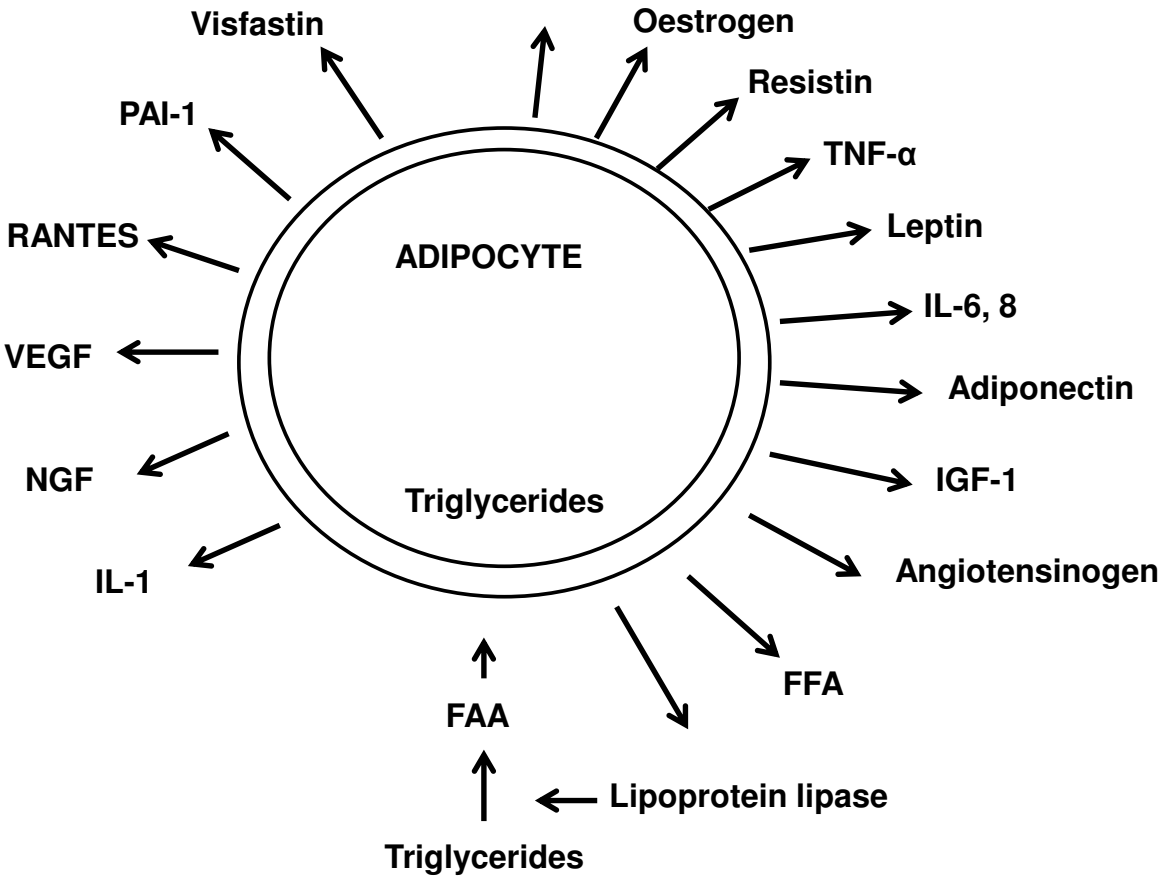

Figure 1.4. A summary of adipose secreted factors, adapted from Gustafson *et al* (2010). Adipose secreted hormones and cytokines are shown. PPAR, peroxisome proliferator-activated receptor; regulated upon activation normal T-cell, RANTES; GH, growth hormone; Vascular endothelial growth factor, VEGF; Normal growth factor, NGF; IGF, insulin-like growth factor; Plasminogen activator inhibitor-1, PAI-1; TNF-α, tumour necrosis factor alpha; IL, interleukin; FFA, free fatty acids.

Adipokine	Primary Source	Receptor	Effects on other adipokines	Action on adipose tissue (AT)	Secretion in response to insulin	Secretion in response to insulin resistance.	Peripheral Function
Leptin	Adipocytes	Leptin receptor	Suppressed TNF-α and IL-6 expression Stimulation of adiponectin expression	Sensitises AT to the action of insulin.	Increased production	Increased leptin in circulation. (leptin resistance can occur with insulin resistance, despite more leptin is present, a response is not guaranteed).	Regulates satiety (acts primarily at the level of the central nervous system to regulate energy intake and expenditure)
Adiponectin	Adipocytes	AdipoR1, AdipoR2, T-cadherin	Suppressed TNF-α and IL-6 expression	Enhances insulin sensitivity. Involved in IR and IRS phosphorylation.	Increased production (required for the normal action of insulin on the AT)	Decreased	Insulin sensitizer, anti-inflammatory Decreases gluconeogenesis Increased glucose uptake
Resistin	Peripheral blood mononuclear cells (human), adipocytes (rodent)	Unknown	Stimulation of TNF-α and IL-6 expression	Induces insulin resistance. Induces adipocyte differentiation.	Decreased production	Increased	Promotes insulin resistance and inflammation through IL-6 and TNF secretion from macrophages.
IL-6	Adipocytes, stromal vascular fraction cells, liver, muscle	IL-6R	Stimulation of leptin and resistin expression. Suppression of adiponectin expression	Elevated lipolysis,		Increased	Reduction in insulin sensitivity
TNF-α	Stromal vascular fraction cells, adipocytes	TNFR	Stimulation of leptin and resistin expression. Suppression of adiponectin expression	Elevated lipolysis		Increased	Inflammation, Antagonism of insulin signalling

Table 1.1. Sources, functions and interactions of adipokines. Adapted from (Karlsson and Beck, Ouchi et al., Rabe et al., 2008, Lago et al., 2009)

1.6.1 TNF-α

TNF-α is associated with insulin resistance in white adipocytes as TNF-α mRNA and protein expression is elevated in adipose tissue from obese humans and rodents (Maeda et al., 2002). Adipocytes from obese subjects have been shown to have elevated $[Ca^{2+}]_i$, additionally, adipocytes with elevated $[Ca^{2+}]_i$ have been demonstrated to have elevated $[cAMP]_i$, therefore resulting in an elevated rate of basal lipolysis. A summary of the lipolytic cascade is presented in Chapter 2, Section 2.1. As TNF-α expression is elevated in obesity, it further enhances basal lipolysis via stimulation of MAP kinases which decrease the protein expression of perillipin (Carmen and Victor, 2006), resulting in enhanced lipolysis (Arner, 2005b). In macrophages it has been demonstrated that TNF-α production is associated with elevated $[Ca^{2+}]_i$ (Seabra et al., 1998). As adipocytes in obese humans and rodents also exhibit elevated $[Ca^{2+}]_i$, it seems reasonable to suggest that elevated adipocyte $[Ca^{2+}]_i$ may also contribute to elevated basal lipolysis by stimulating TNF-α production.

Additionally there are regional variations in TNF-α production, dependent upon the fat deposit from which it is produced. Adipose expression of TNF-α is greater in subcutaneous adipose compared with visceral adipose (Kershaw and Flier, 2004), BMI is also reported to affect regional differences in adipokine release as TNF-α release was greater in subcutaneous adipose tissue when obtained from obese women with a body mass index (BMI) of 42, but not with a BMI of 32 (Fain et al., 2004).

1.6.2 IL-6

Human white adipose tissue produces up to 30% of IL-6 present within the circulation (Guerre-Millo, 2004, Kershaw and Flier, 2004), the remaining IL-6 is produced and secreted by other cell types present within the adipose tissue such as stromal vascular cells, endothelial cells and fibroblasts (Fain et al., 2004). Plasma IL-6 is positively correlated with body mass and inversely correlated to insulin sensitivity (Guerre-Millo, 2004). It is possible that there is an association between obesity, elevated adipocyte $[Ca^{2+}]_i$ and elevated IL-6 secretion/ activity. As yet, this has not been directly studied in adipocytes. It is known, however, that IL-6 secretion from other cell types, e.g. mast cells, is a $[Ca^{2+}]_i$ dependent process (Jeong et al., 2002).

Insulin has been shown to both increase IL-6 mRNA expression and release in adipocyte cell lines (LaPensee et al., 2008), and elevate $[Ca^{2+}]_i$ in primary adipocytes (Draznin, 1988). As IL-6 secretion is dependent on Ca^{2+} and stimulated by insulin, it is possible that elevated $[Ca^{2+}]_i$ by insulin may upregulate IL-6 secretion. Adipocytes with elevated $[Ca^{2+}]_i$ exhibited a 2X elevation in $[cAMP]_i$. Studies in human fibroblasts, which are another IL-6 secreting cell type, demonstrated that treatment with cAMP, cAMP analogues or cAMP activators all resulted in a sustained elevation of IL-6 mRNA levels. cAMP activators were all shown to stimulate IL-6 secretion. Additionally treatment of cells with the Ca^{2+} ionophore A23187 also resulted in an increase in IL-6 expression.

There are several means by which IL-6 can contribute to the induction of insulin resistance. IL-6 reduces insulin-stimulated glucose uptake by serine phosphorylation or IRS-1 and subsequent inhibition of the insulin receptor

kinase (Zhang et al., 1988). IL-6 increases hepatic triglyceride secretion (Nonogaki et al., 1995). In humans, infusion of IL-6 increases plasma fasting triglyceride and VLDL triglyceride levels (Stouthard et al., 1995), suggesting that IL-6 contributes to the development of hypertriglyceridaemia. However, there is evidence to suggest IL-6 may not always contribute to metabolic dysfunction. In vitro investigations have shown IL-6 to increase glucose uptake by increasing GLUT-4 translocation, additionally IL-6 can activate AMPK increasing fat oxidation in muscle and adipose cells (Allen and Febbraio, Galic et al., 2010). A complex interplay between different adipose secreted factors and cytokines may be responsible for the differences in the effects of IL-6 observed between studies

1.6.3 Adiponectin

Adiponectin is highly and specifically expressed in adipocytes, in particular subcutaneous adipose tissue (Kershaw and Flier, 2004). Circulating adiponectin levels are positively correlated with insulin sensitivity and negatively correlated with BMI (Smith, 2002) and insulin resistance (Guerre-Millo, 2004). Adiponectin increases insulin sensitivity by increasing fatty acid oxidation in skeletal muscle by phosphorylation and activation of adenosine monophosphate activated protein kinase activity (AMPK) (Yamauchi et al., 2002), resulting in a reduction in circulating FFAs and intracellular triglyceride deposition in muscle and liver (Diez and Iglesias, 2003). In mice, recombinant adiponectin administration by pancreatic euglycaemic clamp activates liver AMPK reducing hepatic glucose production by 65%, thereby also reducing plasma glucose concentrations (Combs et al., 2001, Yamauchi et al., 2002).

It has been demonstrated in both humans and mice that adiponectin formation is influenced by $[Ca^{2+}]_i$. Chelation of adipocyte $[Ca^{2+}]_i$ by EGTA resulted in a reduction in adiponectin secretion from adipocytes, whereas excess supplementation of Ca^{2+} (20mM) to the adipocyte incubation medium resulted in an elevation of adipocyte adiponectin (Banga et al., 2008). This could be suggestive of a protective mechanism to counteract the detrimental effects of elevated $[Ca^{2+}]_i$. However a reduction in adiponectin expression is associated with obesity and insulin resistance (Diez and Iglesias, 2003). For example adiponectin mRNA levels in white adipocytes were lower in obese mice (~70 to 90% lower) and humans (~50-80% lower) in comparison to wild type mice and normal weight humans (Hu et al., 1996). It has been suggested that hypoadiponectinaemia is related to the development of insulin resistance (Hotta et al., 2001). Additionally adiponectin expression can influence and be influenced by adipokines. Adiponectin reduces the production and activity of TNF-α (Fantuzzi, 2005). TNF-α and IL-6 inhibit adiponectin expression both cultured adipocytes and primary adipose tissue, indicative of TNF-α and IL-6 inhibition of adiponectin release having a role in insulin resistance. Interventions to reduce insulin resistance (weight loss, TZD treatment) increase adiponectin gene expression and plasma levels thereof in adipose tissue (Kershaw and Flier, 2004).

1.6.4 Resistin

In rodents resistin is expressed in adipocytes, whereas in humans resistin is expressed within macrophages (Galic et al., 2010). Resistin expression and secretion is increased in obesity, and is decreased by PPARγ ligands.

In mice infusion or over-expression of resistin results in hyperglycaemia, which has been attributed to elevations in hepatic glucose production. Reductions in serum resistin caused by infusion of resistin antibodies or by resistin gene deletions have been shown to restore hepatic responsiveness to insulin (Banerjee et al., 2004, Steppan et al., 2001). Additionally circulating resistin levels are reduced by rosiglitazone (an antidiabetic drug) (Steppan et al., 2001). The importance of resistin in humans is unclear as investigations into serum resistin levels in obese type 2 diabetics do not all report elevated serum resistin (Savage et al., 2001). To date the effects of elevated $[Ca^{2+}]_i$ on resistin expression have not yet been studied in adipocytes.

1.7 Experimental Aims

There is an increasing awareness of the role of white fat adipocytes in the regulation of energy metabolism. As $[Ca^{2+}]_i$ is an important ubiquitous intracellular signalling molecule, it is possible that $[Ca^{2+}]_i$ has a role in adipocyte function, with dysregulations in adipocyte $[Ca^{2+}]_i$ and altered adipocyte function contribute to the metabolic derangements associated with obesity and hypertension.

L-type Ca^{2+} channels have been suggested to be a functional Ca^{2+} influx pathway in adipocytes, which are activated upon plasma membrane depolarisation. As the ion species which regulate Vm are unknown, I aim to explore adipocyte Vm and the ion conductances which are responsible for this.

Additionally as adipocyte plasma membrane Ca^{2+} influx pathways are poorly described, investigations presented within this thesis aims to identify the Ca^{2+} influx pathways present on the plasma membrane of the white fat adipocyte. This will be attempted by way of $[Ca^{2+}]_i$ imaging in conjunction with known Ca^{2+} antagonists, patch clamp methods and Western blotting.

.

Chapter 2

The ionic control of membrane potential of primary white fat adipocytes and differentiated 3T3-L1 adipocytes

2.1 Adipocyte Lipolysis

One of the main roles of adipocytes is the storage of energy in the form of triglycerides (TG), particularly during times of surplus energy intake. When stored energy is required by other tissues, it is released in the form of non-esterified fatty acids (Chaves et al., 2011). 95% of the total adipocyte volume is comprised of fat droplets (Arner, 2005a). Lipolysis is the stepwise hydrolysis of ester bonds in TG, resulting in the breakdown of diglycerides giving rise monoglycerides and glycerol (Ahmadian et al., 2009). The control of lipolysis comprises various signalling pathways. The cAMP dependent pathway is predominant and the best characterised pathway for the induction of lipolysis, this is summarised in Figure 2.1.

Insulin and adrenaline/ noradrenaline are the main physiological regulators of lipolysis (Lafontan and Langin, 2009). Adrenaline and noradrenaline bind to β-adrenoceptors, stimulating lipolysis. Isoprenaline, a synthetic, non selective β-adrenoceptor agonist can also be used to stimulate lipolysis. For an excellent review on the role of β adrenoceptors in lipolysis see Bartness *et al*, 2010.

Insulin inhibits lipolysis. Insulin's inhibition of catecholamine-induced lipolysis can occur via multiple mechanisms, the cAMP degradation by its stimulation of cAMP phosphodiesterase being the most predominant (Engfeldt et al., 1988). Insulin can also inhibit lipolysis by a direct inhibitory effect on HSL, this has been shown in both human and in cultured 3T3-L1 adipocytes (Engfeldt et al., 1988).

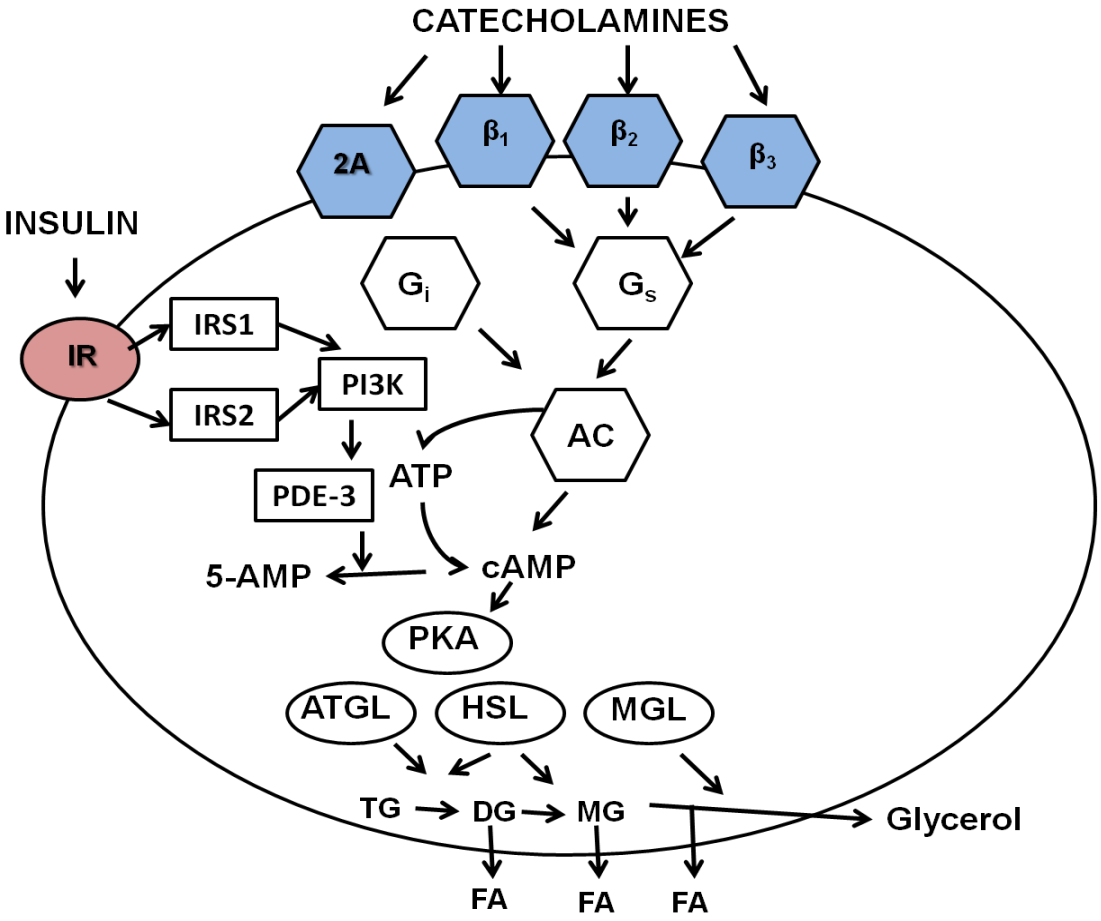

Figure 2.1. The cAMP dependent lipolytic pathway. Adapted from (Arner, 2005a)).($\beta_{1,2,3}$, beta$_{1,2,3}$-adrenergic receptors; 2A, α_2 adrenoceptors, $G_{i,s,}$inhibitory (i) or stimulatory (s) G-proteins; AC, adenylate cyclise; cAMP, cyclic AMP; PKA, protein kinase A; AGTL, adipose tissue specific triglyceride lipase; HSL, hormone sensitive lipase; MGL, monoglyceride lipase; TG, triglycerides; DG, diglyceride, MG, monoglyceride; FA, Fatty acid; IR, insulin receptor; IRS-1,2, insulin receptor substrates 1 and 2; PI3K, phosphoinositide 3-kinase; PDE-3, phosphodiesterase 3. In short catecholamines bind to the β-adrenoceptors, activating stimulatory G proteins (G_s). The alpha subunit of the activated G_s activates adenylate cyclise causing increased cAMP. The increase in cAMP activates PKA, which then goes on to phosphorylate HSL, initiating triglyceride hydrolysis.

2.2 The effects of insulin and catecholamines upon the electrophysiological properties of adipocytes.

Isoprenaline is reported to hyperpolarise the plasma membrane of mouse skeletal muscle fibres (van Mil et al., 1995). The hyperpolarising effect of isoprenaline was attributed to membrane voltage (Vm) alterations caused by stimulation of the Na^+-K^+ pump, Na^+ conductance, and an increase in outward K^+ conductance. Insulin also causes membrane potential alterations in insulin responsive tissues. Zierler (1966) studied the effect of insulin on the resting membrane potential of the rat extensor digitorium longus muscle. High insulin concentrations (0.1 units/ml) caused hyperpolarisation of the RMP of every muscle fibre investigated. The authors suggest a difference in membrane permeability to K^+ and accumulation of $[K^+]_i$ observed was not due to the actions of insulin, but more likely due to the resultant membrane hyperpolarisation that occurred as a result of insulin exposure. The hyperpolarisation observed was attributed to reduced membrane permeability to Na^+ or increased permeability to Cl^-. It is already well characterised that nerve, cardiac and pancreatic beta cell functions depend upon, or are accompanied by, alterations in transmembrane ion gradients. It is possible that the RMP of the white fat adipocyte may play a significant role in its basal function. Inhibition of lipolysis in adipocytes by Ca^{2+} was reported to result following KCl depolarisation of the plasma membrane, inducing opening of VGCCs. The resultant Ca^{2+} influx caused activation of PDE-3, reducing intracellular cAMP, leading to reduced HSL and subsequent inhibition of lipolysis (Xue et al., 2001). Furthermore, modulations in membrane potential induced by hormonal changes may influence the metabolic activity of adipose tissue or even contribute to the development of a dysregulated state. Insulin inhibits lipolysis by PDE-3 activation (see Figure

2.1). Conversely it is also possible, that if indeed insulin does hyperpolarise the plasma membrane of the white fat adipocyte, that this hyperpolarisation could counteract/ prevent the opening of VGCCs, therefore inhibiting Ca^{2+} influx, removing the inhibitory action of Ca^{2+} on lipolysis. Ion channel agonists/antagonists may be used to mimic the regulatory effect of hormones or signalling molecules on the adipocyte. For example, sulphonylurea drugs such as tolbutamide and glibenclamide are used as insulin secretalogues in the treatment of type 2 diabetes, as they cause K_{ATP} channel closure in pancreatic beta cells, mimicking the effect of ATP (Pearson et al., 2006). Understanding adipocyte membrane potential in the basal state and how disease states alter the types of ion channels involved and how they are regulated, may prove to be clinically useful. At present very little is known about the electrophysiological properties of adipocytes and how these may influence adipocyte function.

The electrophysiological characteristics of adipocytes, such as resting membrane potential (RMP), have not been comprehensively studied when compared to the plethora of information available pertaining to other tissue types. As the K^+ ion is a determinant of membrane potential in many cell types it would be interesting to determine if the K^+ ion is involved in adipocyte RMP. The importance of K^+ in RMP is discussed in Section 2.3.1. Initial investigations into white adipose tissue RMP were made using the sharp electrode technique. RMP values obtained from different studies using this method were inconsistent ranging from -21mV to -46mV (Ramirez-Ponce et al., 1990, Stark et al., 1980, Akiyama et al., 1990, Kamei et al., 1992). Other investigations into adipocyte RMP utilised Rb^+ distribution ratio and voltage-sensitive dyes also provided varied RMP values (Davis et al., 1981, Cheng et al., 1980). No investigations into adipocyte RMP within the literature have utilised the whole-cell or

perforated patch clamp techniques, which are reported to be less damaging to the cell membrane and thus better suited to the maintenance of the intracellular ionic mileau (see Section 2.5.4.3).

To date, studies utilising singe-channel patch clamp and molecular biological methods, such as RT-PCR and Western Blot, have indicated that isolated adipocytes of rat and human origin contain voltage-gated potassium channels of the delayed rectifier type. Channel properties were reported to be similar between both species indicative that it could be the same K_v channel, (which had suggested involvement in the regulation of Vm) in adipose tissue from both species.

Hormones influencing adipocyte metabolic activity have been reported to influence transmembrane ionic gradient and membrane potential (Ramirez-Ponce et al., 1991). Insulin and noradrenaline have been shown to modify the resting membrane potential of the white fat adipocyte. Insulin is reported to hyperpolarise adipocyte RMP (Ramirez-Ponce et al., 1991, Beigelman and Hollander, 1962). The extent of insulin's hyperpolarising effect was found to be more pronounced in adipocytes sourced from younger lighter rats (<330g), although RMP of adipocytes from older heavier rats >330g was also modulated by insulin (Beigelman and Hollander, 1963). The effects of insulin are reversible. Conversely catecholamines reversibly depolarise the plasma membrane of adipocytes (Ramirez-Ponce et al., 1991). In contrast to the hyperpolarisation by catecholamines reported in mouse skeletal muscle (Zemkova et al., 1985), and rat mesenteric artery (Goto et al., 2000).

Changes in intracellular cAMP levels via adenylate cyclase (activation/inactivation) are also suggested to be a consequence of the

hormones modulation of membrane properties. Insulin also exerts its inhibitory effect upon lipolysis by activation of G_i proteins which are implicated in Ca^{2+} dependent K^+ channel regulation and in the regulation of inwardly rectifying K^+ channels (Lishko et al.) (Karschin, 1999). Although K_{IR} channels have not yet been confirmed on the plasma membrane of primary adipocytes, small inward currents K^+ have been determined in 3T3-L1s (Straub et al., 2011) 3T3-L1s are also reported to undergo lipolysis (Zhou et al., 2011). G_i proteins inhibit adenylate cyclase and therefore attenuate cAMP accumulation. Thus, evidence indicates that insulin has the potential to alter membrane properties via modulation of either the K^+ channel directly, or indirectly via action upon regulators of this channel type. More insight can be gained in the effects of catecholamines in white adipocytes by looking at brown adipocytes.

As with white fat adipocytes, catecholamines are known to depolarise the brown adipocyte plasma membrane. β-adrenergic stimulation of brown adipocytes by noradrenaline results in elevated intracellular cAMP. cAMP can modulate a variety ionic currents in other cell types, however this is predominantly via the inactivation of K^+ channels and removal of the outwards K^+ gradient. However membrane input resistance in brown fat cells decreased following noradrenaline stimulation and depolarisation, indicative of an increase in channel activity (Horwitz et al., 1969).

2.3 Resting membrane potential

The basis for the resting membrane potential (RMP) are the permeabilities and the equilibrium potentials for the major ion species involved in RMP, typically K^+, Na^+ and Cl^- ions. Physiologically, the cellular permeabilities to K^+ and Cl^- are high, thus the resting membrane potential of many cells, (see Table 2.1) is close to the equilibrium potential of Cl^- and K^+ ions. Table 2.2 shows the ionic concentrations and equilibrium potentials as calculated for each ion involved in RMP in a typical mammalian cell. The equilibrium potential for any particular ion is given by the Nernst equation (see Equation 2.1).

Ion	Ion concentration in plasma (mM)	Ion concentration in cytoplasm (mM)	Reversal Potential (mV)
Na^+	145	12	+67
K^+	4	140	-95
Cl^-	115	4	-90

Table 2.1. Ionic concentrations and Nernst Potentials in a typical mammalian cell as determined at 20°C, taken from Stanfield (1996). The values presented here should be taken as a rough guideline as every cell type is different and ion concentration and permeability for any given cell varies depending upon cellular physiological status.

However as shown in Table 2.2 not all RMPs are close to that of K^+ or Cl^-. In the physiological situation where multiple ion gradients control the resting membrane potential of the cell, the equilibrium potential of the cell (Nernst potential) depends on the relative permeability of the ions. Ion permeability is dependent on the ion's size and mobility, and also the activity of membrane ion channels for that ion. It is the membrane permeability of the cell to other ions such as Na^+ and Cl^- that prevent the cell interior reaching the Nernst potential for K^+ (Wright, 2004).

Tissue/Cell	Membrane Potential (mV)	Major ion involved in membrane potential	References
Pancreatic Beta cell	-62	K^+	(Manning Fox et al., 2006)
Bovine pulmonary artery endotheilial cells	Range from -88mV and 5mV with a mean of -26±3mV	K^+, Cl^- and Na^+	(Voets et al., 1996)
Rabbit articular chondrocytes	-42	Cl^-	(Tsuga et al., 2002)
The red blood cell	-8	Cl^-	(Jay and Burton, 1969)
Neuron	-60	K^+	(Doan and Kunze, 1999)
Skeletal muscle	-95	K^+	(Hille, 2001)
Smooth muscle	-50	K^+	(Hille, 2001)
Astrocyte	-80	K^+	(McKhann et al., 1997)
Adipocyte	~-30	Unconfirmed	(Ramirez-Ponce et al., 1990)

Table 2.2. Resting membrane potentials of various cell types.

Drugs and hormones can affect ion permeabilities and therefore membrane potential by multiple mechanisms, including reduction in the number of ion channels, closure of ion channels, and altered exchanger activity. For example, insulin is reported to affect ion permeabilities in skeletal muscle resulting in membrane hyperpolarisation. Application of insulin caused the rate of active Na^+ /K^+ exchange in skeletal muscle to increase by 60-120%, resulting in a decrease in $[Na^+]_i$ leading to membrane hyperpolarisation (Clausen, 1996).

A $$E_{ion} = \frac{RT}{Zf} \ln \frac{[ion]_o}{[ion]_i}$$

B $$E_{ion} = -60 \log_{10} \frac{[Cl]_o}{[Cl]_i}$$

Equation 2.0-1. The Nernst equation. E= equilibrium potential for the ion under consideration, R= the universal gas constant (8.31j mol^{-1} K^{-1}), Z= the oxidation state of the ion under consideration, T=temperature in Kelvin. $[ion]_o$ and $[ion]_i$ represent extracellular and intracellular ion concentrations. The Nernst equation can be simplified and represented as equation B, at room temperature.

$$Vm = -\frac{-RT}{F} \ln \frac{PK[K]in + PNa[Na]in + PCl[Cl]out}{PK[K]out + PNa[Na]out + PCl[Cl]in}$$

Equation 2.0-2. The Goldman-Hodgkin-Katz equation. Vm is the potential difference that exists across the plasma membrane of the cell. , R= the universal gas constant (8.31j mol^{-1} K^{-1}), Z= the oxidation state of the ion under consideration, T=temperature in Kelvin. P is the relative permeability of the ion given in cm/s.

2.3.1 K^+ channels regulate resting membrane potential

Resting membrane potential is an important ubiquitous property of all cells. K^+ channels stabilise the resting membrane potential of both excitable and non excitable cell types (Sanguinetti and Spector, 1997, Chilton et al., 2005). Generally, transmembrane K^+ -selective leak channels allow the diffusion of K^+ ions down the concentration gradient (the K^+ concentration gradient is established by the activity of ATPases). This creates a charge separation and also a voltage across the membrane. Other examples of K^+ channels involved in the generation of resting membrane potential are discussed briefly heirn. Delayed rectifier K^+ channels set RMP in feline smooth muscle. Opening of the ATP sensitive K^+ channel (K_{ATP}) contributes to RMP in large, cultured primary rat neurons (Kawano et al., 2009), and in pancreatic β-cells. In excitable cells, K^+ channels regulate RMP during the quiescent period between action potentials,

and also govern the return of membrane potential back to the resting state. In cell types expressing outwardly rectifying K^+ channels, K^+ channel closure results in depolarisation of the plasma membrane and subsequent cell specific activity, such as the secretion of insulin from pancreatic β-cells or muscle contraction. Generally, activation of K^+ channels (K_v and K_{ATP}) resulting in an increase in outward K^+ permeability results in a shift in the transmembrane potential towards the Nernst potential for K^+, i.e. membrane hyperpolarisation. K^+ channel regulators such as G proteins (Yamada et al., 1998), and intracellular ATP, (Terzic et al., 1995) can alter channel properties such as subunit assembly, conductance, activation and inactivation. Consequences of such modulation can result in membrane potential changes, or altered intracellular ionic activity due to the induction of voltage-gated ion channel conductance arising from the activation of other voltage-regulated channels that are permeable to other ions.

A large number of genes encode channel subunits, giving rise to a very diverse range of K^+ channel subtypes (Coetzee et al., 1999). The number of K^+ channel phenotypes is even greater. The functional diversity of K^+ channels is extended due to additional processes such as alternative splicing, post-translational modification and the heterologous assembly of pore-forming subunits. This diversity is attenuated by K^+ channel interactions between accessory subunits or regulatory proteins. As the multitude of K^+ channels is vast and beyond the scope of this brief introduction see (Miller, 2000) for a brief and generalised summary of K^+ channels and their characteristics.

2.4 Experimental aims

To date information pertaining to the Vm of adipocytes is limited, additionally the ion species that determine adipocyte Vm are unknown. In this chapter I aim to measure adipocyte Vm and determine the ion conductances that underlie this. Since insulin and β-adrenoceptors are key regulators of adipocyte function I also aim to explore their effect on adipocyte Vm.

2.5 Methods

2.5.1 3T3-L1 adipocyte culture

Cells in culture were kept at 37°C in a humidified atmosphere of 5% CO_2/ 95% air. 3T3-L1 fibroblasts were cultured in maintenance medium comprising Dulbecco's Modified Eagle Medium (DMEM, Sigma D5671) supplemented with Newborn Calf Serum (NCS Sigma N4637, 10% (v/v)), antibiotic/anitmycotic mix (Sigma A5955, 5 ml/500 ml medium), gentamycin (Sigma G1272, 2.5 ml/500 ml medium) and L-glutamine. The 3T3-L1 fibroblasts were grown to 60% confluence in T75 flasks prior to trypsinisation with trypsin and subcultured at a 1:3 split twice a week. To prevent the occurrence of spontaneous differentiation of the 3T3-L1 fibroblasts all maintenance flasks were regularly checked and subcultured at 50-60% confluence (Green and Meuth, 1974).

3T3-L1 fibroblasts intended for differentiation to 3T3-L1 adipocytes seeded in 35mm culture dishes (Corning) and were grown to confluency. Two days post confluency differentiation of the 3T3-L1 fibroblasts was initiated using a series of DMEM based media comprising of 3T3-L1 fibroblast maintenance medium, with foetal calf serum instead of newborn calf serum, with supplementation of porcine insulin (Sigma I5523, 1mg/ml stock in dH_2O:acetic acid (100:1) 200 µl/ 200 ml), IBMX (Sigma I-7018, 0.5 mM), dexamethasone (Sigma D1756, 0.25 µM).

Substitution of the fibroblast maintenance medium for differentiation medium occurred on 'day 0', and was left for 48 hours. On day 2 the medium was exchanged for differentiation medium, excluding dexamethasone and IBMX. Cells were kept in this for a further period of 48 hours, days 2-4. On day 4 this medium was removed and replaced with differentiation medium with the

exclusion of insulin, IBMX and dexamethasone. At this stage, differentiation is apparent as the cells lose their fibroblastic appearance and adopt a round, adipocyte like morphology. During the early stages of differentiation the cells contain multiple small fat droplets. As differentiation progresses the multiple droplets coalesce into a singular large droplet and the cells become macroscopic. The 3T3-L1s were used when the majority of cells in a dish were observed at a later stage of differentiation. The medium was changed every 48 hours. The cells were used within 5 days.

2.5.2 3T3-L1 Oil Red O hematoxylin counter stain

To confirm the presence and accumulation of lipid droplets following cell differentiation, dishes of cells were taken for Oil Red O and hematoxylin counter staining. Oil Red O is a fat soluble dye commonly used for the staining of triglycerides and neutral lipids (Ramirez-Zacarias et al., 1992, Sung et al.).

Tissue culture dishes containing cultures were gently rinsed with 2mls sterile Dulbecco's phosphate-buffered saline (DPBS) (pre-warmed to 37^{o}C so as not to shock the cells). Following aspiration of the DPBS, each culture dish was incubated in 2ml 10% (v/v) formalin in dH_2O for 30 minutes.

Stock solution of Oil Red O (300mg Oil Red O in 100mls 99% (v/v) isopropanol was used to prepare a working solution. Three parts Oil Red O stock (30ml) were mixed with two parts (20ml) dH_2O. This was allowed to sit for ten minutes and filtered prior to use.

Following formalin incubation, and each plate rinsed in 2 ml sterile dH_2O, and then incubated in 2ml of 60% (v/v) isopropanol for 5 minutes. The isopropanol was poured away and 2 ml of Oil Red O working solution was added and left to stand at room temperature for 5 minutes. Warm tap water, applied using a

pipette, was used to rinse each dish multiple times over until the water ran clear. To visualise the cells nuclei, each plate was counter-stained with hematoxylin (Jensen et al., 2004). Each dish was incubated for 1 minute in 2ml hematoxylin (stock solution composition 5g hemotoxylin, 50ml absolute ethanol, 100g ammonium sulphate, 100ml dH_2O, 30g sodium iodate; Working solution composition: 100ml filtered stock solution and 4ml glacial acetic acid), and rinsed with warm water as described above. To maintain staining, dishes were kept wet with water. Cells were observed and images taken using a phase contrast microscope at x10 magnification.

2.5.3 Rhodamine 123 staining of primary adipocytes

Within suspensions of primary adipocyte preparations, both adipocytes and fat droplets (as a result of lipolysis) are present. The adipocyte nucleus nub was used as a morphological indicator to distinguish between adipocytes and fat droplets. If the nucleus nub of a primary adipocyte is attached in the "face down" orientation to the glass cover slip, (plating is described in Chapter 3, Section 3.9.2) it can be difficult to distinguish a primary adipocyte from a lipid droplet. To improve the likelihood of patching a mature adipocyte it is necessary to visualise them; to facilitate this, intact cells can be loaded with lipophillic dyes. For this purpose Rhodamine 123 was chosen.

The adipocytes were loaded with 10-20µg/ml Rhodamine 123 in Ca^{2+} Hank's buffer. Rhodamine 123 was prepared from a 2mg/ml stock solution in DMSO. The adipocytes were loaded with dye for 5 minutes in the dark at 22^{o}C and then visualised under a fluorescent microscope. Cells were illuminated with an excitation wavelength of 450-490nm. Emitted light was filtered using a long-pass barrier filter at 510nm (Karl Zeiss filter set 10 488010-9901-000). The

emitted light was detected using a photonics ISIS camera. A typical view of a group of adipocytes stained with rhodamine 123 is shown in Figure 2.2. Of the five adipocytes present in the image, the protruding nucleus is only visible in two of the adipocytes shown; without the presence of rhodamine 123, it would have been difficult to distinguish the other adipocytes from fat droplets. No fat droplets are seen within this image.

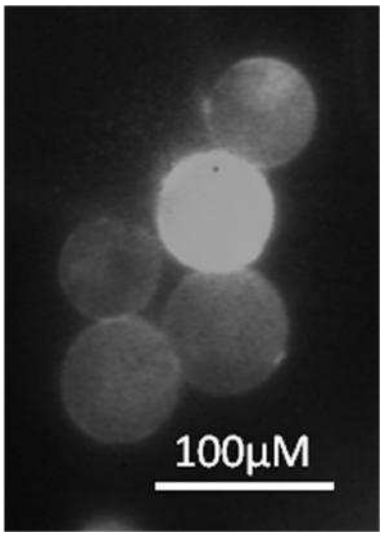

Figure 2.2. A fluorescent image of primary adipocytes loaded with 10-20µg of Rhodamine 123, viewed at X20. The grey / white colouration is indicative of the presence of the Rhodamine 123 within the adipocyte. Fat droplets fail to fluoresce and are not visible following fluorescent illumination.

2.5.4 Patch clamp

2.5.4.1 Patch clamp pipettes (perforated patch)

Patch clamp pipettes were pulled from thin-walled borosilicate capillaries (GC150TF, Harvard apparatus) using a two-stage vertical pipette puller (Narishige, Japan). The diameter of the patch pipette tip of each batch of pipettes pulled was assessed using the bubble number method. Patch clamp pipettes with bubble numbers of 7 were used. The tips of the patch pipettes

were coated close to their tips with Sylgard (Dow Corning Corp) to reduce their electrical capacitance. (Sakmann, 2009). The pipettes were fire-polished before use. Pipette resistances were typically between 2.5 and 5MΩ.

Pipettes were assembled in a standard polycarbonate pipette holder. Electrical coupling was provided by using an Ag/AgCl wire. The adipocytes were washed with Hank's solution prior to observation. A coarse, three-way, mechanical manipulator was used to bring the pipette close to the cell, such that both the pipette and the cell could be visualised within the same field. A fine three-way hydraulic micromanipulator was used to position the tip of the pipette onto the cell.

The bath was electrically grounded via a salt bridge comprising 150mM KCl in 2% (v/v) agar. On contact with the batch solution, the pipette current was adjusted to zero by application of an offset voltage. The offset voltage was taken as the zero reference potential for all experimental measurements. Posteriori corrections were made for liquid junction potentials, these are discussed in Chapter 4, Section 4.3.3.

Membrane voltages (perforated patch) and membrane currents (cell-attached patch) were recorded using an Axopatch-1D patch clamp amplifier (Axon instruments).

2.5.4.2 Microscope set up

The 35mm dishes containing 3T3-L1 cells were mounted directly onto the stage of the inverted microscope. To reduce the volume of the petri dishes, and permit a more rapid solution change, a perspex insert was used. The volume of the

dish was reduced from 2.5ml to 500µl. With the insert, complete solution changeover could occur within 60 seconds. Primary adipocytes were attached to a glass coverslip as described in Chapter 3, Section 3.9.2. To image these cells prior to patching, a bespoke perspex chamber was used with a glass floor. Again, solutions could be changed within 60 seconds.

To perifuse the microscope chamber, solutions were gravity fed, through polythene tubing, all drug additions were made via bath perifusion. Solutions were removed via aspiration by a vacuum pump. To exchange the perifusion solutions electrically controlled two-way valves were utilised. Solutions were warmed to the desired temperature by passing through a heated electrical resistor that was controlled by a feedback circuit (designed by Dr P.A. Smith). A thermocouple was used to monitor and set the temperature of the perifusion solution.

To form a seal, the microelectrode was gently brought to the surface of the cell until contact was made, gentle suction was applied as necessary by application of negative pressure via a syringe connected to the pipette holder by polythene tubing. Seal formation was monitored by applying short positive voltage pulses to the cell membrane. Contact with the cell and seal formation is indicated by a reduction in the test pulse current response, indicative of increased resistance at the pipette tip, caused by occlusion of the pipette tip by the cell. Seals >20GΩ were considered acceptable. Following gigaseal formation, the appropriate patch clamp configuration was carried out.

2.5.4.3 The perforated patch, whole-cell configuration of the patch clamp technique.

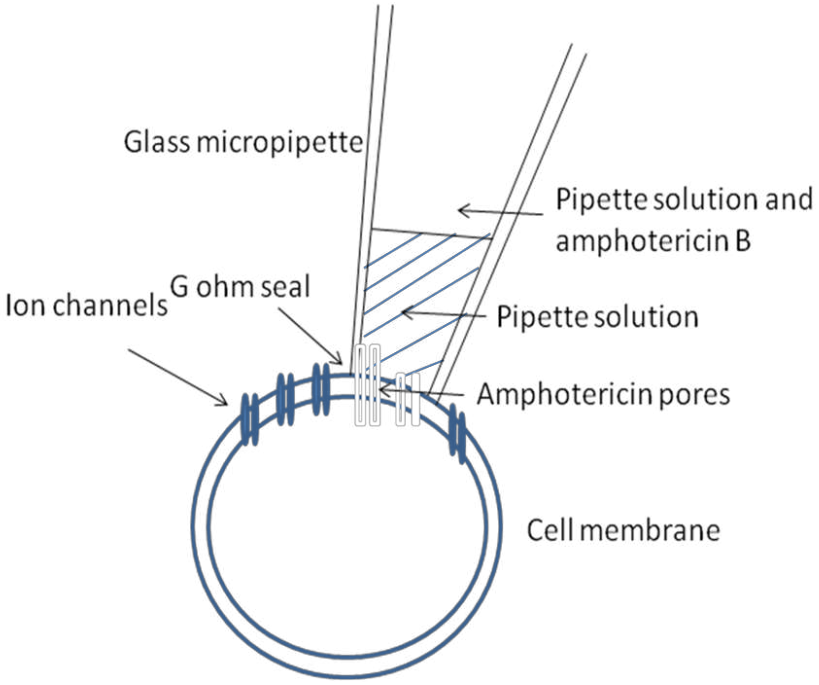

Figure 2.3. The formation of the perforated patch, patch-clamp configuration. In this configuration, amphotericin B, a pore forming antibiotic is added to the pipette solution and this is back filled. The pipette tip does not contain amphotericin. The amphotericin B migrates to the pipette tip and incorporates with the membrane patch. A low resistance pathway formed between the interior of the cell and the patch pipette. Adapted from (Molleman, 2003).

Resting membrane potentials were recorded from primary epididymal white fat adipocytes and 3T3-L1 adipocytes using a variant of the whole-cell patch clamp technique, the perforated patch configuration. The perforated patch technique is shown in Figure 2.3. The advantage of this method is that the patch of the cell membrane is not disrupted, and as the pores produced by amphotericin are permeable to monovalent cations only, anions and multivalent ions do not permeate through the pores due to the absence of dialysis. Moreover, intracellular constituents and signalling molecules essential for normal cell function are not exchanged with the pipette solution. The maintenance of the intracellular milleu in this configuration also prevents channel run-down, giving

this configuration a distinct advantage over the traditional whole-cell patch configuration (Carrier, 1995).

Membrane voltages were recorded using an Axopatch 1D patch clamp amplifier (Axon instruments) at both room temperature (22^{o}C) and at 32^{o}C. The pipette solution comprised (in mM) 76K_2SO_4, 10KCl, 10NaCl, 10 HEPES. The solution was adjusted to pH 7.4 with NaOH. A stock solution of amphotericin B in DMSO (50mg/ml) was prepared, protected from exposure to light and stored at -20^{0}C for a period of one week. To induce perforation of the adipocyte cell membrane, 0.1 µg/ml of amphotericin B was applied to the pipette filling solution. The tip of the patch pipette was filled with amphotericin B free solution by capillary action, and the remainder of the pipette 'back-filled' with amphotericin B containing solution. Normal Hank's solution (see Appendicies) was perifused in the bath containing adipocytes during seal formation. This was to reduce amphotericin B build-up at the tip of the pipette and subsequently improve the likelihood of obtaining a high resistance seal in the cell-attached configuration before perforation of the adipocyte cell membrane occurred. Following the formation of the high resistance seal, the holding potential of the pipette tip was set at -30mV. Test pulses of 0.2mV were repetitively applied to monitor changes in the access resistance. As the amphotericin B diffused to the pipette tip and incorporated with the membrane patch, it resulted in subsequent perforation of the adipocyte membrane. The resistance of the patch decreased and cell capacitive currents in the form of capacity current transients appeared. When the whole-cell configuration was ascertained as determined by the development of capacitance transients (Figure 2.4), the capacitive transients were compensated, the current clamp applied and the membrane potential measured.

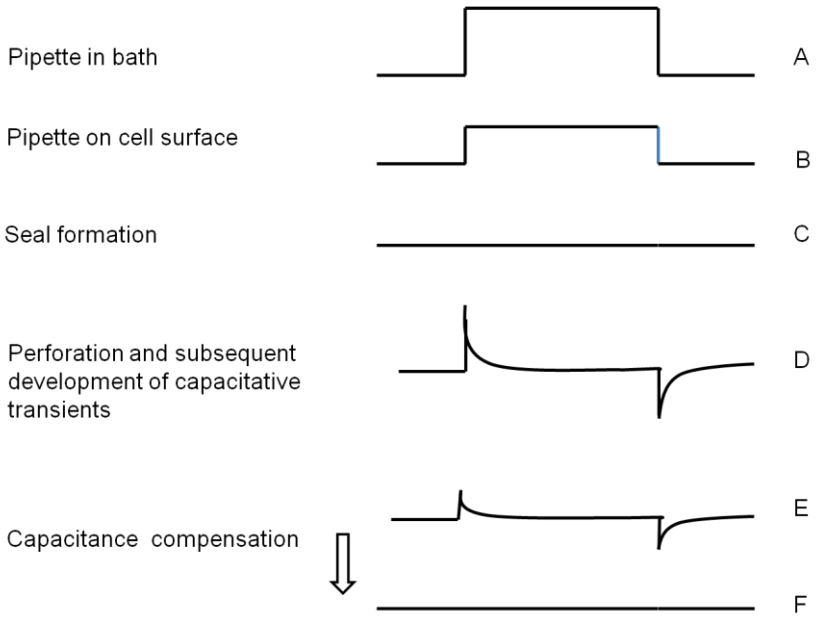

Figure 2.4. Seal formation with subsequent development of capacitance transients as observed during establishment of a perforated patch protocol. (A) Current response as the pipette is immersed in the bath solution. (B) Increase in resistance at the pipette tip as it makes contact with the cell surface as manifest by a reduction in current response. (C) Gigaseal formation. (D) Development of the capacitive transients as access resistance decreases during perforation. (E & F) Compensation for the capacitive transient.

One of the limitations of the perforated patch configuration is that the voltage of the pipette is not necessarily the same as the voltage of the clamped cell membrane. Such an error is introduced by a high series access resistance can be problematic, (series resistance arises as a result of anything in series with the cell such as the patch pipette; perforation; clogging of the pipette tip).

The series resistance and membrane resistance acts as a voltage divider to all imposed voltages. Voltage error is at a minimum in instances when the series resistance is small in comparison to the membrane resistance. Typically, series resistance has to be two orders of magnitude smaller than the membrane resistance to keep the voltage error low.

The mean series resistance of the 3T3-L1 adipocytes was 32±1MΩ and the mean capacitance was 15.6±13.9pF (n=100) as determined by electronic capacitance compensation. The capacitance of the primary adipocytes could not be compensated, as the cells were too large. The mean diameter of the primary adipocytes was 78.18μM±0.5 (n=634). The diameter of the differentiated 3T3-L1s was not measured.

Ccell=specific capacitance X cell area

Ccell=1Fcm^{-2} x Area(cm^2)

2.5.4.4 Measurement of RMP

For this, the P-clamp amplifier was used in current clamp mode (Figure 2.5). In current clamp mode, the patch clamp amplifier 'measures' Vm of the cell by varying the voltage command to maintain a constant current, I_{out}, of zero.

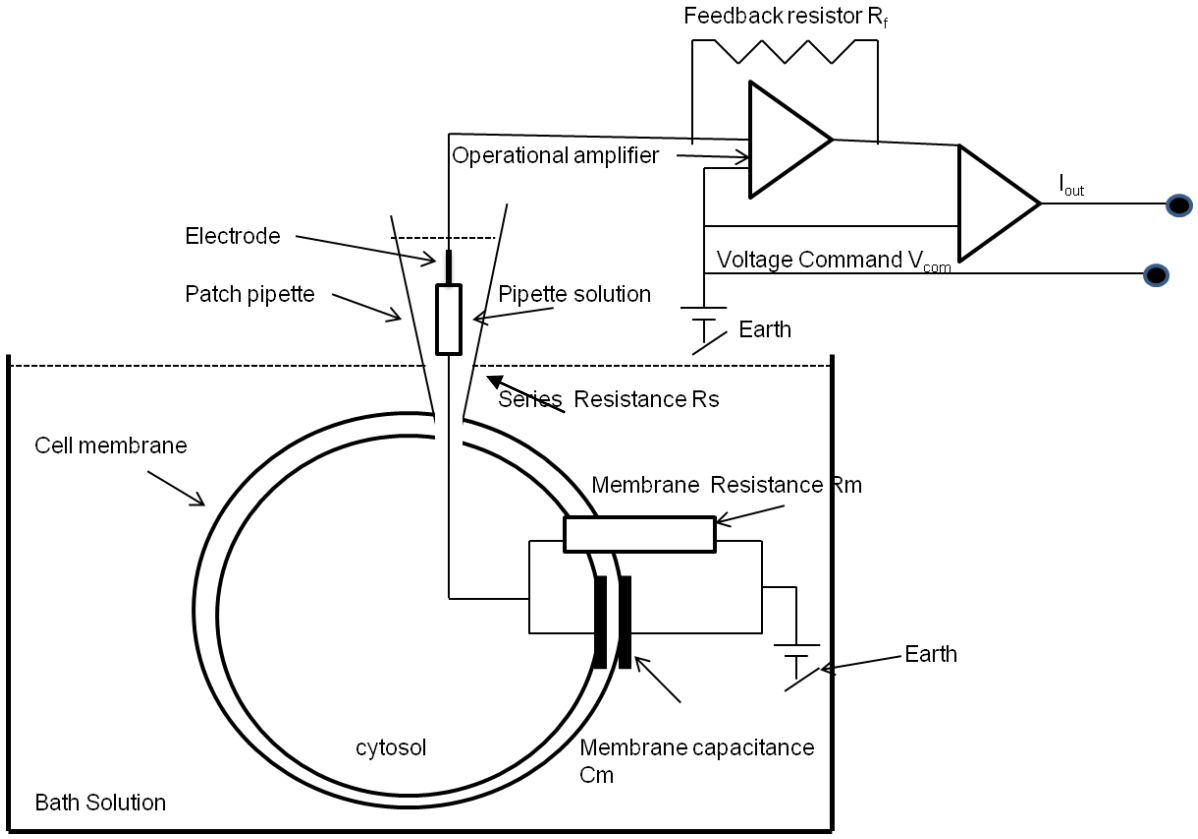

Figure 2.5. A simplified diagram of the perforated patch circuit and patch clamp amplifier. R_f: feedback resistor, V_{com}: command voltage, V_{pip}: pipette potential, I_{out}: output current.

2.5.4.5 Prediction of $[ion]_i$

The Nernst equation can be transformed to give $[ion]_i$ on the basis of known membrane potential responses (as observed experimentally) to a given extracellular ion concentration. The Nernst equation was used to predict values for adipocyte $[K^+]_i$, $[Na^+]_i$ and $[Cl^-]_i$.

A $$E_{ion} = -60 \log_{10} \frac{[Cl]_o}{[Cl]_i}$$

B $$10\left(\left(\frac{ECl}{60}\right) + Log_{10}[Cl]_o\right) = [Cl]_i$$

Equation 2.3. The Nernst equation (A). (B) is the Nernst equation, fully transformed to give an estimate of $[Cl^-]_i$.

2.5.4.6 Input resistance measurements

Plasma membrane input resistances for primary and 3T3-L1 adipocytes in both 138mM Cl^- and 5mM Cl^- bath solutions were calculated by measuring the changes in membrane potential during the application of current pulses. The calculation used to determine input resistance is shown in Equation 2.4.

$$Input\ Resistance = \frac{Change\ in\ V}{Change\ in\ I}$$

Equation 2.4. The calculation used to determine input resistance. V=voltage, *I*=current.

2.5.4.7 Statistical analysis

Membrane potential data are expressed as box and whisker representations showing the median Vm, the 25 and 75% confidence intervals and the

maximum and minimum membrane potential values observed for each cell type. Statistical analysis was performed using Graphpad PRISM version 5 (graphpad software, San Diego, California USA). All statistics are expressed as described within each figure legend.

2.5.5 Microscopic demonstration of differentiated 3T3-L1 adipocytes

To confirm 3T3-fibroblast differentiation into 3T3-L1 adipocytes, lipid accumulation was monitored by staining with Oil Red O, throughout the differentiation process.

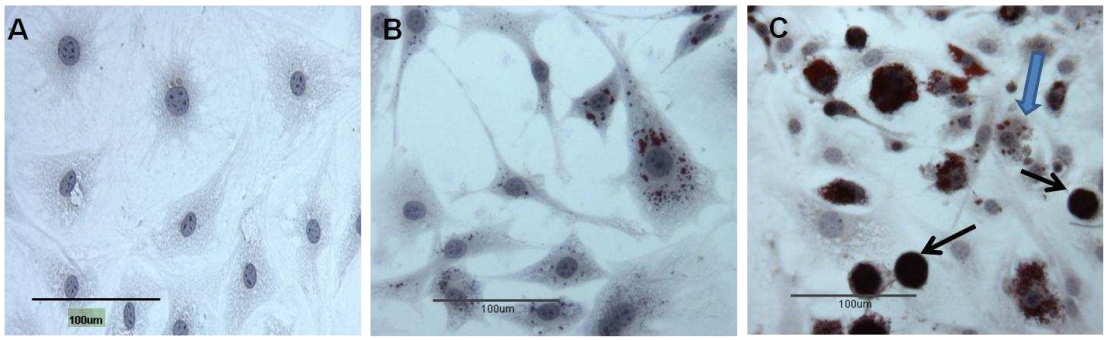

Figure 2.6. Oil Red O stain with the haematoxylin counter stain. All images are at X20 mag. Image A shows 3T3 fibroblasts prior to the induction of differentiation. Image B was taken 96 hours (day 4) into the differentiation process, image C shows a heterogeneous population of 3T3 fibroblasts and 3T3-L1 adipocytes following completion of the differentiation protocol. Adipocytes selected for patching are shown by arrows. 3T3-L1 adipocytes were stained at passage 15.

The differentiation of 3T3-L1 fibroblasts to adipocytes is characterised by the accumulation of lipid droplets, which is visible in some cells by the presence of red stain (Figure 2.6C). As the cells accumulate lipid, they become less flat and adopt a rounded shape. 3T3-L1 fibroblasts at an intermediate stage of differentiation show multiple lipid droplets and a centralised nucleus. Fully-differentiated 3T3-L1 adipocytes are spherical in shape and contain a coalesced fat droplet, (as indicated by the blue arrow (Figure 2.6C)). Some cells within the population failed to differentiate. The presence of non-

differentiated cells within the differentiated population of adipocytes is due to the proliferation of fibroblasts that have lost their capacity to differentiate (Green and Meuth, 1974). Figure 2.7 illustrates the typical patch clamp arrangement for both primary (Figure 2.7A) and 3T3-L1 (Figure 2.7B) adipocytes.

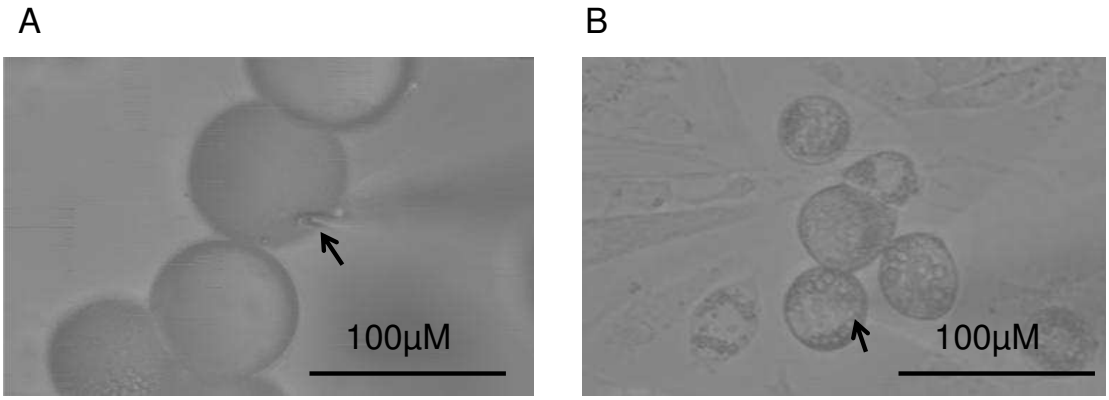

Figure 2.7. A typical image of a group of A) primary adipocytes and B) differentiated 3T3-L1 adipocytes. Cells were viewed at x20 under an air objective lens. The shadow of the cell-attached patch pipette is highlighted with an arrow in both cases. In B, the adipocyte chosen for study was spherical in shape indicative of the cell being in a late stage of differentiation. In B, there are cells at various stages of the differentiation process, cells at an intermediate stage of differentiation have multiple fat droplets as in Figure 2.7C. Cells that have not differentiated are visible in the background (flattened fibroblasts).

2.5.6 Ionic basis of adipocyte resting membrane potential

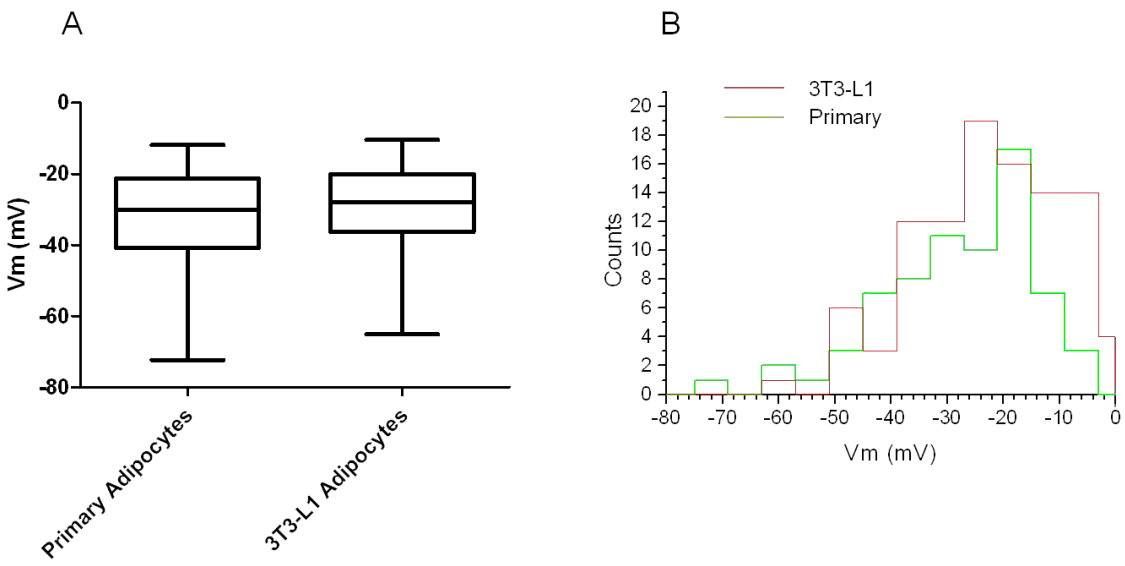

Figure 2.8. Comparison of the data spread of RMPs. (A) and distribution of RMPs (B) of primary adipocytes (n-68) and 3T3-L1 adipocytes (n=88). In (A) the data are shown as Median ± 25% and 75% confidence intervals, with the maximum and minimum values for data shown.

Figure 2.8 shows the distribution of membrane potentials of primary white fat adipocytes and differentiated 3T3-L1 adipocytes, measured in the absence of insulin with the perforated patch clamp configuration.

The median resting membrane potentials of the primary adipocytes and the differentiated 3T3-L1s were not significantly different (Mann-Whitney, $P>0.05$). Figure 2.8A, with a similar distribution of values Figure 2.8B. These data suggest that the two adipocyte models used in this study may have similar ionic mechanisms of resting membrane potential.

The lab has extensive experience with the use of mouse islet β-cells. Islets were prepared and supplied by Dr P.A Smith. To confirm the accuracy and validity of the perforated patch clamp technique used in this study, the membrane potential of the mouse islet β-cells was measured in the absence of glucose, in both 5.6mM and "elevated" 50mM extracellular K^+ (Figure 2.9).

The mean series resistance and cell capacitance were 32.9±1MΩ and 12.6±4.4pF respectively (n=8).

The concentration of extracellular K^+ was altered by equimolar substitution of bath Na^+. In physiological $[K^+]_o$ (5.6mM), the Vm of the β-cell was ~-71mV (n=8), which was significantly depolarised to ~-21mV in elevated (50mM) $[K^+]_o$ (Friedman's, P<0.001) Figure 2.9.

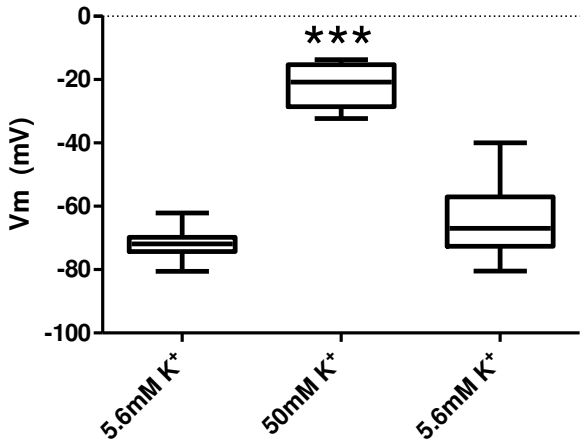

Figure 2.9 Membrane potential of primary mouse beta cells. Membrane potentials were measured in the absence of glucose in 5.6mM K^+ (control), in 50mM K^+ and then recovery in 5.6mM (n=8) . ***.P<0.001 (Friedman's).

I assume the mouse beta cells possess $[K^+]_i$ of 140mM, and $[Na^+]_i$ of 10mM as per a generic cell, (see Table 2.2). On the basis of the membrane potential responses observed experimentally (Figure 2.9) the GHK equation (Equation 2.2) was used to determine the permeability ratio of Na^+ to K^+ (assuming PCl^- is negligible) : 0.02.

Since K^+ is the major ion involved in controlling the membrane potential of most cell types (Hille, 2001), conditions of 50mM $[K^+]_o$ were applied to adipocytes to investigate the role of the K^+ ion, if any in adipocyte RMP.

If we assume that the adipocyte Vm is solely dependent on K^+, and the median adipocyte Vm in Figure 2.10 being -41mV in 5.6mM $[K^+]_o$, the predicted $[K^+]_i$ is 26mM as per the Nernst equation (Equation 2.3). On the basis of the predicted $[K^+]_i$ value, and assuming exclusive involvement of K^+ in adipocyte Vm, elevation of $[K^+]_o$ to 50mM would result in a membrane depolarisation to +17mV.

However elevation in extracellular K^+ by equimolar substitution of Na^+ with K^+ from 5.6mM to 50mM did not affect membrane potential of either primary (Figure 2.10A) or 3T3-L1 (Figure 2.10B) adipocytes. Furthermore addition of known L-type Ca^{2+} channel blocker verapamil at 20μM failed to block any voltage-gated or passive Ca^{2+} current. Addition of verapamil did not affect membrane potential in either adipocyte model.

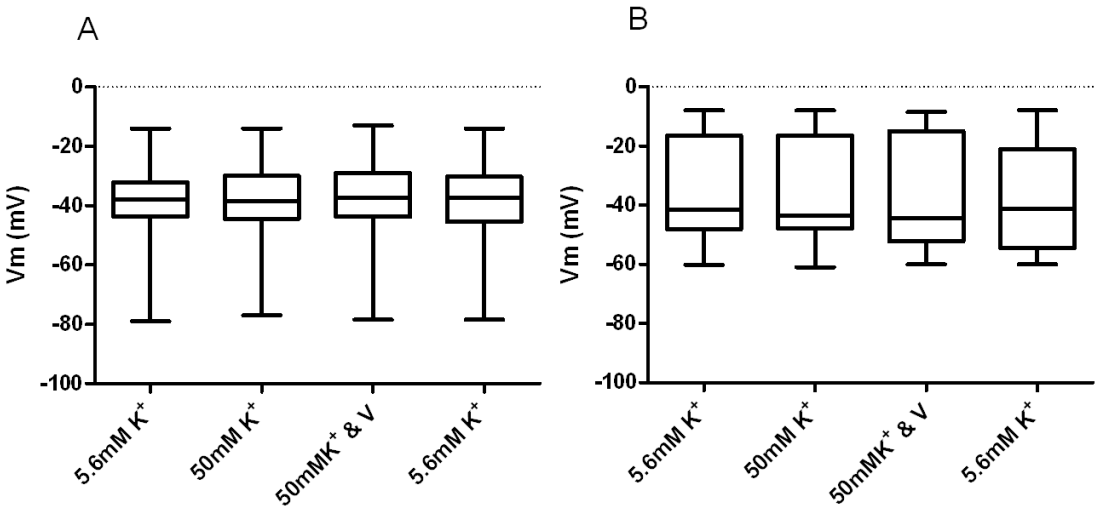

Figure 2.10. The effect of elevation of extracellular K^+ from 5.6mM to 50mM on the membrane potential in the absence and presence of 20μM verapamil (V). (A) primary adipocytes (n=8) and (B) differentiated 3T3-L1 adipocytes (n=11). (Friedman's).

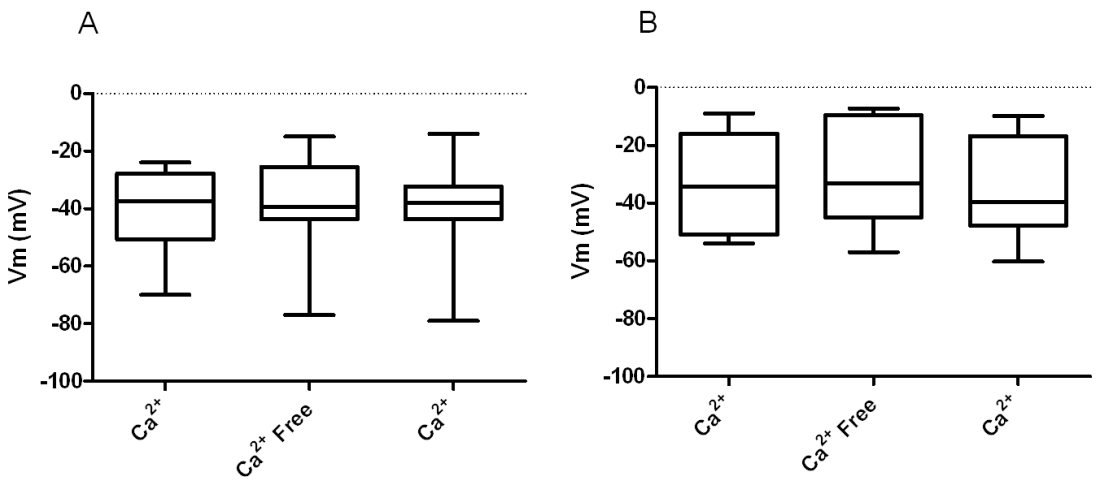

Figure 2.11. The effect on membrane potential of extracellular Ca^{2+} removal by equimolar substitution with Mg^{2+}. In (A) primary adipocytes (n=8) and (B) differentiated 3T3-L1 adipocytes (n=11) (Friedman's).

Equimolar substitution of extracellular Ca^{2+} with Mg^{2+} did not have an effect on membrane potential in either primary or differentiated 3T3-L1 adipocytes (Figure 2.11).

Since $[K^+]_o$ appeared not to be involved in controlling Vm, another ion capable of generation of a negative membrane potential was sought; the involvement of Cl^- in the generation of the resting membrane potential in both adipocyte models was explored. The effect of removal of extracellular chloride was initially explored by equimolar substitution of Cl^- with Aspartate (Asp^-).

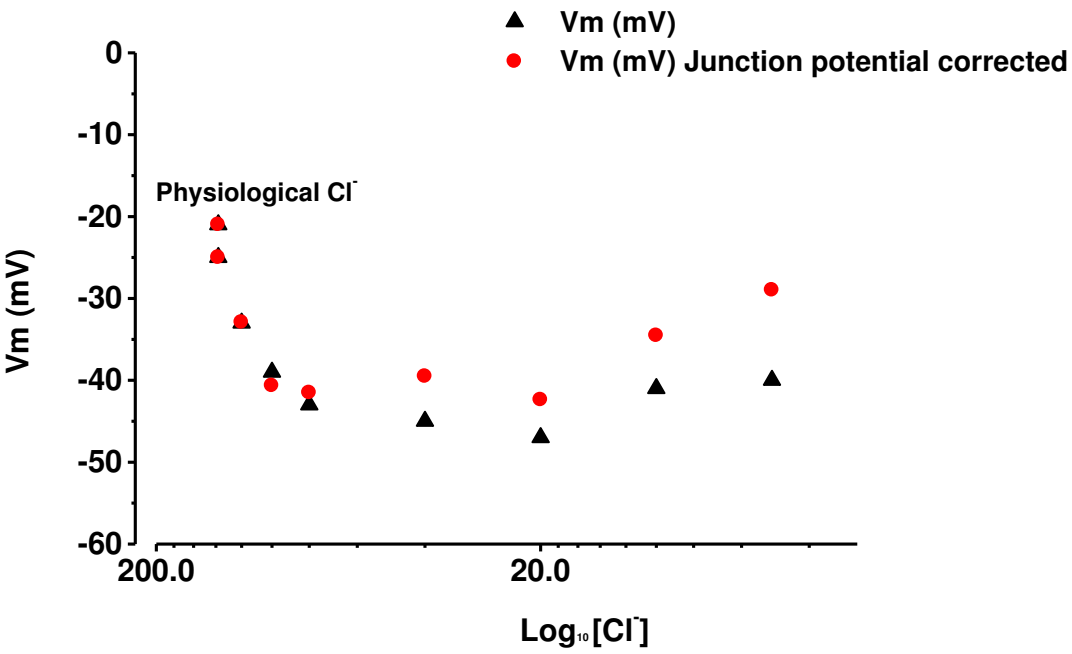

Figure 2.12. Representative trace, of the effect of perifusion of decreasing concentrations of extracellular chloride on membrane potential in the primary white adipocyte. Extracellular chloride was removed by direct equimolar substitution with sodium aspartate from 138mM extracellular chloride to 5mM extracellular chloride. Extracellular chloride substitution with aspartate caused a partially reversible hyperpolarisation of the plasma membrane in the primary adipocyte. Junction potentials were determined experimentally, and membrane potential measurements corrected. Black triangles represent raw data. Junction potential corrected membrane potentials are shown as red circles (n=5).

Incremental substitution of extracellular Cl^- from 138mM to 80mM by replacement with aspartate resulted in a concentration dependent hyperpolarisation of the primary adipocyte. (Figure 2.12). Initially Na-Aspartate was used as a substitute for extracellular chloride. It was hypothesised that the net Cl^- current would be outward resulting in depolarisation of the adipocyte plasma membrane. However, as the opposite was observed it is suspected that, aspartate was entering the adipocyte causing membrane hyperpolarisation. To test this hypothesis, another Cl^-

substitute, gluconate, was utilised and similar experiments carried out (Figure 2.13).

Having determined that the Cl^- ion is involved in the regulation of resting membrane potential in 3T3-L1 cells, the incremental substitution protocol was repeated in primary white fat adipocytes. Membrane potential values were taken after stabilization of the membrane potential value shortly following exchange of the extracellular solution. The effect of extracellular chloride removal on membrane potential recorded in 3T3-L1 and primary adipocytes was similar, with maximal depolarisation of the plasma membrane from a median of ~-30 to -40mV to a median of -7mV (Figure 2.14). Junction potentials were measured for each chloride solution tested. Junction potentials were measured as follows. The patch pipette was filled with 3M KCl solution. The pipette was immersed in the perifusion medium in 138mM Cl^- solution, with the voltage zero'd. The perifusion media was exchanged for one containing 5mM Cl^-, and the potential change (if any) was measured. Following each junction potential measurement the pipette containing 3mM KCl was changed. The voltage offset caused by the junction potential increased with every decreasing concentration of chloride, most notably from 40mM $[Cl^-]_o$ onwards. Junction potentials have been subsequently compensated in all figures depicting experimental data. Figure 2.15 illustrates a typical experiment using this protocol. The effect on membrane potential of extracellular chloride removal suggests the presence of chloride channels on the plasma membrane of both adipocytes and 3T3-L1 adipocytes. This will be discussed further in Chapter 4.

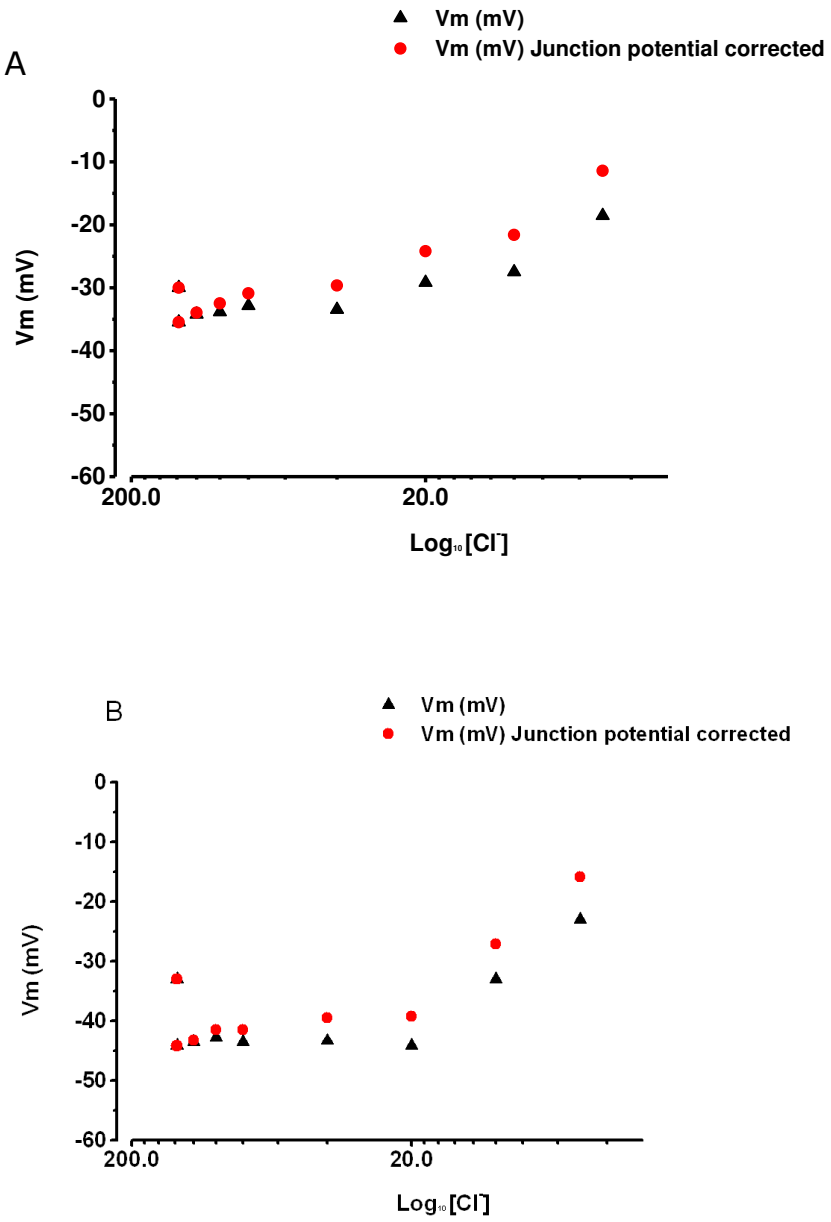

Figure 2.13. Representative traces, of the effect of decreasing concentrations of extracellular chloride on adipocyte membrane potential. Extracellular chloride removal causes a reversible depolarisation of the plasma membrane of both the primary adipocyte (A) from -35mV to –10mV, (n=9) and the 3T3-L1 adipocyte (B) from -40mV to -10mV, (n=14). Due to Cl^- ions leaving the cell, ECl^- becomes more +ve. Membrane potential measurements were corrected for junction potentials, n=9. The input resistance of the primary adipocyte (A) in 138mM extracellular Cl^- was 2.08GΩ. in 5mM extracellular Cl^- the input resistance was 0.41GΩ.

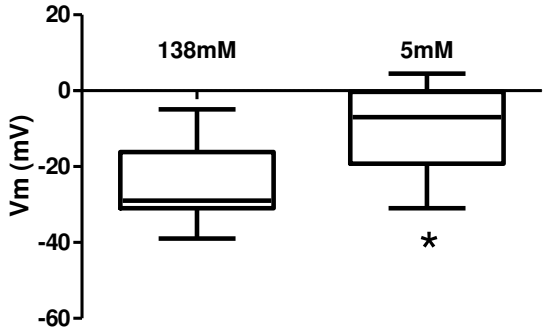

Figure 2.14. Membrane potential change of primary adipocytes in 5mM $[Cl^-]_o$. Pooled membrane potentials, as were recorded in 138mM $[Cl^-]_o$, and 5mM $[Cl^-]_o$, n=9. *P<0.05 (Friedman's).

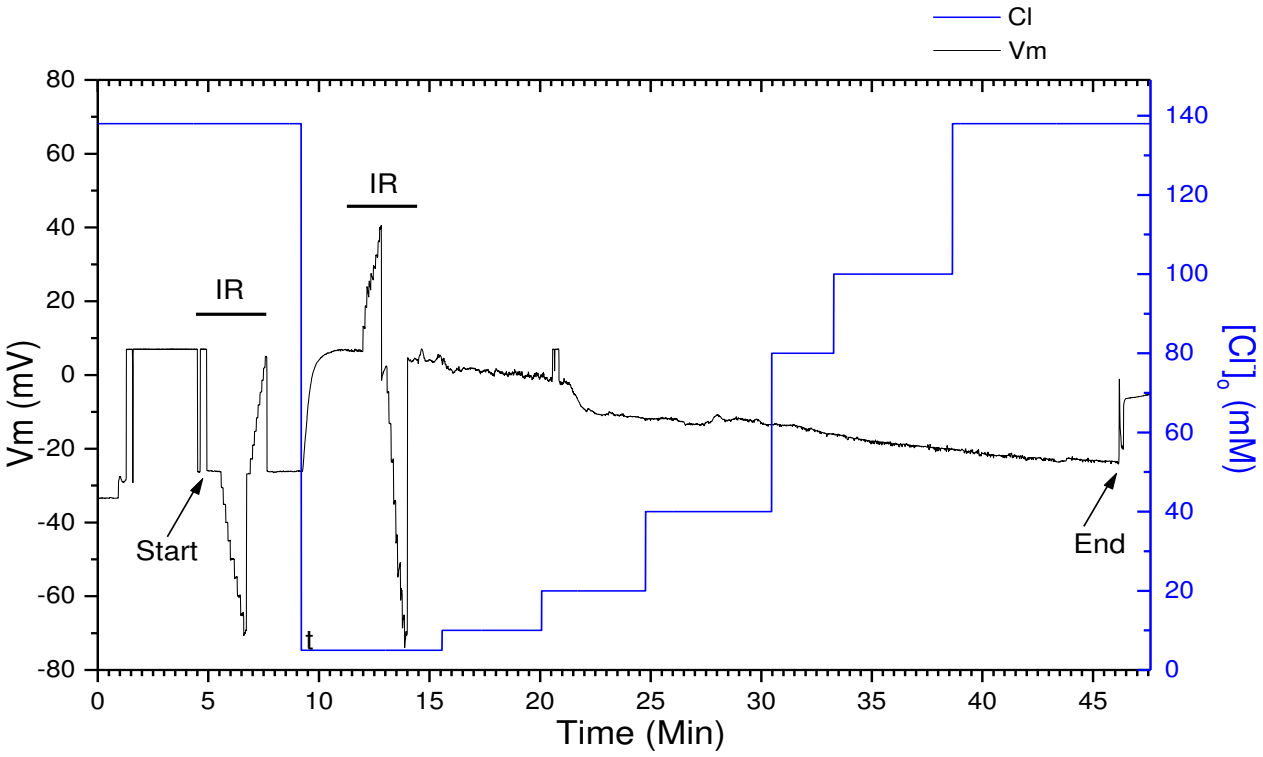

Figure 2.15. A representative trace showing the effect of removal of extracellular Cl^- by substitution with gluconate on the membrane potential of 3T3-L1 cells. The concentration of extracellular Cl^- present in the extracellular medium is represented by the blue line. The change in Vm (mV) arising as a result of buffer substitution is represented in black. The staircase changes in voltage (labelled as IR) input resistance are a result of incremental stepwise current injection from -9pA to +9pA. To measure input resistance, the slope of the voltage values obtained at each step were noted. There is no correction for junction potentials in this figure. Note recovery of Vm on return to 138mM $[Cl^-]_o$..

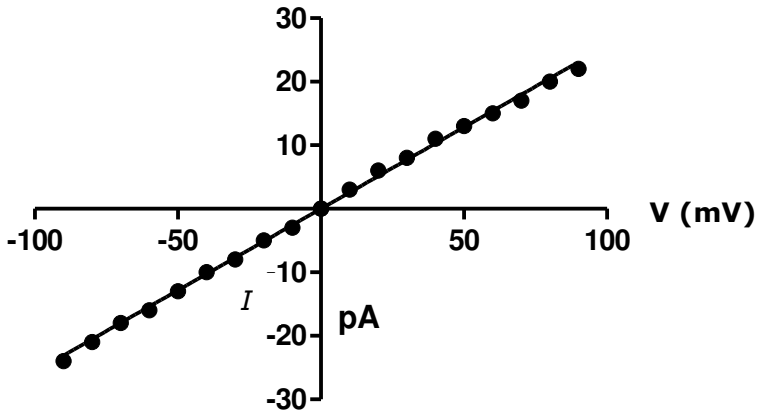

Figure 2.16. A representative determination of input resistance. This measurement was taken from a primary adipocyte in 138mM Cl^-. To measure input resistance current was injected in 10pA increments from -90pA to +90pA and the corresponding change in membrane voltage noted for each current injection step. The values for current and voltage were plotted and in accordance with Ohms law, V=I/R and therefore the slope was taken as the input resistance value. The input resistance in this example is 0.25GΩ.

In addition to measuring changes in membrane potential, the input resistance of the adipocyte plasma membrane was measured as both an indicator of cell integrity and as an indicator of ion channel activation. A low resistance, i.e. high conductance would suggest open channels and vice versa. A representative trace showing a membrane potential experiment with input resistance determination is shown in Figure 2.16. To measure the input resistance of the primary adipocyte plasma membrane, current was injected in an incremental and stepwise manner. This is indicated by the triangular peaks in the Vm record (Figure 2.15) showing negative deflection for the injection of negative currents and positive deflection for the injection of positive currents. After the first input resistance measurement in 138mM Cl^-, the extracellular Cl^- was dropped to 5mM. A rapid depolarisation from ~-20mV to ~0mV was observed. After the measurement of input resistance, bath Cl^- was switched to 10mM, 20mM, 40mM 80mM, 100mM, 120mM back to 138mM. Hyperpolarisation resulted with each increment in extracellular Cl^-

concentration. The start and end membrane potential values in 138mM extracellular chloride solution used in this illustrative trace were similar at -28mV and -27mV respectively. The ability of extracellular Cl^- removal to reversibly depolarise the 3T3-L1 adipocyte plasma membrane suggests that Cl^- has a role in the generation of resting membrane potential in these cells.

The basal input resistances of primary white fat adipocytes with resting membrane potential values between -20 and -40mV ranged from 0.25GΩ and 2GΩ. As the plasma membrane hyperpolarises with increasing $[Cl^-]_o$ the input resistance increases ($P<0.05$, Pearson). There was no significant correlation between input resistance and membrane potential in 5mM extracellular Cl^- for either the primary (Figure 2.17) or 3T3-L1 adipocytes (Figure 2.18).

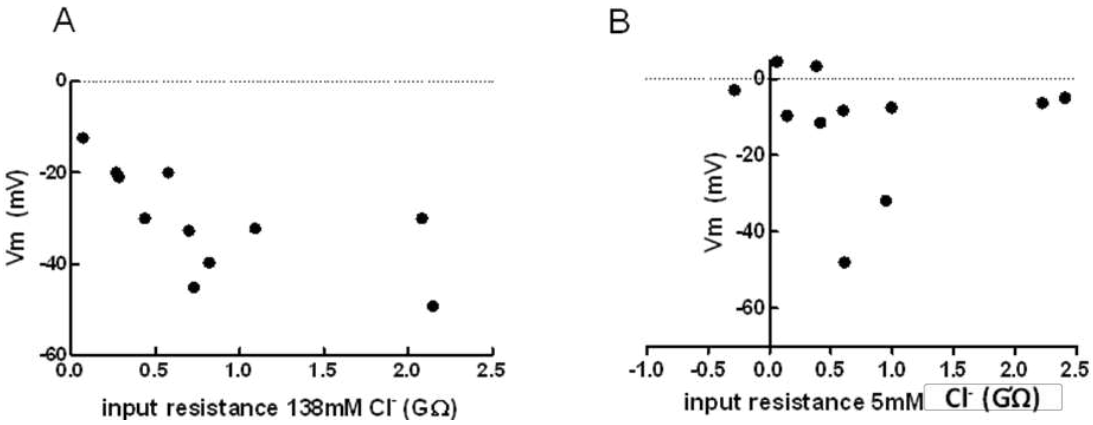

Figure 2.17. Correlation analyses between input resistance and membrane potential in primary white fat adipocytes. (A) 138mM extracellular chloride and (B) in 5mM extracellular chloride. In 138mM extracellular chloride the input resistance is significantly correlated with membrane potential ($P<0.05$, Pearson). 7 out of 11 adipocytes tested had RMP's of between -20 and -45mV. All of these adipocytes had input resistances of between 0.25 and 2GΩ. In 5mM extracellular Cl^- ,there was no correlation between Vm and input resistance.

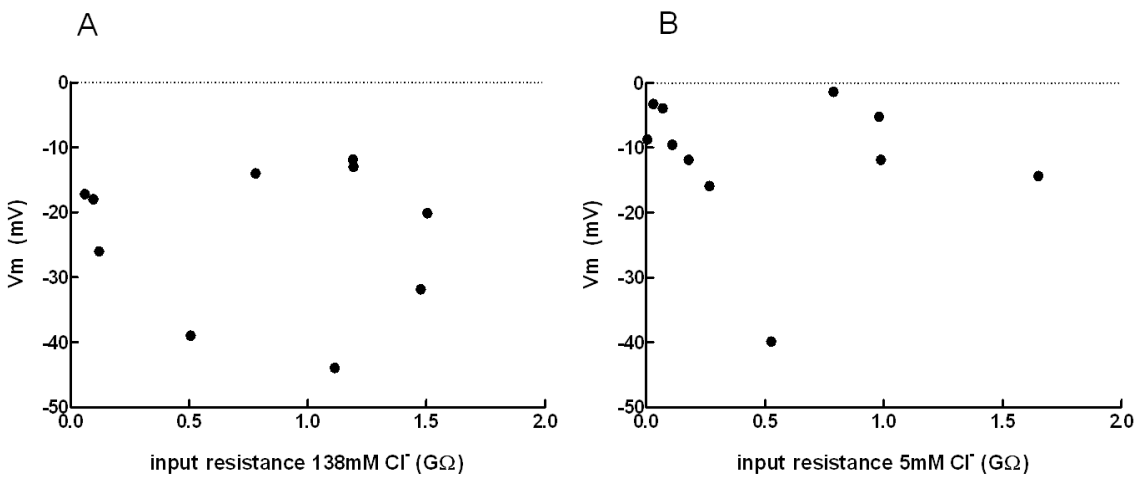

Figure 2.18. Correlation analysis between input resistance and membrane potential in differentiated 3T3-L1 adipocytes. (A) 138mM extracellular Cl^- n=10 (B) and 5mM extracellular Cl^- (n=11).

For primary adipocytes, the pooled input resistance in 138mM Cl^- was 0.8±0.2GΩ (n=11), and in 5mM Cl^- 0.7±0.2GΩ (n=11). One data set was excluded on the basis of non-linearity. For the 3T3-L1, the input resistance in 138mM Cl^- was 0.6±0.2GΩ (n=10), whereas in 5mM Cl^-, it was 0.5±0.2GΩ (n=11). A parametric paired t test was conducted for analysis involving both adipocyte models.

Although the input resistance appears high, values reported here are lower than those reported for other cell types such as smooth muscle cells (3.8GΩ) and neurons, (5.3GΩ). (Klockner and Isenberg, 1985, Pixley and Pun, 1990). The greater the input resistance, the less conductance there is across the membrane, and the less likely it is that ion channels will be open. Conversely, it is possible that if fewer ion channels are open, the ions that transition through these may have a more significant effect on the membrane responses of the cell.

Additionally measurements of input resistance in single cells are high, both isolated smooth muscle + rabbit portal vein are reported to have IR values ~0.3GΩ at resting membrane potentials of ~-50mV (Wilde and Lee, 1989).

2.5.7 Determination of $[Cl^-]_i$

On the basis of $[Cl^-]_o$ being 135mM and ECl^- being -30mV (the median membrane potential of adipocytes). If we assume only Cl^- is involvement in adipocyte RMP then we can calculate from the Nernst equation (See Equation 2.3) a value for $[Cl^-]_i$ of 42mM. As such, on reduction of $[Cl^-]_o$ to 5mM the Vm would be expected to depolarize to +52mV. Such a membrane potential response was not observed, this supports the role of an additional ion involved in adipocyte Vm.

2.5.8 The effect of Na^+ on adipocyte Vm

When two or more ions contribute to the cells resting membrane potential, the membrane potential will not be at the equilibrium potential for either ion. To test the hypothesis that Na^+ has a role in adipocyte resting membrane potential, RMP, extracellular Na^+ was removed from the bath solution by equimolar substitution with NMG. NMG is a cationic compound which cannot permeate cation channels (Clifford et al., 1998).

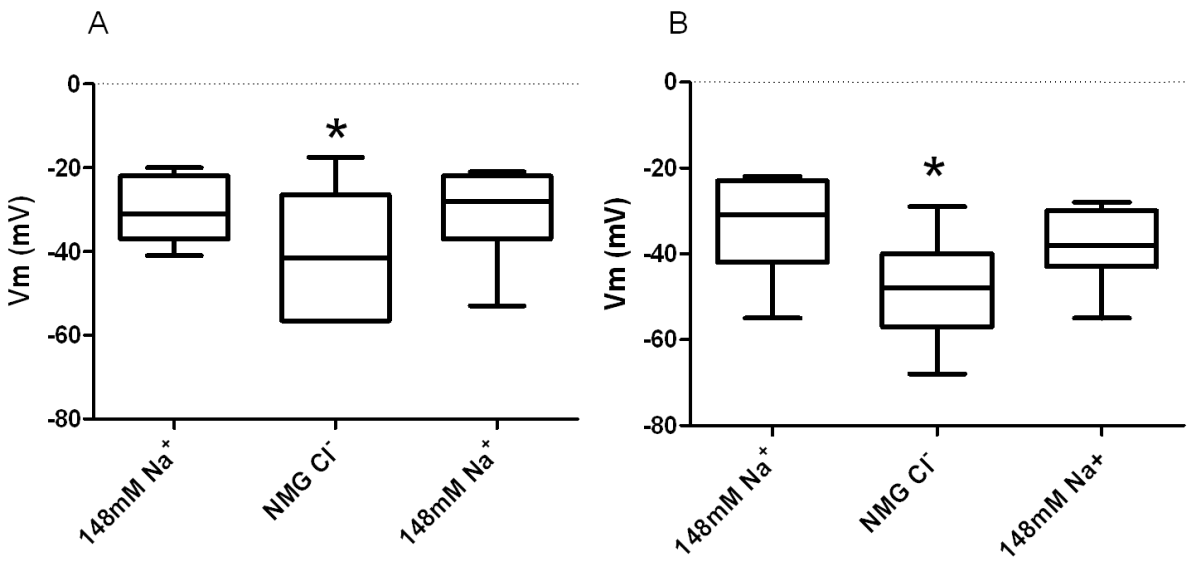

Figure 2.19. The effect of removal of extracellular Na^+ on adipocyte membrane potential. (A) primary adipocytes, n=7 and (B) 3T3-L1 adipocytes, n=7. Removal of extracellular Na^+ caused a significant and reversible hyperpolarisation of the adipocyte plasma membrane P<0.05 (Friedman's) in both adipocyte models.

Input resistances were measured to determine any changes in membrane permeability that may result as a consequence of ion channel activity. Data are presented as Mean ± SEM. For the primary adipocytes the input resistance in Na^+ was 0.4±0.5GΩ, in NMG Cl 1±0.7GΩ and upon return to Na^+ reversed back to 0.6±0.4GΩ, with a significant difference in input resistance between Na^+ and NMG Cl^-, P<0.05 (Friedman's). For the 3T3-L1 adipocytes, the input resistance in Na^+ was 0.5±0.2GΩ, in NMG Cl^- 0.4±0.1GΩ, and upon return to Na^+ 0.2±0.1GΩ (Friedman's).

Removal of Na^+ from the bath solution resulted in a reversible & significant hyperpolarisation of both the primary and the 3T3-L1 adipocyte plasma membrane of 10mV (P<0.05, Friedman's) (Figure 2.19). Since these experiments suggest an involvement of Na^+ on RMP. 2-APB a blocker of non-

selective ion channels was used to investigate the channel types which may underlie this permeability (Figure 2.20).

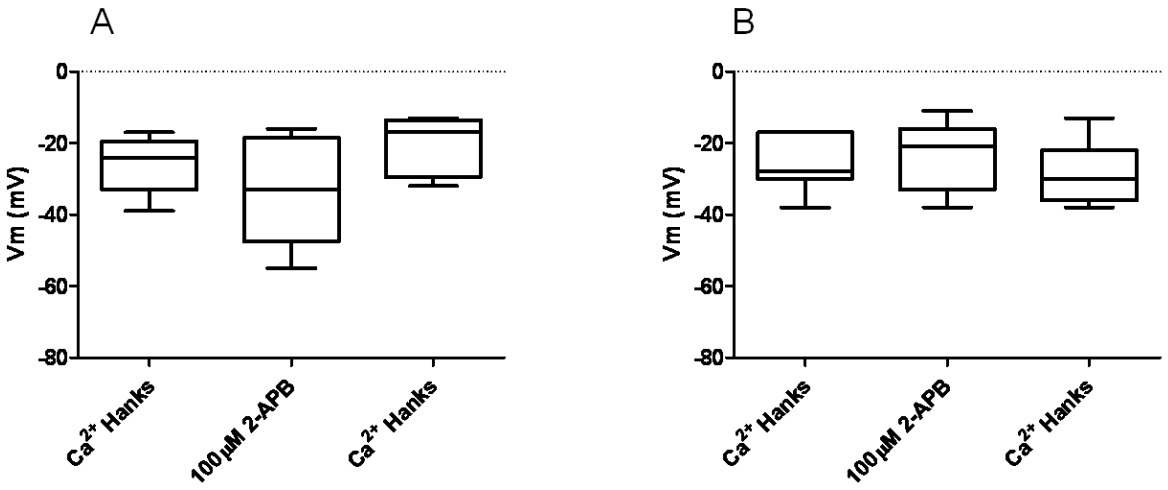

Figure 2.20. The effect of 100µM 2-APB on adipocyte membrane potential. (A) primary adipocytes n=5, and (B) 3T3-L1 adipocytes, n=7. 100µM 2-APB did not have any significant effect on membrane potential in either of the adipocyte models tested (Friedman's).

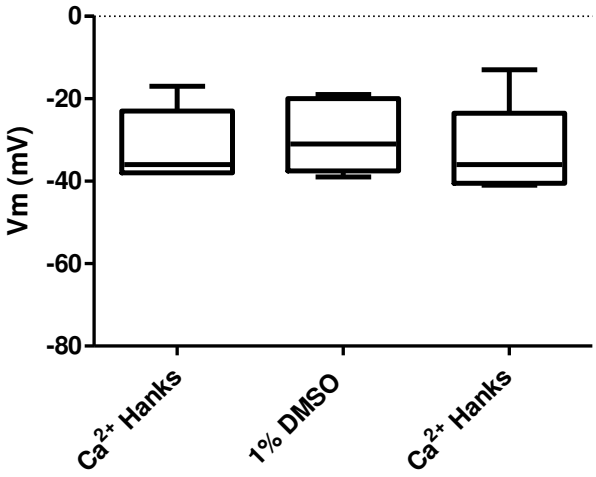

Figure 2.21. The effect of the DMSO vehicle control on membrane potential in differentiated 3T3-L1 adipocytes. Perifusion of 1% (v/v) DMSO in the perifusion media did not cause any significant change in membrane potential, n=5 (Friedman's).

Neither 2-APB or its vehicle DMSO (Figures 2.20 and 2.21) affected Vm of either adipocyte model. See appendicies for an investigation into the effects

of 2-APB in rat dorsal root ganglions. Dorsal root ganglions are reported to express non selective cation channels (Elg et al., 2007).

2.5.9 The effect of insulin and isoprenaline on adipocyte membrane potential

Isporenaline and insulin have been reported to alter membrane potential of both adipocytes and in other target tissues (Section 2.2). To explore the possibility that these hormones may change membrane potential of adipocytes the effect of insulin and isoprenaline on the resting membrane potential of primary (A) and 3T3-L1 (B) adipocytes was investigated.

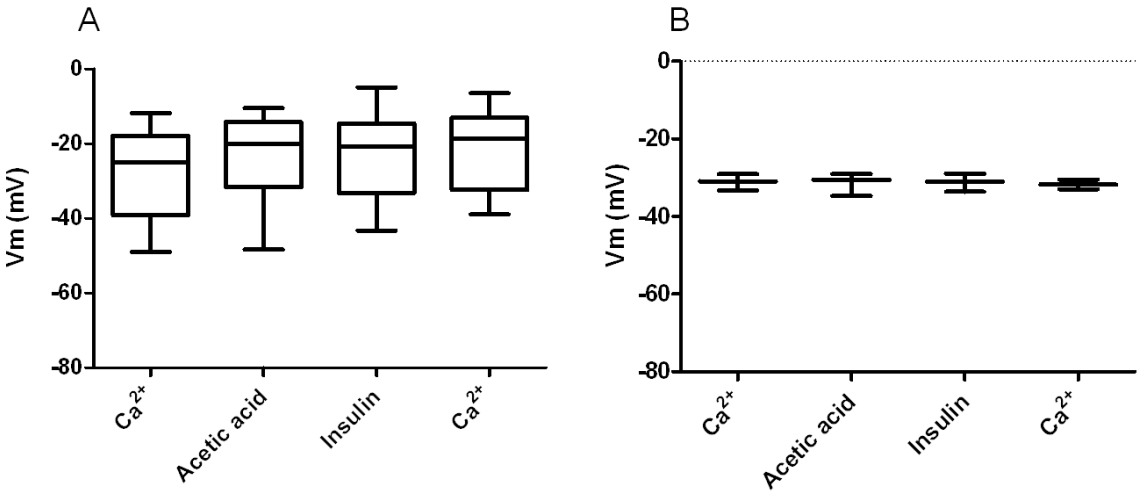

Figure 2.22. The effect of 100nM insulin and the acetic acid vehicle control on membrane potential. (A) primary adipocytes (n=12) and (B) differentiated 3T3-L1 adipocytes at 32^0C (n=3, note the lack of 25%/75% quartiles due to the small n). Neither insulin nor acetic acid had a significant effect on membrane potential (Friedman's) in either adipocyte model tested.

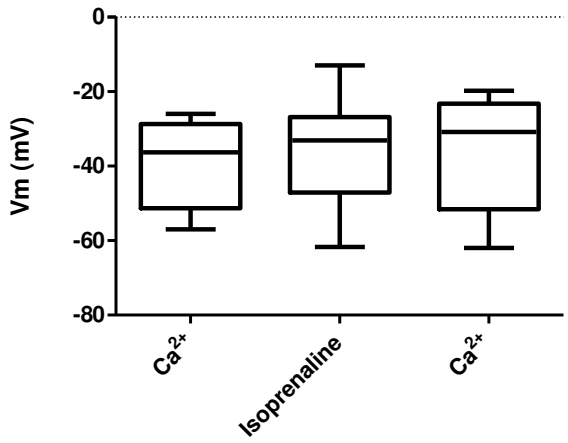

Figure 2.23.**The effect of perifusion of 10μM isoprenaline on the membrane potential of differentiated 3T3-L1 adipocytes.** Of the total population (n=12) 64% of the 3T3-L1 depolarise as a result of isoprenaline perifusion at 32°C. This effect on Vm is not statistically significant (Friedman's).

Figure 2.22 shows that neither 100nM insulin or the vehicle control for insulin, acetic acid, have no significant effect on membrane potential in either primary (A) or differentiated 3T3-L1 adipocytes (B). Figure 2.23 shows that 10μM isoprenaline does not have an effect on the membrane potential of 3T3-L1 adipocytes. The vehicle for isoprenaline, DMSO, did not have an effect on 3T3-L1 RMP (Figure 2.21).

2.6 Discussion

2.6.1 Tissue culture

Differentiation of 3T3 fibroblasts to 3T3-L1 adipocytes occurs only after cessation of cell proliferation. At this point, the cells incorporate an increased amount of fatty acid precursors into triglycerides, as visualised by the formation of multiple small fat droplets, which over time incorporate into large fat droplets. Differentiated 3T3-L1 adipocytes adopt an appearance which is similar to, but not identical to that of the mature adipocytes (Figure 2.6 and Figure 2.7). 3T3-L1 adipocytes express markers of adipocyte differentiation such as PPARɣ and C/EBPα (Ntambi and Young-Cheul, 2000, Guo and Liao, 2000), incorporate glucose into triglyceride in response to insulin (Green and Kehinde, 1975, Mehra et al., 2007, Straub et al., 2011), and secrete adipose specific adipokines such as adiponectin and resistin (Soares et al., 2005, Kershaw and Flier, 2004, Kamigaki et al., 2006). To confirm that the 3T3-L1s were successfully accumulating lipids during the differentiation process and adopting an adipocyte phenotype, Oil Red O was used to monitor lipid accumulation within the 3T3 fibroblasts during the differentiation time-course. The differentiation end point (Figure 2.6C) was a heterogenous population of 3T3-L1 adipocytes at varying stages of the differentiation process; this is not uncommon as others also do not observe 100% differentiation (Green and Meuth, 1974, Green and Kehinde, 1975). It is possible that the cells are not asynchronous with regard to the time-frame and extent of lipid accumulation. It is also likely that not all cells are capable of differentiation, and that the non-differentiating cells continue to proliferate maintaining the monolayer during the differentiation time-course. The presence of non-differentiated adipocytes within our culture is not

problematic with regard to this study as only fully-differentiated single adipocytes were selected and utilised for patching, as indicated in Figure 2.6C.

2.6.2 Comparison of RMP in primary adipocytes, 3T3-L1 adipocytes and fibroblasts

Primary adipocytes and differentiated 3T3-L1 cells are both widely used adipocyte experimental models, each with their respective advantages and disadvantages. Primary adipocytes are considered the most physiological adipocyte model. Their large lipid droplet and increased buoyancy render conventional tissue culture methods and experimental manipulations ineffective (Poulos et al., Ailhaud, 2001). Primary adipocytes cannot proliferate and as such cannot be maintained and utilised experimentally over extended periods of time unlike their 3T3-L1 counterparts (Ntambi and Young-Cheul, 2000). The quality of the cell preparation and indeed the variability between different preparations can also determine experimental success. Over-digestion with collagenase can potentially increase membrane permeability and increase membrane fragility. A need to repeatedly source and prepare tissue can introduce variability due to the differences between donors; however, this can also be considered a favourable trait as the heterogeneity between different rat donors and also individual adipose cells within a preparation is more representative of physiological diversity.

There are very few published electrophysiological studies on adipocytes. So far there is no direct experimental comparison of the electrophysiology of primary and 3T3-L1 adipocytes, the results presented here are the first. The resting membrane potential of primary white fat adipocytes has previously been determined. See Table 2.3 for a summary.

Vm (mV)	Technique used to observe membrane potential	Species	Tissue Preparation	References
-28.7	Cl^- distribution ratio	Rat (120-140g)	Isolated cells from epididymal fat pads.	Perry and Hales, 1969
-46	Microelectrode	Rat	Epididymal fat pad tissue explant	Stark et al., 1980
-75	Rb^+ distribution	Rat (130-180g)	Epididymal fat pad tissue explant	Davis et al., 1981
-21	Microelectrode	Rat (400-500g)	Mesenterial fat pad tissue explant	Akiyama et al., 1990
-34	Microelectrode	Rat (120-180g)	Epididymal fat pad tissue explant	Ramirez-Ponce et al., 1990
-58	Voltage sensitive dye	Rat (150-200g)	Isolated cells from epididymal fat pads.	Cheng et al., 1980
-34	ZnO nanoelectrodes	Human	Isolated cells	Al-Hilli and Willander, 2009
-17 to -69	Microelectrode	Rat (110-405g)	Epididymal fat pad tissue explants	Beigelman and Hollander, 1962
-27 to -29	Microelectrode	Rat (210g)	Epididymal fat pad tissue explants	Beigelman and Shu, 1972
-21	Microelectrode	Rat (400-500g)	Mesenterial fat pad tissue explants	Kamei et al., 1992
-22	Microelectrode	Rat (400-500g)	Epididymal fat pad tissue explants	Kamei et al., 1992
-22	Microelectrode	Guinea Pig (600-700g)	Mesenterial fat pad tissue explants	Kamei et al., 1992
-23	Microelectrode	Guinea Pig (600-700g)	Epididymal fat pad tissue explants	Kamei et al., 1992

Table 2.3. A comparison of the techniques used and the resting membrane potentials for white fat adipocytes sourced from different species.

The most commonly reported adipocyte RMP values fall within the range of -20 and -46mV, with discrepancies occurring between the RMP obtained via Rb^+ distribution and the values obtained by the sharp microelectrode technique. Rb^+ permeates K^+ channels and mimics the distribution of K^+ across the plasma membrane. Through using this technique it is already assumed that K^+ is the predominant contributor to membrane potential. A

problem with ion distribution determinations is that is difficult to determine if a singular ion, and which ion determines membrane potential. Accurate estimations of intracellular water space also need to be determined and shown to be constant throughout. Determining intracellular water space in adipocytes is difficult (Cheng et al., 1980, Ailhaud, 2001). Impaling a tissue segment or a cell with a microelectrode can cause severe ionic leaks at the junction between the electrode and the cell membrane. This can compromise the certainty and reproducibility of potentials derived by this method. In particular, methods involving repeated electrode contact on agitated tissue segments such that multiple perforations occurred, the leakiness of the membrane increases giving rise to variable membrane potential measurements (Beigelman and Hollander, 1962). Difficulties arise when using adipocytes as they comprise predominantly of lipid and only have a thin rim of cytoplasm. Microelectrode impalement can be interfered by the clogging of the electrode tip with fat. The whole-cell patch configuration is believed to be less damaging to the cell, and thus give rise to more accurate recordings of a cell's electrical signals (Li et al., 2004). Attempts at ascertaining the whole-cell configuration of the patch clamp technique within this study on primary adipocytes were unfortunately unsuccessful due to persistent clogging of the patch pipette tip with lipid. Even less detrimental to the integrity of the cell membrane is the perforated patch configuration of the whole-cell technique. The integrity of the cytoplasmic components are maintained as electrical contact to the interior of the cell is established via perforation using pore-forming antibiotics, such as amphotericin or nystatin. It is likely that variations between primary tissue explants, adipocyte preparations, and the methods used to study adipocyte RMP are accountable for the variation in adipocyte RMPs reported. Generally the RMP of white adipocytes is notably

more depolarised than that of brown adipocytes, as determined by microelectrode impalement at 29°C, -50mV to -60mV (Nedergaard, 1981, Girardier et al., 1968) and of "excitable" cells such as neurons which have a resting membrane potential of ~-60mV (Doan and Kunze, 1999). In this study, the mean RMP for both the 3T3-L1 (-28±1.23mV, n=88) and the primary adipocytes (-31±1.57mV, n=68) as shown in Figure 2.8 are similar to the RMP values most commonly reported in the literature for this cell type (Table 2.3).

2.6.3 The involvement of K^+ in RMP of 3T3-L1 adipocytes or primary adipocytes

The lack of change in adipocyte membrane potential in response to elevated extracellular K^+ (50mM), suggest K^+ ions are not involved in the RMP of either primary epididymal white fat adipocytes or differentiated 3T3-L1 adipocytes.

Increasing $[K^+]_o$ to 80mM depolarised adipocyte resting membrane potentials, from -24mV to -12mV, when compared to the RMP in the absence of extracellular K^+(Beigelman and Shu, 1972). Earlier studies suggested that the adipocyte responses to changes in $[K^+]_o$ were only observed in white fat adipocytes in rats weighing less than 215g (Beigelman and Hollander, 1964). This could be an explanation as to why no membrane potential effects were seen in adipocytes in this study, as rats used to source tissue weighed between 250-340g. Adipocyte size influences basal and insulin-stimulated lipid synthesis, the basal rate of lipolysis and how the cell responds to insulin in an antilipolytic capacity (Jacobsson and Smith, 1972). Large cells are less likely to take up glucose and exogenous fatty acids in response to insulin (Smith, 1971, Lonn et al., 2010). Adipose tissue deposits sourced from

heavy/ overweight rats contain larger cells, the increase in adipocyte size may influence the electrophysiological properties of the plasma membrane, however no report as yet has investigated the differences in plasma membrane properties, e.g. ion channel density between obese and lean tissues.

If only K^+ ions were involved in setting adipocyte resting membrane potential, we would expect the resting membrane potential of adipocytes to be approximately -90mV, assuming $[K^+]_i$ to be 135mM with $[K^+]_o$ to be 5.6mM where elevation of $[K^+]_o$ to 50mM would depolarise the adipocyte plasma membrane to approximately -26mV. The theoretical adipocyte resting membrane potential based on the Nernst potential for K^+ was not observed. Additionally 50mM $[K^+]_o$ did not significantly depolarise the plasma membrane of the adipocyte. The K^+ gradient would make no contribution to RMP if it was membrane impermeable. However, the presence of K^+ channels in the plasma membrane of adipocytes has been recorded. Initially, an outwardly rectifying K^+ conductance was described by microelectrode recording in rat white adipose tissue (Ramirez-Ponce et al., 1991). Studies using inside-out patches and whole cell patch configuration have provided evidence of the existence of voltage-dependent K^+ channels in isolated white fat adipocytes from rat, (Ringer et al., 2000, Lee and Pappone, 1997). Whole-cell patch clamp studies also describe a voltage-dependent K^+ conductance in subcutaneous and visceral preadipocytes (Ramirez-Ponce et al., 2003) and in mature white fat adipocytes differentiated from epididymal pre-adipocytes. (Ramirez-Ponce et al., 1996, Lee and Pappone, 1997).

A practical limitation of applying the whole-cell configuration to adipocytes is persistent clogging of the patch pipette tip due to the high lipid content of adipocytes, as was experienced during whole-cell patch clamp attempts upon

primary adipocytes within this laboratory. The risk of washout of channel regulators in whole cell configuration has also been reported as the electrode solution dialyzes that of the cell interior. The size of the cell under study determines the likelihood of dialysis of pipette solution with the cell interior, with smaller cells more likely to undergo dialysis in comparison to larger cells. Ramirez ponce *et al* (1996) reported adipocyte diameters of 20-60 μM. Images of adipocytes in studies conducted by Lee and Pappone (1997) and Ramirez Ponce *et al* (1996) are inclusive of scale bars. The diameters of the adipocytes under study within the investigation conducted by Ramirez Ponce *et al* (1996) were varied in size, with an approximate diameter of 30μM. The diameter of the adipocytes studies in the literature is generally 2-3 times larger than that reported for islet cells (12μM diameter). Islet cells are a prominent cell type used in patch clamp investigations (Perez-Armendariz et al., 1991), so it is likely that washout of intracellular constituents when conducting whole cell investigations with adipocytes, may be less of a technical issue, than with other smaller cell types. Despite the observed technical difficulties in applying the whole-cell configuration to adipocytes, in the study by Lee and Pappone (1997) whole-cell findings were re-enforced by replicate investigations in the perforated patch configuration, no difference in observations utilising the two techniques was reported (Lee and Pappone, 1997). Ramirez ponce *et al* (2003) utilised human pre-adipocytes differentiated into mature adipocytes in culture. The adipocyte morphology resembled that of the 3T3-L1 cells used in this study at an intermediate stage of differentiation (Figure 2.6B). In the study by Ramirez ponce *et al* (2003), differentiation was assessed by eye on the basis of lipid droplet accumulation, however lipid stains such as Oil Red O or Sudan black were not utilised to confirm the inclusions seen as being lipid, although in earlier studies by the

same group utilising rat pre-adipocytes differentiated in culture, did confirm lipid accumulation with Oil Red O (Ramirez-Ponce et al., 1996). The K^+ currents observed in the 1996 and 2003 studies by Ramirez ponce between differentiated adipose cells of rat and human origin were not dissimilar. A voltage-gated outward current with sigmoidal activation kinetics, and an activation threshold of ~-30mV was demonstrated in white adipocytes (Lee and Pappone, 1997, Ramirez-Ponce et al., 1996). Macroscopic current amplitudes ranged between 0.5nA to 6nA (Ramirez-Ponce et al., 1996). In white adipose tissue, the single channel conductance of these channels was reported to be 16.4pS (Ringer et al., 2000), whereas in brown adipose tissue it was 17pS (Russ et al., 1993). The channels responsible for this current were highly selective for K^+ with a selectivity sequence of $K^+ > NH_4^+ > Cs^+ > Na^+$. This sequence did not differ between adipocytes of rat or human origin (Ramirez-Ponce et al., 1996, Ramirez-Ponce et al., 2003). Pharmacological K^+ channel blockers (tetraethylammonium (TEA), 4-aminopyridine (4-AP), barium and cobalt) were used to confirm the identity of these channels as K^+. In white rat adipocytes, the IC_{50} for TEA blockade was 1.5mM (Ringer et al., 2000), similar to the IC_{50} of TEA blockade in brown adipose tissue of 1.8mM (Russ et al., 1993). No difference in K^+ channel properties were observed between isolated white adipocytes sourced from Sprague Dawley, Zucker lean and Zucker obese rats (Lee and Pappone, 1997).

Similarities between the observations of different investigators, and across differing primary tissue sources suggests that voltage-gated K^+ conductance is a universal property of primary adipose tissue, including brown adipose tissue (Russ et al., 1993, Lucero and Pappone, 1989). It was proposed that the voltage-gated K^+ channel observed in brown adipose tissue was similar to the delayed rectifier channel found in nerve. If this is the case, it would

suggest that the activity of these channels in brown cells is dependent upon depolarisation/excitability (Lucero and Pappone, 1989).

Regarding the reported differences in RMP between white adipose tissue and brown adipose tissue, ~-30mV for white adipose tissue, (see Table 2.3) and -51mV for brown adipose tissue (Girardier et al., 1968), a non-voltage dependent K^+ channel was identified in brown adipocytes but not in white adipocytes (Russ et al., 1993). It is possible that this channel contributes to steady state RMP in brown adipose tissue and is not expressed in WAT.

As an addition to the current work, it would be of interest to determine the presence of K^+ channels on the plasma membrane surface of our primary and 3T3-L1 adipocytes. It is possible that K^+ channels are present on the adipocyte plasma membrane, however they may be non functional or inactivated. cAMP is known to inactivate delayed rectifier K^+ channels when applied directly (Chung and Kaczmarek, 1995), or via pharmacological induction of elevated cAMP (Garber et al., 1990). cAMP is involved in a variety of adipocyte functions, differentiation, adipokine secretion (Path et al., 2001) and lipolysis (see Chapter 2, Section 2.1). Our adipocytes were not stimulated by catecholamines to undergo lipolysis or subject to pharmacological elevation in cAMP by agents such as dibutyryl adenosine 3',5'-cyclic monophosphate (DBcAMP, a cAMP analogue), aminophylline or pentoxifylline (PDE inhibitors). It is a possibility that the rats would be exhibiting a sympathetic nervous system response prior to culling, which may result in adipose tissue lipolysis, however there was no membrane potential response to elevated extracellular K^+ in either the primary or 3T3-L1 adipocyte model, therefore the likelihood of inhibition of delayed rectifier K^+ channels by elevated cAMP is unlikely.

Since K^+ lacked a contribution to adipocyte RMP, the role of Cl^- and Na^+ on adipocyte RMP were investigated.

2.6.4 Membrane potential of beta cells

It is well established that K^+ ions are the major determinant of resting membrane potential in pancreatic beta cells. Eradication of the outward K^+ gradient either by closure of the K^+ ATP channel or elevations in extracellular K^+ gives rise to membrane depolarisation of the pancreatic beta cell (Smith et al., 1990, Manning Fox et al., 2006, Antunes et al., 2000). The resting membrane potential values obtained here for mouse beta cells (as shown in Figure 2.9) are similar to those previously reported in the literature, ~-62mV (Smith et al., 1990, Manning Fox et al., 2006) with depolarisation of Vm in 50mM extracellular K^+ going to ~-20mV. This indicates that our membrane voltage measurements by the perforated patch method are comparable to membrane voltage measurements previously made by others using either the whole-cell patch configuration or the perforated patch configuration (Manning Fox et al., 2006, Smith et al., 1990). The observation of membrane depolarisation in elevated extracellular K^+ is indicative that our perforated patch method is valid and confirms suitability of the experimental method utilised. It also confirms that K^+ is not a determinant of adipocyte RMP.

2.6.5 Cl^- ions are involved in adipocyte RMP

Cl^- is generally present at lower intracellular concentrations than extracellular levels (see Table 2.2). Generally, the transmembrane Cl^- gradient carries an inward negative charge, which either contributes to a hyperpolarised RMP or it is in equilibrium with Vm. Our adipocytes do not have a hyperpolarised RMP when compared to brown adipocytes or neurons, however, reduction of $[Cl^-]_o$

from 138mM to 5mM depolarized the plasma membrane, a finding that indicates Cl^- ions have a role in adipocyte RMP, and the presence of Cl^- channels (This is further investigated in Chapter 4) (see Figure 2.14). Radioisotopic determination of rates of K^+, Na^+ and Cl^- efflux and intracellular concentrations in isolated fat cells support the hypothesis that Cl^- is a major determinant of adipocyte resting membrane potential (Perry and Hales, 1969). The membrane potential we observed for primary adipocytes (-28mV) is identical to the membrane potential reported by Perry *et al* (1969) as determined by radioisotopic methods. Microelectrode studies by Biegelman *et al* (1972) also suggested a role of Cl^- in the resting membrane potential of primary adipocytes, although this was in conjunction with K^+ (Beigelman and Shu, 1972).

It is not entirely uncommon for Cl^- ions to be a major determinant of RMP. Cl^- ions determine the resting membrane potential of the red blood cell, which has a resting membrane potential of -8mV. The plasma membrane of the red blood cell is thousands of times more permeable to Cl^- ions than Na^+ or K^+ ions (Jay and Burton, 1969). The calculated Nernst potential for Cl^- ions in the red blood cell matches experimental observations of resting membrane potential made by investigators Jay and Burton (Jay and Burton, 1969). Cl^- ions are also implicated in the resting membrane potential of bovine pulmonary artery cells. When the Cl^- ion component is eliminated the cell hyperpolarises from -26mV towards the Nernst potential for K^+ ions, -62mV (Voets et al., 1996). The resting membrane potential of rabbit articular chondrocytes, -42mV, has also been reported to be maintained by Cl^- ion conductance (Tsuga et al., 2002). It seems reasonable to conclude that Cl^- ion conductance contributes to the resting membrane potential of adipocytes. Multiple ion conductances often determine membrane potential at rest. We

suggest that the other ion conductance involved in adipocyte RMP is that of the Na^+ ion.

Input resistances were calculated prior to and post extracellular Cl^- removal, (1) to eliminate the possibility that the adipocyte plasma membrane was leaky, and (Hulme et al.) to investigate the hypothesis that an increase in channel activity would increase the permeability and hence decrease the resistance of the adipocyte plasma membrane. If the plasma membrane of the cell was leaky, a low input resistance would result regardless of ion channel activity due to high membrane permeability. It would be expected that adipocytes with "leaky" membranes would be unable to maintain their ionic mileau, and as such it is expected they would have resting membrane potentials in 138mM Cl^- of close to 0mV. Conversely, regarding channel activity, a decrease in ion channel activity would decrease the permeability and hence increase the input resistance of the adipocyte plasma membrane. There was no significant difference in mean input resistance in either primary or 3T3-L1 adipocytes between 138mM Cl^- and 5mM Cl^- bath solutions.

2.6.6 Na^+ ions contribute to adipocyte RMP

The data presented Figure 2.19 suggest that Na^+ has a role in the RMP of both the primary adipocyte, and 3T3-L1 adipocyte. It is known that Na^+ conductance contributes to RMP in brown adipocytes (Girardier et al., 1968).

For Na^+ to contribute to RMP, a Na^+ selective pathway in the plasma membrane is required. Na^+ currents are carried by a number of channel types and transporters including ligand-gated sodium channels, voltage-gated sodium channels, non-selective cation channels. It is unlikely that voltage-gated Na^+ channels contribute to adipocyte RMP. No evidence of an inward current that would be indicative of an inward voltage-gated Na^+ or Ca^{2+}

conductance has been reported (Lee and Pappone, 1997, Ramirez-Ponce et al., 2002). Secondly, I-V relationships for estimation of R_{IN} were linear (Figure 2.16) and did not indicate any voltage-dependent components. Store-operated calcium channels (SOCs) are also Na^+ permeable (Arnon et al., 2000); it is unlikely that Na^+ permeable SOCs are involved in adipocyte RMP, as their main role is regulation of store-operated calcium entry and are only active in response to internal Ca^{2+} store emptying (Parekh and Putney, 2005).

It was hypothesised that the Na^+ currents carried by non selective cation channels are involved in the membrane potential responses observed. Na^+ conductance via non-selective cation channels are suggested to be involved in the generation of resting membrane potentials in bovine pulmonary artery cells (Voets et al., 1996) and in rabbit arterial smooth muscle cells, where the non-selective cation channel conductance is twice that of the K^+ channel conductance (Bae et al., 1999). Single channel data has provided evidence for the presence of non-selective cation channels in both primary white adipocytes and brown adipocytes (Halonen and Nedergaard, 2002, Ringer et al., 2000, Weber and Siemen, 1989). In the current investigations, buffer substitution of Na^+ for K^+ had no effect on adipocyte membrane potential, however removal of extracellular Na^+ by equimolar substitution with NMG Cl^- caused a hyperpolarisation of the adipocyte plasma membrane. As NMGCl can't permeate non selective cation channels this is indicative of non-selective cation channel conductance (Figure 2.19).

Currently, the channel selectivity for non-selective cation channel antagonists is poor. To ascertain in a general context, the presence of non selective cation channels on the plasma membrane of our adipocytes, 2-Amioethoxydiphenylborate (2-APB), a TRP channel inhibitor, was utilised (See Table 2.6). The consensus is that maximal block of non-selective cation

channels by 2-APB occurs a concentration of ~100uM. If this is the case, it would be expected that 2-APB inhibits Na^+ influx causing hyperpolarisation of plasma membrane. In experiments presented here, there was no membrane potential effect of 2-APB in either adipocyte model (Figure 2.20).

Table 2.6 summarises the TRP channel types blocked by 2-APB, and the inhibitory concentration. TRPC and TRPCM channels are the predominant TRP channel types that are blocked by 2-APB. To confirm the effects of 2-APB blockade on non-selective cation channels, rat DRG neurons were sourced as a positive control. In rat DRG neurons, single cell RT PCR identified TRPC1 & TRPC6 mRNA (Alessandri-Haber et al., 2009). DRGs from mouse had an abundant expression of TRPC1, TRPC3 and TRPC6 mRNA, with lower levels of expression of TRPC2, TRPC4 and TRPC5 mRNA (Elg et al., 2007). Expression of multiple TRPC channel types within one tissue is not uncommon (Abramowitz and Birnbaumer, 2009), this may complicate my interpretation of the observed 2-APB effect.

Proteins	**Concentration/ IC50***
TRPC1	>80% inhibition @80μM
TRPC3	>90% inhibition @ 90μM
TRPC5	19μM*
TRPC6	10.4uM*
TRPM2	>95% inhibition 30μM
TRPM3	87.5% inhibition @ 100μM
TRPM7	178μM*
TRPM8	
Voltage operated K^+ channel	5μM

Table 2.6. A Comparison of the potencies of 2-APB in inhibiting a range of channels and proteins from (Togashi et al., 2008). Note, 2-APB was used at 100μM within this investigation.

Using the perforated patch clamp technique, 20mM OAG (synthetic cell permeable diacyl glycerol analogue) was used with primary rat DRG neurons to activate the TRPC channels, (Vazquez et al., 2003, Hofmann et al., 1999, Venkatachalam and Montell, 2007). It was hypothesised, that this would result in a cellular influx of Na^+ resulting in membrane depolarisation, which would then be ameliorated following application of 100μM inhibitory concentration of 2-APB in the presence of 20mM OAG. Unfortunately due to time constraints it was not possible to fully optimise seal formation on the DRGs within these patch clamp investigations. As most TRP channels are permeant to Ca^{2+} ions (Hofmann et al., 1999, Nilius and Voets, 2005), calcium imaging was used as an alternative approach utilising the same method as described in Chapter 3, Section 3.9.3. The results and discussion of this experiment are presented in appendicies. In short the findings in this study were inconclusive; as such the presence of NSCC on the plasma membrane of white adipocytes is yet to be fully ascertained.

2.6.7 The effect of insulin on adipocyte membrane potential

Insulin and the catecholamines, adrenaline, noradrenaline and isoprenaline are known to modulate metabolic activity in white fat adipocytes. Insulin was originally reported to hyperpolarise the resting membrane potential of the insulin responsive tissue, skeletal muscle (Zierler, 1966). This was proposed to be via accelerated Na^+ efflux activated by insulin. An increase in permeability, and inward flux of Cl^- ions was also considered a potential consequence of insulin. In contrast to published observations in adipocytes, insulin was not reported to increase permeability of the plasma membrane to K^+ (Zierler, 1966),

In adipocytes, insulin is antilipolytic (Ahmadian et al., 2009, Jacobsson and Smith, 1972). As insulin is membrane impermeable, it is likely that its membrane potential effects occur due to altered ion flux via modulation in ion channel function, or via altered trafficking and channel expression. It has been suggested that the functional effect of insulin occurs via modulation in membrane potential. Intracellular recording demonstrated that insulin hyperpolarised the RMP of white adipocytes by 13.5mV, potentially by reducing intracellular cAMP concentrations and increasing outward K^+ conductance (Ramirez-Ponce et al., 1991, Ramirez-Ponce et al., 1998). K^+ channel current density in differentiated adipocytes was larger in the presence of insulin when compared to non-insulin exposed cells, indicating that insulin may also modulate K^+ currents by up-regulation of K^+ channel trafficking to the plasma membrane (Ramirez-Ponce et al., 2002). Rb^+ fluxes suggested that insulin caused a 9mV hyperpolarisation of the white adipocyte plasma membrane (Davis et al., 1981). The hyperpolarisation of white adipocytes observed in insulin by Davis *et al* (1981) is identical to the mean change from RMP of -9mV in the presence of insulin, as determined by microelectrode impalement (Beigelman and Hollander, 1962). In the case of Beigelman and Hollander *et al* (1962), there was a large distribution of resting RMP values (-17 to -69mV) and membrane potential change in the presence of insulin. Such a large spread of data, may mask any significance. In our adipocytes, insulin caused a 5mV depolarisation in median resting membrane potential (Figure 2.22), however this effect was not statistically significant, a finding in agreement with observations by Stark *et al* (1980). The reasons for the difference in the reported effects of insulin and those shown here are unknown.

2.6.8 The effect of isoprenaline on adipocyte membrane potential

There was no membrane potential effect of isoprenaline this is unlikely to be due to an absence of β-adrenoceptors since their functional presence has already been shown in differentiated 3T3-L1 cells within our laboratory (Pulbutr, 2009).

The lack of a membrane potential effect observed with isoprenaline is in contrast to that reported by others. Noradrenaline causes depolarisation of the white adipocyte RMP by ~8.5mV (Ramirez-Ponce et al., 1991). Brown adipose tissue segments also depolarised from -50mV to ~-30mV following adrenoceptor stimulation with noradrenaline (Schneider-Picard et al., 1985).

Based on observations by Hamida *et* al (2011) demonstrating the functional effect of depolarisation on the stimulation of lipolysis, the lack of membrane potential effect of isoprenaline in 3T3-L1 cells could indicate that lipolysis was not stimulated as catecholamine resistance has been demonstrated in human adipocytes sourced from populations of normal healthy individuals (Lonnqvist et al., 1992). Hamida *et al* (2011) also demonstrated resistance to isoprenaline-induced lipolysis in human abdominal subcutaneous adipocytes, however the BMI and health status of the donors was unknown (Hamida et al., 2011). Although not demonstrated here, previous work within this laboratory has demonstrated that application of 10μM isoprenaline is suitable for the induction of lipolysis of adipocytes (Pulbutr, 2009). The EC_{50} of isoprenaline for the induction of lipolysis, as consistently reported by others, is 0.1μM (Langin et al., 2005, Tebar et al., 1993). Inhibition of lipolysis under elevated concentrations of isoprenaline (100μM), and its binding to α-adrenoceptors has been reported (Skomedal et al., 1984). The concentrations of isoprenaline used in this study were sufficiently lower, also previous

studies in our laboratory did not show α-adrenoceptor involvement in isoprenaline-stimulated lipolysis (Pulbutr, 2009). Conversely, α-adrenoceptor involvement is implicated in the membrane depolarisation of brown adipose tissue (Schneider-Picard et al., 1985) partly mediating K^+ efflux (Weber and Siemen, 1989).

2.6.9 The involvement of cAMP in the mediation of the membrane potential effects of insulin and isoprenaline

The existence of K^+ currents reported in adipocytes has lead to the hypothesis that, as with brown adipocyte (Girardier et al., 1968, Horwitz et al., 1969, Lucero and Pappone, 1990), both insulin and noradrenaline act by modulating K^+ conductances. Elevating intracellular cAMP (reported to block K^+ channels) indirectly by addition of forskolin (50μM), or directly, in addition with phosphodiesterase inhibitor IBMX, reduced voltage rectification in adipocytes. It was suggested that noradrenaline induced increases in $[cAMP]_i$, and blocked outward K^+ conductance resulting in depolarisation. This effect in white adipose tissue may depend on the adipocyte source. Mesenterial adipocytes did not show a membrane potential effect of isoprenaline (50nM) (Akiyama et al., 1990), however the membrane potential response was significantly depolarised in the presence of theophylline, an agent known to elevate cAMP (Stefanovich, 1979), again confirming a requirement for cAMP involvement in the membrane responses seen (Akiyama et al., 1990).

If the membrane potential effects of insulin and isoprenaline are dependent on a functional K^+ conductance, this could explain the absence of any membrane potential effect in our adipocyte models as they are not responsive to modulations in K^+. Functional studies assessing lipolysis in brown adipocytes investigated the effect of ouabain (an Na^+/K^+ ATPase

inhibitor) and theophylline (inhibitor of cyclic AMP breakdown). The authors observed no effect of theophylline on noradrenaline-stimulated lipolysis, suggesting that the effect of noradrenaline may be independent of adenylate cyclise activation and subsequent augmentation of intracellular cAMP levels. However there was a requirement for inward K^+ conductance through the Na^+/K^+ ATPase. Removal of extracellular K^+ by substitution with choline, an impermanent cation, impaired free fatty acid release to a similar extent as ouabain (Herd et al., 1973). K^+ channel inhibition may not be the only mechanism involved in the induction of lipolysis, however it is possible that the mechanism of regulation of lipolysis differs between brown and white adipocytes.

2.6.10 Summary

Data show that the K^+ conductance through K^+ ion channels, is not a determinant of membrane potential in either primary adipocytes or in differentiated 3T3-L1 cells. The membrane potential of both primary adipocytes and differentiated 3T3-L1 adipocytes is ~-30mV. The major ion involved in adipocyte membrane potential is Cl^-, with a minor role of Na^+. Data also suggest a role of non selective cation channels as a cellular Na^+ entry pathway in adipocytes. Neither insulin nor isoprenaline had an effect on the Vm of either adipocyte model, as such, any functional effects of insulin or β-adrenoceptor stimulation on adipocytes are unlikely to be modulated by alterations in membrane potential. Additionally, membrane responses were similar between the 2 adipocyte models for all investigations within this chapter; suggesting a similar mechanism for the regulation of Vm between primary and differentiated 3T3-L1 adipocytes.

Chapter 3

Investigation into the presence of Ca^{2+} influx pathways on the plasma membrane of white fat adipocytes

3.1 Introduction

Ca^{2+} is a ubiquitous second messenger that is involved in signal transduction within numerous cell types. Changes in the concentration of intracellular Ca^{2+} ($[Ca^{2+}]_i$) instigate a range of cellular functions from muscle contraction, neurotransmitter release, exocytotic release from endocrine cells and gene expression (Catterall et al., 2003b). $[Ca^{2+}]_i$ needs to be tightly controlled to maintain appropriate cellular homeostasis and function. Dysregulated Ca^{2+} signalling can result in abhorrent cell function and the development of a disease state. Examples include dysregulations in the inositol triphosphate (IP3) pathway in neurons in the development of Alzheimer's disease (Stutzmann et al., 2004), dysregulated Ca^{2+} signalling by L-type VGCCs in muscle disorders (MacLennan, 2000) and dysregulated Ca^{2+} handling by the ryanodine receptor (RYR) Ca^{2+} channel in the control of sarcoplasmic Ca^{2+} release in cardiomyopathies (Kranias and Bers, 2007). In the non-excitable smooth muscle, a switch in expression of L-type VGCCs to T-type channels contributes to the development of vascular disease (House et al., 2008).

Sources of Ca^{2+} are derived from Ca^{2+} release from the intracellular stores, or via extracellular Ca^{2+} influx. There are numerous Ca^{2+} influx pathways (see Chapter 1, Section, 1.2.1) including ligand-gated ion channels, store-operated ion channels, and, as discussed herein, voltage-gated Ca^{2+} channels and the sodium calcium exchanger.

3.1.1 Voltage-gated calcium channels

Voltage-gated calcium channels (VGCCs) are multi-subunit, transmembrane proteins which mediate Ca^{2+} entry in a variety of cell types in response to depolarized membrane potentials (Arikkath and Campbell, 2003). The presence and function of VGCCs in excitable cell types such as neurons, muscle cells, and cardiac muscle cells is well established (Ertel et al., 2000). VGCCs are increasingly being reported in non-excitable cell types, regulating functions such as endocrine secretion and gene expression (Catterall et al., 2003b, Tsien et al., 1991). There is increasing evidence for the contribution of L-type Ca^{2+} channels in insulin action. L-type Ca^{2+} currents in both primary, and islet cell lines are implicated in insulin secretion (Satin et al., 1995, Jung et al., 2009). It is possible that L-type Ca^{2+} currents have a role in insulin signalling as they have been described in insulin target tissues such as the liver and skeletal muscle, although characterisation of their role is needed. Adipose tissue is a target tissue for insulin action. Ca^{2+} influx by VGCCs is suggested to influence insulin responsiveness in white adipose tissue, however to date evidence is limited; this point is expanded upon in Section 3.7.

3.1.2 The sodium calcium exchanger

The Na^{+}/Ca^{2+} exchanger (NCX) is regarded as an essential Ca^{2+} signalling component which is present on the plasma membrane of many cell types, in particular the heart (Philipson and Nicoll, 2000). The NCX is a bi-directional exchanger which can operate as a means of both Ca^{2+} efflux or influx. The NCX utilises the electrochemical gradient of Na^{+} to mediate the counter transport of $3Na^{+}$ ions for $1Ca^{2+}$ ion (Reuter et al., 2005). The stoichiometry of the NCX is the exchange of $3Na^{+}$ ions to $1Ca^{2+}$ ion (3:1), although exchange ratios of 1:1 and

4:1 have been suggested (Iwamoto and Kita, 2004, Dong et al., 2002). The calcium efflux mode of NCX is referred to as the "forward mode", whereby NCX extrudes Ca^{2+} from the cytoplasm. It is generally accepted that under normal physiological conditions, the NCX works as a Ca^{2+} extrusion mechanism. Net Ca^{2+} efflux via the NCX is accomplished using energy derived from the Na^+ gradient set up by the ATP-dependent Na^+ pump (Li et al., 1994).

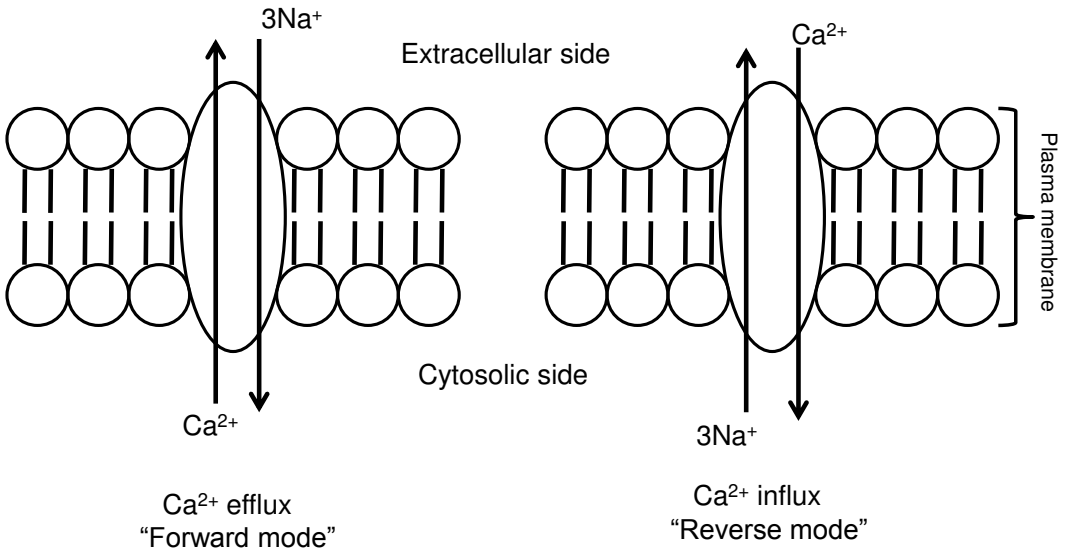

Figure 3.1. The sodium-calcium exchanger, a representation of Ca^{2+} efflux and Ca^{2+} influx modes.

Alterations in membrane potential or in Na^+ and Ca^{2+} gradients can initiate the "reverse mode" of exchange such that Ca^{2+} is transported into the cell, with Na^+ being extruded (Altimimi and Schnetkamp, 2007). Elevated $[Na^+]_i$ or reductions in $[Na^+]_o$ are reported to alter the mode of exchange from the forward to the reverse mode (Rathi et al., 2004). The NCX is also reported to operate in the reverse mode at membrane potentials of ~-40mV, however this is dependent upon Ca^{2+} and Na^+ concentration gradients. A visual overview of the "forward"

and "reverse" modes of NCX is shown in Figure 3.1. The structure of the NCX is shown in Figure 3.2.

The physiological role of the forward mode of the NCX has been well characterised in heart muscle. During cardiac excitation-contraction coupling, Ca^{2+} enters cardio myocytes upon membrane depolarisation through Ca_v1. VGCCs (Quednau et al., 1997); or via Ca^{2+} induced Ca^{2+} release. Following each cardiac contraction, Ca^{2+} is extruded via the NCX, ensuring cardiac relaxation and maintaining Ca^{2+} homeostasis (Reuter et al., 2005). The physiological role of the reverse mode of the NCX is less well characterised. Leblanc and Hulme (1990) proposed that Ca^{2+} influx via the NCX is involved in cardiac action potentials (Leblanc and Hume, 1990), however the function of the reverse mode of the NCX is well characterised under pathological conditions. For example, in ischemia associated reperfusion injury, there is an increase in cardiomyocyte $[Na^+]_{i.}$ This is suggested to induce $[Ca^{2+}]_i$ overload by the reverse mode of the NCX (Iwamoto et al., 1996b). Additionally platelets from diabetic patients exhibit abnormal Ca^{2+} homeostasis, which has also been suggested to occur as a result of Ca^{2+} influx via the reverse mode of the NCX (Li et al., 2001).

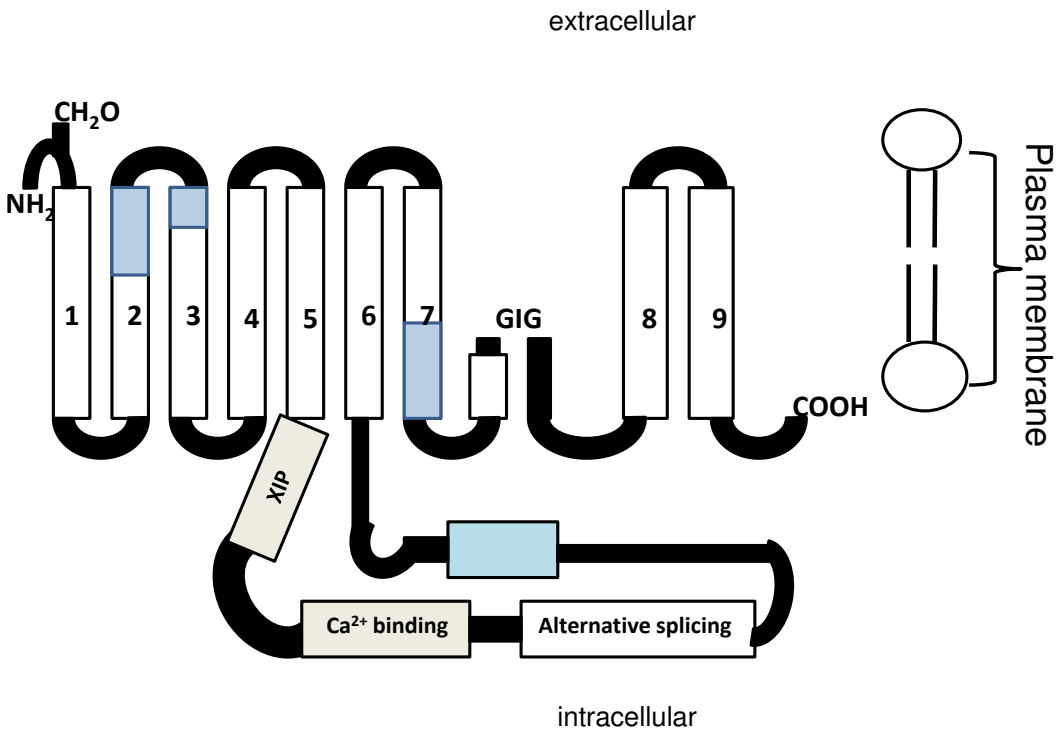

Figure 3.2. Model of the Na^+/Ca^{2+} exchanger, (adapted from Philipson and Nicoll (2000)). The NCX is modelled to comprise 9 segments. The N-terminus is glcosylated and located extracellularly. The α-repeat regions in transmembrane segments 2, 3 and 7 are represented by blue shading. Segment 6 has previously been suggested to be a transmembrane segment, however it is also suggested to be part of the large intracellular loop region (as represented by the shaded triangle). The XIP region, Ca^{2+} binding site and the region where alternative splicing occurs are all shown on the large intracellular loop. GIG represents a Glycine, Leucine, Glycine segment.

3.1.3 Voltage-gated Ca^{2+} channel structure

Structural knowledge of a protein aids supported hypothesis of biochemical function or molecular binding partners and their mode of interaction with the protein. Understanding protein interactions with its subunits, substrates, and regulators aids the identification of physiological function and cellular role of the protein, how it is regulated, and how expression and function may alter in a disease state. Structure prediction methods such as homology searches (Hanlon et al., 1999), hydropathy profiles and for some subunits, electron microscopy (Wang et al., 2004) and x-ray crystallography have been utilised to establish the

structure of VGCCs (Opatowsky et al., 2004, Van Petegem et al., 2004). Excellent general reviews on the structure and classification of VGCCs are available (Lipscombe et al., 2004, Catterall, 2000, Catterall et al., 2003a, Ertel et al., 2000) as only a brief summary will be presented in this introduction.

Multiple systems of classification exist for VGCCs. The first system of classification split the Ca^{2+} channels into two groups, high voltage activated (HVA) and low voltage activated (LVA). This system based on observations made through the utilisation of electrophysiological and pharmacological techniques. When Barium (~100mM) was used as a charge carrier in single-channel studies HVA channels activate at membrane potentials positive to ~-20mV and thus need to be subject to greater levels of depolarisation to activate (Catterall et al., 2003b, Jones, 1998). Members of the HVA channel family were first discovered in skeletal, smooth and cardiac muscles. HVA channels were named L-type channels as they had a LARGE and LONG-LASTING current, comprising a large single-channel Ca^{2+} conductance (~25pS) with slow current decay (Fox et al., 1987).

The next system of classification was based on the type of α_1 subunit the channel comprised of. The nomenclature of the α_1 gene products was based on their order of discovery. α_{1s} was the first channel isoform to be cloned within a laboratory, this was derived from skeletal muscle. α_{1A-} α_{1I} are subsequently discovered subunits, however this system of nomenclature was found to cause confusion as no identification of channel properties or structure is given (Catterall et al., 2003b, Catterall et al., 2003a). In 2000, Ertel *et al* (2000) suggested a system of nomenclature for VGCCs that was based on the channels structural relationships as well as conforming to the system of nomenclature used for other VGCC families, (i.e. Na^+ and K^+). Ca^{2+} channels were renamed such that the chemical symbol of the permeating ion was used in conjunction with the channels primary

regulator (e.g. voltage), denoted in subscript. The first numerical indicator identifies the order of discovery of the α_1 subunit within that α_1 gene family. In the instance where a splice variant of a particular channel needs to be identified, lower case letters are used (Ertel et al., 2000). An overview of Ca^{2+} channel nomenclature/classification is shown in Table 3.1, additionally the structure of VGCCs is shown in Figure 3.3.

Current Nomenclature	**Former Nomenclature**	**Ca^{2+} channel Classification**	**Generic Ca^{2+} channel classification**
$Ca_v1.1$	α_{1S}	L-type	HVA
$Ca_v1.2$	α_{1C}		
$Ca_v1.3$	α_{1D}		
$Ca_v1.4$	α_{1F}		
$Ca_v2.1$	α_{1A}	P/Q-type	
$Ca_v2.2$	α_{1B}	N-type	
$Ca_v2.3$	α_{1E}	R-type	LVA
$Ca_v3.1$	α_{1G}	T-type	
$Ca_v3.2$	α_{1H}		
$Ca_v3.3$	α_{1I}		

Table 3.1. **An overview of Ca^{2+} channel nomenclature and classification**. High voltage activated, HVA; Low voltage activated, LVA.

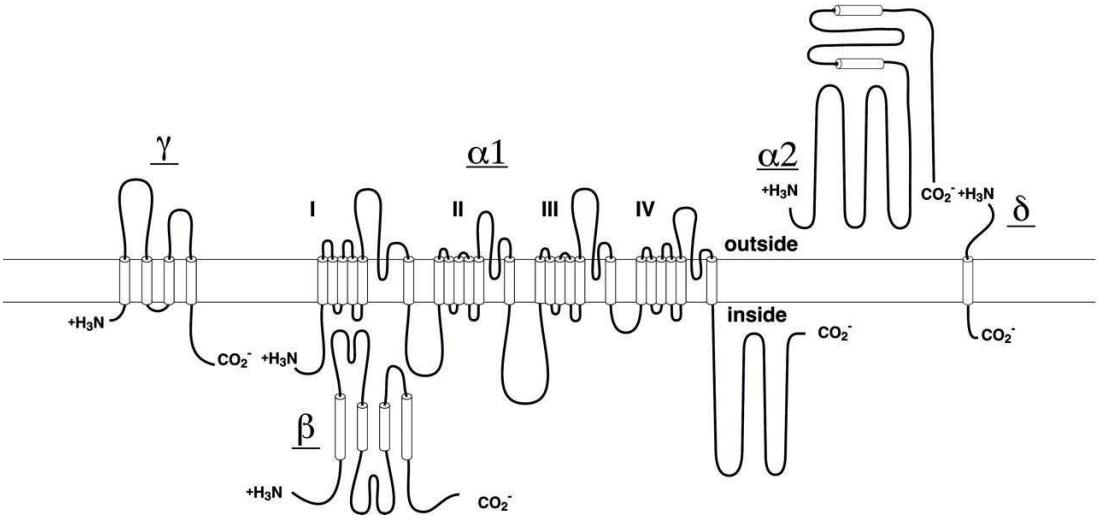

Figure 3.3. The subunit structure of VGCC channels, reproduced with permission (Catterall et al., 2005). The illustrated model depicts the subunit composition and structure of a skeletal muscle Ca^{2+} channel. Cylinders are representative of α helices. VGCCs are comprised of a transmembrane alpha subunit (190-250kDa), a regulatory cytoplasmic beta (β) subunit (52-62kDa), with gamma, delta and γ-subunits completing the complex, however the γ subunit is omitted in neuronal VGCCs (Catterall, 2000). The α_1-subunits incorporate the conduction pore, voltage sensor and gating apparatus, as well as the sites of regulation by drugs, toxins, and second messengers (Catterall et al., 2005). The VGCC protein is organised into 4 homologous domains (I-IV) with 6 transmembrane segments (S1-S6) within each domain. The membrane-spanning S4 segments of each domain are highly-conserved amphipathic helices, comprising of positively charged residues at every 3rd or 4th position (Catterall et al., 2005, Hui et al., 1991). The S4 segment of VGCC is the voltage sensor.

Sole expression of the α_1-subunit is sufficient for Ca^{2+} channel activity, however co-expression of the α_1-subunit with the $\alpha_2\delta$-subunit increases the surface expression of the channel, macroscopic current amplitude, and alters the voltage-dependence of channel activation/inactivation (Felix et al., 1997). More recently a role of the $\alpha_2\delta$-subunit in regulating the surface distribution of VGCCs in response to epigenetic cues has been suggested, also that these subunits aid association of the channel complex with lipid rafts, pertaining to areas of elevated VGCCs expression or "hot-spots" (Robinson et al., 2010). Lipid rafts are increasingly reported to be involved in protein compartmentalisation (Chini and Parenti, 2004, Hardie and Muallem, 2009). Lipid rafts are specialised microdomains which compartmentalise cellular signals by acting as a central point for the organisation

of signalling molecules. $\alpha_2\delta$ direction of channels to hotspots serves to amplify calcium signalling in accordance with local demand, as well as drive the VGCCs towards raft-associated proteins known to regulate channel activity, such as G-proteins and kinases (Robinson et al., 2010). However the role of $\alpha_2\delta$ in membrane targeting is controversial as some studies where $\alpha_2\delta$ was co-expressed with α_1 failed to yield channel expression on the cell membrane. Discrepancies may be attributed to the expression system used, however it is likely that the $\alpha_2\delta$ subunit cooperates with the β-subunit to ensure expression of the mature channel complex on the cell membrane surface (Herlitze et al., 2003).

β-subunits associate with the α_1-subunit via a high affinity interaction between a highly conserved motif of the I-II cytoplasmic linker of the α_1-subunit known as the alpha interaction domain (AID) and the guanylate kinase (GK) domain of the β-subunit (Pragnell et al., 1994, Karunasekara et al., 2009). The AID is located in the intracellular loop joining the first and second repeats of the α_1-subunit. β-subunit association with the AID within the α_1-subunit aids trafficking of the membrane protein to the cytoplasm (Jarvis and Zamponi, 2007) by binding to and antagonising an endoplasmic reticulum retention signal present on the intracellular loop I-II of the α-subunit (Herlitze et al., 2003). Functional $Ca_v\beta$s increase whole-cell current by increasing the number of channels expressed on the plasma membrane and by increasing their open probability (Po) (Dalton et al., 2005). Ca^{2+} channels expressed in Xenopus oocytes show greater whole-cell current amplitude and an increased number of drug binding sites when the α_1-subunit is co-expressed with the β-subunit (Herlitze et al., 2003). Rabbit CHO transformants comprising the α_1-subunit in conjunction with the β-subunit show a 100-fold increase in current amplitude and an increase in the number of DHP binding sites as well as improved DHP binding capacity (Nishimura et al., 1993). The interaction between the α_1 and β-subunits is reversible, indicating that the β-

subunit acts as a regulatory protein rather than a subunit. The β-subunit is unique in comparison to other auxiliary subunits by way of it being located entirely within the cytoplasm (Karunasekara et al., 2009).

Site-directed mutagenesis studies identified three essential residues within the AID required for the successful interaction of the α_1-subunit with the β-subunit (Hui et al., 1991). The mutations showed abolition of the coupling between α_1 and β and as a result also the β-subunit regulation of trafficking of α_1 to the plasma membrane.

To summarise, VGCCs are a diverse group of channels, their structural and function diversity is owed not only by the numerous genes and splice isoforms of the α_1-subunit, but also the association of auxiliary subunits. Post-translational modifications have a role in mediating channel function, adding further to the functional diversity of the channel by influencing its tertiary structure. Dysregulations in gene transcription and translation into VGCC channel protein can give rise to a disease state, as can altered regulation by substrates.

3.2 Regulation of voltage-gated Ca^{2+} channels

3.2.1 Regulation of voltage-gated Ca^{2+} channels by phosphorylation

Calcium current through VGCC channels is regulated by numerous hormones and substrates by way of second messenger induced channel phosphorylation. The most characterised second messenger system of VGCC phosphorylation is that of cAMP-dependent phosphorylation by protein kinase A (PKA), although phosphorylation by protein kinase C (PKC) and, more recently protein kinase D (PKD), have roles in the regulation of VGCCs.

The cardiac $Ca_v1.2$ channel is regulated by phosphorylation by PKA (Dai et al., 2009). Stimulation of this channel occurs via PKA and cyclic adenosine monophosphate (cAMP)-dependent mechanisms, as such this channel is heavily involved in the response to β adrenergic stimulation in the "fight or flight" response (Dai et al., 2009). $Ca_v1.2$ assembles with the β_2–adrenoceptor into a signalling complex with G_s protein, adenylate cyclase, PKA and PP2A. G-protein coupled receptors in the heart activate G-proteins which act as either stimulatory G_s or inhibitory G_i signals for adenylate cyclase (AC). Increased AC activity gives rise to elevated intracellular cAMP. cAMP binds to the regulatory subunits of PKA. cAMP binding to PKA releases the catalytic subunits which are then free to phosphorylate their channel substrates. PKA phosphorylation sites of functional importance as determined by observing a reduction in current upon mutation of said residues (serine to alanine) are located on both the $\alpha_{1\chi}$ (Ser1928) and β (Ser 459, Ser478, Ser 479) subunits. Not all β subunits have PKA phosphorylation sites; the PKA phosphorylation sites are conserved in β_2 splice variants with the exception of β_1 β_3 β_4 $\beta_{2\chi}$. Phosphodiesterase regulates the phosphorylation cascade via the degradation of cAMP to 5-AMP (Kamp and Hell, 2000).

PKA stimulation of VGCCs also occurs as a result of strong depolarisation. The voltage-dependent conformational change is suggested to expose phosphorylation sites coupling voltage-gating and phosphorylation of the Ca^{2+} channel (Catterall, 2000). Facilitation of this regulation requires PKA to be located in close proximity to the channel. In skeletal muscle, PKA is associated with the channel by an A-Kinase anchor protein (AKAP). AKAPs anchor cAMP-dependent protein kinase to specific substrates and cellular compartments, targeting kinases to intracellular sites, facilitating phosphorylation events close to their substrates. AKAPs comprise of a targeting domain, enabling direction to the appropriate cellular location, and a kinase-anchoring domain comprising an α-helix which binds to the

regulatory subunit of PKA. This regulatory mechanism is important in the regulation of the contractile force in skeletal muscle (Catterall, 2000). The association of AKAP is required for the β-AR regulation of $Ca_v1.2$ channels in cardiac myocytes (Gao et al., 1997).

Cardiac $Ca_v1.2$ channels are also regulated by the PKC kinases (classical cPKCs, novel nPKCs and atypical aPKCs) (Tafti and Hantash, 2008). PKC is stimulated by numerous pathways including; various G_q protein coupled receptors; α_1 adrenoceptors intracellular and extracellular ATP; glucocorticoids; arginine-vasopressin (McHugh et al., 2000); phospholipase C; and occasionally Ca^{2+} (Kamp and Hell, 2000).

Both the α and β-subunits are substrates for PKC phosphorylation. PKC phosphorylation sites on the α_{1c}-subunits are on the N-terminal domain at Threonine 27 and Threonine 31 (Kamp and Hell, 2000). Mutation studies, whereby threonine residues 27 and 31 were singly converted to alanine abolished the channels sensitivity to modulation by PKC, suggestive of a requirement for both sites to be phosphorylated in the regulation of channel activity (McHugh et al., 2000). Conversely threonines 27 and 31 are not involved in the regulation of the brain isoform of $Ca_v1.2$. $Ca_v1.2$ activity in rat myoblast L6 cells is shown to be both up-regulated and down-regulated by PKC activity depending on the isoform activated; nPKC isoforms are reported to enhance activity in the basal state whilst cPKCs are reported to inhibit basal channel activity (Tafti and Hantash, 2008).

Recently, PKD was shown to regulate the human cardiac $Ca_v1.2$ channel. Single-channel activity in HEK234 cells stably expressing $Ca_v1.2$ was observed in the presence of an active mutant of PKD. Current amplitude was unaltered in comparison to the control. Expression of the dominant-negative mutant of PKD saw significant reduction of calcium channel currents. Mutation studies identified

the functional target residues of PKD as being Ser1884 on the C-terminal domain of human $Ca_v1.2$. As currents were neither enhanced or reduced by PKD activity, a role of PKD regulation of channel activity in the basal state was suggested (Aita et al., 2011).

3.2.2 Regulation of voltage-gated Ca^{2+} channel by lipids

Lipids are increasingly being recognised as signalling molecules in their own right. However, in comparison to signalling proteins, lipids are harder to study due to technical difficulties (Hardie and Muallem, 2009). Lipid regulation of VGCCs is not fully understood, although there is growing evidence that phosphatidylinositol 4,5-bisphosphate (PIP_2) and free fatty acids regulate the activity of VGCCs. Arachidonic acid (AA) (polyunsaturated fatty acid) regulates the activity of α_1 VGCCs (Hardie and Muallem, 2009).

External application of AA inhibits VGCC current at both the single-channel and the whole-cell current level with IC_{50}s ranging from 1-10μM. Inhibition of channel activity in the presence of AA has been reported in skeletal ($Ca_v1.1$), smooth muscle and rat cardiac myocytes ($Ca_v1.2$) (Xiao et al., 1997), SCG neurons ($Ca_v1.3$), and recombinant $Ca_v1.3$ channel currents in HEK 293 cells. It has been suggested that AA maintains VGCCs in a closed state as opposed to an inactivated state (Roberts-Crowley et al., 2009).

3.3 Regulation of the NCX

3.3.1 Regulation of the NCX by Ca^{2+} and Na^+

In addition to its role as a transport substrate for the NCX, Ca^{2+} also has a regulatory role in the activation of the NCX. Regulatory Ca^{2+} binds to a high

affinity binding site within the intracellular loop region (Matsuoka et al., 1997) which contains 2 Ca^{2+}-binding domains. Conversely, high levels of cytosolic [Na^+] inhibits the NCX by facilitating Na^+-dependent inactivation (Iwamoto et al., 2004b, Dong et al., 2002, Lytton, 2007). Excised patch-clamp investigations demonstrated a time-dependent change in exchange currents when elevated (~100mM) Na^+ was applied to the cytosolic side of the membrane surface. Initially, a rapid outward Ca^{2+} current was observed which declined over a 20 second period to a steady state value amounting to ~10% of the original peak current amplitude. This time-dependent decline in outward current was attributed to Na^+-dependent inactivation (Chernysh et al., 2008). Amelioration of Na^+-dependent inhibition of the exchanger can be achieved by elevated concentrations of Ca^{2+} although the site of Ca^{2+} action is unclear. Additionally, ATP is also known to prevent Na^+-dependent inactivation of the NCX (Hilgemann and Ball, 1996). Different models of inactivation have been proposed, including exchanger inactivation following the binding of Na^+ to the intracellular transport site of the NCX. Alternatively, Na^+ has also been suggested to bind to a regulatory site distal from the Na^+ binding site (Lytton, 2007).

As mentioned above, ATP protects against Na^+-dependent inactivation, the proposed mechanism is by stimulating phosphatidylinositol-4,5-bisphosphate (PIP_2) synthesis (Hilgemann and Ball, 1996). PIP_2 is reported to bind to the exchanger inhibitory peptide (XIP) region of the exchanger (Figure 3.2). The XIP region is suggested to exert an auto-inhibitory function on exchanger activity following its interaction with a binding site located elsewhere on the exchanger. The precise location of the XIP binding site is not yet known, however it has been suggested to be situated within the central hydrophilic domain (Maack et al., 2005). $PIP_{2,}$ through binding to the XIP region of the exchange protein, prevents the auto-inhibitory action from occurring. In support of this hypothesis, mutation

studies conducted within the XIP region of the exchanger have demonstrated both enhanced and reduced susceptibility to Na^+-dependent inactivation (Matsuoka et al., 1997). When compared to the wild type NCX, an NCX mutant with an XIP corresponding to the mutant with increased susceptibility to Na^+-dependent inactivation was shown to bind PIP_2 with low affinity (He et al., 2000).

3.3.2 Regulation of the NCX by phosphorylation

NCX1 on rat smooth and cardiac muscle is phosphorylated by protein kinase C (Linck, 1998). PKC activation is reported to stimulate the NCX (Ballard and Schaffer, 1996, Zhang et al., 2006, Iwamoto et al., 1996a). Site-directed mutagenesis studies identified three phosphorylation sites for the regulation of NCX1 by PKC: Ser-249, Ser-250 and Ser-357. Additionally, deletion of the cytoplasmic loop in NCX3 mutants abolished responsiveness to phorbol 12-myristate 13-acetate (PMA), a potent PKC activator, implicating the cytoplasmic loop in PKC regulation of the exchanger (Iwamoto et al., 1998, Zhang and Hancox, 2009).

The involvement of PKA in the regulation of NCX is unclear. It has been established that that NCX plays an important role in the maintenance of Ca^{2+} homeostasis in the heart (Ballard and Schaffer, 1996), with β-adrenoceptor activation stimulating myocardial contraction and relaxation, which is suggestive of a role of PKA in the regulation of NCX1 (Zhang and Hancox, 2009). Conversely, a number of investigators also report a lack of β-adrenoceptor stimulation of NCX1 by isoprenaline, abrogating a role of PKA in NCX1 regulation (Main et al., 1997, Lin et al., 2006, Ginsburg and Bers, 2005). Discrepancies between investigations could be indicative of either a minor role of PKA in the regulation of

NCX1, or a secondary effect upon NCX regulation by way of alterations in $[Ca^{2+}]_i$ or $[Na^+]_i$ management (Ginsburg and Bers, 2005)

3.4 Inactivation of voltage-gated Ca^{2+}Channels

3.4.1 Ca^{2+}-dependent inactivation of voltage-gated Ca^{2+}Channels

Ca^{2+} is a ubiquitous second messenger, as such Ca^{2+}-dependent inactivation is an essential regulatory mechanism ensuring optimal $[Ca^{2+}]_i$. Ca^{2+}-dependent inactivation was discovered following the finding that Ca^{2+} channel inactivation is faster in the presence of Ca^{2+} than in the presence of Ba^{2+} or any other monovalent/divalent cation (Hering et al., 2000). Ca^{2+} dependent inactivation is considered as a means of negative feedback control, preventing excessive Ca^{2+} entry (Hofer et al., 1997). Cardiac $Ca_v1.2$ channels predominantly inactivate by Ca^{2+}-dependent inactivation, although they can also undergo voltage-dependent inactivation (Cens et al., 2006). Ca^{2+}-dependent inactivation determines the duration of Ca^{2+} current in $Ca_v1.1$-$Ca_v1.4$ channels (Catterall, 2000). These VGCC channels are usually subjected to fast Ca^{2+}-dependent inactivation and slow voltage-dependent inactivation (McDonald et al., 1994).

3.4.1.1 Time course of Ca^{2+} dependent inactivation

Ca^{2+}-dependent inactivation is a common property of $Ca_v1.2$, $Ca_v1.3$ and $Ca_v2.2$ channels (Liang et al., 2003). Ca^{2+} dependent inactivation can be induced by elevations in $[Ca^{2+}]_i$ of only a few micromoles. Ca^{2+} entry during a maintained depolarisation enhances Ca^{2+} channel closure. In instances of long-lasting membrane depolarisation (~1 second), channel inactivation follows a biphasic time course comprising of both "fast" and "slow" components. In multiple

investigations the fast component of Ca^{2+} channel inactivation was significantly reduced in external Ba^{2+}. The slow component remained unaltered, suggesting that the fast component of inactivation is Ca^{2+} mediated (Lin et al., 2012). The fast component of Ca^{2+} dependent inactivation occurs within 10's of milliseconds (Brehm and Eckert, 1978), (Neely et al., 1994). It has been proposed that the rate of Ca^{2+}-dependent inactivation is limited by the rate at which channel conformational changes can take place within the channel protein (Sherman et al., 1990).

Following Ca^{2+}-dependent inactivation channels are subject to additional closure by slow voltage-dependent inactivation (Hering et al., 2000), this occurs within ~100's milliseconds. Prior to opening channels have to recover from inactivation, if a pulse arrives before completion of inactivation, there will be a reduction in Ca^{2+} entry.

3.4.1.2 Mechanism of Ca^{2+} dependent inactivation

The majority of Ca^{2+}-dependent inactivation of a channel occurs via a reduction in the open probability of available channels (Po) (Hofer et al., 1997) with only a small proportion of Ca^{2+}-dependent inactivation occurring via an alteration to the open channel. Studies investigating $Ca_v1.2$ channels in HEK293 cells indicate that $[Ca^{2+}]_i$ inactivates 80% of this channel type (Lacinová and Hofmann, 2005). The remaining 20% of $Ca_v1.2$ channels available for opening were inactivated by Ca^{2+}-dependent and voltage-dependent mechanisms (Lacinová and Hofmann, 2005). The suggested Ca^{2+} site responsible for Ca^{2+}-dependent inactivation is an EF motif located in the α_1 subunit of the channel (Bernatchez et al., 1998). Ca^{2+} is suggested to bind with an interaction of 1:1 Ca^{2+} to binding site, with a reported K_i of ~4μM (Hofer et al., 1997). The helix loop helix (EF) Ca^{2+}-binding motif has

been located close to the IVS6 region of the α_1-subunit. In cardiac VGCC channels, it is suggested that this motif is responsible for Ca^{2+}-dependent inactivation (Hofer et al., 1997). Studies on the role of the S6 segment in $Ca_v1.2$ channel blockade by drugs by point substitution mutations in segments IIIS6 and IVS6 (from valine to alanine) show altered drug sensitivity to phenylalkylamines and 1,4 dihydropryidines along with altered inactivation kinetics in comparison to wild type $Ca_v1.2$. Ca^{2+} inactivation is susceptible to alterations in the composition of the intracellular domain linkers, highlighting the importance of the IIIS6 and IVS6 segments in Ca^{2+}-dependent inactivation. Ca^{2+} entry is determined by the following factors: membrane potential, the kinetics of Ca^{2+} channel opening, the kinetics of inactivation processes, and the kinetics of recovery form inactivation (Hering et al., 2000). Development and recovery from inactivation in Ca^{2+} channels are affected by structural changes in the α_1-subunit pore forming segments, intracellular loops and carboxyl (C) terminus. Auxiliary subunits and intracellular proteins also influence the inactivation process, in particular the β-subunit. In VGCCs β-subunits 1-4 produce different channel inactivation behaviours. β_2 produces slow inactivation β_1 and β_4 produce intermediate inactivation behaviour with β_3 producing fast inactivation. The modulatory effect of the β-subunit upon channel inactivation is dependent upon the alpha subunit isoform as β-subunit modulations in channel inactivation characteristics have not yet been observed in Ca_v1. Ca^{2+} channels (Walker et al., 1998).

It has been demonstrated that stimulation of β-adrenoceptors which instigate the phosphorylation of Ca^{2+}-dependent channels in a cAMP-dependent manner as a result of PKA activation, significantly reduces Ca_v1. Ca^{2+} channel inactivation. Inhibition of channel dephosphorylation also reduced Ca^{2+}-dependent inactivation (Rankovic et al., 2011). These findings indicate that phosphorylation of $Ca_v1.x$ Ca^{2+} channels maintain the channels in a state of high open probability and that

dephosphorylation of the channels may be involved in Ca^{2+}-dependent inactivation. Ca^{2+} can also activate the Ca^{2+}-dependent protein phosphatase calcineurin, which itself is regulated by the Ca^{2+} binding protein calmodulin. Calcineurin activation results in dephosphorylation and therefore inactivation of the Ca^{2+} channel (Armstrong, 1989). Other potential contributors/ mechanisms involved in Ca^{2+}-dependent inactivation are Ca^{2+} binding to an EF motif in the C terminal domain, Ca^{2+} binding to calmodulin a Ca^{2+} binding protein and Ca^{2+} binding directly to the channel (de Leon et al., 1995). Although as discussed above, the various motifs involved in Ca^{2+}-dependent inactivation have been identified, the structural rearrangement of the channel protein that occurs during the inactivation process is yet to be elucidated.

3.4.2 Voltage-dependent inactivation (VDI) of voltage-Gated Ca^{2+} channels

Channel inactivation by way of voltage is defined as the current decay that occurs during prolonged periods of depolarisation. Voltage-dependent inactivation regulates Ca^{2+} entry, preventing toxic Ca^{2+} overload under these circumstances (Cens et al., 2006). Neuronal $Ca_v2.1$ channels inactivate primarily by voltage-dependent inactivation although they can also inactivate by Ca^{2+}-dependent means. The kinetics of VGCC channel inactivation as studied using barium as a charge carrier in heterologous expression systems, have been investigated and compared across different channel subtypes (Hering et al., 2000). The inactivation sequence for VGCCs is as follows, from the fastest to the slowest: $Ca_v3.1$> $Ca_v2.3$>$Ca_v2.2$>$Ca_v2.1$>$Ca_v1.1$-$Ca_v1.4$ (Hering et al., 2000).

As with Ca^{2+}-dependent inactivation, the kinetics of Ca^{2+} channels are determined by the properties of both their α_1-subunits and the α_1-subunit interactions with

other channel subunits. Interaction of the α_1-subunit with the β-subunit, also influence inactivation properties. Chimeras created between non-inactivating $Ca_v1.x$ and fast-inactivating R-type rat brain Ca^{2+} channels have demonstrated that multiple structural domains are involved in voltage-dependent inactivation; substitution of linker region I-II and domain II &III S6 regions of $Ca_v2.3$ with $Ca_v1.2$ sequence, abolished inactivation implicating these regions II and III in voltage-dependent inactivation. A model of inactivation was proposed whereby the I-II linker forms a hinged lid which docks at domains II and III of the S6 region (Stotz et al., 2000), a similar mechanism to that observed during voltage-dependent inactivation in K^+ (Armstrong and Bezanilla, 1973, Murrell-Lagnado and Aldrich, 1993) and Na^+ channels (Kass, 2004).

Regulation of activation and inactivation of α_1 by the β-subunits are separate events (Olcese et al., 1994). The N-terminus of the β-subunit is one of the structural determinants important for setting the rate and voltage at which α_1 inactivates. One hypothesis is that the β-subunit interacts with a highly conserved sequence motif in the intracellular loop of $\alpha_{1,}$ that connects the first and second of the four repeat domains (Olcese et al., 1994). Another hypothesis is that the N terminus of the β-subunit may not interact with α_1, but rather set the special conformation of β so that other β-subunit motifs interact with α_1 (Pragnell et al., 1994). As with β-subunit activation of α_1, the rate at which α_1 inactivates is dependent on the β-subunit subtype (Ellinor et al., 1993).

Ca^{2+} channels undergo more than one conformational change during activation/inactivation. There is a slight delay prior to channel opening, with a sigmoidal time-course for the development of inward current upon depolarisation. The channel must pass through multiple closed states prior to opening (Jones, 1998).

3.5 Calcium channel / Exchanger pharmacology

3.5.1 Voltage-gated calcium channel pharmacology

Multiple VGCC channel types are present in mammalian cells. VGCCs differ in their voltage dependence, kinetics, and single-channel properties, they also differ in their pharmacology. Drugs and toxins are essential research tools for distinguishing between different classes of Ca^{2+} channel, especially in tissues which comprise more than one VGCC channel type, such as the neuron (Cena, 1998). A summary of current VGCC channel ligands is shown in Table 3.2. VGCC agonists and antagonists used in particular areas of research are summarised briefly in Table 3.3

Peptide voltage-gated Ca^{2+} channel ligands						
Blocker	Derived from	Block	Mode of action	Binding site	Reversibility	Reference
ώ-Aga-IVA	African Funnel Web spider (*Agenelopsis aperta)*	$Ca_v2.2$	Gating modifier Antagonism of voltage sensor movement	S_3-S_4 linker of α_1	Poor reversibility, channel activity can be recovered following repetitive depolarisation	(Mynlieff and Beam, 1992, Aosaki and Kasai, 1989)
GVIA ώ-conotoxin	Marine snail venom (*Conus geographus)*	$Ca_v2.1$ $Ca_v2.3$ $Ca_v3.1$, 3.2, 3.3	Occlusion of channel pore	Pore region of α_1 subunit		
Inorganic voltage-gated Ca^{2+} channel ligands						
Lead Copper Zinc Aluminium Cobalt Cadmium		Non-selective $Ca_v1.2$ IC_{50} 4μM	Physical Pore occlusion or surface charge screening altering gating properties			(Busselberg et al., 1994). (Lory et al., 1990)

Organic voltage-gated Ca^{2+} channel ligands						
Ligand	Classification	Blocks	Mode of action	Binding site	Reversibility	Reference

Nifedipine	DHP Antagonist	$Ca_v1.2$	DHP antagonists bind with high affinity to the inactivated state of the channel at depolarised membrane potentials ($\sim K_d$<1nM) than at hyperpolarised membrane potentials ($\sim K_d$ 10nM to 1μM).	The transmembrane segments IIIS5, IIIS6 and IVS6 of the α_1 subunit. Within these segments, single amino acid residues responsible for high affinity drug binding have been identified for the DHPs, PAAs and BZPs. It has been suggested that DHP and BZP binding sites are located in close proximity.	Yes	
Amlodipine	DHP Antagonist	$Ca_v1.2$			Yes	
Nitrendipine	DHP Antagonist	$Ca_v1.2$, $Ca_v1.3$			Yes	(Xu and Lipscombe, 2001)
Nimodipine	DHP Antagonist	$Ca_v1.2$ IC_{50} 139nM, $Ca_v1.3$ IC_{50} 2.7μM			Yes	(Xu and Lipscombe, 2001)
Bay K	DHP Agonist	Used as a research tool to enhance single channel activity of $Ca_v1.$, thus improving their detection	Stabilises the open conformation of the channel. No change in the IV relationship		Yes	(Fox et al., 1987)
Verapamil	PAA Antagonist	$Ca_v1.3$	Pore block from the intracellular side.		Yes	(Hockerman et al., 1997)
Desmethoxyverapamil	PAA Antagonist				Yes	
Methoxyverapamil	PAA Antagonist				Yes	
Diltiazem	BZPs Antagonist				Yes	

Table 3.2. A brief overview of Ca^{2+} channel ligands used in research

Ca^{2+} Channel	**Tissue expression of Ca^{2+} channel**	**Ca^{2+} Channel blockers used in research**	**Used in research for the following conditions:**
$Ca_v1.1$, $Ca_v1.2$, $Ca_v1.3$, $Ca_v1.4$	Neurons, endocrine, skeletal muscle, cardio vascular system	Dihydropyridines Phenylalkylamines, Benzothiazepines	Cardiac disorders
$Ca_v2.1$	Neurons	w-agatoxin IVA from spider, w-conotoxin MVIIC from marine cone snail.	Epilepsy, migrane symptoms
$Ca_v2.2$	Neurons	w-conotoxin MVIIA from marine cone snail, CVID from marine cone snail.	Pain
$Ca_v2.3$	Neurons	SNX-482 from tarantula	Diabetes symptoms
$Ca_v3.1$, $Ca_v3.2$, $Ca_v3.3$	Neurons, Smooth muscle, sinoatrial node	Nickel Ethosuximide, Zonisamide	Arrhythmias, epilepsy, pain

Table 3.3. Outline of Ca^{2+} channel blockers, the channels they are effective against and the areas of research in which they are used. Adapted from Mohan and Gandhi (2000).

3.6 Pharmacology of the NCX

Unlike VGCCs where selective inhibitors for various channel types have been identified (see Section 3.5.1), many NCX inhibitors used in research are not sufficiently selective to allow exchanger characterisation in intact cells. This is due to non-specific effects of NCX antagonists upon other transporter types (Annunziato et al., 2004). The NCX also operates in both Ca^{2+}-influx and Ca^{2+}-efflux modes, as such, blockade of the reverse mode of exchange may not confirm the presence of the NCX if it is operating in the forward mode. A summary of NCX inhibitors used in research is presented within Table 3.4

Inhibition of the reverse mode of the NCX does represent a novel potential therapeutic strategy to treat conditions of dysregulated Ca^{2+} influx, e.g. ischaemia-reperfusion injury, as demonstrated by preliminary investigations in animal models and primary tissue preparations of brain (Annunziato et al., 2004), heart (Feng et al., 2006, Takahashi et al., 2003, Magee et al., 2003) and kidney (Matsuda et al., 2005, Ogata et al., 2003). Clinical trials are currently not possible with NCX inhibitors, as currently available reverse-mode NCX inhibitors do not exhibit the required levels of selectivity and efficacy to permit such investigations (Toth et al., 2009). If the NCX is a Ca^{2+} influx pathway in white adipocytes, it is possible that dysregulated Ca^{2+} influx could occur by the reverse mode of the NCX. Inhibition of Ca^{2+} entry by NCX could also have applications in adipocytes. SN-6 and KBR-7943 were used in the current study to investigate the presence of NCX1 and NCX3 within primary white fat adipocytes.

Classification of NCX inhibitor	NCX inhibitor used in research	Isoform selectivity	IC_{50}	Inhibition upon mode of exchange	Reported inhibition upon other channel types	References
Inorganic Cation	Ld^{3+}, Mn^{2+}, Cd^{2+}, Ni^{2+}	NCX1 NCX2			VGCC	(Annunziato et al., 2004)
Amilioride Analogue	Amilioride	No isoform selectivity reported	1mM	Ca^{2+} efflux and Ca^{2+}influx modes	Na^+/H^+ exchange VGCC Na^+ channels	(Alvarez de la Rosa et al., 2000, Blaustein and Lederer, 1999, Annunziato et al., 2004)
Amilioride Analogue	Benzamil	No isoform selectivity reported	100μM	Ca^{2+}efflux and Ca^{2+} influx modes	Na^+/H^+ exchange	(Watano et al., 1996)
Amilioride Analogue	3,4-dichlorobenzamil	NCX1	17-30μM	$Ca^{2=}$ efflux and Ca^{2+} influx modes	$Ca_v1.1$-$Ca_v1.4$ VGCCs T-Type VGCCs	(Watano et al., 1996)
Peptide	XIP		K_i 0.1 to 1.0μM		Calmodulin	(Li et al., 1991, Annunziato et al., 2004)
Benzyloxyphenyl	SN-6	NCX1 NCX2 NCX3	2.9μM 16μM 8.6μM	Ca^{2+} influx Ca^{2+} influx Ca^{2+} influx	Non reported at concentrations up to 30μM.	(Iwamoto et al., 2004b, Iwamoto, 2004, Iwamoto et al., 2004a, Matsuda et al., 2001)
Benzyloxyphenyl	SEA0400	NCX1 NCX2	56nM 980nM	Ca^{2+} influx Ca^{2+} influx	Inhibition of Ca^{2+} influx observed in hepatocyte NCX knockouts.	(Reuter et al., 2002, Iwamoto et al., 2004a)
Benzyloxyphenyl	YN-244769	NCX3	18nM	Ca^{2+} influx		(Iwamoto et al., 1996b, Iwamoto and Kita, 2006)
Benzyloxyphenyl	KBR-7943	NCX3 NCX1 NCX3 NCX1	1.2-2.4nM >30μM	Ca^{2+} influx Ca^{2+} efflux	Inhibition of Ca^{2+} influx observed in hepatocyte NCX knockouts. @~30μM, $Ca_v1.1$-$Ca_v1.4$ VGCCs, Na^+ pump, voltage-dependent Na^+ channels, NCKX	(Reuter et al., 2002, Iwamoto and Kita, 2004, Iwamoto et al., 1996b)

Table 3.4. Brief overview of Na^+/Ca^{2+}(NCX) inhibitors used in research. VGCC, voltage gated calcium channel; XIP, exchanger inhibitory peptide; (2-[2-[4-(-nitrobenzyloxy)phenyl]-ethyl]isothiourea methanesulfonate), KBR-7943

3.7 Evidence for voltage-gated Ca^{2+} channels in white adipocytes

3.7.1 Experimental evidence for voltage-gated Ca^{2+} channels in white adipocytes

The presence and role of VGCCs in excitable cells is well-characterised, however to date the evidence for their existence in adipocytes is limited. There is no direct electrophysiological evidence for the presence VGCCs on the membrane surface of the white fat adipocyte. Elucidation of the presence of VGCCs on the membrane surface of the white adipocyte has been determined indirectly through the utilisation of intracellular fluorescent Ca^{2+} indicators such as aqueorin (Pershadsingh et al., 1989) or Fura 2 in conjunction with conditions of elevated extracellular K^+ (~30mM or higher). Conditions of elevated extracellular K^+ are used to probe for the presence of VGCCs, in a variety of cell types (Yaguchi and Nishizaki, 2010), including adipocytes. Elevations in extracellular K^+ depolarize the plasma membrane (Beigelman and Shu, 1972) by eradicating the outward K^+ gradient resulting in opening of the VGCCs and subsequent cellular Ca^{2+} influx. Reversal of any K^+-induced increase in $[Ca^{2+}]_i$ by VGCC specific antagonists such as nifedipine or nitrendipine ~10μM is also indicative of VGCC on the plasma membrane surface.

Initially, Draznin *et al* (1987) demonstrated that addition of 40mM K^+ to Fura-2 loaded primary adipocytes resulted in a significant increase in $[Ca^{2+}]_i$ which was ameliorated following addition of $Ca_v1.2$ Ca^{2+} channel blocker nitrendipine (25μM) (Draznin et al., 1987a). Subsequent studies by other groups in primary adipocytes confirmed these findings. Elevation of

extracellular K^+ from ~5.6mM to 30mM resulted in a significant increase of $[Ca^{2+}]_i$ (Gaur et al., 1996b, Kelly et al., 1989). A similar Ca^{2+} response to that induced by 30mM $[K^+]_o$ was observed upon addition of Bay K 8644 indicative of Ca^{2+} by VGCCs. The increase in $[Ca^{2+}]_i$ produced by 30mM K^+ was blocked upon addition of dihydropryidine VGCC antagonist nimodipine (100nM) (Gaur et al., 1998b). Concentrations of up to 60mM $[K^+]_o$ have been used to induce elevations in $[Ca^{2+}]_i$. Pershadsingh *et al* (1989) demonstrated a reversible and significant elevation in $[Ca^{2+}]_i$ in primary white adipocytes upon exposure to medium containing 60mM K^+. The effect of K^+ on $[Ca^{2+}]_i$ was blocked upon addition of VGCC antagonist diltiazem (10μM) (Pershadsingh et al., 1989). Radioligand binding studies carried out on purified adipocyte plasma membranes using [^{3}H]PN-200-110, (a dihydropryidine which binds the $Ca_v1.2$. Ca^{2+} channel α-subunit with high affinity Kd=~0.14nM (Dacquet et al., 1989)) and monoclonal antibodies raised against the α_1-subunit of L-type VGCCs purified from rabbit skeletal muscle demonstrated the presence of L-type Ca^{2+} channels in rat adipocytes (Gaur et al., 1998a) (Note study was conducted before the revised nomenclature for $Ca_v1.1$-$Ca_v1.4$ channels was established). Immunoassay procedures within the same investigation allowed detection of the β and α_2-δ VGCC auxhillary subunits (Gaur et al., 1998a). Contrary to the reports above, depolarising conditions of 70mM $[K^+]_o$, when applied to murine 3T3-L1 adipocytes, an established adipocyte model, did not induce a significant increase in $[Ca^{2+}]_i$; This observation was used in support of the argument against Ca_v1. VGCCs within this cell type (Yorek et al., 1999).

3.7.2 Functional evidence for $Ca_v1.3$ voltage-gated Ca^{2+} channels in white fat adipocytes

Ca^{2+} influx by $Ca_v1.2$/ $Ca_v1.3$ Ca^{2+} channels are implicated in insulin-stimulated glucose uptake in adipocytes. In radioactive glucose uptake studies, treatment of adipocytes with 30mM KCl decreased the half-maximal response to insulin stimulated 2-deoxyglucose (2-DOG), glucose transport by ~50%. On the contrary, treatment of adipocytes with ionomycin (3µg/ml), an ionophore which would cause Ca^{2+} influx independently of VGCC channels, did cause a significant increase in $[Ca^{2+}]_i$, however there was no reduction in insulin stimulated glucose transport (Kelly et al., 1989). Similar findings were observed by Draznin *et al* (1987b).

Insulin and growth hormone (GH) are reported to increase $[Ca^{2+}]_i$ in white adipocytes, with suggested Ca^{2+} influx through VGCCs. The elevation in $[Ca^{2+}]_i$ observed following preincubation of adipocytes with growth hormone (500ng/ml) for 3 hours was blocked following addition of 30µM verapamil or 100nM nimodipine, indicative of the Ca^{2+} entry occurring through $Ca_v1.2$/ $Ca_v1.3$ VGCCs (Gaur et al., 1996a). The insulin-induced increase in $[Ca^{2+}]_i$ is controversial. Draznin *et al* (1987) report an insulin-induced increase in $[Ca^{2+}]_i$ (Draznin et al., 1987a), which is inhibited following application of 25µM nifedipine. Other groups have not observed a $[Ca^{2+}]_i$ increasing effect of insulin (up to 20nM) (Kelly et al., 1989, Blackmore and Augert, 1989). In addition the dihydropryidine Ca^{2+} channel blocker amlodipine has been shown to improve whole body glucose tolerance in rats which had the insulin resistant state induced by cyclosporine (Yavuz et al., 2004).

3.7.3 Clinical evidence for voltage-gated Ca^{2+} channels in white fat adipocytes

An association has been demonstrated in a variety of paradigms between elevated Ca^{2+} influx through VGCCs and reduced insulin-stimulated glucose transport. This has been demonstrated in subcutaneous adipose tissue from the agouti mouse model (Kim et al., 1996), in 3T3-L1 adipocytes (Whitehead et al., 2001), and in primary rat adipocytes (Draznin et al., 1989). Evidence of amerlioration of exacerbated cellular $[Ca^{2+}]_i$ and improved insulin responsiveness has been demonstrated in insulin resistant men as those receiving treatment with nitrendipine, exhibited an improved glucose tolerance as determined by an oral glucose tolerance test. This has also been demonstrated in elderly (aged 65+) obese and hypertensive subjects (Byyny et al., 1992). Older hypertensive, and particularly older obese hypertensive, patients manifest significant insulin resistance when compared to normal body weight controls as determined by the 2-DOG uptake assay. Adipocytes from abdominal wall fat biopsy exhibited elevated $[Ca^{2+}]_i$ in all elderly subjects in comparison to those from young controls. Administration of 10mg nitrendipine twice daily for one month, restored adipocyte 2-DOG uptake to control values in hypertensive subjects (obese and normal weight). Oral glucose tolerance tests following nitrendipine therapy demonstrated restoration of plasma insulin to control values in obese hypertensive individuals (Beer et al., 1993, Byyny et al., 1992). Treatment of non-obese hypertensive subjects with amlodipine reduced plasma glucose levels, indicative of an improved insulin effectiveness despite insulin levels remaining similar prior to and post treatment (Harano et al., 1995).

3.8 Experimental aims

Calcium influx pathways within the adipocyte are poorly defined. The observation that application of $Ca_v1.2$ and $Ca_v1.3$ calcium channel blockers restore adipocyte responsiveness to insulin in vitro, as well as ameliorate insulin resistance in a clinical setting indicates a functional role of either, or, or both $Ca_v1.2$, $Ca_v1.3$ VGCCs in adipocytes. Additionally, The NCX has been shown to be an important Ca^{2+} pathway in numerous cell types (Blaustein and Lederer, 1999). To date there is only one published suggestion of NCX mediated Ca^{2+} influx in white fat adipocytes (Pershadsingh et al., 1989): although evidence supporting the existence of the reverse mode of the NCX has been demonstrated previously within this laboratory (Pulbutr, 2009). I aim to confer findings by others by exploring changes in $[Ca^{2+}]_i$ and routes of calcium entry with known pharmacological blockers of $Ca_v1.2$ and $Ca_v1.3$ channels and the reverse mode of the NCX, in the rat epididymal adipocyte. Elevated concentrations of $[K^+]_o$ have been used by other research groups, in conjunction with known pharmacological blockers of $Ca_v1.2$, $Ca_v1.3$ to determine the presence of this channel type on the adipocyte plasma membrane. I aim to confirm findings by others and determine whether conditions of 50mM $[K^+]_o$ is a suitable method to identify VGCCs in adipocytes. Investigations were conducted both at basal and following acute insulin exposure with the intention of identifying changes in $[Ca^{2+}]_i$ between the two conditions, as well as investigate the hypothesis that insulin does alter adipocyte $[Ca^{2+}]_i$ by attenuating Ca^{2+} influx from the extracellular environment.

3.9 Methods

All experiments were carried out using variations of a modified Hank's buffer solution that contained (in millimoles): 5.6 KCl, 138 NaCl, 1.2 NaH_2PO_4, 10 HEPES, 2.6 $CaCl_2$, 1 $MgCl_2$, 4.3 $NaHCO_3$, and 5 glucose, 0.1% (wt/vol) BSA (pH 7.4 with NaOH). For Ca^{2+}-free solutions, $CaCl_2$ was replaced by equimolar substitution with $MgCl_2$, total Mg^{2+} was 3.6mM. For the high potassium solutions, the concentration of KCl was elevated from 5.6mM to 50mM. This was osmotically compensated via a subsequent reduction in NaCl from 138mM to 94mM. All drug stocks were made in DMSO and diluted to the desired concentration in the appropriate Hank's buffer.

3.9.1 Adipocyte isolation and loading

Epididymal fat pads were excised from male Wistar rats, body weight (250-340g), fed ad libitum (Charles River Laboratory, Kent, UK). Rats were killed by stunning followed by cervical dislocation in accordance with UK Home Office guidelines. The white adipocytes were isolated from the epididymal fat pads using a modified version of Rodbell's procedure (Rodbell, 1964). The dissected fat pads were transported in Hank's solution containing 2.6mM Ca^{2+} (supplemented with 0.1% BSA (wt/vol) and 5mM glucose). To prepare the fat pad for dissection, it was placed in a Petri dish with Hank's solution. The eppididymis and major blood vessels were removed to reduce the likelihood of isolating other cell types along with adipocytes. The dissected fat pads were washed with Hank's solution to remove any residual blood or fur. Manually the fat pads were transferred (while cutting) to a glass vial containing 5mls of 0.5mg/ml type II collagenase (Sigma) in Hank's

supplemented with 0.01% wt/vol BSA and 5mM glucose. The fat pads were then minced with scissors until the fragments were approximately 1/2cm square.

The minced tissue was then transferred to a 25ml Nalgene conical flask. The scintillation vial was washed with a further 5ml of Hank's, this was also transferred to the conical flask, giving a final volume of collagenase of 10ml. Adipose tissue was subject to enzymatic digestion for 6-8 minutes at 37^{o}C in a Grant water bath (Griffin and George 896331), with agitation at 240 shakes per min Following digestion (ascertained by eye based on lack of tissue lumps and uniform milky consistency) the digest, followed by 50ml of Hank's solution, were filtered through a 250μM nylon mesh (Normesh limited, Oldham, UK). This diluted out the collagenase so that it was no longer active on the adipose tissue. Filtering the sample also removed any large lumps of tissue that were not digested in the previous step. The filtrate was collected in a 50ml syringe and adipocytes allowed to separate from the modified Hank's buffer for five minutes. The adipocytes, due to their high lipid content, float and form a visible white layer situated on top of the Hank's solution. This characteristic of the adipocytes aids in the isolation process as cell debris and other contaminating cell types present within the adipose tissue explants (fibroblasts, macrophages, stromal cells, monocytes and preadipocytes (Vazquez-Vela et al., 2008)) sink to the bottom. The infranatrant and debris were removed by drainage of the Hank's buffer. The adipocytes and the Hank's solution surrounding the adipocytes were retained and subject to washing with 50mls of the Hank's buffer. The process of draining, floatation and washing was repeated twice. After the final wash the adipocytes were resuspended in 10mls of Hank's BSA 0.01% (wt/vol) and placed in a Petri

dish, and kept at room temperature (21-22^{o}C). The adipocytes were taken immediately for imaging.

3.9.2 Plating

To image the adipocytes, they were plated onto glass cover-slips. Circular glass cover-slips, 13mm in diameter, thickness 0 (BDH biosciences 406/0189/10), were coated with 50µl poly-D-lysine (P7886; Sigma) at 100µg/ml in Dulbecco's PBS 1x (Na^{+} Mg^{2+} free). The poly-D-lysine was applied to the centre of the cover slip. The cover-slips were left to air-dry overnight. To attach the adipocytes to the cover-slips, the coated cover-slips were inverted and placed on a suspension of freshly isolated adipocytes, and left for ten minutes. The cover-slip with the attached adipocytes were incubated with Fluo 4-AM (at a final concentration of 1µM in 0.1% BSA (wt/vol), 5mM glucose, Hank's solution) for 30 minutes in the dark at room temperature (21^{o}C-22^{o}C). Loading was performed at room temperature to reduce the likelihood of dye compartmentalisation in accordance with the manufacturer's recommendations (Invitrogen). Prior to imaging, the cover-slip containing Fluo-4-loaded adipocytes was mounted in a bespoke perspex chamber with a glass floor. The adipocytes were washed by perifusion for 10 minutes in Ca^{2+}-containing Hank's solution. To perifuse the microscope chamber, solutions were gravity-fed through polythene tubing. A peristaltic pump was used to aspirate away the bath solution. All drug additions were made via bath perifusion. Exchange between solutions was performed using an electrically controlled two-way valve.

3.9.3 Imaging

To enable imaging of adipocyte $[Ca^{2+}]_{i,}$ adipocytes were loaded with the fluorescent Ca^{2+} indicator dye Fluo-4 AM (acetoxymethyl). Fluo-4 is an analog of Fluo-3 with the two chlorine substituents replaced by fluorines. Manufacturers report increased fluorescence excitation at 488 nm resulting in higher fluorescence signal levels (Invitrogen). Fluo-4 AM can be used at lower dye concentrations to generate the same fluorescence signal intensity (Gee et al., 2000). Lower loading concentrations and dye loading times of Fluo-4 AM make its use in cells a less invasive practice (Gee et al., 2000).

Cells loaded with Fluo-4 were imaged using an inverted Axiovert 135TV microscope (Carl Zeiss Ltd, Welwyn Garden City, UK) using continuous episcopic illumination. The light source was provided by a xenon arc lamp. To monitor changes in $[Ca^{2+}]_i$, cells were illuminated continuously throughout the experiment. The dye was excited at 485nm with the lowest light intensity that allowed binocular visualisation of the fluorescent signal when the observer was dark adapted. To reduce the risk of photo-bleaching, care was taken not to use a higher light intensity than necessary, i.e. within the lower limits of camera detection. Excitation light was prevented from interfering with the emission light through the utilisation of a 510nm long pass filter. Emission light was detected using a Photonics Science ISIS camera. Adipocytes were visualised using a x20 air objective lens. Live cell recordings were captured at 1 Hz using an 8 bit DT3155 frame grabber card and Imaging workbench software (INDEC Biosystems, Santa Clara, CA, USA).

3.9.4 Selection criteria for cell analysis

Fields of adipocytes for investigation were chosen based on the following criteria: an obvious adipocyte like structure (cygnet ring shape with a protruding nucleus); even dye loading, avoiding cells that looked punctuate (Punctuation is indicative of dye compartmentalisation within organelles); also with as many cells present in the field of view as possible. No preference was given to cells based on the following: cell size; group or single. Contamination by other cell types within the fat tissue (vascular smooth muscle, fibroblasts, and macrophages) was not observed within any of the adipocyte preparations, presumably having been efficiently removed during the adipocyte isolation procedure. Contaminating cell types can easily be identified as they have morphologies quite distinct from that of an adipocyte. Contaminating cell types are likely to be smaller in size, elongated, spindle like in shape.

3.9.5 Two point calibration

In order to ascertain the extent of fluorescence intensity change as a result of a change in intracellular calcium within an experiment, both the maximum and the minimum values of fluorescence had to be established for each cell within a particular experimental run. This was achieved by carrying out a two-point calibration which determined the maximum and minimum fluorescence values for the Fluo-4 indicator within each individual adipocyte. The maximum fluorescence value ($[F_{max}]$), i.e., the value of the calcium-saturated Fluo-4 indicator, was determined by perifusing Triton X-100 in increasing concentrations: 0.0125% (v/v), 0.025% (v/v), 0.05% (v/v), and

0.1% (v/v) in Ca^{2+} modified Hank's 0.01% (wt/vol) BSA. This was done to determine the "ideal" Triton X-100 response, whereby the fluorescence value would reach maximum value followed by a decline to the basal value. The concentration of Triton X-100 was not increased any further following observation of the maximum fluorescence value. The minimum value of fluorescence [F_{min}] was taken as the fluorescence of the Fluo-4 in the absence of extracellular Ca^{2+}, obtained by perfusion of the adipocytes with the calcium chelating agent EGTA (10mM).

The cellular Kd of Fluo-4 was taken as being 345nM (Takahashi et al., 1999, Gee et al., 2000, Paredes et al., 2008). Ca^{2+} indicators can be used to measure Ca^{2+} concentrations between the 0.1Kd-10xKd range (Paredes et al., 2008). However the Kd is variable and subject to environmental conditions including pH, and temperature. To keep these factors as uniform as possible, the pH and temperature of the buffers used were controlled as rigorously as possible. A thermocouple was used to set and monitor the temperature of the perifusion solution. It was assumed that the Fluo-4 bound to Ca^{2+} with a 1:1 stoichiometry, and also that the dye was predominantly located in the cytosol.

3.9.6 Analysis protocol and statistics

Using Imaging workbench 5.2, analysis regions of interest (Draznin et al.) were selected such that the first ROI (0) was always designated as the background. Subsequent ROIs were drawn around each adipocyte. The time-course and mean fluorescence intensity was then calculated for each cell.

The experimental data was further analysed using Microcal ORIGIN 5.0 (Microcal Software Inc., Northampton, MA). Macros were created (see Appendices for the macro scripts) to subtract the background fluorescence (ROI-0) for each cell, calibrate, and correct for linear trend. The macros were named Data and Calibrate respectively.

3.9.7 The data macro

The imaging workbench file comprises multiple data columns containing information pertaining to the fluorescence, the total pixel area and the total fluorescence for each cell. Only the initial value for the total pixel area per cell is used for the analysis as it was assumed that the size of the cell would remain constant throughout the protocol.

The background fluorescence was monitored through the course of the experiment and an average of the fluorescence background is subtracted from the average fluorescence for each cell. The average intensity per cell was ascertained by counting the magnitude of every pixel and then dividing by the number of pixels.

3.9.8 The calibrate macro

The raw fluorescence trace minus the background was displayed and cells were selected on the basis of having a Triton X-100 response. From all of the selected cells, a new trace was then displayed showing the average values for all cells. Two sets of timing were utilised, one to mark out the calibration timings. Using this information, the macro finds a minimum fluorescence value and subtracts it from each cell. This is the fluorescence that is left following Triton X-100 application in EGTA. We assume that this value is constant throughout the protocol and that the fluorescence left is inaccessible and not subject to change. The second set of timings allowed for correction of any linear trend. The calibration trace was then re-analysed, and the maximum fluorescence intensity value found, i.e., the dye saturation point with Triton X-100. Equation 3.1 was then utilised to determine $[Ca^{2+}]_{i.}$

$$[Ca^{2+}]_i = Kd \times \frac{(F - F\,min)}{(F\,max - F)}$$

Equation 0-1.1 Determination of $[Ca^{2+}]_i$. Calibration of a single wavelength indicator can be carried out following determination of the maximum and minimum fluorescence values of the indicator (Fmax +Fmin) in Ca^{2+} saturated and Ca^{2+} free following subtraction of the background fluorescence, Kd represents the equilibrium dissociation constant of the fluorescent indicator. The cellular Kd of Fluo-4 was taken as being 345nM (Takahashi et al., 1999, Gee et al., 2000, Paredes et al., 2008)

Measurements for $[Ca^{2+}]_i$ were taken after every change in the perifusion solution, following stabilisation of the $[Ca^{2+}]_i$ signal.

Graphpad PRISM version 5 software (Graphpad software, San Diago, California, USA) was used for statistical analysis. Data were subject to exclusion on the basis of the following criteria: If the basal $[Ca^{2+}]_i$ was

<50nM, or >300nM, if the adipocyte was unresponsive to the Triton X-100 calibration procedure; or if the $[Ca^{2+}]_i$ continuously decreased throughout the experiment, adipocytes that did not respond to extracellular Ca^{2+} removal were also excluded.

Data were output as $[Ca^{2+}]_i$, and expressed as mean ± S.E.M. For each protocol presented at least 3 different adipocyte preparations were used and "n" the number of adipocytes given as the sum total from these preparations. Normality testing was carried out for each experiment. Due to the non-parametric distribution of data, the Friedman's test was carried out with the Dunns post-test. Statistical significance was considered when $p<0.05$.

3.9.9 Optimisation

Attempts to carry out the experiments at 32°C (to model physiological conditions as closely as possible) were not successful due to loss of fluorescent signal. This could be attributed to either dye loss or loss of Ca^{2+} from the cell, possibly by an active transport mechanism. To test the possibility that the dye was being extruded by the multiple drug resistant transporter (MDR), adipocytes were loaded with a substrate for multiple drug resistant proteins, calcein AM (1μM) (Glavinas et al., 2004). Probenecid, a blocker of calcein transport (Webster and Carlstedt-Duke, 2002) did not show any improvement to signal retention within the adipocyte. Photo-bleaching was also considered a possibility, although the signal loss was not constant and stabilized at a $[Ca^{2+}]_i$ value of approximately 50nM. To account for the decline in fluorescence signal intensity, any linear trend was corrected for during the analysis. Experimental temperature was also investigated, and it

was determined that the fluorescent signal within the cell could best be maintained when the experiments were performed at 22^{o}C

3.9.10 Protein extraction and Western blots

3.9.10.1 Brain and heart sample preparation

Brain was dissected out of a male Wistar rat (weighing approximately 200-220g) and washed thoroughly in Hank's supplemented with 0.1% wt/vol BSA, to reduce blood contamination. Tissues were transferred to a fresh tube containing lysis buffer. The lysis buffer comprised, in mM Tris 20, EGTA 1, 1 NaF, 10 Beta glycerophosphate and 0.1% (v/v) Triton X-100 pH 7.6. One protease inhibitor tablet (Rigo et al.) was added per 10mls of buffer. Brains were weighed and typically 1g of tissue was added to 10ml of complete lysis buffer. Brain tissue was homogenised using a hand held homogeniser (Ultra-Turrax T18, IKA Laboretechnik, Germany) until a uniform consistency was obtained. Samples were assembled on a rotating wheel and spun for 1 hour at 4^{o}C. To separate the non-solubilised matter from the protein, the samples were centrifuged at 15,000g for 10 minutes at 4^{o}C. The supernatant was transferred to a clean microfuge tube, 50µl of this was kept for the determination of sample protein concentration. The remainder of the supernatant was re-suspended in lysis buffer.

3.9.10.2 Adipocyte sample preparation

Primary white adipocytes were isolated from the epididymal fat pads of Wistar, diabetic fatty Zucker and the lean control Zucker rats as described in Section 3.9.1. The excess Hank's buffer was removed from the adipocyte suspension. 500µl of packed cell volume was transferred to a 1.5ml microfuge tube and an equal volume of lysis buffer (as above) added. For

solubilisation, the samples were assembled on a rotating wheel and left to spin for 45 minutes at 4°C. To separate out the fat and non-solubilised matter, the samples were centrifuged at 15,000g for 10 minutes at 4°C. The upper layer of fat was removed and the supernatant containing the cell lysate was transferred to a clean microfuge tube, 50µl of this was aliquotted and kept for determination of sample protein concentration. The remainder of the supernatant was re-suspended in one fifth sample volume of a 6X concentrated stock of solubilisation buffer.

3.9.10.3 Lowry assay

To determine the protein content of all samples, the Lowry assay was carried out. Stock solutions of 1mg/ml bovine serum albumin in dH_2O were used to set up the standard curve. The dilutions are shown in Table 3.5.

Tube Number	Concentration of BSA (mg/ml)
0	0
1	0.05
2	0.10
3	0.15
4	0.20
5	0.25
6	0.30
7	0.35
8	0.40
9	0.45

Table 3.5. The dilutions of the 1mg/ml BSA stock used to create the standard curve for the protein assay. Each concentration was made up in a separate 1.5ml microfuge tube. A new standard curve was constructed for every sample set to be assayed for protein concentration. All standards and samples were assayed in triplicate.

The adipose protein samples were diluted 1:10 (20µl in 180µl dH_2O) to a total volume of 200µl. The control protein samples of brain and heart were diluted to 1:20 and 1:40. To prepare the Lowry AB solution 20mls of Lowry A (composition see Appendicies) was mixed with, 100µl NaK tartrate and 100µl 1% $CuSO_4$ were added. 1ml of Lowry AB solution was added to each standard and sample. The Lowry AB and sample/ standard mixture was incubated for ten minutes at room temperature. Following incubation, 100µL of 1:1 Folin reagent (Sigma): dH_2O was added to each sample and standard and the mixture immediately vortex mixed. 200µl of each sample and standard were transferred in triplicate into a clean 96-well plate. The plate was incubated at room temperature for 45 minutes. The plate was then read at 750nm with a Spectra MAX 340pc plate reader. Protein standard curves and sample concentrations were determined by the Softmax Pro software (Molecular Devices). All protein samples were diluted to equivalent protein concentrations (1mg/ml) using 1:1 solution of 1X solubilisation buffer and lysis buffer.

3.9.10.4 SDS-PAGE gels

Protein samples were denatured by being assembled on a heat block set to 95^{o}C for 5 minutes. Samples were vortexed and then centrifuged for one minute at 13,000rpm. Whilst sample preparation took place, 1X electrophoresis buffer was prepared by dilution of the 10X stock. 7.5% pre-cast SDS-PAGE gels (Lonza, 58501) were initially used in this study. Due to difficulties detecting protein at a loading concentration of 20µg/µl and a limited volume of 20µl with the pre-cast gels, home-made gels were utilised

instead. These had a maximum loading volume of 40µl, enabling loading of 40µg/µl of normalised protein sample.

3.9.10.5 Composition of SDS-PAGE gels

Gels were made according to the composition described in Table 2.6

Component	Stacking Gel (ml) 4%	Resolving Gel (ml) 7%
H_2O	4.880	8.160
30% acrylamide	1.040	3.680
Resolving gel buffer, 1.5M Tris-HCl		4.000
Stacking gel buffer, 0.5M Tris-HCl	2.000	
10% SDS	0.080	0.160
10% APS	**0.040**	**0.080**
TEMED	**0.008**	**0.016**
Total Volume	8.0	16.10

Table 3.6. The composition of 7% SDS polyacrylamide gels. Volumes stated above are for the preparation of two gels. Ammonium persulfate (APS), and tetramethylethylenediamine (TEMED) are shown in bold as these components were added to the gel mix immediately before casting.

Ammonium persulfate (APS) and tetramethylethylenediamine (TEMED) cause polymerisation of the gel and as such were added to the gel composition last of all. Gels were cast in a Bio-Rad Mini PROTEAN gel apparatus and overlaid with water-saturated butanol. Resolving gels were left to polymerise for 20 minutes. Following gel polymerisation, the saturated butanol was washed away with dH_2O. Residual water was removed by blotting (with filter paper) between the glass plates. APS and TEMED were added to the stacking gel mix, and this poured on top of the resolving gel. A 10-well 1.5mm Bio-Rad comb was inserted into the resolving gel in between the gel plates. The stacking gel was left to polymerise for 20 minutes.

The gels were locked into the gel holder and placed into the electrophoresis tank (Bio-Rad Mini PROTEAN). The tank was then filled with 1X electrophoresis buffer. To aid determination of the molecular weight of the proteins at a later stage, dual colour Bio-Rad precision plus protein standards ranging from 10kD to 250kD were utilised (cat no 161-0374). To load the samples and molecular weight markers into the gel, loading tips were used. The loading tips were always washed between sample loading by dipping the end of the tip into the electrophoresis buffer. This removes excess sample accumulation at the end of the pipette tip. Typically 1µl of molecular weight marker was loaded into the appropriate well. The control samples of heart and brain protein were loaded at 10-15µg/ul. Adipocyte protein concentrations were initially loaded at 20µg/µl. This was later increased to 40µg/µl for all adipocyte samples and 25µg/µl protein for the heart and brain samples. The gel was run at 200V for 40 minutes (Bio-rad PowerPac^{TM} 200) until the dye front had run to the bottom of the gel. The gel was removed from the cassette and carefully separated away from the glass plates.

3.9.10.6 Electrotransfer

In preparation of the transfer two pieces of pre-cut filter paper, two sponge pads, and nitrocellulose membrane were placed in cold transfer buffer; these were allowed to soak for 10 minutes. The stacking gel was removed from the resolving gel. To carry out the transfer all components were assembled as shown in Figure 3.4. After addition of each component, all bubbles were removed by using a roller.

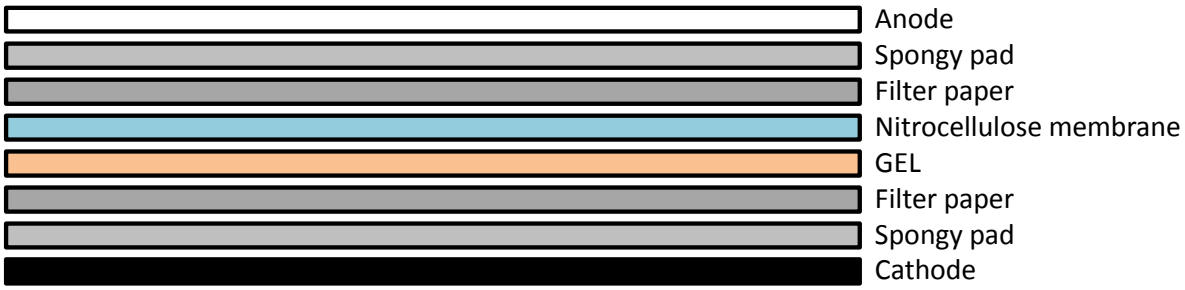

Figure 3.4. **The order of assembly of the Western blot transfer.** The black side of the cassette was placed down and the cassette opened out. All components were assembled as depicted above and the cassette locked.

Transfer of proteins from the gel to the nitrocellulose was carried out using the Bio Rad Mini PROTEAN apparatus with ice pack inserts. The tank was then filled with transfer buffer and transfer was performed for 1 hour at 100V. To assess the quality/ success of the transfer ponceau solution (0.1% (w/v) ponceau solution in 5% (v/v) acetic acid, Sigma) was added to the nitrocellulose membrane. The appearance of red bands was indicative of protein, and as such a successful transfer. The membrane can be cut at this stage to separate the blot up for incubation with different antibodies, or simply to remove any excess membrane. To de-stain, the membrane was washed with Tris-Buffered Saline Tween 20 buffer (TBST). Non-specific protein binding was reduced by incubating the membrane in 5% (v/v) Marvel dried milk in TBST at room temperature, on a shaking platform for one hour.

3.9.10.7 Antibody incubation

Due to the difficulties in extracting an appropriate amount of protein from the adipocyte samples, in particular those from Zucker rats (due to a noticeably increased amount of fat), samples were conserved as much as possible. This was achieved by cutting the membrane horizontally in 4 locations. Each

section was probed separately for the protein of interest and the β-actin loading control. Membranes were enclosed within custom sized heat-sealed bags. Primary antibodies were diluted in 5% (v/v) milk in TBST, and subsequently added to the bag containing corresponding membrane segments, and then sealed. Membrane segments were incubated overnight with shaking. Primary antibodies used within this investigation are shown in Table 3.7

Antibody	Supplier Cat no	Host Species	Band Size kDa	Working dilution	Species Reactivity	Blocking condition
$Ca_v1.3$ (a1D)	Alomone ACC-005A	Rabbit (polyclonal)	265	1:200	Mouse, rat	5% v/v milk TBST
β-actin	Sigma	Rabbit	42	1:20,000	Human, rat, rabbit	5% v/v milk TBST
(Na^+/Ca^{2+} exchanger) NCX1	Abcam Ab6495	Mouse (monoclonal)	120	1:200 -1:500	Mouse, rat, cow, guinea pig, rabbit	5% w/v milk TBST
(Na^+/Ca^{2+} exchanger) NCX3	Santa Cruz SC-48896	Goat (polyclonal)	64	1:200 Range (1:100-1:1000)	Mouse, rat, human	5% w/v milk TBST

Table 3.7. The primary antibodies used within this investigation.

The plastic bag containing primary antibody and the nitrocellulose membrane was cut. The primary antibody in 5% v/v milk TBST was poured into a universal tube and placed into the freezer for storage for re-use. (primary antibodies were used no more than 3 times). The membrane was placed into the glass dish where it was rinsed in TBST (Glass dishes were washed in 70% (v/v) IMS dH_2O). The membrane was then washed in TBST for 3 periods of 5 minutes, followed by 3 periods of 15 minutes in TBST. After washing, the infra-red dye labelled secondary antibody (Li-COR™) was diluted to 1 in 10,000 in 5% (w/v) milk in TBST. The Donkey anti-mouse 926-68072, goat anti-rabbit 926-68021 and donkey anti-goat 926-68074 (Li-COR™) secondary

antibodies were used as appropriate. The secondary antibody was added to the glass container containing the washed blot, and left to incubate at 37^{o}C, on a shaking platform for one hour. Following incubation with the secondary antibody the membrane the TBST washing steps were repeated. The membrane was then rinsed in dH_2O and taken for scanning with the Odyssey infrared imaging scanner, with the Odyssey software version 2.1 (LI-COR Bioscience, USA). Densitometry analysis was also performed using the Odyssey software. All data from independent protein preparations for each adipocyte sample type were expressed as the ratio to optical density values for the corresponding β-actin control.

3.10 Results

3.10.1 Adipocyte morphology and loading

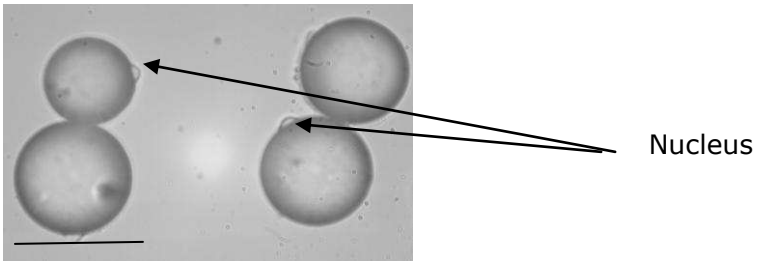

Figure 3.5. A representative image of primary white fat adipocytes isolated from rat epididymal fat pads. This is light microscope image of 4 adipocytes, taken at x20 magnification using an air objective lens. The distinct cygnet ring shape of the cell is characterised by the nucleus being pushed out to one side by intracellular lipid droplet which constitutes approximately 95% of the cells volume (Arner, 2005a). The scale bar represents 100μM.

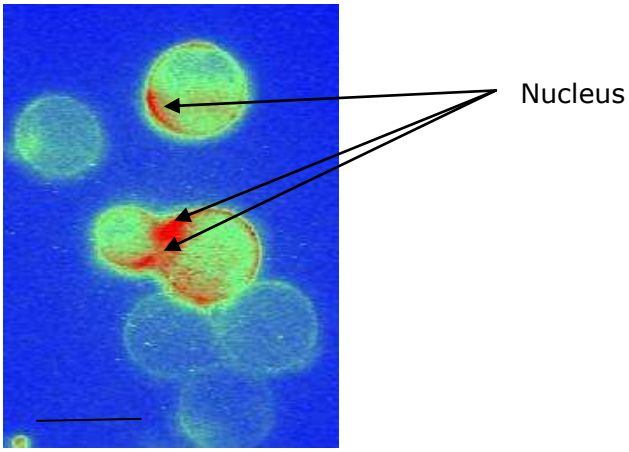

Figure 3.6. A representative field of Fluo-4 loaded primary white fat adipocytes. Viewed at x20 under an air objective lens. The image given is a pseudo colour image using a hot to cold look up table (LUT). The red colour is representative of high Ca^{2+} and / or dye content. The blue colour is indicative of the absence of Ca^{2+}/dye. The scale bar represents 100μM.

Figure 3.5 is a representative image of adipocytes, as observed following cellular isolation and plating onto glass cover slips. Figure 3.5 shows four adipocytes, all are roughly spherical in shape with a protruding nucleus.

Figure 3.6 shows a field of adipocytes comprising seven cells, following incubation for 30 minutes in Fluo 4-AM. The size, loading and location of the adipocytes varied within this population. These cells also have the typical spherical appearance characteristic of adipocytes. The nucleus nub as shown in Figure 3.5 is visible in 3 cells within Figure 3.6. The dark red region located to the side of the adipocyte is indicative of either a high $[Ca^{2+}]_i$ and/or dye content within this region. The cells are varied in the extent to which they are loaded. Some cells are brighter and more uniformly loaded than others. Analysis was carried out to ascertain whether the vicinity of the cell with respect to other members of the adipocyte population was a factor that would influence experimental outcome. No correlation was seen between adipocyte locale and likelihood of success of dye loading or responsiveness to Ca^{2+}. Adipocytes had an average calculated diameter of 78.8 ± 1.79μm with a mean cell volume of 268nL ± 16.85nL (n=43), Figure 3.7 shows that adipocytes used in this study had a median basal $[Ca^{2+}]_i$ of 118nM.

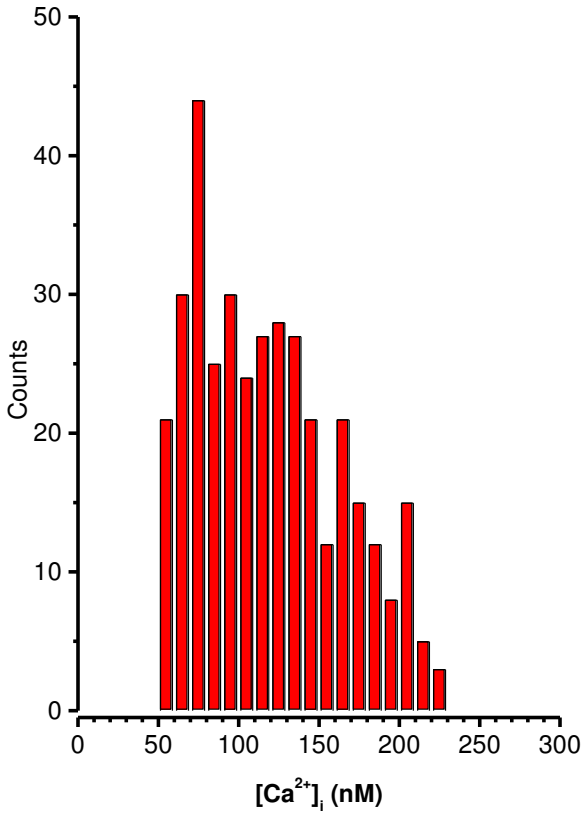

Figure 3.7. Distribution of basal $[Ca^{2+}]_i$ in adipocytes from all experimental protocols. Median $[Ca^{2+}]_i$ is 118nM (n=368). The distribution is not Gaussian, warranting the use of non-parametric statistical analysis. Also note the cut off at 50nM $[Ca^{2+}]_i$ in accordance with the exclusion criteria outlined in the materials and methods. Note, in subsequent figures the mean $[Ca^{2+}]_i$ is between 100 and 150, as determined by the mean for all basal $[Ca^{2+}]_i$'s recorded for each experimental protocol. Means are represented in subsequent figures to enable comparison with the published literature.

3.10.2 Adipocytes have functional Ca^{2+} influx pathways

To confirm the presence of Ca^{2+} influx pathways within white fat adipocytes, adipocyte responsiveness to changes in extracellular calcium concentration was investigated. It was hypothesised that upon removal of extracellular Ca^{2+} there may be a reversible decrease in $[Ca^{2+}]_i$, with $[Ca^{2+}]_i$ returning to basal levels following re-perifusion of extracellular Ca^{2+}.

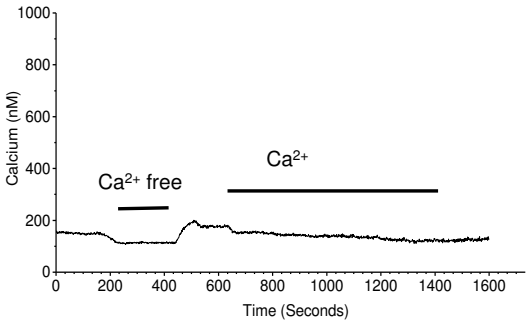

Figure 3.8. A typical background subtracted and calibrated $[Ca^{2+}]_i$ trace for an adipocyte displaying responsiveness to extracellular Ca^{2+} removal. Only one trace is shown for clarity, note a reduction in $[Ca^{2+}]_i$ upon perifusion of extracellular Ca^{2+} free at approximately 200 seconds, and a recovery of $[Ca^{2+}]_i$ upon re perifusion of extracellular Ca^{2+} at 400 seconds.

There was a mixed cellular response to extracellular Ca^{2+} removal/ reperfusion and the Triton X-100 calibration step at the end of the protocol. Correction for linear reduction in fluorescence intensity was carried out in adipocytes where applicable. Initially, only adipocytes that were responsive to extracellular Ca^{2+} removal and the Triton X-100 calibration step were taken for further analysis, giving rise to a trace as shown in Figure 3.8. Only adipocytes responsive to changes in extracellular Ca^{2+} are presented within this thesis as it was hypothesised that these adipocytes were viable and responsive to changes in $[Ca^{2+}]_o$. The level of $[Ca^{2+}]_i$ for the responsive cells was calculated on the basis of the maximum and minimum fluorescence intensity values for each individual cell. Values for $[Ca^{2+}]_i$ were taken from the time-course for each cell after each intervention following stabilisation of the Ca^{2+} signal. Responsive cells from at least 3 different adipocyte preparations were pooled and used for statistical analysis.

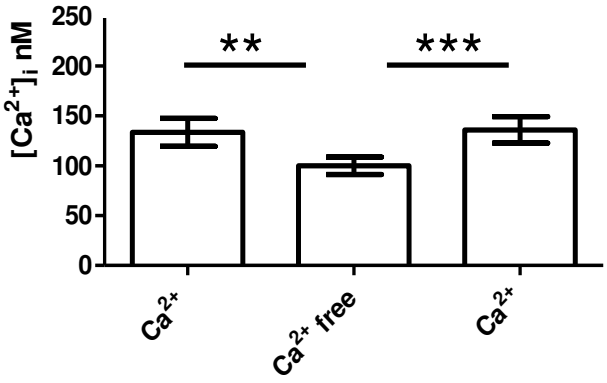

Figure 3.9 Shows adipocytes which are responsive to changes in extracellular Ca^{2+}. Background subtracted and calibrated data using adipocytes from at least 3 preparations, n=38 cells. The results show that Ca^{2+} influx and efflux pathways are present. When Ca^{2+} is removed from the extracellular media the $[Ca^{2+}]_i$ significantly decreases by 26%. Upon re addition of 2.6mM extracellular calcium in the perifusion media the $[Ca^{2+}]_i$ returns to the original baseline value. Data are presented as mean ± SEM (**P<0.01, ***P<0.001), Friedman's.

Figure 3.9 shows that the adipocytes used in this study are responsive to changes in extracellular Ca^{2+}, suggestive of the presence of calcium influx pathways.

3.10.2.1 Investigation into the presence of $Ca_v1.2$ and $Ca_v1.3$ VGCCs in white fat adipocytes

To test the hypothesis that the increase in $[Ca^{2+}]_i$ observed upon reperifusion of extracellular Ca^{2+} was by way of either $Ca_v1.2$ or $Ca_v1.3$ channels, adipocytes were exposed to 20μM nifedipine, (a dihydropryidine (DHP)), to screen for $Ca_v1.2$ VGCCs, and 20 μM verapamil, to screen for $Ca_v1.3$ VGCCs (Koschak et al., 2001, Xu and Lipscombe, 2001, Lipscombe et al., 2004).

In Figure 3.10a and 3.10b there was a significant reduction in $[Ca^{2+}]_i$ upon extracellular calcium removal P<0.05. This effect is reversible upon re-perifusion of extracellular Ca^{2+}. There is no significant effect of either

nifedipine or verapamil upon $[Ca^{2+}]_i$. To eliminate any confounding effect of the DMSO vehicle, the same perifusion protocol was repeated in the absence of blocker, with the DMSO (0.1 %v/v) vehicle only. Adipocytes responded to DMSO perifusion by a significant 28% increase in $[Ca^{2+}]_i$ when compared to recovering $[Ca^{2+}]_i$ values (Figure 3.11).

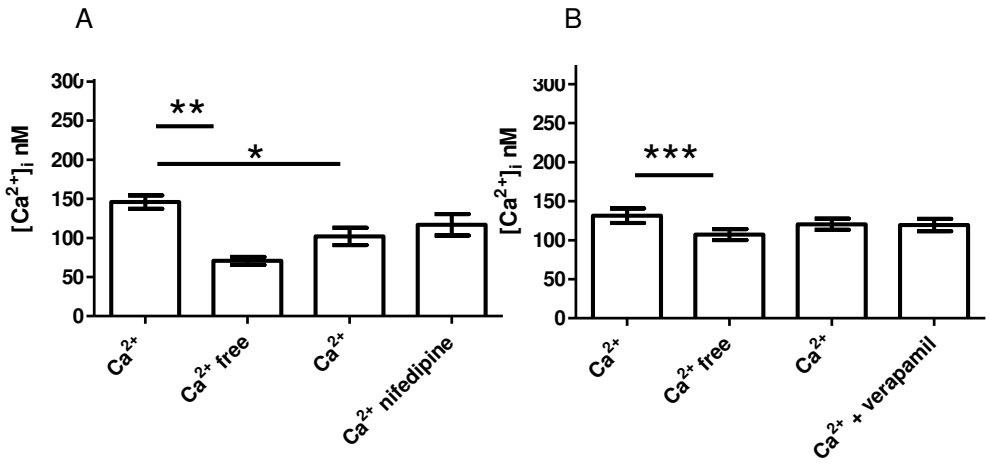

Figure 3.10. The effect on $[Ca^{2+}]_i$ of perifusion of $Ca_v1.2$ and $Ca_v1.3$ VGCC blockers. (A) nifedipine 20μM, (n=21) and (B) Verapamil 20μM, (n=22) is shown. Data are expressed as mean ± SEM (*P<0.05, **P<0.01, ***P<0.001) Friedman's.

Extracellular Ca^{2+} removal resulted in a significant reversible decrease in $[Ca^{2+}]_i$. In this instance, $[Ca^{2+}]_i$ incompletely recovers. Perifusion of DMSO significantly increases $[Ca^{2+}]_i$ by 22% when compared to recovering Ca^{2+}. The reason for the DMSO effect on increasing $[Ca^{2+}]_i$ was unknown. The extent of the change in Ca^{2+} due to the DMSO vehicle with nifedipine and verapamil were corrected for accordingly.

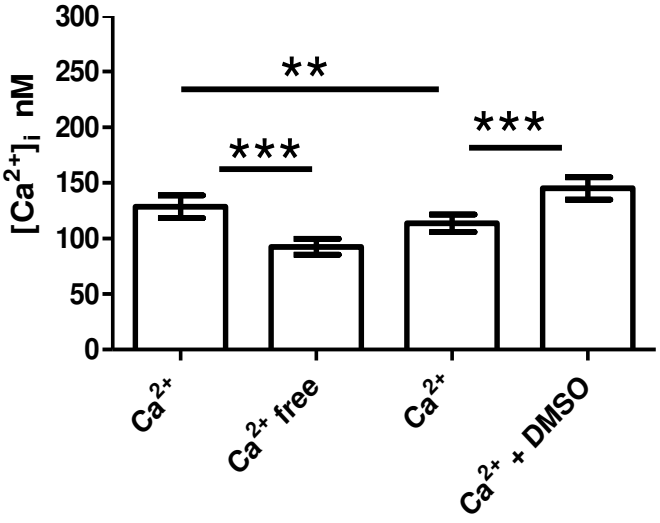

Figure 3.11. The effect on $[Ca^{2+}]_i$ of perifusion of 0.1%v/v DMSO (n=33). Data are expressed as an ± SEM (**P<0.01, ***P<0.001) Friedman's.

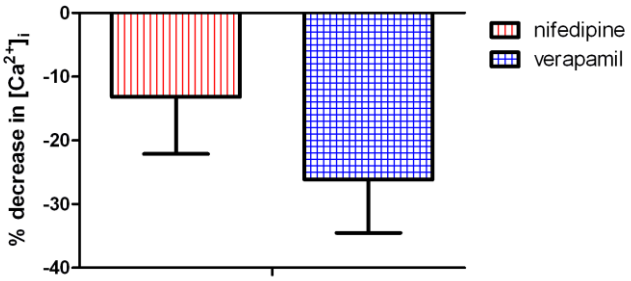

Figure 3.12. The effect of perifusion of the $Ca_v1.2$ blocker nifedipine, (n=23) and the $Ca_v1.3$ blocker verapamil (n=11) on adipocyte $[Ca^{2+}]_i$ levels, post correction for effect of the DMSO vehicle. Experimental data for this figure were sourced from Figure 3.10 and 3.11. Values are shown as % change in $[Ca^{2+}]_i$ when compared to recovering Ca^{2+}in the presence of the DMSO vehicle. The $[Ca^{2+}]_i$ levels in the presence of verapamil (mean=-26.1 ± 8.3) after correction for the DMSO vehicle effect is significantly different when compared to recovering $[Ca^{2+}]_i$ levels. Nifedipine (mean -13.18 ± 8.9) did not cause a significant reduction in $[Ca^{2+}]_i$. Data are presented as Mean ± SD.

Data were taken for correction for the effect of the DMSO vehicle from Figure 3.10 and 3.11. The inhibitor was included in the perifusion medium, providing constant exposure of the cells to nifedipine or verapamil during the course of

the experimental protocol. Ca^{2+} channels flicker on and off, as such it is likely that any open channels if they are $Ca_v1.2$ or $Ca_v1.3$ channels will be blocked. Following this correction verapamil (20μM) is shown to inhibit basal Ca^{2+} influx when compared to nifedipine (20μM) indicative of a role of $Ca_v1.3$ VGCCs in basal Ca^{2+} influx (Figure 3.12).

To investigate a possible role of $Ca_v1.2$/ $Ca_v1.3$ VGCCs, on Ca^{2+} re-entry in the white fat adipocyte, Ca^{2+} channel blockers were added in the absence of extracellular Ca^{2+}, prior to re-addition of extracellular Ca^{2+}.

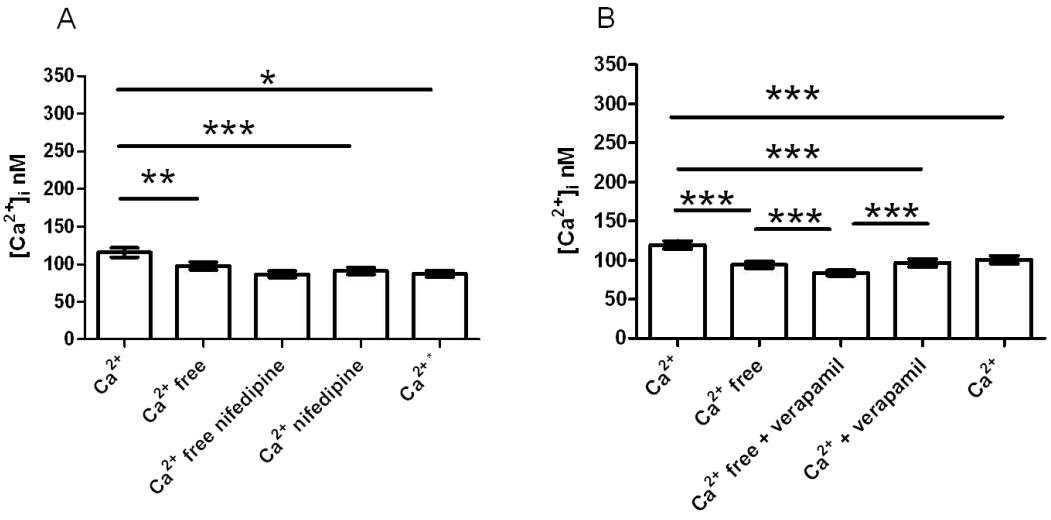

Figure 3.13. The effect of perifusion of 20μM VGCC blockers on Ca^{2+} re-entry in white fat adipocytes. (A) Nifedipine, (n=40) and (B) Verapamil (n=80) on Ca^{2+} re entry. Data are presented as mean ± SEM (*P<0.05, **P<0.01, ***P<0.001), Friedman's.

Figure 3.13A shows the addition of 20μM nifedipine had no effect on $[Ca^{2+}]_i$ in the absence of extracellular Ca^{2+}, however nifedipine irreversibly prevented $[Ca^{2+}]_i$ recovery upon re-perifusion of extracellular Ca^{2+}. Similar observations were made for 20μM verapamil (Figure 3.13B).

To investigate if $Ca_v1.2$/ $Ca_v1.3$ channels were open, the channel agonist Bay K 8644 was employed (Figure 3.14). When Ca^{2+} was removed from the

extracellular media, $[Ca^{2+}]_i$ decreased by 20%, whilst addition of Bay K 8644 had no effect on $[Ca^{2+}]_i$ in the absence of extracellular Ca^{2+}. Upon re-addition of 2.6mM extracellular Ca^{2+} in the perifusion media, $[Ca^{2+}]_i$ fully recovered, Bay K 8644 (1μM) had no significant effect on $[Ca^{2+}]_i$ in adipocytes in either the presence or absence of $[Ca^{2+}]_o$.

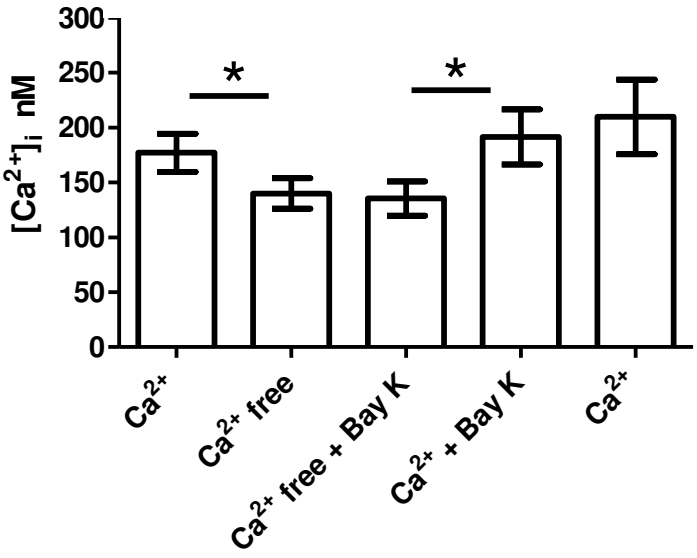

Figure 3.14. The effect of perifusion of 1μM Bay K 8644 on $[Ca^{2+}]_i$ in white fat adipocytes. The results are expressed as mean ± SEM (n=14), (*P<0.05) Friedman's.

To investigate any confounding effect of the DMSO vehicle the same perifusion protocol was carried out in the absence of any $Ca_v1.2/Ca_v1.3$ VGCC agonist/ antagonist with the DMSO (0.1%v/v) vehicle only. Figure 3.15 shows that there was no significant effect of DMSO in the absence of $[Ca^{2+}]_i$, or on its recovery on re-perifusion of extracellular Ca^{2+}.

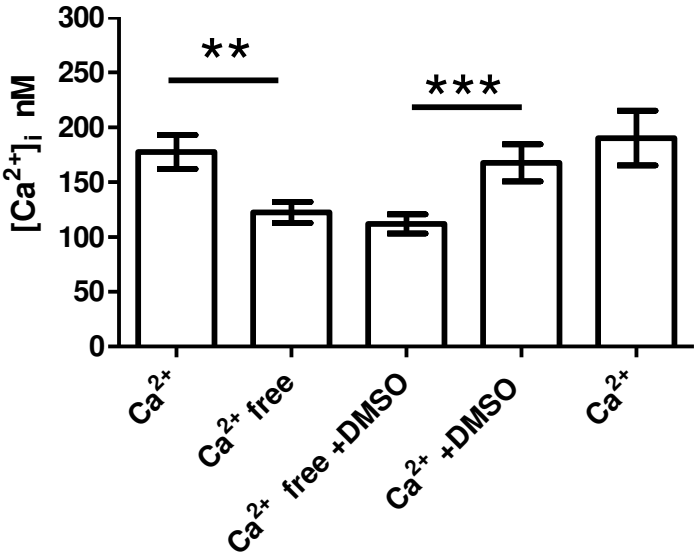

Figure 3.15. The effect on $[Ca^{2+}]_i$ of perifusion of 0.1%v/v DMSO. Data are expressed as mean ± SEM (n=25). (**P<0.01, ***P<0.001) Friedman's.

Subsequent experiments were carried out to investigate whether elevation of extracellular K^+, would elicit the presence of VGCCs. Conditions of high extracellular K^+ (50mM) are often used to probe for the presence of VGCCs, and have been used to do so in a variety of cell types (Yaguchi and Nishizaki, 2010), including adipocytes. Perifusion of 50mM K^+ did not significantly affect $[Ca^{2+}]_i$ of the total population (n=17). However, 58% (n=10) responded by exhibiting increased $[Ca^{2+}]_i$ of 18±4.3% upon K^+ perifusion. To determine whether a subset of the adipocyte population were exhibiting Ca^{2+} entry by VGCCs, the data for the K^+ responsive adipocytes were subject to further analysis. Of the adipocytes that did show an increase in $[Ca^{2+}]_i$ in response to 50mM K^+, there was no significant effect of verapamil (Figure 3.16B).

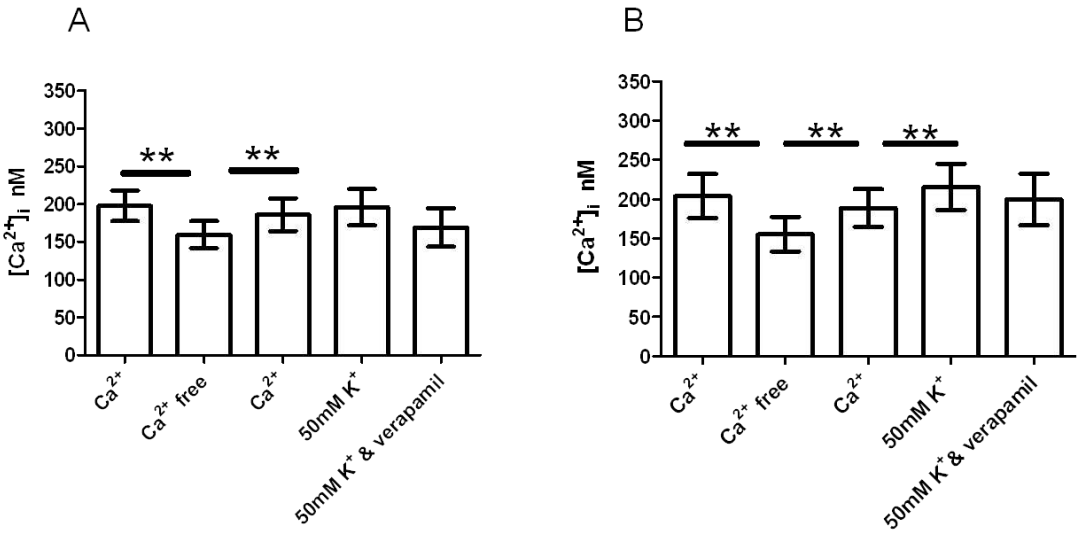

Figure 3.16. The effect of perifusion of 50mM K^+ on $[Ca^{2+}]_i$ in white fat adipocytes. All adipocytes are shown in A (n=17). In B, only adipocytes that responded to 50mM K^+ with a significant increase in $[Ca^{2+}]_i$ are shown (n=10). Data are expressed as mean ± SEM (**P<0.01, ***P<0.001) Freidman's.

Hyperinsulinaemic individuals exhibit insulin resistance (Shanik et al., 2008). Both insulin resistance and hyperinsulinaemia are associated with type 2 diabetes (Shanik et al., 2008). In vitro insulin resistance can be induced in isolated white rat adipocytes upon exposure to elevated concentrations of insulin (Marshall and Olefsky, 1980, Shanik et al., 2008). The effect of 30 minute acute insulin (100nM) application on $[Ca^{2+}]_i$ was then investigated.

In Figure 3.17A extracellular Ca^{2+} removal resulted in a mean decrease in $[Ca^{2+}]_i$ of -30% (P<0.005). $[Ca^{2+}]_i$ was restored to basal levels following re-perifusion of 2.6mM Ca^{2+}. Perifusion of 100nM insulin for 30 minutes did not result in a significant change in $[Ca^{2+}]_i$. 65% of the adipocyte population responded by increasing $[Ca^{2+}]_i$, 35% of the adipocyte population responded by decreasing $[Ca^{2+}]_i$.

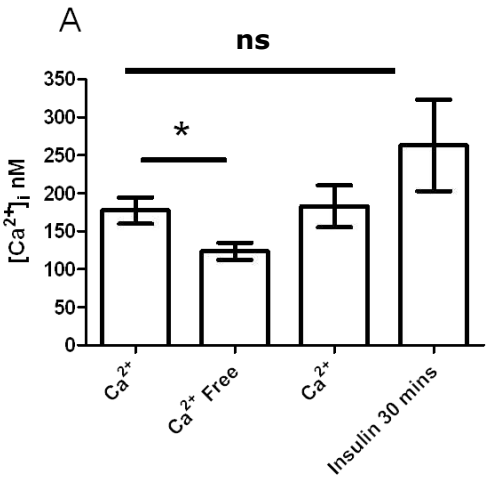

Figure 3.17. The effect of acute insulin exposure on $[Ca^{2+}]_i$ in white fat adipocytes. In A, the effect of perifusion of 100nM insulin for 30 minutes on $[Ca^{2+}]_i$, in adipocytes that are responsive to changes in extracellular Ca^{2+}. Data in A are expressed as mean ± SEM (n=17) (*P<0.05) Friedman's

Insulin had no effect on basal $[Ca^{2+}]_i$. Insulin did not affect the nature of response to extracellular Ca^{2+} removal (Figure 3.17). There was no significant difference in $[Ca^{2+}]_i$ pre and post insulin exposure. Furthermore perifusion of 20μM verapamil in insulin did not affect $[Ca^{2+}]_i$ in the absence of $[Ca^{2+}]_o$. $[Ca^{2+}]_i$ values returned to basal levels upon re-perifusion of $[Ca^{2+}]_o$ in the presence of insulin and verapamil. Removal of extracellular verapamil had no further effect on $[Ca^{2+}]_i$ (Figure 3.18).

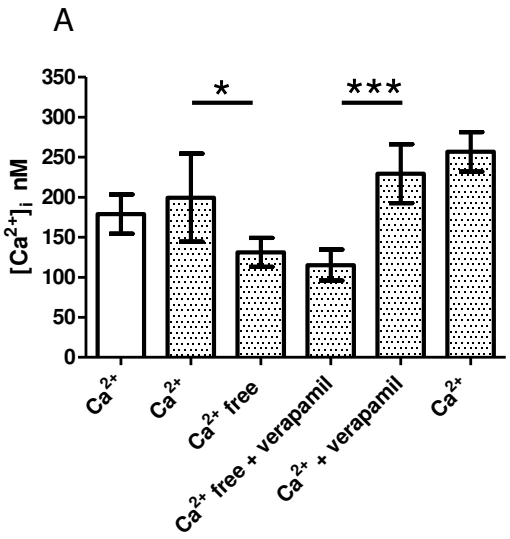

Figure 3.18. The effect of perifusion of 20μM verapamil in 100nM insulin on Ca^{2+} re-entry pathways in the white fat adipocyte (n=7). Shaded bars indicate the presence of insulin in the perifusion media. Data are expressed as mean ± SEM (*P<0.05, **P<0.01, ***P<0.001) Friedman's

Figure 3.19A shows that insulin had no effect on either the ability of 50mM $[K^+]_o$ to elevate $[Ca^{2+}]_i$, or the subsequent effect of verapamil at inhibiting Ca^{2+} influx. To ascertain, in the adipocytes that did respond by elevated $[Ca^{2+}]_i$ in 50mM extracellular K^+ whether Ca^{2+} entry was occurring by VGCCs, subanalysis were performed. Of the adipocytes that responded by an increase in $[Ca^{2+}]_i$ there was no significant effect of verapamil in insulin (Figure 3.19B).

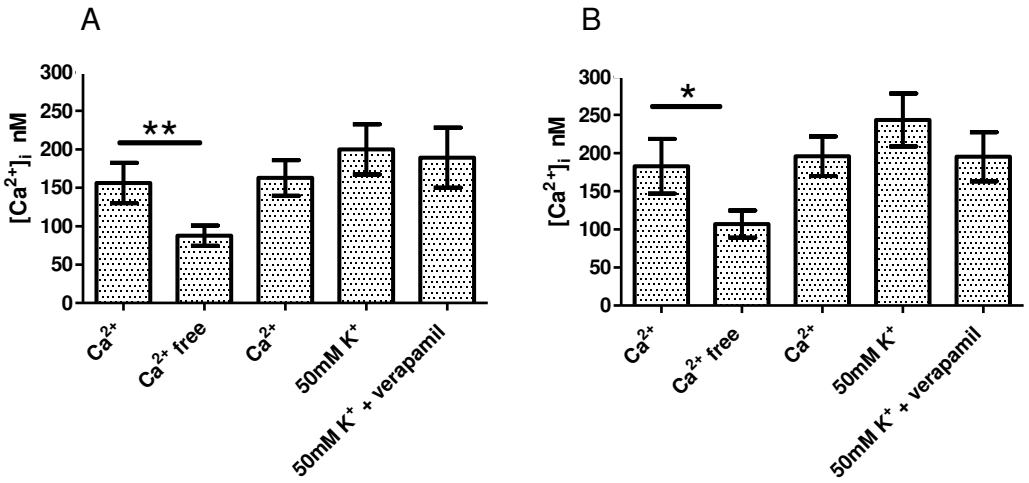

Figure 3.19. The effect of perifusion of 100nM insulin on $[Ca^{2+}]_i$ in the presence and absence of 2.6mM Ca^{2+} is shown. As is the effect of 50mM K^+ in the presence and absence of 20μM verapamil. Shaded bars represent the presence of insulin in the perifusion media. A shows all experimental data (n=11). B shows only adipocytes that responded to 50mM K^+ by an increase in $[Ca^{2+}]_i$ (n=8). Data are expressed as mean ± SEM (*P<0.05, **P<0.01) Friedman's.

In Chapter 2, it was demonstrated that elevated $[K^+]_o$ did not affect the Vm of white adipocytes. Reductions in $[Cl^-]_o$ were shown to depolarise the plasma membrane. As such, it was further investigated whether the presence of $Ca_v1.3$ could be elicited by depolarising the adipocyte plasma membrane with reduced $[Cl^-]_o$ and subsequent perifusion of verapamil.

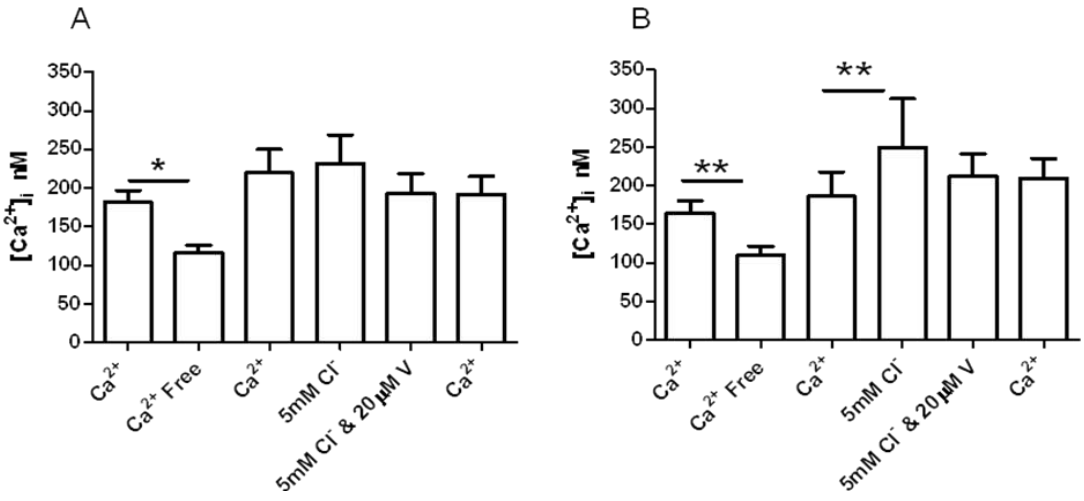

Figure 3.20. The effect of extracellular Cl^- reduction from 138mM to 5mM on $[Ca^{2+}]_i$ in the primary white fat adipocyte. A) shows all adipocytes tested, n=15. B) shows only the adipocytes that responded to extracellular Cl^- removal by increasing $[Ca^{2+}]_i$ n=12 out of 15. There was no significant effect of verapamil at reducing $[Ca^{2+}]_i$. Data are expressed as mean

Adipocytes were first subject to extracellular Ca^{2+} removal to confirm the presence and activity of Ca^{2+} regulatory mechanisms within this adipocyte population. Having ascertained adipocyte responsiveness to alterations in $[Ca^{2+}]_o$ ($P<0.05$, Wilcoxon), the concentration of extracellular Cl^- was reduced from 138mM to 5mM. No significant increase in $[Ca^{2+}]_i$ occurred. To ascertain the role of L-type VGCCs in the response to 5mM Cl^-, only adipocytes that responded by showing an increase in $[Ca^{2+}]_i$ in response to a reduction in extracellular Cl^- are shown in B, n=12 out of 15 ($P<0.05$ Wilcoxon). There was no significant effect of verapamil (V) (20μM) at reducing $[Ca^{2+}]_i$ levels in these adipocytes.

To test the hypothesis that the reverse mode of the NCX was acting as a Ca^{2+} entry pathway, adipocytes were exposed to reverse mode NCX inhibitors SN-6 and KBR-7943.

3.10.2.2 Investigation into the presence of the reverse mode of the sodium calcium exchanger in white fat adipocytes

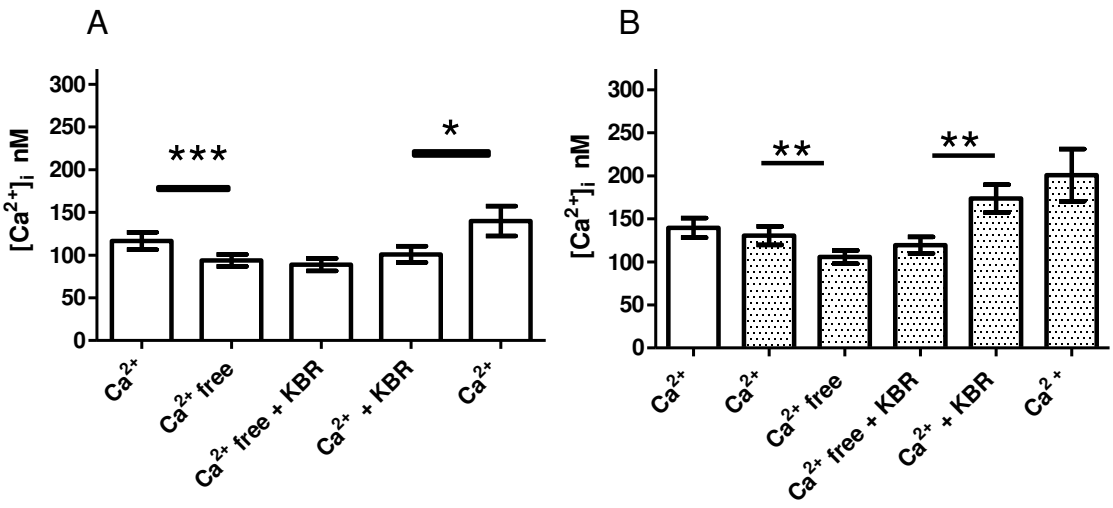

Figure 3.21. The effect of 10μM KBR-7943 upon Ca^{2+} re-entry within the white fat adipocyte. In (A) the effect of KBR-7943 in the absence of insulin is shown (n=18). In (B), shaded bars indicate the presence of 100nM insulin in the perifusion media (n=40). Background subtracted and calibrated data using adipocytes from at least 3 separate adipocyte preparations are shown. Data are expressed as Mean ± SEM (* P<0.05, **P<0.01, P<0.001) Friedman's.

In Figure 3.21 extracellular Ca^{2+} removal resulted in a significant decrease in $[Ca^{2+}]_i$, indicative of functional Ca^{2+} efflux pathways in the primary white adipocytes used within this investigation. In Figure 3.21, perifusion of 10μM KBR-7943 in the absence of extracellular Ca^{2+} did not affect $[Ca^{2+}]_i$. Re-addition of extracellular Ca^{2+} in the presence of KBR-7943 did not cause any significant increase in $[Ca^{2+}]_i$, with washout of KBR-7943 resulting in recovery of $[Ca^{2+}]_i$ to a value similar to that observed at the start of the perifusion protocol. Indicative of an inhibitory effect of KBR upon Ca^{2+} re entry in non insulin conditions.

In Figure 3.21B 100nM insulin was added to the perifusion media ~5 minutes into the perifusion protocol. $[Ca^{2+}]_i$ values did not differ in the presence or absence of insulin. Upon re-addition of extracellular Ca^{2+} there was no inhibitory effect of KBR-7943 on Ca^{2+} re-entry, as $[Ca^{2+}]_i$ recovered to a value similar to basal $[Ca^{2+}]_i$ with no further change in $[Ca^{2+}]_i$ on KBR-7943 washout.

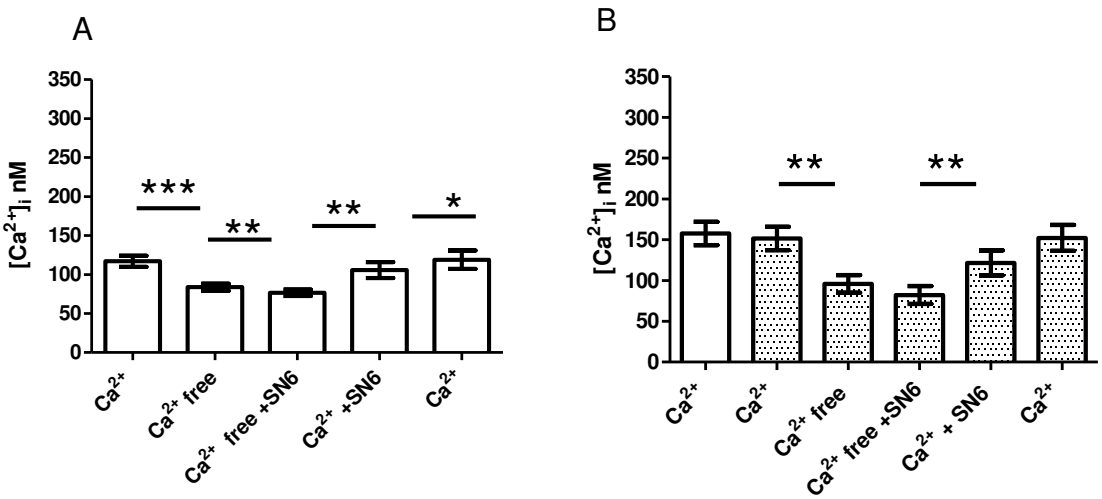

Figure 3.22. The effect of 10μM SN-6 upon Ca^{2+} re-entry within the white fat adipocyte. In (A) the effect of SN-6 in the absence of insulin is shown (n=39). In (B), shaded bars indicate the presence of 100nM insulin in the perifusion media (n=28). Background subtracted and calibrated data using adipocytes from at least 3 separate adipocyte preparations are shown. Data are expressed as Mean ± SEM (* P<0.05, **P<0.01, P<0.001) Friedman's.

In Figure 3.22 perifusion of SN-6 in the absence of extracellular Ca^{2+} resulted in a significant reduction in $[Ca^{2+}]_i$. SN-6 addition in Ca^{2+} free resulted in a further significant decrease in $[Ca^{2+}]_i$. Re-addition of Ca^{2+} to the perifusion media in the presence of 10μM SN-6 resulted in a significant increase in $[Ca^{2+}]_i$. Upon SN-6 washout, $[Ca^{2+}]_i$ significantly increased further, indicating a partial inhibitory effect of SN-6 upon Ca^{2+} re entry.

In summary adipocytes have functional Ca^{2+} influx pathways. Verapamil was shown to block basal Ca^{2+} influx, suggestive of the presence of $Ca_v1.3$ channels on the plasma membrane of white adipocytes. Conditions of elevated extracellular K^+ do not significantly increase $[Ca^{2+}]_i$. Acute insulin exposure does not increase $[Ca^{2+}]_i$. Additionally SN-6 and KBR-7943 were shown to inhibit Ca^{2+} re-entry in non insulin conditions, suggestive of the presence of the reverse mode of the NCX in white fat adipocytes.

3.11 The behaviour of the NCX at -30mV with extracellular Ca^{2+} concentrations of 2.6mM and 50µM.

To predict the direction of exchange of the NCX and $[ion]_i$ at -30mV for 2.6mM $[Ca^{2+}]_o$ and 50µM $[Ca^{2+}]_o$, Equation 3.2 was used.

$$E_{NaCa} = \frac{nE_{Na} - 2E_{Ca}}{n-2}$$

Equation 3.2. Equation describing the mode of exchange of the NCX (Stys et al., 1992). This equation was transformed to provide a model of the mode of exchange of the NCX at extracellular $[Ca^{2+}]_i$ concentrations of 2.6mM and 50µM. E_{NaCa}, E_{Na} and E_{Ca} are the reversal potentials of the exchanger, Na^+ and Ca^{2+} respectively, n represents the exchanger stoichiometry. In this instance the exchanger stoichiometry is assumed to be $3Na^+ : 1Ca^{2+}$, so n=3.

Figure 2.23 shows the expected equilibrium isotherms for Na^+ and Ca^{2+} under the different extracellular $[Ca^{2+}]_o$ conditions, $[Ca^{2+}]_o$=2.6 and nominally $[Ca^{2+}]_o$ free.

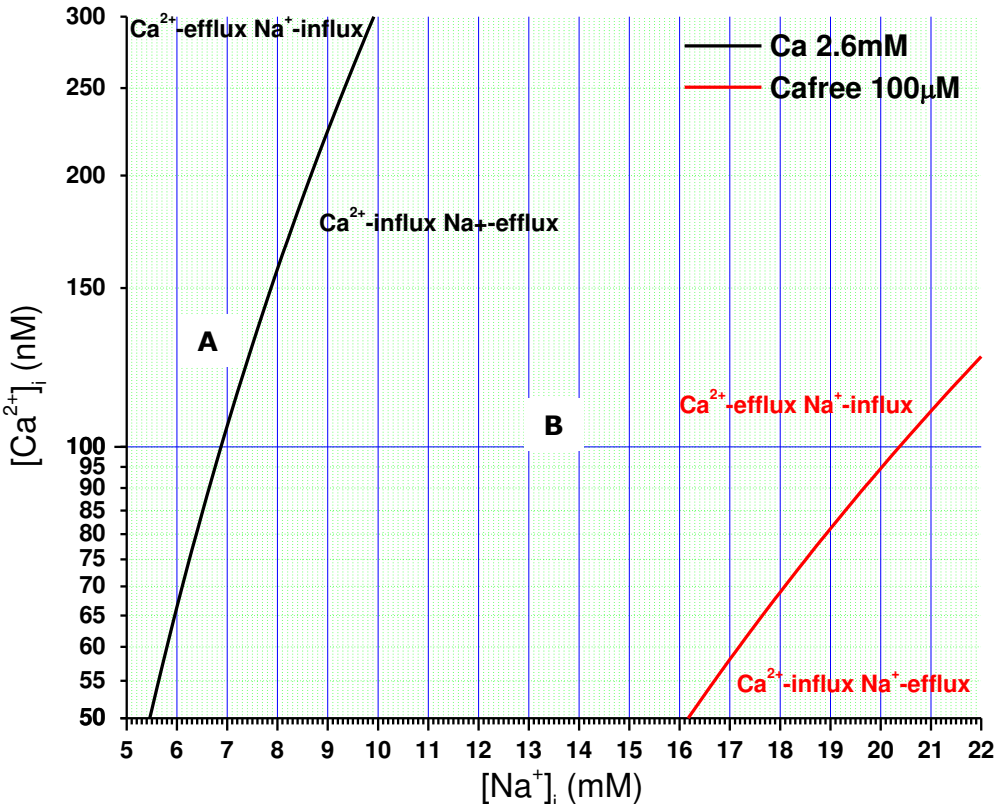

Figure 3.23. Steady state [ion]$_i$ in the presence and absence of extracellular Ca^{2+} at -30mV in white adipocytes. (A) In the presence of 2.6mM extracellular Ca^{2+} with a resting $[Ca^{2+}]_i$ of 120nM this model predicts $[Na^+]_i$ to be 7.3mM, at NCX equilibrium. When the extracellular buffer is switched to extracellular Ca^{2+} free the exchanger now operates in Ca^{2+} efflux mode and $[Na^+]_i$ increases. (B) Upon re addition of $[Ca^{2+}]_o$ as per the protocols in Figures 3.21 and 3.22 the exchanger will tend to increase $[Ca^{2+}]_i$ by operating in reverse mode, i.e. Ca^{2+} influx mode.

Figure 3.23 shows that at -30mV in 2.6mM $[Ca^{2+}]_o$ the NCX will operate in Ca^{2+} efflux mode, only when $[Ca^{2+}]_o$ is removed. When $[Ca^{2+}]_o$ is re-added the exchanger will then operate in Ca^{2+} influx mode. The higher the $[Na^+]_i$ value the more likely the exchanger will operate in reverse mode in 2.6mM $[Ca^{2+}]_o$ to result in Ca^{2+} influx.

The experiments in section 3.11.3 were carried out to confirm the presence of $Ca_v1.3$ and the NCX Ca^{2+} influx pathways in primary white adipocytes

3.11.1 Protein expression of the α_1 subunit of $Ca_v1.3$ voltage-gated Ca^{2+} channels in rat white adipocytes

Western blotting experiments were performed to explore the protein expression of the α_1 subunit of $Ca_v1.3$ adipocytes. An expected band of ~265kDa was detected by the $Ca_v1.3$ antibody (Alomone) in rat heart (positive control tissue) and in rat white adipose samples from Wistar, Zucker lean and Zucker obese rats. Due to antibody batch-to-batch variations and time constraints, only a limited number of immunoblots was obtained (n=6, Wistar; n=2, Zucker lean/obese), see Figure 3.23.

The intensity of the $Ca_v1.3$ protein bands was measured. β-actin was used as a loading control, as such $Ca_v1.3$ protein levels were normalised to β-actin. Data are expressed in terms of fold of heart tissue intensity. Due to the low n statistics cannot be performed to compare the protein expression of $Ca_v1.3$ in Zucker rats compared to Leans or controls, however the figure has been included as an indicator of $Ca_v1.3$ expression between the Zucker rats, the lean controls and the Wistars. The expression of the α_1 subunit of $Ca_v1.3$ in Zucker obese rats appears to be less than half of the expression levels observed for the Wistars or the Zucker leans, suggestive of a reduction in $Ca_v1.3$ α_1 subunit expression in adipocytes from obese rats (Figure 3.24).

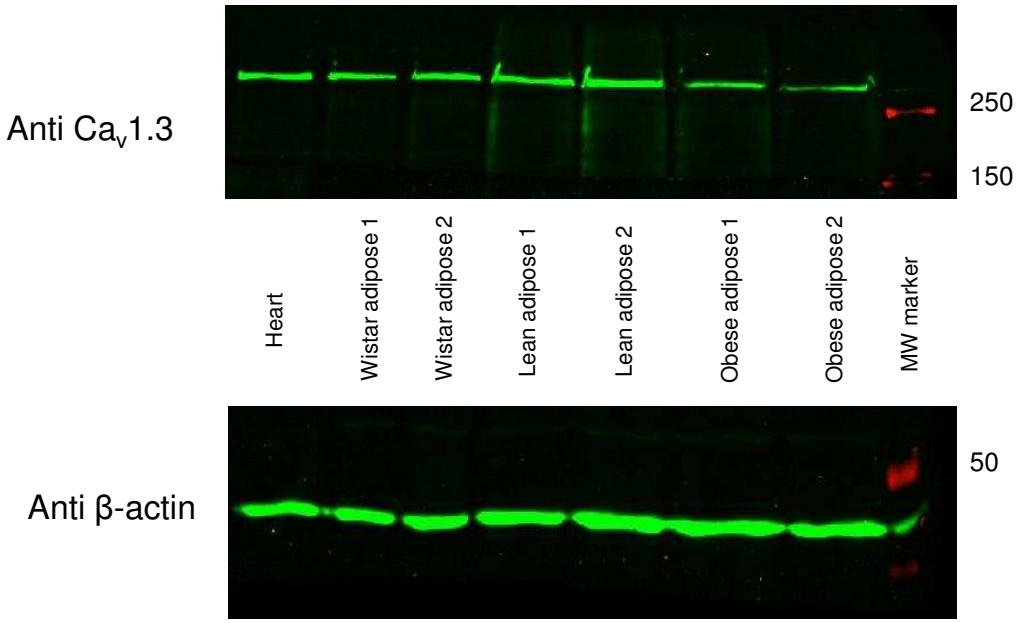

Figure 3.24. Representative Western blot of $Ca_v1.3$ and β-actin expression in heart, and in white adipocytes from Wistar, Zucker Lean and Zucker obese rats. Protein sample of 25µg was loaded for heart, and 40µg for each adipocyte sample. Only the upper portion of the blot is shown, to conserve the samples, the mid and lower portions of the blot were probed for the presence of NCX1 and NCX3.

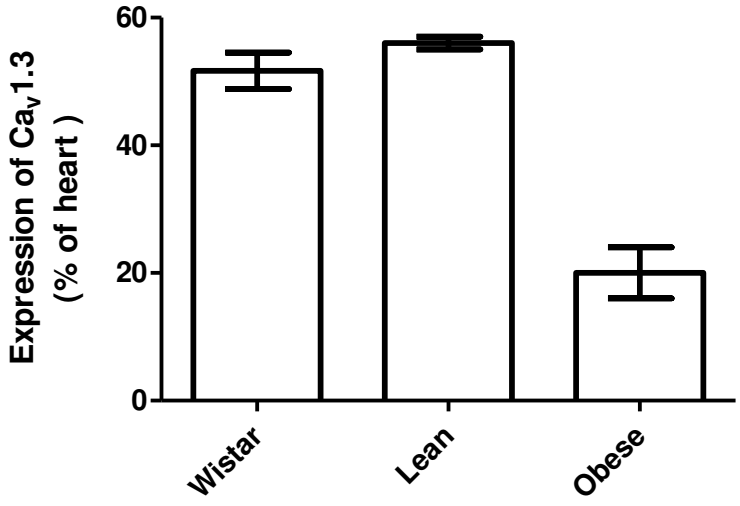

Figure 3.25. Expression of the α_1 subunit of $Ca_v1.3$ in, Wistar, Zucker obese and Zucker lean control rats. The protein levels of $Ca_v1.3$ (at ~265kDa) were normalised to β-actin and shown as a % expression relative to heart. Data are expressed as mean ± SEM for the Wistar sample (n=6). For the Zucker Lean and Obese samples data are expressed as the mean and range (n=2).

The specificity of the primary antibodies were examined, by probing the protein samples in the absence of primary antisera, (Figure 3.26), no non-specific binding was detected.

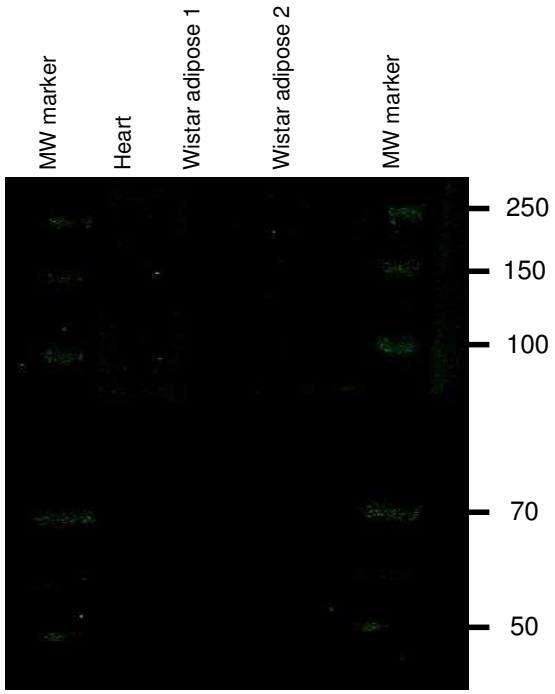

Figure 3.26. Representative non primary control of $Ca_v1.3$ and β-actin expression in heart, and in white adipocytes from Wistar rats. (Samples were loaded with 25μg protein for heart and 40μg protein for each adipocyte sample). Samples were incubated without primary antibodies, followed by green anti rabbit secondary antibody at 1:10,000 dilution for 1 hour at 37°C.

In summary, the presence of the α_1 subunit of $Ca_v1.3$ had been confirmed in primary white adipocytes from Wistar rats, although further experiments are required to confirm the reduction in $Ca_v1.3$ expression observed in adipose protein samples from obese Zucker rats, when compared to Wistars and Zucker leans.

3.11.2 Protein expression of NCX1 and NCX 3 in rat white adipocytes

Western blotting was performed to confirm the protein expression of both NCX1 and NCX3 in primary white fat adipocytes. Rat heart was used as the positive control for the detection of NCX1 (Ankorina-Stark et al., 2002) and rat brain for the detection of NCX3 (Ankorina-Stark et al., 2002). The expected band size for NCX1 according to Manufacturers was 120kDa, a band of ~130kDa was detected in the brain sample but not in the heart or adipose tissue samples. No bands of the expected size in accordance with the manufactures guidelines (Santa Cruz) ~64kDa were detected for NCX3 in any of the tissues investigated (Figure 3.27).

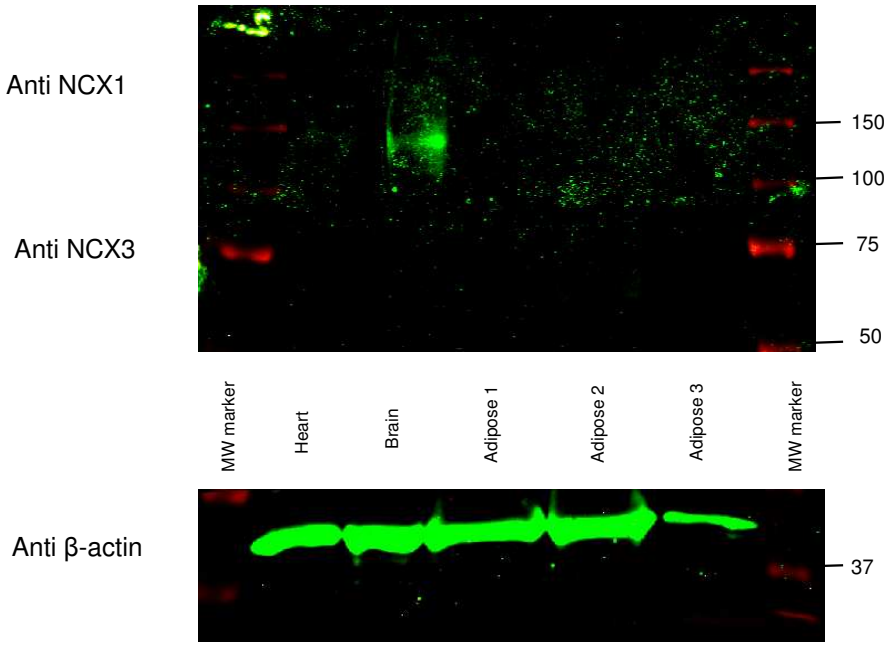

Figure 3.27. Western blots of NCX1, NCX3 and β-actin expression in heart, brain, and white epididymal adipose tissue from Wistar rats. Tissue lysates of heart, brain and adipose tissue were separated by SDS-PAGE prior to Western blot analysis. Positions of molecular weight markers in kDa are indicated. A representative blot of one of three independent experiments is shown, each with different distinct samples. 25µg of protein was loaded for heart and brain tissue samples. 40µg of protein was loaded for each adipose tissue sample.

3.12 Discussion

3.12.1 Resting Ca^{2+} levels in adipocytes

Our median resting Ca^{2+} value of 118nM is similar to those reported in the literature for experiments conducted in primary white adipocytes (Table 3.8). Differences in resting $[Ca^{2+}]_i$ between our investigations and others could be attributed to differences between different strains of rat.

The significant decrease in $[Ca^{2+}]_i$ during the perifusion of extracellular Ca^{2+} free (Figure 3.9) and subsequent recovery of $[Ca^{2+}]_i$ upon re-perifusion of Ca^{2+} is indicative of functional Ca^{2+} influx pathways in un-stimulated adipocytes.

Extracellular divalent cations (Ca^{2+}, Mg^{2+}) have been reported to close voltage gated channels and elevate the resting membrane resistance, providing a membrane stabilising effect (Hille, 2001). Another suggestion is that the interaction between the ionic lipid bilayer and the divalent cations provides a barrier to pore growth. To the contrary, lowered extracellular divalents have the opposite (destabilising) effects.

The $[Ca^{2+}]_i$ response observed upon extracellular Ca^{2+} removal was unlikely to occur as a result of membrane destabilisation. In all experiments presented within this thesis, the extracellular Ca^{2+}, in extracellular Ca^{2+} free buffer, was replaced by equimolar substitution with Mg^{2+}, a divalent equivalent to Ca^{2+}.

Strain of Rat	Weight (g)	Ca^{2+} indicator	Experimental Temp	Technique	Ca^{2+} in buffer	Resting Ca^{2+} value obtained (nM)	References
Sprague Dawley	90-150	Fura-2	30°C	Cuvette	2.5mM	~165	Kelly, Deeny et al. 1989
CD strain	160-180	Fura-2	37°C	Perifusion	KRB	~100	(Gaur et al., 1998b)
CD strain	150-200	Fura-2	37°C	Perifusion	KRB	~200	(Gaur et al., 1998a)
Sprague Dawley	250	Aequorin	22°C	Cuvette	1.4mM	100	(Pershadsingh et al., 1989)
Sprague Dawley	225-250	Fura-2	37°C	Cuvette	3mM	140-370	(Draznin et al., 1987a)

Table 3.8. A summary of resting white adipocyte $[Ca^{2+}]_i$ values obtained in other studies from epididymal fat pads except in * where $[Ca^{2+}]_i$ was measured in adipocytes from both epididymal and perirenal fat pads.

Other studies investigating the presence of $Ca_v1.x$ channels within the adipocyte utilised cuvette-based imaging techniques (Draznin et al., 1987b, Kelly et al., 1989, Klip and Ramlal, 1987, Draznin et al., 1989, Akiyama et al., 1990). Imaging of single cells ensures that the responses seen were those of the adipocyte, as adipose tissue comprises various cell types, including; vascular cells; endothelial cells; and immune cells (Kershaw and Flier, 2004, Fantuzzi, 2005). Thus, it is a possibility that contamination of the adipocyte preparation with other cell types may contribute to the fluorescence responses seen within cuvette experiments. Attempts to replicate the results of others, using the cuvette method within this laboratory were unsuccessful. The adipocytes were not uniformly distributed across the volume of the cuvette, due to their elevated lipid content, they floated to the top of the cuvette away from the light path of the spectrophotometer. Another limitation of cuvette-based imaging is that only the effects of cumulative drug addition can be measured. The effects of drug washout or isotonic solution substitution, for example switching from 5.6mM K^+ to 50mM K^+ for the induction of a VGCC channel response, cannot be measured within the same sample. Finally, the use of cuvettes to investigate $[Ca^{2+}]_i$ assumes a homogenous distribution of fluorescent indicator with stable light emission properties throughout the adipocyte cytosol. Investigators have observed that fluorescent indicators can be trapped within subcellular compartments (Yorek et al., 1999). The subcellular compartments may differ in their Ca^{2+} concentration from that of the cytosol. Live cell imaging in a perifusion system enables the selection of cells for investigation, allowing exclusion of cells that appear punctuate (an indicator of dye accumulation within other compartments). The strengths of imaging are that the effects of drug washout, along with changes in the composition of the perifusion solution can be monitored on a cell-to-cell basis in real time. It allows the identification of, if

any, different groups of responsive cells to any particular intervention and, as the imaging technique is in real time, the identification of brief changes in response.

3.12.2 A role of voltage-gated Ca^{2+} channels in Ca^{2+} influx in the white fat adipocyte?

The presence and function of VGCC is well established in excitable cell types (Fleischmann et al., 1994). Activation of $Ca_v1.1$-$Ca_v1.3$ Ca^{2+} channels in excitable cell types induces rapid elevations in $[Ca^{2+}]_i$ resulting in muscle contraction and nervous transmission/secretion. The α_1 subunit of VGCCs are increasingly being reported in "non-excitable" cell types such as fibroblast endocrine, and immune cells, where the role of VGCCs is less well understood (Fleischmann et al., 1994), however has been speculated to have a role in signalling processes. In the instance of T-lymphocytes, both the α_1 and β subunits are expressed, however depolarisation induced Ca^{2+} entry does not play a critical role in the function of this cell type (Badou et al., 2006). As the adipocyte is also known to possess a signalling function it is possible that the α_1 subunit of $Ca_v1.3$ has a role within this. Conversely the role of Ca^{2+} entry by VGCCs in sperm is well characterised and is reported to regulate flagellar movement, aiding propulsion of the sperm along the reproductive tract (Lishko et al., 2012).

$Ca_v1.2$ channels activate at -35mV (Lipscombe et al., 2004); are blocked by the dihydropryidines (DHP) nifedipine and nitrendipine (Lipscombe et al., 2004, Koschak et al., 2001, Xu and Lipscombe, 2001). $Ca_v1.3$ channels activate at -40mV to -55mV and are blocked by the phenylalkylamine (PAA), verapamil (Xu and Lipscombe, 2001). The inhibitory potency of DHPs and PAAs is increased at

depolarised membrane potentials. (In this current investigation nifedipine and verapamil were used to investigate L-type VGCC in basal Ca^{2+} influx in rat white adipocytes).

Nifedipine failed to significantly inhibit basal Ca^{2+} influx ameliorating a major role of $Ca_v1.2$ VGCCs in basal Ca^{2+} influx, whereas verapamil (20μM) significantly inhibited basal Ca^{2+} entry suggesting that $Ca_v1.3$ may be involved.

The reported IC_{50}s of nifedipine and verapamil are varied, depending on the cell type and means by which this was studied. The IC_{50} of verapamil is reported to be 4μM in rat ventricular calls and motor neurons (Diochot et al., 1995). The IC_{50} of nifedipine is reported to be 36nM in rat aortic smooth muscle (Hirakawa et al., 1994), in rat neurons 5μM of nifedipine inhibits 32 ± 1% of calcium current (Lorenzon and Foehring, 1995). Verapamil is reported to block $Ca_v1.2$ channels with an IC_{50} of 30μM (Dilmac et al., 2004) so it is possible that some blockade of $Ca_v1.2$ may occur alongside $Ca_v1.3$ if both channel types are present (Dilmac et al., 2004) as 20μM verapamil was used in this study. Also, the DHP and PAA receptor site are in close proximity and have shared amino acid residues within the binding site (Catterall et al., 2003b, Mohan and Gandhi, 2008). Conversely, incomplete inhibition of $Ca_v1.3$ VGCCs has been reported upon application of DHPs (Xu and Lipscombe, 2001).

VGCC sensitivity to PAAs like verapamil also depends upon the gating properties of the channel molecule (Hering et al., 1997). For blockade by PAAs to occur, the channels have to pass through an open conformational state. It has been proposed that PAAs block the channel from the intracellular side (Hering et al., 1997). In cell types that possess hyperpolarised membrane potentials channel blockade by PAAs is prevented at "rest". The observation that verapamil blocked

basal Ca^{2+} influx is suggestive that there may be open VGCCs present on the plasma membrane at rest, as such adipocytes may possess a more depolarised resting membrane potential. Fleischmann *et al* (1994) suggested a theoretical "window current" for steady state cellular Ca^{2+} influx in $Ca_v1.x$ VGCCs at membrane potentials between -40 and -20mV. Fleischmann *et* al *(1994)* reports the existence of a non inactive current in non spiking muscle cells, at ~-30mV, where channel inactivation is incomplete. Gaur *et al* (1996b) suggested that VGCCs may have a role in maintaining the level of resting $[Ca^{2+}]_i$. Additionally treatment of adipocytes with nimpodipine, a $Ca_v1.2$ VGCC blocker, was shown to significantly reduce $[Ca^{2+}]_i$, as attributed to a reduced basal Ca^{2+} influx by VGCCs (Gaur et al., 1996b). Resting membrane potentials of white fat adipocytes have been measured by others (Perry and Hales, 1969, Ramirez-Ponce et al., 1990, Kamei et al., 1992, Beigelman and Shu, 1972) and were investigated within this study (see Chapter 2). The most commonly reported adipocyte RMP values occur between -20 and -46mV (See Chapter 2, Section 2.7.2). It seems reasonable to propose on the basis of the afore mentioned literature reports that $Ca_v1.3$ may have a role in basal Ca^{2+} influx in white adipocytes. However, this seems unlikely, as the VGCCs undergo voltage dependent inactivation. As the plasma membrane of the adipocyte is stably depolarised at rest, the channels are likely to reside in the inactivated state. Once VGCCs have been subject to voltage dependent inactivation they need to be hyperpolarised for a period of milliseconds to remove the inactivation. Inactivated channels cannot return to their conducting state until the inactivation has been removed. Inactivation overrides the likelihood of the activation process to open the channels (Hille, 2001). As such it is questionable as to the likelihood of VGCCs maintaining basal Ca^{2+} in adipocytes.

A limitation of using pharmacological methods to determine the presence of specific channel types is that there are increasing reports of non specific drug effects upon other channels and transporters. In the instance of the work presented, here as basal Ca^{2+} influx was not inhibited by nifedipine (Figure 3.12), it is possible that the inhibitory effect of nifedipine upon Ca^{2+} re-entry was due to a non-specific effect of nifedipine upon another channel type, possibly the NCX. The dihydropryidine antagonist nicardipine (0.1-10μM) has been reported to inhibit Na^{+}/Ca^{2+} exchanger (NCX) activity in rat cardiac sarcolemmal membranes (Takeo et al., 1985).

In addition to blocking basal Ca^{2+} influx, verapamil was also shown to inhibit Ca^{2+} re-entry in primary white fat adipocytes (Figure 3.13B). Diltiazem, verapamil and nifedipine at concentrations up to 10μM are reported to not have an effect on the NCX, (at least in cardiac sarcolemmal vesicles (Hata et al., 1988)). So, a non specific inhibitory effect of nifedipine or verapamil at 20μM (as used in this study) upon the NCX is possible.

3.12.3 Bay K 8644 had no effect of increasing adipocyte $[Ca^{2+}]_i$

The major actions of Bay K 8644 to promote Ca^{2+} influx have been suggested to occur by the drug increasing $Ca_v1.x$ channel openings in Mode 2. At the whole-cell level, if Bay K 8644 was promoting longer channel open times, an increase in cellular $[Ca^{2+}]_i$ would be expected.If our adipocytes did possess depolarised membrane potentials of approximately -20mV to -30mV as reported, an effect of Bay K 8644 at increasing $[Ca^{2+}]_i$ would be expected. Such responses have been observed in human mesangial cells where a significant increase in $[Ca^{2+}]_i$ of 18% above baseline $[Ca^{2+}]_i$ occurred in the presence of Bay K 8644, with this effect being eliminated following removal of extracellular Ca^{2+} (Hall et al., 2000).

The concentration of Bay K 8644 used in the current study (1μM) was consistent with that used by other studies that did observe increased membrane currents upon addition of Bay K 8644 (Sanguinetti and Kass, 1984, Hall et al., 2000). The lack of effect of Bay K 8644 in affecting adipocyte $[Ca^{2+}]_i$ (Figure 3.14) is unlikely to be attributed to the effects of other channel types, as the actions of Bay K 8644 to increase $[Ca^{2+}]_i$ are reported to be specific to $Ca_v1.x$ VGCCs. It is possible that adipocytes possess a very low functional VGCC channel density on the membrane surface of the adipocyte. Additionally, stimulated Ca^{2+} influx by Bay K 8644 through a small number of channels may not be sufficient to increase mean cellular $[Ca^{2+}]_i$. It is also possible that by stimulating cellular Ca^{2+} influx by Bay K 8644 triggers Ca^{2+}-dependent inactivation of the VGCCs, or other cellular Ca^{2+} extrusion mechanisms are initiated to prevent cytotoxic Ca^{2+} overload. The final possibility is that the VGCCs are not actually present and the observed effects of the pharmacological agents on reducing $[Ca^{2+}]_i$ (see Figures 3.12 and 3.13) are due to non-specific effects of nifedipine and verapamil on other Ca^{2+} influx pathways such as the sodium-calcium exchanger.

3.12.4 High $[K^+]_o$ induced increase of $[Ca^{2+}]_i$ was not inhibited by $Ca_v1.3$ voltage-gated Ca^{2+} channel blocker verapamil

Perifusion of adipocytes in high K^+ solution was another experimental approach utilised to investigate the presence of VGCC on the plasma membrane of rat white adipocytes. In excitable cells such as neurons/ muscle, exposure to elevated extracellular K^+ decreases the outward K^+ gradient resulting in depolarisation of the plasma membrane. The resultant plasma membrane depolarisation causes the opening of VGCCs and subsequent influx of extracellular Ca^{2+}. Elevated conditions of extracellular K^+ are reported to cause

elevations in $[Ca^{2+}]_i$ in white fat adipocytes, suggesting that elevated $[Ca^{2+}]_i$ can occur through membrane-induced depolarisation and Ca^{2+} entry through VGCCs (Draznin et al., 1989, Shi et al., 2000, Huang et al., 2004, Gaur et al., 1996a), however in Chapter 2, no membrane potential effect of K^+ was observed in either primary or differentiated 3T3-L1 adipocytes. In Chapter 3, 58% of the adipocyte population tested underwent a K^+-induced increase in Ca^{2+}, however this was not statistically significant (Figure 3.16A, 3.16B). These findings contradict previously published observations by other investigators (Draznin et al., 1989, Huang et al., 2004, Shi et al., 2000), with the exception of observations made by Yorek *et al* (1999) whereby exposure of 3T3-L1 adipocytes to 70mM K^+ did not cause an increase in $[Ca^{2+}]_i$. Yorek *et al* (1999) utilised cell mounting and perifusion-based methods, similar to those utilised within this study. Thus differences in experimental approach may be accountable for the observed differences in adipocyte $[Ca^{2+}]_i$ response to elevated extracellular K^+. Another difference is that cuvette methods observe changes in $[Ca^{2+}]_i$ responses within a cellular population, where as perifusion based methods allows the study of single cells, reducing the likelihood of obtaining $[Ca^{2+}]_i$ measurements from contaminating cell types. The advantage of cellular perifusion with ion substituted solutions is that this approach does not cause an osmotic effect upon cells under study. The fact that the cells in the present study displayed stable dye loading characteristics and reversible $[Ca^{2+}]_i$ responses to extracellular Ca^{2+} removal suggest that they were viable.

To further investigate whether extracellular Ca^{2+} was indeed entering the adipocyte by VGCCs, a subanalysis was performed. Of the adipocytes that responded to 50mM extracellular K^+ by increasing $[Ca^{2+}]_{i,}$ there was no significant effect of 20μM verapamil at inhibiting Ca^{2+} entry (Figure 2.16B)

contrary to the studies of Draznin *et al* (1988) and Gaur *et al* (1996) who reported an inhibitory effect of 30μM verapamil on high K^+ induced increase in $[Ca^{2+}]_i$ in white adipocytes.

3.13 Low $[Cl^-]_o$ induced increase of $[Ca^{2+}]_i$ was not inhibited by $Ca_v1.3$ voltage-gated Ca^{2+} channel blocker verapamil

The observation that elevations in $[K^+]_o$ from 5mM to 50mM do not cause depolarisation of the adipocyte plasma membrane is of particular interest. Results in Chapter 2 show that removal of extracellular Cl^- depolarised the plasma membrane of both adipocyte models. The following hypothesis were tested; 1) does removal of extracellular Cl^- result in increased Ca^{2+} influx from the external environment; 2) whether this influx was via L-type calcium channels. There was no significant increase in $[Ca^{2+}]_i$ following extracellular Cl^- removal, and furthermore perifusion of 20μM verapamil did not inhibit Ca^{2+} influx in the adipocytes that did show elevations in $[Ca^{2+}]_i$ (Figure 3.20). The obvious conclusion is that depolarisation of the adipocyte plasma membrane does not cause Ca^{2+} entry via L-type calcium channels. Thus, either the channels are not present; not functioning as a Ca^{2+} influx pathway, or they are inactive.

To further investigate the possibility that extracellular Ca^{2+} was entering the adipocyte by $Ca_v1.2$/ $Ca_v1.3$ VGCCs, the calibrated single-channel traces of the Ca^{2+} response in K^+ during the time-course of the protocol were re-investigated for the presence of Ca^{2+} spikes, indicative of transient Ca^{2+} influx by way of VGCCs with subsequent channel closure. None of the records obtained in this project displayed any transient increase in $[Ca^{2+}]_i$. The increase in $[Ca^{2+}]_i$ observed upon solution exchange to 50mM K^+ occurred over a time-course that was of the order of minutes, indicative of Ca^{2+} entry from a source other than

VGCCs. It is possible that the increase in $[Ca^{2+}]_i$ observed in 50mM K^+ responsive adipocytes was due to activation of the sodium calcium exchanger (NCX). The NCX is a bidirectional transporter exchanging $3Na^+$ for $1Ca^{2+}$. The NCX is electrogenic, depolarization of the membrane from resting Vm can reverse the exchanger's direction (Torok, 2007). On the basis of the adipocyte plasma membrane being depolarised at rest it is possible that the NCX will be functioning in the reverse mode (Na^+ efflux and Ca^{2+} influx). In addition, the concentration of Na^+ is low in the high K^+ solution (138mM Na^+ in 5.6mM K^+ and 93.6mM Na^+ in 50mM K^+). This was to maintain the osmolarity of the solution, however the low concentration of extracellular Na^+ will activate the reverse mode of the NCX (Rathi et al., 2004), which may lead to an increase in $[Ca^{2+}]_i$. It is likely under conditions of low extracellular Na^+ that the NCX is operating as a Ca^{2+} influx pathway accountable for the increase in $[Ca^{2+}]_i$ observed upon perifusion of 50mM K^+ Hank's solution. This observation supports the hypothesis that functional NCX is present on the plasma membrane surface of adipocytes. This was further investigated in Section 3.10.2.2.

3.13.1 Investigation into the effect of insulin on $[Ca^{2+}]_i$ and Ca^{2+} influx pathways in rat white adipocytes

Insulin has been reported to increase $[Ca^{2+}]_i$ in white adipocytes. Studies suggest that insulin-induced increases in $[Ca^{2+}]_i$ contribute to the development of insulin resistance. The increase in $[Ca^{2+}]_i$ in insulin was reported to be via enhanced Ca^{2+} entry via VGCCs (Draznin et al., 1987a, Draznin et al., 1989) as treatment of adipocytes with 30μM verapamil reduced $[Ca^{2+}]_i$ from 239nM to 128nM and restored adipocyte responsiveness to insulin as determined by the 2-deoxyglucose (2-DOG) uptake assay in human gluteal adipocytes (Draznin et al.,

1988). This data corroborated earlier findings by Draznin *et al* (1987) in rat adipocytes, whereby insulin was demonstrated to enhance $[Ca^{2+}]_i$ in rat epididymal adipocytes by ~30% (Draznin et al., 1987a, Draznin et al., 1988), an effect inhibited by 25μM nifedipine. In contrast to observations within this study, significant effects of insulin on increasing $[Ca^{2+}]_i$ were observed within 10 minutes in adipocytes from both human and rat (Draznin et al., 1987a, Draznin et al., 1988). Later studies by other laboratories demonstrated that insulin was not found to increase $[Ca^{2+}]_i$ (Blackmore and Augert, 1989, Kelly et al., 1989, Schwartz et al., 1991, Gaur et al., 1998b). The reasons for the observed differences in insulin effect between investigations are unknown.

Ca^{2+} re entry by VGCCs was also compared in the presence and absence of insulin. The verapamil response at inhibiting Ca^{2+} re-entry was significant in non-insulin exposed adipocytes (Figure 3.13), however when insulin is present the inhibitory response of verapamil was lost (Figure 3.18A). These data suggest that in the presence of 100nM insulin, $[Ca^{2+}]_i$ is not re-entering the adipocyte by VGCCs. In this study insulin did not have an effect on membrane potential (Chapter 2 Figure 2.22), so it is unlikely that the loss of inhibition on Ca^{2+} re-entry is due to a membrane potential effect. Insulin also did not significantly increase $[Ca^{2+}]_i$.

The majority of studies that did not observe an effect of insulin on $[Ca^{2+}]_i$ were those that subjected adipocytes to acute exposure conditions. To observe an inhibitory effect on glucose transport, some studies do incubate adipocytes in insulin for periods of up to 4 hours (Marshall and Olefsky, 1980). To confirm adipocyte responsiveness to insulin, the 2-[N-(7-nitrobenz-2-oxa-1,3-diazol-4-yl)amino]-2-deoxy-D-glucose (2-NBDG glucose) uptake assay was attempted in adipocytes in real time, using the protocol described by Nakata *et al* (2006). As

a positive control, protocols were also repeated in pancreatic β cells (Yamada et al., 2000, Nakata et al., 2006). The adipocytes and pancreatic β-cells under study failed to maintain 2-NBDG as determined by a distinct lack of fluorescent signal.

3.13.2 Protein expression of the α_1 subunit of $Ca_v1.3$ in white adipocytes

Even though pharmacological inhibitors of VGCCs are used to indicate the presence of this channel type upon the plasma membrane of the cell under study, it is possible that non-specific effects of inhibitors occur on other Ca^{2+} influx mechanisms. On the basis of the results in sections 3.10.2.1, Western blots were carried out to examine the expression of the $Ca_v1.3$ VGCC proteins in the white fat adipocyte. Investigation into the expression of the α_1 subunit was attempted. This is the largest and most important subunit as it incorporates the conduction pore, voltage sensor and the sites of regulation by drugs/phosphorylation, as well as the gating apparatus.

As protein bands of the expected size ~265kDa were observed in preparations adipocyte protein lysates, see Figure 3.24. Results indicate that $Ca_v1.3$ is likely to be present on the adipocyte plasma membrane. Data in Figure 3.25 are suggestive of a reduction in $Ca_v1.3$ expression in adipose tissue in adipocytes sourced from obese rats. As obesity is associated with insulin resistance (IR) it is likely that $Ca_v1.3$ expression is reduced in IR. Solid conclusions cannot be drawn at this stage due to the low experimental n.

To confirm the bands detected by the anti $Ca_v1.3$ antibody were not due to non-specific binding of the primary antibody to another protein product requires the

use of the anti $Ca_v1.3$ blocking peptide. Again, due to limited manufacturer supply these studies could not be performed. However, to confirm the bands visualised were not a result of non-specific secondary antibody binding, a repeat set of samples was run and exposed to the anti rabbit secondary antibody only (Figure 3.26). No non-specific binding of the secondary antibody was shown.

3.14 Investigation into the presence of the reverse mode of the NCX in rat white adipocytes

Verapamil was shown to inhibit Ca^{2+} re-entry in primary adipocytes (Figure 3.12). Upon acute insulin exposure this inhibitory action of verapamil was apparently lost (Figure 3.18), data that suggests Ca^{2+} re-entry by some other means under acute insulin exposure, which was no longer occurring by $Ca_v1.3$ VGCCs. Additionally elevated $[K^+]_o$ prepared by isotonic substitution of $[Na^+]_o$ a measure which is expected to reverse the NCX (Ca^{2+} influx) (Rathi et al., 2004). In the absence of insulin exposure of adipocytes to 50mM $[K^+]_o$ resulted in a small increase in $[Ca^{2+}]_i$ (Figure 3.16). These data together suggest another Ca^{2+} influx pathway.

It has also been reported that the NCX operates in the reverse mode of exchange at membrane potentials of approximately ~-40mV (Watano et al., 1996). In Chapter 2, the mean resting membrane potential of adipocytes subject to perforated patch investigation was found to be approximately -34mV, as such it would be reasonable to suggest that the NCX is operating in reverse mode. As acute insulin (100nM) exposure did not have an effect on the resting membrane potential of adipocytes tested within this study (Chapter 2, Figure 2.22), it is therefore possible that the reverse mode of the NCX is acting as a Ca^{2+} re-entry pathway under both non insulin and insulin conditions.

Fluo-4 $[Ca^{2+}]_i$ imaging data show KBR-7943 inhibits Ca^{2+} re-entry in non insulin conditions (Figure 3.21A). There was no inhibitory effect of KBR-7943 upon Ca^{2+} re-entry in 100nM insulin (Figure 3.21B). Initially, data are suggestive of the reverse mode of the NCX acting as a Ca^{2+} re-entry pathway in non insulin conditions. Further to these observations, modelling of the behaviour of the NCX under conditions used within this investigation (-30mV, and $[Ca^{2+}]_o$ =2.6mM and nominally $[Ca^{2+}]_o$ free) was carried out and described in Figure 3.23. It was determined that the NCX would only operate in the Ca^{2+} influx mode following extracellular $[Ca^{2+}]_o$ removal and subsequent re-addition of 2.6mM $[Ca^{2+}]_o$.

KBR-7943 does have inhibitory effects on other channel types. At concentrations of approximately 30μM, KBR-7943 has been reported to inhibit Ca^{2+} influx by the NCKX and VGCCs (Iwamoto et al., 1996b). KBR-7943 was used at 10μM within this investigation, however non-specific effects of KBR-7943 have been reported when used at 5μM. KBR-7943 at 5μM was reported to decrease Ca^{2+} transients in heart tubes from NCX1 knockout mouse embryos (Reuter et al., 2002), suggesting that the inhibitory effects of KBR-7943 occur by other mechanisms. As such, it is possible that KBR-7943 is inhibiting Ca^{2+} entry via VGCCs. In support of this, the data for the inhibitory effects of KBR-7943, in insulin conditions is similar to the data obtained when verapamil was used to inhibit Ca^{2+} re-entry (+/- insulin) within the white fat adipocyte, Figure 3.18.

Verapamil as discussed in Chapter 3 Section 3.5.1 is an L-type Ca^{2+} channel blocker, however it is also reported to have non-specific inhibitory effects on the reverse mode of the NCX. Hata *et al* (1988) reported an inhibitory effect of verapamil at inhibiting Na^+-dependent Ca^{2+} uptake in rat sarcolemmal vesicle preparations at concentrations >10μM (Hata et al., 1988). Additionally Erdreich *et al* (1983) reported verapamil inhibition of Na^+ dependent Ca^{2+} uptake in rat

brain synaptic plasma membrane vesicles with an IC_{50} of 175μM. The differences in verapamil concentration required to observe an inhibitory effect upon the NCX may vary between sample preparations, possibly dependent upon the isoforms of NCX expressed and the level of NCX expression. Verapamil was used at 20μM in experiments conducted within this thesis so it is possible, that the drug may inhibit the reverse mode of the NCX.

It is also a possibility that the effects of KBR-7943 observed in experiments conducted within this chapter are attributable to inhibition of store-operated Ca^{2+} entry (SOCE) (Parekh and Putney, 2005). The current literature report low mRNA expression levels of SOC channels belonging to the TRPC family in human white adipocytes

SN-6 inhibited Ca^{2+} re-entry in absence of insulin, suggestive of the presence of the reverse mode of the NCX, the inhibitory action of SN-6 upon Ca^{2+} re-entry was lost in insulin. SN-6 has been shown not to inhibit VGCCs at concentrations of up to 30μM, rendering SN-6 a more selective reverse mode NCX inhibitor than KBR (Iwamoto et al., 2004a). SN-6 was used at 10μM within this investigation, as such it is likely that SN-6 when used at this concentration does not differentiate between different NCX isoforms. SN-6 is reported to inhibit Na^+ dependent radioactive Ca^{2+} uptake in CCL39 cells with IC_{50} values of 2.9μM, 16μM and 8.6μM for NCX1, NCX2, and NCX3. This rules out the likelihood of SN-6 and KBR-7943 acting upon different NCX isoforms. No IC_{50} for SN-6 inhibition of NCX are reported in adipocytes. To confirm this suggestion, a positive control for SN-6 is required to ensure the drug is functional at inhibiting Ca^{2+} influx via the NCX. This could have been done either by conducting a repeat perifusion protocol with Fluo-4 $[Ca^{2+}]_i$ imaging and SN-6 in heart or brain tissue, both of which are known to express the NCX.

Investigations by Pershadsingh *et al* (1989) used similar methodologies to those used in this thesis to identify both VGCC and NCX in WAT. Pershadsingh *et al* (1989) showed that perifusion of primary white adipocytes from epididymal fat pads with Na^+-free buffer, as prepared by iso-osmotic substitution of NaCl with choline-chloride or KCl showed a two fold increase in $[Ca^{2+}]_i$ above basal levels. The increase in $[Ca^{2+}]_i$ following exchange of the medium to one that contained 60mM $[K^+]_o$ was however attributed to Ca^{2+} entry by VGCCs as diltiazem (10μM) blocked the increase in $[Ca^{2+}]_i$ observed in 50mM K^+. These authors assumed an adipocyte resting membrane potential of -58mV and were therefore expecting depolarisation of the adipocyte membrane upon exchange of the extracellular solution to 50mM K^+ (Pershadsingh et al., 1989). However, this does not account for the increase in $[Ca^{2+}]_i$ observed upon exchange of buffer to choline-chloride, as these conditions are not reported to cause Ca^{2+} influx by VGCCs. As such Ca^{2+} re-entry within the white fat adipocytes used within this investigation was suggested to be occurring by way of both VGCCs and the reverse mode of the NCX.

To further investigate the presence of NCX on the membrane surface of the white fat adipocyte, Western blotting was carried out. A band of ~120kDa, most likely representative of protein expression of NCX1 was only detected within the brain sample. This is not entirely unlikely as NCX1 expression has also been reported in the brain (Iwamoto and Kita, 2006). A prominent NCX1 expression in the protein sample from heart tissue was expected as shown by Sugano *et al* (2011) using the Abcam NCX1 antibody, this was not seen in our hands; this result could arise due to incomplete inhibition of *in vitro* proteolysis by the protease inhibitors used within the sample preparation, or that degradation of the protein sample occurred prior to addition of the protease inhibitor cocktail to

the sample, suggesting that further optimisation of the protein sample preparation is required. Additionally the Abcam antibody is a monoclonal antibody. It is possible that if any post translational modifications have occurred, or indeed the sample is degraded, then detection of protein by a monoclonal antibody is much less likely than by a polyclonal antibody.

Western blotting failed to determine the presence of NCX3 in any of the tissues tested. In accordance with the manufactures guidelines, bands of 64kDa are indicative of the presence of the NCX3 protein. The literature report an expected band size of 103kDa for NCX3 (Lytton, 2007). According to UniProt, the NCX has various isoforms of varying molecular weights from 31kDa-103kDa. Several putative modification sites have been identified on NCX3 which could also influence the proteins migration behaviour. As the NCX3 antibody is polycolonal, it should detect both phosphorylated and post-translationally modified forms of NCX3. Additionally, the Manufacturers (Santa Cruz) state that the NCX3 antibody detects all isoforms of NCX3, eliminating the possibility of non-detection due to varying isoform expression.

NCX3 was not detected in the positive control, brain protein lysate, suggestive of a problem with the sample preparation. Again it is possible that the protease inhibitor used for sample preparation did not inhibit *in vitro* proteolysis, or that the proteolysis occurred within the sample prior to the addition of protease inhibitors. Bands for the reference protein β-actin were detected, abrogating technical issues in the running of the gel. With regard to the adipose tissue samples, it is possible that there was not enough protein sample loaded to allow detection of NCX1 or NCX3; or that the collagenase type II used for adipose protein preparations may contain esterases which could degrade the NCX protein; or simply, that there was indeed no NCX1 or NCX3 expressed within

these tissue samples; or finally an inability of the antibody to detect NCX1 protein under the experimental conditions used within this investigation. Additionally as NCX1 protein was not detected in various heart preparations, whereby NCX1 expression is well established, it was considered that the detection of NCX1 by the antibody used under experimental conditions presented here was unreliable

3.15 Summary

Primary white adipocytes are responsive to changes in $[Ca^{2+}]_o$. Fluo 4 imaging in conjunction with verapamil suggests a role of $Ca_v1.3$ in Ca^{2+} influx in adipocytes. Conditions of elevated $[K^+]_o$ cannot be used to determine the presence of VGCCs in adipocytes, neither can depolarising conditions of $[Cl^-]_o$ since neither affected $[Ca^{2+}]_i$. The presence of the α_1 subunit in adipocytes however, was confirmed by Western blot.

The results of the $[Ca^{2+}]_i$ determinations conducted here are in support of the reverse mode of the NCX in white fat adipocytes as both SN-6 and KBR-7943 inhibited Ca^{2+} re-entry in non insulin conditions. Additionally, modelling of the behaviour of the NCX under conditions used within this investigation were in support of the reverse mode of the NCX following $[Ca^{2+}]_o$ removal and re-addition. Unfortunately Western blot investigations were not able to confirm the presence of the NCX in adipocytes.

The inhibitory effect on Ca^{2+} re-entry of verapamil, SN-6 and KBR was lost in insulin, suggestive of another Ca^{2+} influx pathway in acute insulin exposure conditions.

Chapter 4

Evidence of spontaneously active ion channels in differentiated 3T3-L1 adipocytes

4.1 Introduction

The original aim of this study was to determine the presence of voltage-gated calcium channels in the plasma membrane of primary white fat adipocytes. Voltage-gated calcium channels are often identified indirectly by depolarising the cells plasma membrane with elevated extracellular [K^+], which removes the outward K^+ gradient, the resultant effect of this is elevated $[Ca^{2+}]_i$. Ca^{2+} influx pathways can then be explored by use of calcium channel antagonists. We failed to observe an increase in $[Ca^{2+}]_i$ in primary adipocytes upon perifusion of extracellular K^+, which then prompted investigation into why no effect of 50mM $[K^+]_o$ was observed. Investigation into the ions involved in adipocyte membrane potential demonstrated that K^+ is not involved in adipocyte RMP. Moreover, further investigations showed that Cl^- ions are involved in the RMP of both primary adipocytes and 3T3-L1 adipocytes. Thus, there is a requirement for Cl^- channels in the plasma membrane of adipocytes. Consequently, we investigated the presence of Cl^- channels in differentiated 3T3-L1 adipocytes using the cell attached patch clamp technique. Chloride channels are reviewed in the following section to aid in the understanding of the type of chloride channel that we may expect to find on the 3T3-L1 adipocyte plasma membrane.

4.2 Chloride channels

Cl^- channels are ubiquitously expressed anion selective pores, which allow the passive diffusion of negatively-charged ions down their electrochemical gradient (Suzuki et al., 2006). Cl^- channels are present both in the plasma membrane and in the membranes of intracellular organelles including the endocyotic and synaptic vesicles (Jentsch, 1996, Jentsch et al., 2002). Cl^- channels are permeable to numerous anions, including iodide, nitrates, bicarbonates, thiocyanates and bromide (Suzuki et al., 2006). Cl^- unlike Ca^{2+} does not appear to have a role as second messenger (Jentsch, 1996), however Cl^- channels do have important roles in cellular physiology. Chloride flux through Cl^- channels are involved in regulation of excitability of nerve and muscle, cell volume regulation, pH regulation of intracellular organelles and control of transepithelial transport (Nilius and Droogmans, 2003, Jentsch et al., 2002).

Cl^- channels have been classified functionally in accordance with their gating mechanisms and are grouped into 5 categories as follows:- voltage-dependent chloride channels (CIC); cystic fibrosis transmembrane regulator (CFTR) which is regulated by protein kinases; volume-regulated chloride channels (VRAC) (Nilius et al., 1996), which are regulated by cell swelling; glycine or У-amino butyric chloride channels (GABA) which are opened upon ligand binding (Nilius and Droogmans, 2003); finally, Ca^{2+}-activated chloride channels which are regulated by elevations in $[Ca^{2+}]_i$. A summary of Cl^- channel conductances is shown in Table 4.1. The molecular structures of CIC channels, CFTR channels and GABA-chloride channels has been determined (Nilius and Droogmans, 2003), however the structures of VRAC and Ca^{2+} gated Cl^- channels have yet to be elucidated.

4.2.1 Voltage-dependent/gated Cl^- channels

The ClC channels belong to a large gene family of Cl^- channels, comprising 9 genes (in mammals). They are grouped into one of three branches on the basis of their sequence homology, see Figure 4.1. The first branch comprises plasma membrane channels, whereas the channels encoded by branches two and three are Cl^- channels of the intracellular membranes (Jentsch et al., 2002). The first branch comprises ClC-1 which is expressed in skeletal muscle (Suzuki et al., 2006). ClC-2, a ubiquitously expressed channel activated either by hyperpolarisation or cell swelling, and finally ClC-Ka and ClC-Kb, otherwise known as ClC-K1 and ClC-K2 in the rat, respectively, which are exclusively expressed within the kidneys (Jentsch, 1996, Estevez et al., 2001). Unlike other ClC channel which yield Cl^- currents by themselves, ClC-Ka and ClC-Kb require association with a 40kDa β-subunit "barttin" in order to conduct Cl^- currents (Estevez et al., 2001, Planells-Cases and Jentsch, 2009). The second branch comprises ClC-3, ClC-4 and ClC-5, which are expressed in the brain and kidneys. Inactivation of ClC-5 gives rise to kidney stones (Jentsch, 1996). The third branch comprises ClC-6 and ClC-7 which are found ubiquitously and believed to be present on intracellular membranes; we would not expect to observe CIC-6 and CIC-7 on the plasma membrane surface of our 3T3-L1 adipocytes, as such they are not reviewed in this section.

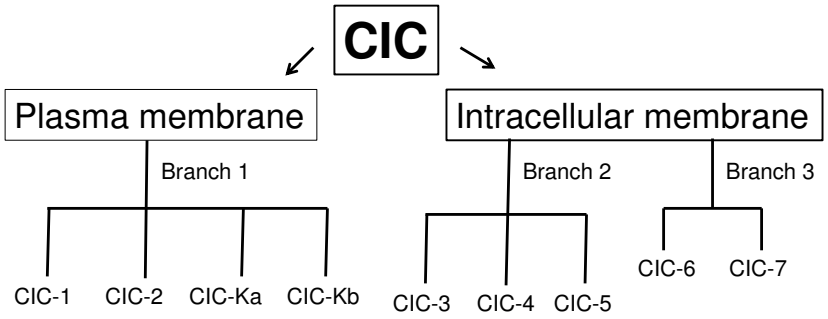

Figure 4.1. The groupings of CIC chloride channels

The structural determination of ClC channels arose following the identification of channel homologues in *Escherichia coli* (EcClC) and in *Salmonella typhimurium* (StClC) (Dutzler, 2004). X-ray structures of bacterial ClC channels show that the EcClC channel is a dimeric complex comprising 2 identical subunits which comprise 10-12 transmembrane segments (Mindell et al., 2001). The ion conduction pathway does not occur at the interface between the 2 associating subunits, instead, each subunit comprises a central ion-conducting pore and selectivity filter (Dutzler, 2004, Dutzler et al., 2002, Fahlke et al., 1998). Each pore can be gated independently (Mindell et al., 2001). Concatermeric studies of ClC-0 (the torpedo Cl^- channel) together with either ClC-1 or ClC-2 also support the dual pore hypothesis (Weinreich and Jentsch, 2001). If the CIC channel does have 2 pores, and hence 2 conducting pathways, we would expect to see 2 sets of conductance on our single channel records. However, the dual pore model is reported not to be applicable to every ClC isoform since site-directed mutagenesis and single-channel patch clamp studies have challenged this model with respect to the ClC-1 isoform (Fahlke et al., 1998). Each subunit comprises two halves which span the membrane in opposite directions (Dutzler et al., 2002). The molecular weights of the channel complex vary from ~60kDa to 110kDa. The ClC family are anion-selective with selectivities of $Cl^- > I^-$ (Estevez et al., 2001, Dutzler et al., 2002).

Some ClC channels are depicted as being Cl^- activated, owing to observations that in order for Cl^- channels to be gated by voltage there is a requirement for the presence of Cl^- within the channel pore. One suggested model is that the pore comprises of two anion binding sites, one mediating conduction selectivity (towards the intracellular side) and the other gating selectivity (towards the extracellular side). The passage of Cl^- is blocked by a glutamate-side chain closer

to the extracellular side. The property of Cl^- activation is hypothesised to act by Cl^- both entering the pore, and inducing conformational changes mediating the movement of the glutamate side-chain, allowing diffusion of Cl^- through the channel (Dutzler et al., 2002). Another model states that the channel harbours 2 Cl^- ions, with the entry of a 3rd Cl^- ion into the channel pore inducing conduction (Corry et al., 2004). In contrast to voltage-gated Ca^{2+} and K^+ channels, primary sequence analysis of voltage-gated Cl^- channels does not reveal a voltage-sensing domain, like the S4 segment (Jentsch et al., 2002). However, mutations in domain 1 of CIC-1 indicate that the charged amino acid residues within this transmembrane domain may act as a voltage sensor (Fahlke et al., 1995). When aspartic acid at the extracellular end of domain 1 was switched for glycine, there was altered voltage dependence within this channel (Jentsch et al., 2002, Fahlke et al., 1995). Alongside voltage regulation, currents through ClC Cl^- channels are also regulated by pH and extracellular [Ca^{2+}] (Estevez et al., 2001, Weinreich and Jentsch, 2001).

4.2.2 CIC-1

ClC-1 is expressed in skeletal muscle and acts as a membrane potential stabiliser. The membrane potential stabiliser effects evident from ClC-1 mutations gives rise to myotonia congenital, characterised by defective muscle relaxation. Various mutations are involved in the pathogenesis of mytonia (Schmidt-Rose and Jentsch, 1997). ClC-1 is voltage-gated by 2 mechanisms, a fast voltage-gate (acting on individual pores) and a slow voltage-gate (acting on both pores as a common gate), with channel closure occurring upon membrane depolarisation (Weinreich and Jentsch, 2001). Whole-cell current measurements indicate that the channel exhibits inward rectification. Low intracellular pH causing slowing of gating kinetics in combination with an increased channel open probability at

negative charges were utilised in order to resolve the channel events of ClC-1. Single-channel recording shows that the ClC-1 channel has 2 open conductance levels of 1.2pS and 2.4pS. Channel properties were reported to be in concordance with the presence of 2 independently gated conductance states (Saviane et al., 1999). In agreement with the dual pore model, concatemers of ClC-0 and ClC-1 also showed 2 independent conductance levels of ~8pS (ClC-0) and ~1.8pS (ClC-1) (Weinreich and Jentsch, 2001). ClC-1 is inhibited by the compound 9-AC (IC50 10.6μM). The ClC-1 ClC-0 concatamer is inhibited by 9-AC with an IC50 of 8.2μM (Weinreich and Jentsch, 2001).

4.2.3 ClC-2

ClC-2 is, according to northern blot analysis, ubiquitously expressed; however immunohistochemical analysis indicates elevated expression levels in the brain (Jentsch et al., 2002). ClC-2 is involved in cell volume control, and in setting intracellular Cl^- concentration (Schmidt-Rose and Jentsch, 1997). Investigations on the single channel level with equal Cl^- concentration in the intracellular and extracellular solution have shown that ClC-2 is activated by hyperpolarisation, with slow gating properties, exhibiting a single channel conductance of 2-3pS (Weinreich and Jentsch, 2001). ClC-2 is also activated by cell swelling and acidic pH, where elevated pH in excess of pH 7.4 result in channel closure. Disruption to ClC-2 gives rise to testicular and retinal degeneration (Jentsch et al., 2002). Multiple agents are used as ClC-2 antagonists, however none of the following inhibitors is specific to this channel type: 0.5mM 5-nitro-2-(3-phenylpropylaminobenzoic acid (NPPB), 1mM 9-AC and diphenylcarbonate (DPC) reversibly inhibit ClC-2 currents (Furukawa et al., 1998). The inorganic cations $Cd^{2+}$and Zn^{2+} (IC_{50} 23μM) block hyperpolarisation activated Cl^- current (Clark et al., 1998).

4.2.4 ClC-Ka /ClC-Kb

CIC-Ka and CIC-Kb are exclusively expressed in the kidney and inner ear, therefore we would not expect to observe this Cl^- channel type in the 3T3-L1 adipocytes. As such, this channel type will not be reviewed in this thesis. For excellent literature on CIC-Ka and CIC-Kb channels see the following references. (Planells-Cases and Jentsch, 2009) (Corry et al., 2004, Jentsch et al., 2002).

4.2.5 ClC-3, CLC-4 and CLC-5

CLC-3, 4 and 5 are endosomal Cl^- channels (Jentsch et al., 2005), and therefore are unlikely to be involved in regulation of Vm within 3T3-L1 adipocytes. CLC-3 and CLC-4 are close homologues of CLC-5 (Kornak et al., 2001) with ~80% sequence homology (Jentsch et al., 2005). CLC-5 is a renal chloride channel expressed on the endosomes of the renal and intestinal epithelia, where it functions as a Cl^-/H^+ exchanger, exchanging $2Cl^-$ with $1H^+$. This activity is highly voltage dependant, outwardly rectifying and active at voltages positive to +20mV, however as plasma and intracellular membranes do not display voltages of +20mV, it is unclear as to the mechanism of activity of CLC-5 in the physiological setting (Gunther et al., 2003). Again, see the following literature for further information pertaining to this group of channels.
(Piwon et al., 2000), (Hara-Chikuma et al., 2005, Mohammad-Panah et al., 2003). (Nilius and Droogmans, 2003). (Wrong et al., 1994). (Piwon et al., 2000, Gunther et al., 2003, Luyckx et al., 1999),.

4.2.6CFTR (Cystic fibrosis transmembrane conductance regulator)

The sequence encoding the CFTR protein has been localised to chromosome 7. The gene product, the CFTR protein, comprises 1,480 amino acids.

Hydrophobicity analysis of the cDNA sequence show the CFTR protein is organised into a doubly repeating motif of 6 transmembrane domains with a nucleotide binding fold (NBF). The two halves of the protein are linked by the regulatory (R) domain. The R domain is highly charged and suggested to serve a regulatory function as it possesses several phosphorylation sites for Ca^{2+} calmodulin kinase, cyclic AMP dependent protein kinase A (PKA) and protein kinase C (PKC) (Fuller and Benos, 1992, Harris, 1992, Seibert et al., 1999). The predicted structure of CFTR is resemblant of the ATP-binding cassette superfamily of proteins. CFTR activates upon phosphorylation of the regulatory domain and the subsequent hydrolysis of ATP (Fuller and Benos, 1992) as channel activity is absent in when non-hydrolyzeable ATP analogues are present (Schultz et al., 1995).

Expression of CFTR is primarily within the epithelial lining of numerous tissue types, including pancreatic ducts, sweat glands, kidney tubules, lung and jejunum (Harris, 1992, Antigny et al.). Mutations within the gene encoding CFTR, the most commonly reported mutation associated being F508 with the deletion of phenyalanine at position 508, give rise to cystic fibrosis. Cystic fibrosis is potentially fatal, manifesting symptoms of reduced permeability to chloride within exocrine glands affecting both absorptive and secretory processes (Quinton, 1990). The defective CFTR protein has a reduced if not absent expression within the apical membrane (Schultz et al., 1999), with the CFTR protein that is incorporated having a shorter half life (Antigny et al.). The CFTR channel does still retain chloride channel functionality, although there is reduced Cl^- ion conductance (Fuller and Benos, 1992). Typically CFTR Cl^- conductance's are ~10pS (Jentsch et al., 2002, Tabcharani et al., 1990), an outwardly rectifying channel with a linear current voltage (I-V) relationship in symmetrical Cl^- solutions (Anderson et al., 1991). Asymmetrical Cl^- solutions cause rectification of

the I-V relationship. The permeability sequence of CFTR is reported as $BR^->Cl^->I^->F^-$ (Anderson et al., 1991). To date there are no specific blockers of CFTR channel (Sheppard, 2004), although sulphonylureas, disulfonic stilbenes and the arylaminobenzoates have been reported to interact directly with the CFTR channel resulting in blockade (Schultz et al., 1999).

4.2.7 Volume-regulated anion channels

Regulation of cell volume is essential for the maintenance of cell integrity in the face of internal and external challenges. Alterations in cell volume arise as a result of various physiological processes, such as glycolysis, cell division, secretion events and muscle contraction (d'Anglemont de Tassigny et al., 2003). Cell swelling also occurs in pathophysiological conditions, e.g, ischaemic stroke, and hypoxic and ischaemic insults. Ultimately swelling occurs either due to an increase in extracellular hypotonicity or under isosmoitc conditions when intracellular osmolytes are increased (Jentsch et al., 2002, Chamberlin and Strange, 1989). Conversely, extracellular hypertonic conditions drive water out of the cell. In response to altered cell volume, transport processes are activated which alter the concentration of intracellular solutes. The responses to cell shrinkage and swelling are termed regulatory volume increase (RVI) and regulatory volume increase (RVI), respectively. In the defence against cell swelling, K^+ channels and Cl^- channels (volume-regulated anion channels, VRAC) are activated. Cl^- channels participate in regulatory volume decrease (RVD). Upon increased cell volume, an outwardly-rectifying Cl^- current is activated giving rise to Cl^- efflux in conjunction with (in the presence of a significant water permeability of the plasma membrane) water loss. As well as maintaining cell volume, the VRAC channels also participate in pH regulation and regulation of membrane potential (Nilius and Droogmans, 2003). The swelling-activated anion

selective conductance is designated $I_{CL,swell.}$ $I_{CL,swell}$ shows increased permeability to various anions with a permeability sequence as follows, $SCN^->I^->Br^->Cl^->F^->$ $Gluconate^-$. The mechanism underlying $I_{CL,swell}$ activation is yet to be elucidated, however it is known that activation is dependent on the presence of intracellular ATP, although hydrolysis is not required as non hydrolysable ATP analogues also induced activation of $I_{CL,swell}$ (Jentsch et al., 2002). Various single channel conductances have been reported for volume-activated Cl^- channels. Small conductance VRAC recorded from Ehrlich ascites cells and chord plexus have a single channel conductance derived from nonstationary noise analysis of macroscopic current of 0.1pS to 8pS. Given the small conductance, it would be very difficult to observe conductances due to the activity of this channel type. The channel density for a small conductance channel is estimated to be 50,000-70,000 channels per cell. Intermediate-conductance VRAC channels have been observed in glia cells, osteoblasts, ostoclasts, epididymal cells and muscle cells showing conductances of 20-90pS. Large conductance channels, 200pS to 400pS, have been described in cardiac myocytes, astrocytes and neuroblastoma cells. Discrepancies between single-channel conductance levels could be attributed to the derivation of conductance values from noise data, or it could be indicative of a broad population of VRAC channels. The pharmacology of this channel type is indicative of the latter (Jentsch et al., 2002). The channel blockers as characterised for voltage-activated Cl^- current (DIDs, SITS, 9-AC) have a low affinity for volume-activated Cl^- currents. The inhibitors for VRAC current vary in potency between cell types. This could be attributed to either a variety of different channel types or differing mechanisms of volume sensitive activation. NPPB, flufenamic acid, niflumic acid, 1-9-d-deoxyforskolin and verapamil induce half-maximal block of VRAC at concentrations ranging from the μM range to the mM range (Nilius et al., 1996). Despite the electrophysiological characterisation

of VRAC, their molecular identification has yet to be determined. Various proteins have been proposed as molecular candidates for VRAC; P-glycoprotein (P-gp); pI_{CLn} (a ubiquitously expressed cytoplasmic protein involved in regulating the assembly of the cells RNA splicing machinery (Pesiridis et al., 2009); phospholemman, a cardiac sarcolemmal protein (Moorman et al., 1992); CLC-2, but have since been dismissed (Suzuki et al., 2006, d'Anglemont de Tassigny et al., 2003, Nilius et al., 1996).

P-glycoprotein is a member of the ABC transporter family, as is CFTR. The structural and sequence similarities between P-glycoprotein and CFTR prompted investigation into P-glcoprotein as a VRAC (Valverde et al., 1992). Despite the original finding that P-glycoprotein increased swell-activated Cl^- currents, the notion of P-glycoportein as a VRAC was discarded as other labs were unable to replicate the original findings (Suzuki et al., 2006, Jentsch et al., 2002, De Greef et al., 1995). pI_{CLN} has been implicated either as a VRAC or one of its regulators (Nilius et al., 1996). Hydropathy investigations failed to detect any transmembrane domain, however oocytes injected with PI_{CLN} mRNA exhibited a VRAC current with similar properties of anion selectivity, outward rectification and inactivation at positive potentials, to those observed in mammalian cells (Paulmichl et al., 1992). The similarities in electrophysiological characteristics led suggestion that PI_{CLN} was the mammalian channel. This notion was disbanded following findings that PI_{CLN} was a cytosolic protein, instead it is suggested to be a potential regulator of the unidentified channel as monoclonal antibodies raised against PI_{CLN} blocked hypotonicity activated IC_{SWELL} (Krapivinsky et al., 1994).

Phospholemman (PLM) is a molecular candidate for VRAC (Moorman et al., 1992). PLM molecules can form Cl^- channels. PLM when expressed in Xenopus oocytes

exhibits similar electrophysiological properties to CLC-2, activation by hyperpolarisation and low pH with slow gating kinetics. PLM and CLC-2 are however structurally different. PLM comprises only one transmembrane segment and has only 72 amino acids (Moorman et al., 1992). It is still unresolved as to whether this is a molecular candidate for $I_{CL,swell}$ (Nilius et al., 1996).

4.2.8 Calcium-activated chloride channels

CaCC are activated by elevations in $[Ca^{2+}]_i$ (Jentsch et al., 2002), and are expressed in both excitable and non-excitable cell types, such as neurons, cardiac and smooth muscle cells, epithelial, endothelial and blood cells (Nilius and Droogmans, 2003). They participate in physiological processes, such as neuronal excitability, transepithelial transport, oocyte fertilisation (Eggermont, 2004). Study of channel properties by investigation of macroscopic current is indicative of both small and intermediate conductance Cl^- channels. Small conductance channels (1-3pS) were identified in cardiac myocytes and smooth muscle cells. Common features of CaCCs is that they are activated in a voltage-dependent manner by way of elevated $[Ca^{2+}]_i$, although there are two proposed mechanisms of Ca^{2+}-induced channel activation between different tissues. Ca^{2+} may bind directly to the channel (observed in vascular endothelial cells and guinea pig hepatocytes (Koumi et al., 1994)) or it may activate the channel indirectly by phosphorylation of Ca^{2+}/calmodulin-dependent protein kinase as observed in T84 intestinal epithelial cells owing to the observation that CaCCs have been stably activated in excised patch experiments, indicative of direct Ca^{2+} activation (Koumi et al., 1994, Van Renterghem and Lazdunski, 1993). Others have observed channel rundown under these circumstances (Hartzell et al., 2005, Wagner et al., 1991), suggesting either that there is more than one channel isoform, or that different regulatory pathways exist (Eggermont, 2004). CaCCs are outwardly

rectifying displaying slow activation, >100ms at positive potentials, deactivating at negative potentials (Eggermont, 2004). As the kinetics of CaCCs are both Ca^{2+} and voltage-dependent, fast activation occurs in conditions of elevated $[Ca^{2+}]_i$ in conjunction with strong depolarisation. The permeability sequence of CaCCs is $I^- > NO_3^- > Cl^- > F^- > CH_3SO_4^-$ (Evans and Marty, 1986). The molecular biology of CaCCs is still unresolved, further data is required as CLCA have not been biophysically characterised (Eggermont, 2004). Pharmacological inhibitors of CACC are poorly selective, limiting the structural and functional characterisation of these channels (Eggermont, 2004), although block by DIDs and niflumic acid has been reported (Jentsch et al., 2002, Koumi et al., 1994)

4.2.9 Glycine and γ-amino butyric acid ($GABA_A$) activated chloride channels

The expression of these channel subtypes was originally believed to be limited to the CNS, however glycine and GABA receptors have in recent years been reported in both brown and white adipose tissues (Nicolaysen et al., 2007). GABA is a neutral amino acid which is released from the GABAergic neurons. GABA and glycine are major inhibitory neurotransmitters in mammalian CNS, as they are ligands for the $GABA_A$ chloride channel and glycine receptor. Within the CNS, $GABA_A$ and glycine receptor activation results in cellular Cl^- influx with hyperpolarisation, which subsequently inhibits neuronal activity as this response contributes to the early part of the inhibitory post synaptic potential. GABA also binds the $GABA_B$ receptors, however this will not be discussed herin as the $GABA_B$ channel is coupled via G proteins to calcium and potassium channels (Clement, 1996). Glycine and $GABA_A$ receptors belong to the ligand-gated ion channel superfamily along with nicotinic acetylcholine receptors, and $5HT_3$ receptors; which exhibit primary sequence homology and conserved structural attributes

between members (Jentsch et al., 2002). $GABA_A$ receptors are reported to be heterooligomeric pentamers comprising α, β and either У, δ, or ε subunits (Farrar et al., 1999), arranged around a central pore, with each subunit comprising 4 transmembrane domains. The N and C terminus are extracellular. Multiple $GABA_A$ subunits have been cloned. In humans, six α subunit (~53kDa) isoforms have been identified, with three β subunits (~57kDa), and three У subunits with additional δ, ε, π, θ subunits. Within each subunit class, isoforms share 70% sequence homology, however this falls to 30% between classes. $GABA_A$ receptors are reported to have varying single channel conductances varying from 12pS, 17-20pS, 27-30pS (Jentsch et al., 2002, Bormann, 1988) dependent on the combination of subunits within the channel. Glycine receptors are also reported to have multiple conductance states. Seven single channel conductances have been observed; 12pS-14pS; 18pS-23pS; 24pS-36pS; 42pS-49pS; 59-72pS; 80-94pS; 105pS-112pS, with native glycine receptors and heteromeric receptors having a smaller single channel conductance than homomeric receptors (Jentsch et al., 2002). Glycine and the $GABA_A$ show permeability sequence of $SCN^->I^->Br^->Cl^->F^-$ (Bormann, 1988, Jentsch et al., 2002). The GABA binding site is situated between the α and β subunits. The actions of GABA are modulated by various chemical substrates of which there are multiple sites within the $GABA_A$ receptor complex (Teuber et al., 1999). Drug binding to one site induces a conformational change in the $GABA_A$ receptor which alters the affinity of the other binding sites to drugs of other classes. $GABA_A$ is activated by muscimol and inhibited competitively by bicuculline and allosterically by benzodiazepines and barbiturates (Bormann, 1988, Eldefrawi and Eldefrawi, 1987). $GABA_A$ & glycine receptors are targets for a range of pharmaceutical drugs such as; antiepileptics (Rigo et al., 2002); anxiolytics (Ran et al., 2004); sedatives; hypnotics (Moraga-Cid et al.); muscle relaxants (Young et al., 1974).

Channel Type	Conductance (pS)	Activated by	Pharmacology	Gating	Permeability	Distribution	Presence in Adipocyte?	References
CIC-1	1.2 and 2.4	Voltage	Inhibited by 9-AC (IC50 10.6μM)	Voltage, exhibits both fast and slow gating properties		Skeletal muscle	Maybe	(Weinreich and Jentsch, 2001)
CIC-2	2-3	Hyperpolarisation, Cell swelling, acidic pH	Inhibited by 1mM 9-AC, 0.5mM NPPB. Cd^{2+} and Zn^{2+} (IC_{50})	Slow gating properties		Ubiquitous with elevated levels in the brain	No	(Jentsch et al., 2002, Furukawa et al., 1998, Clark et al., 1998)
CIC-Ka/ CIC-Kb						Exclusive to kidneys and inner ear	No	(Planells-Cases and Jentsch, 2009)
CIC-3, CIC-4 and CIC-5	Unknown	Voltages positive to +20mv				Endosomal chloride channels	No	(Jentsch et al., 2005, Gunther et al., 2003)
CIC-6, CIC-7						Predominant on the endosomes/	No	(Jentsch et al., 2005)

						lysosomes		
CFTR	10	Phosphorylation of regulatory domain and subsequent ATP hydrolysis				Epithelial lining	Maybe	(Tabcharani et al., 1990)
VRAC	Small =0.1-8 Intermediate = 20-90 Large=200-400	Increase in cellular volume. $[ATP]_i$ required	DIDS, SITS, 9-AC. Half maximal block induced by NPPB, verapamil, flufenamic and niflumic acid		$SCN^->I^->Br^->Cl^->F^-$	Ehrlich ascites, glia, osteoblasts, osteoclasts, epididymal and muscle cells.	No	(Jentsch et al., 2002)
Ca^{2+} activated Cl^-	1-3	Activated in a voltage dependent manner by $[Ca^{2+}]_i$	DIDs and niflumic acid	Slow	$I^->NO_3^->Cl^->F^->CH_3SO_4^-$	Excitable and non excitable cells		(Nilius and Droogmans, 2003, Nilius et al., 1996, Jentsch et al., 2002)
$GABA_A$	12 17-20 27-30	GABA and glycine	TBPS, bicuculine, picrotoxin		$SCN^->I^->Br^->Cl^->F^-$	Central nervous system	No	(Bormann, 1988, Jentsch et al., 2002)

Table 4.1 A summary of the characteristics of Cl^- channels. NPPB, 5-nitro-2-(3-phenylpropylaminobenzoic acid). DPC, diphenylcarbonate. DIDs 4, 4'-diisothiocyanatostilbene-2, 2'-disulfonic acid. SITS, stilbene isothiocyanate sulfonic acid. TBPS tert-butylbicyclophosphorothionate. 9-AC, 9-Anthracene Carboxylic acid. NB the single channel conductance (pS) of chloride channels, is dependent upon the recording conditions ie, Vm, $[Cl^-]_i$ $[Cl^-]_o$ and temperature.

4.3 Experimental aims

In Chapter 2 it was demonstrated that the Cl^- ion contributes to the membrane potential of both primary adipocyte and differentiated 3T3-L1 adipocytes. As such, there is a requirement for the presence of Cl^- channels within the plasma membrane of both adipocyte models. In this chapter the cell attached configuration of the patch clamp technique was used to investigate the presence of Cl^- channels on the plasma membrane of differentiated 3T3-L1 adipocytes.

4.4 Methods

4.3.1 Characterisation of chloride channels in differentiated 3T3-L1 adipocytes

The cell-attached configuration of the patch clamp technique was used to measure and investigate single-channel currents in 3T3-L1 adipocytes. Differentiated 3T3-L1 cells with a round morphology and a coalesced fat droplet, were selected for patching (see Chapter 3, Figure 3.7). Membrane currents were measured with the Axopatch 1D patch clamp amplifier (Axon instruments), filtered with an 8 pole Bessel filter at 2KHz and digitised at 10kHz prior to storage in the pClamp software programme. Currents flowing through the membrane patch were recorded at various pipette holding potentials. All experiments were performed at 22^{o}C. The membrane potential across the patch (Vm) was calculated by subtraction of the pipette holding potential (Vp) from resting membrane potential (Putney et al.), Vm=Vr-Vp. The resting membrane potential was assumed to be approximately -30mV as measured using the perforated patch configuration (See Chapter 3, Section 3.6.2).

All procedures for pipette pulling and sylgard coating were as outlined in Chapter 3, Section 3.5.4.1. To reduce noise in the recording introduced by the patch pipette, thick walled borosilicate capillaries were utilised (GC150F, Harvard apparatus). Pipette resistances were typically 10MΩ. For the pipette solution, a variety of ion-substituted solutions were used, comprising either Cl^- or gluconate (Yavuz et al.) as the major anion and either Na^+ or K^+ as the major cation. The composition of the pipette solutions are described in Table 4.2. The pH of the KCl, NaCl and NaGlu pipette solutions were adjusted to pH 7.4 with 1M NaOH.

Pipette solutions	**Composition of the pipette solutions (mM)**						
	KCl	NaCl	$MgCl_2$	$CaCl_2$	TES	NaGlu	Total Cl^-
KCl	140		1.1	2.6	10		147
NaCl		140	1.1	2.6	10		147
NaGlu			1.1	2.6	10	140	7

Table 4.2. A summary of the composition of all pipette solutions utilised in the single channel recording. TES= [N-Tris(hydroxymethyl) methyl-2-aminoethane sulfonic acid. NaGlu= Sodium Gluconate.

4.3.2 Optimisation of single channel recording methods

HEPES was initially used as a pH buffer, but was later substituted by TES in the composition of the pipette solution. HEPES has been reported to block Cl^- channel conductance in cultured Drosophilia neurons, giving rise to flickering and multiple sub-conductance levels (Yamamoto and Suzuki, 1987). HEPES, when present on either the intracellular or extracellular side of the membrane at 10mM concentrations or higher, is also reported to block ion conductance of an outwardly-rectifying anion channel in human pancreatic carcinoma epithelial-like cells (Hanrahan and Tabcharani, 1990). An example of a single-channel recording obtained when HEPES was used as the pipette solution with KCl is shown in Figure 4.2. In the recordings descried here, ion channel conductance was not observed at every membrane voltage tested. At the membrane

potentials where single channel currents were observed, the currents were not the typical square shape as expected for unitary single channel current events (Armstrong and Hille, 1998). Instead they appeared to have multiple conductance levels, and the inconsistency in open/ closed conductance is indicative of flickering and therefore suspect open channel block of the Cl^- channels.

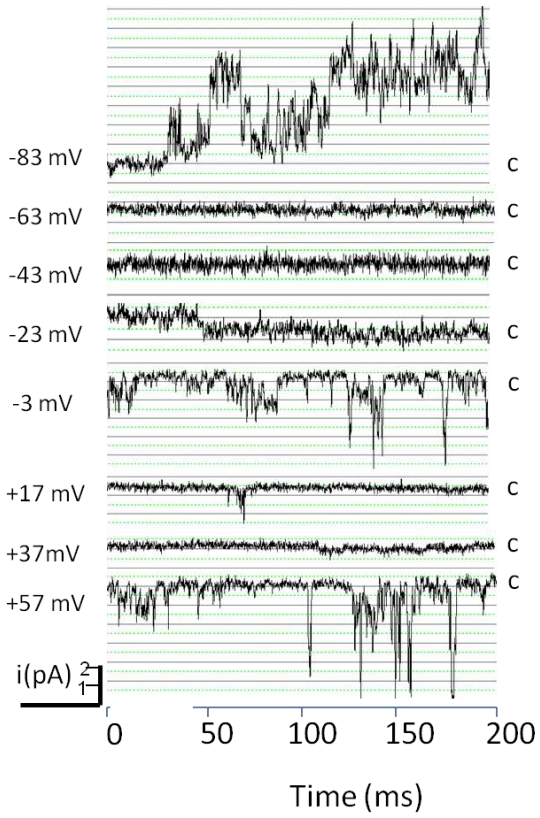

Figure 4.2. A single-channel recording of single-channel currents from 3T3-L1 adipocytes when HEPES KCl is used as the pipette solution. C shows the absence of channel activity. Each solid line represents a 1pA increment in ion channel current. The membrane potential of the cell at which currents were recorded are shown on the left-hand side. Vm values were corrected for experimental liquid junction potentials during the analysis. Outward currents are shown as downward deflections and inward currents are shown as upward deflections.

4.3.3 Measurement of liquid junction potentials

Liquid junction potentials arise wherever two solutions comprising different ion activities and concentrations are in contact. The magnitude of the resultant junction potential is dependent on the ions that are present in the pipette and the bath solutions, in particular the concentration, valency and mobility of the ions. In the cell attached configuration, when the recording pipette is first inserted into the bath solution, voltage offsets arise as a result of the ions in the pipette and bath solutions moving down there concentration gradients. The resultant voltage offsets are corrected by the amplifier when the current is zeroed in the voltage-clamp configuration. Following gigaseal formation between the patch pipette and the cell membrane, the pipette solution is no longer in contact with the bath solution. The junction potential disappears, however the offset that arises as a result of amplifier compensation is still present. The amplifier offset is of equal magnitude to the junction potential, but of opposite sign.

To measure the liquid junction potential for the cell attached configuration, the original reference electrode containing 150mM K^+ was substituted for one containing 3M KCl. K^+ and Cl^- have similar motilities and as such, the high concentration of K^+ and Cl^- prevent the formation of a liquid junction potential at the reference to bath junction. The patch pipette was filled with pipette solution, (either KCl, NaCl or NaGlu) and was subsequently submerged in the bath containing Hank's solution. The voltage offset that occurred as a result of the formation of a liquid junction potential between the pipette and the Hank's solution was compensated to zero. Immediately following compensation, the bath solution was exchanged and pipette solution perifused in place of the Hank's. The resulting offset was measured.

Each measurement was repeated 6 times for each of the 3 pipette solutions. The 3M KCl reference electrode was replaced for a fresh electrode following each measurement. The following formula was used to calculate the correct Vm, Vm=RMP-(VP+LJP).

4.3.4 Comparison of experimental and calculated liquid junction potentials

With KCl solution as the pipette solution, single-channel currents were recorded in the cell-attached configuration. Currents were recorded at room temperature ~22^{o}C, at various membrane potentials. Membrane potentials were corrected for junction potentials in the analysis See Table 4.3. Junction potentials were calculated both experimentally (n=7 for each pipette solution) and using the liquid junction potential calculator provided within Clampex. The junction potentials for the KCl solution between the experimental and calculated values in Clampex were similar. For NaCl and NaGlu, the experimental and computerised cell potential values were dissimilar. The calculated potential is sensitive to the selection of the single ion activity parameter. This could be a source of discrepancy between the calculated and the experimental values. Experimentally-derived junction potential values were used for correction of our Vm values.

Pipette solution (major cation/anion pairs)	Junction potentials for the cell attached configuration	
	Experimental	JPCalc v7 in Clampex
KCl	+2.65	+3.2
NaCl	-2.48	-0.6
NaGlu	+4.59	+10

Table 4.3. A comparison of experimental and calculated junction potentials for the cell attached configuration of the patch clamp technique. For pipette solutions containing the various anion/ cation pairs (n=7 for each pipette solution).

4.4 Data recording and analysis

Data were collected with the Clampex software, and subsequently analysed using pCLAMP. The median amplitudes of the membrane currents observed were determined as multiple levels of channel openings were presented. The median current-voltage relationships were plotted for each cell-attached patch clamp experiment. The conductance was determined from the slope of the current-voltage plot. The mean ± S.E.M of the channel conductances obtained for each pipette solution were compared with the Mann-Whitney test.

4.5 Results

4.5.1 Investigation into the identity of the channels present on the membrane surface of the 3T3-L1 adipocyte

With KCl-rich pipette solution, multiple levels of spontaneous single-channel currents were recorded (Figure 4.3). Single channel currents were present at all membrane potentials tested (-60mV to +60mV). Channel open and closed times were varied and inconsistent. The single-channel current amplitude was also varied, this being indicative of either single channel sub states, or conductance occurring simultaneously through more than one channel type present in the patch of the pipette. Multiple levels of single channel conductance were observed when KCl, NaCl or NaGlu were used as the pipette solution (data not shown). When the median current-voltage relationship was derived from the data in Figure 4.3, as shown in Figure 4.4, data show a channel reversal potential of 0mV, with an expected outward chloride current at -30mV. To investigate the presence of non selective cation channels in the plasma membrane of the white fat adipocyte, single-channel experiments were initially carried out with NMGCL. Cell attached patch clamping on 3T3-L1 adipocytes was time consuming, as such, due to time constraints, the methodology to investigate non selective cation channels was changed, and the perforated patch clamp configuration used instead. The results are described, in Chapter 2.

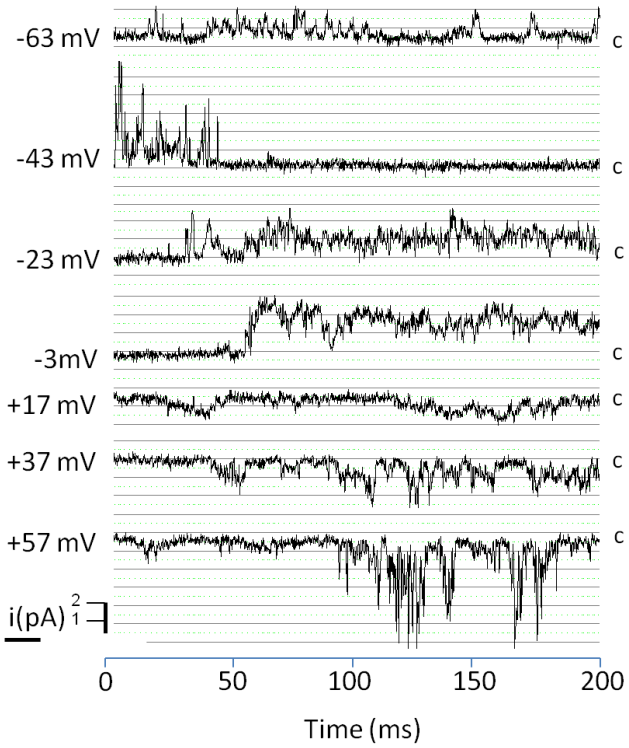

Figure 4.3. A representative trace, from a single patch, of single-channel currents recorded in 3T3-L1 adipocytes when TES KCl is used as the pipette solution. C shows channel closure. Each solid line represents a 1pA increment in ion channel conductance. As such, various levels of channel opening, possibly substates, were observed. Channel opening time also varied. The membrane potential of the cell at which currents were recorded are shown on the left hand side. Vm values were corrected for experimental liquid junction potentials during the analysis. Inward currents are shown as downward deflections and outward currents are shown as upward deflections.

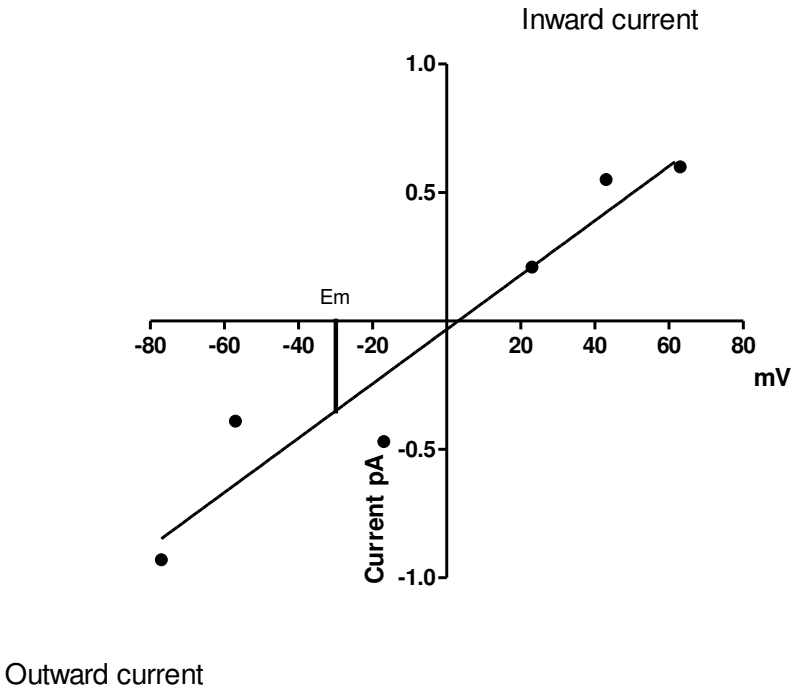

Figure 4.4 The median current voltage relationship derived from the data obtained from the single channel recording in Figure 4.3 (in differentiated 3T3-L1 adipocytes with TES KCL as the pipette solution). Data points were corrected for LJP and for membrane potential, such that the reversal potential for the channel is shown. The reversal potential for the channel is at 0mV. At the equilibrium potential (Em) of -30mV an outward chloride current would be expected.

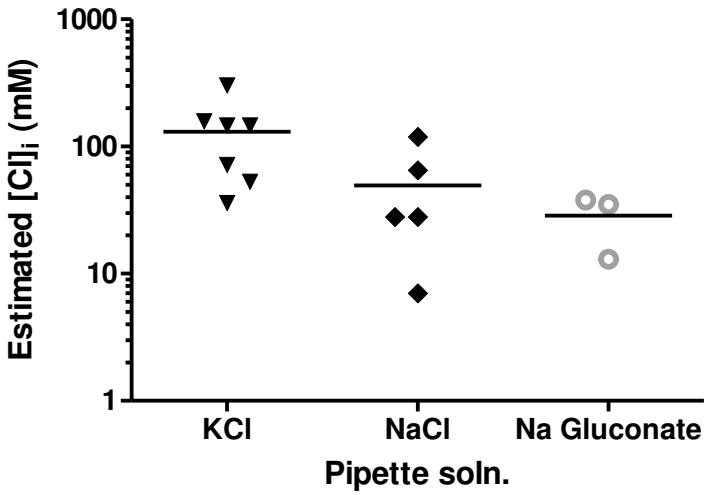

Figure 4.5. Determination of $[Cl^-]_i$ for each of the pipette solutions used within this investigation. Values were determined on the basis of the reversal occurring at the equilibrium potential, as given by the Nernst equation (see Chapter 2, Equation 2.1). All values are corrected for liquid junction potentials.

The values for $[Cl^-]_i$ as calculated by the Nernst equation (Figure 4.5) for each of the pipette solutions used are in excess of the $[Cl^-]_i$ reported for a generic cell (see Chapter 2, Table 2.1). Additionally the channel type patched within this investigation does not reverse at the Cl^- reversal potential, see Table 2.1. Both observations are in support of a non selective cation channel conductance in adipocytes.

4.5.2 Determination of ion channel conductance

The slope conductance was determined for the KCl, NaCl and NaGlu pipette solutions to identify the ion responsible for the currents observed in the single-channel traces. The median currents from each single channel patch experiment were plotted against holding potentials (Vm had previously been corrected for junction potential). The slope conductance was acquired from the plot, and used to represent single channel conductance (У) (Figure 4.4). For the KCl solution, only 7 out of 20 I-V plots were linear; for the NaCl pipette solution, 5 out of 18 traces were linear and for the NaGlu solution, 3 out of 13 traces were linear. Only linear traces (see Figure 4.6) were used in the calculation of slope conductance (Table 4.4). The occurrence of non-linear current traces could be indicative of rectification or the presence of multiple ion conductances. Further analysis with the plotting of all channel conductances obtained at each holding potential for each pipette solution failed to show any clustering or trend, and was not pursued any further. Channel conductances observed for each pipette solution were intermediate, with no difference between them. It is unlikely that a single ion is responsible for the conductance's observed. Additionally, to aid identification of channel types present in 3T3-L1 adipocyte membranes, reversal potentials were calculated from each IV plot for each solution tested. No clustering or trend was observed (Figure 4.5). No conclusion could be made

pertaining to the identity of the channel types present in the plasma membrane of 3T3-L1 adipocytes.

Chloride channels are reported to have multiple levels of ion conductance. To ascertain whether the channels present in the membrane patch were chloride channels, Cl^- was removed from the pipette solution by direct equimolar substitution with gluconate. It was hypothesised that if the currents were passing through chloride channels, the removal of the Cl^- ion would significantly reduce the number of channel currents observed. To account for large variance of the data and a low experimental number of repeats, conductance measured using pipette solutions in which Cl^- was the major cation were compared with the conductances obtained where Glu^- was the major cation using a Mann Whitney U test. There was no significant difference between the two sets of slope conductance. It is possible that there may be some ion current passing through non selective cation channels, which may account for the single channel conductance seen when NaGlu was used as a pipette solution.

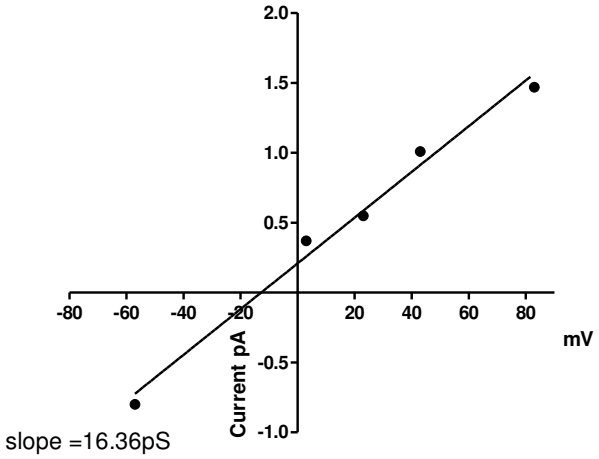

Figure 4.6. A representative graph of showing the median current voltage relationship obtained from a single channel current recording from a 3T3-L1 adipocyte, data points were corrected for LJP. The pipette used in this recording was filled with KCL solution. In this representative graph a single channel conductance of 16.36pS was found.

Pipette Solutions (major cation/anion pairs)	Conductance (pS), mean ±SEM
KCl	18.2±4.6
NaCl	25.31±4.8
NaGlu	10.3±4.

Table 4.4. The slope conductance of the median current voltage relationship obtained from each experimental pipette solution (n=3-7). There was no significant difference in conductance between any combination of pipette solution used, nor when solutions where chloride was the major anion were pooled and compared against NaGlu.

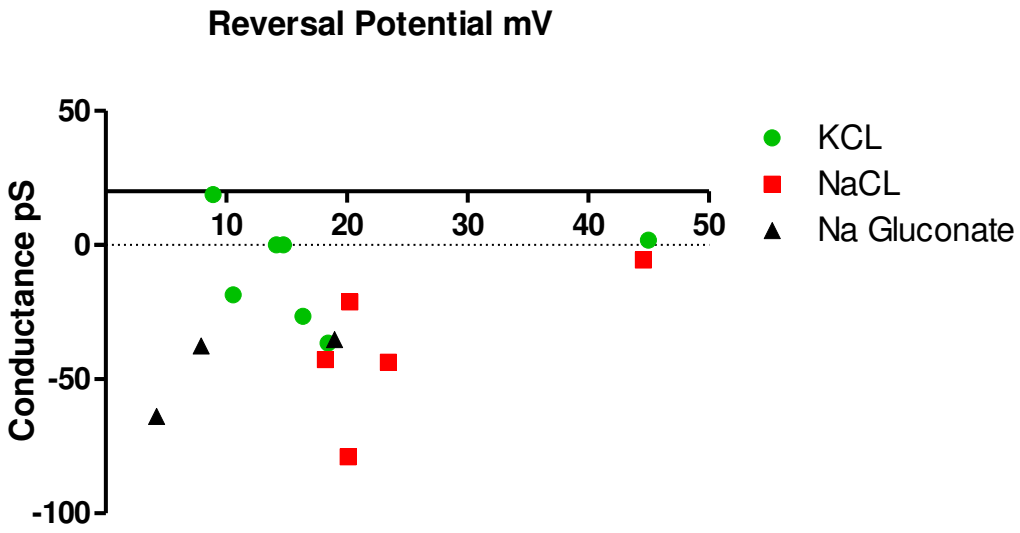

Figure 4.7. A plot of single channel conductance Vs reversal potential for all linear single channel recordings in all solutions tested. (n=3-7).

4.5.3 GHK modelling

Since substitution of $[Na^+]_o$ for $[K^+]_o$ did not have any significant effect on adipocyte Vm (See Figure 2.10), this data suggests they permeate across the cell membrane via a non selective cation channel. To model this $[Na^+]_i$ and $[K^+]_i$ and $[Na^+]_o$ and $[K^+]_o$ were represented as monovalent $[M^+]_i$ and $[M^+]_o$

respectively, as they cannot be distinguished between in terms of any effect on Vm.

$$Vm = -60Log_{10}\left(\frac{P_cCl_o + P_{NS}M_i}{P_cCl_i + P_{NS}M_o}\right) \quad \text{A}$$

$$Vm = -60Log_{10}\left(\frac{Cl_o + \alpha M_i}{Cl_i + \alpha M_o}\right) \quad \text{B}$$

Equation 4.1 GHK determination of $[M^+]_i$. Equaiton A represents the GHK formula for this scenario, B is a simplified version of A where values of α and $[Cl^-]_i$ were determined that would predict Vm as obtained from the following $[Cl^-]_o$ substitution experiment. α = P_{Ns}/P_{Cl} , with P_{Ns} representing the relative permeability for the non selective cation channel.

Extracellular conditions of :-

Decreasing $[Cl^-]_o$ from 138mM to 5mM $[Cl^-]_o$, giving rise to, Vm=0 (see Figure 2.14)

Using values of P_{NS}/P_{Cl}=0.36, $[Cl^-]_i$ was predicted to be 10mM and $[Na^+]_i$ + $[K^+]_i$ (ie $[M^+]_i$) 145mM. However, the median Vm in 5mM $[Cl^-]_o$ depolarised to -7mV (see Figure 2.14), modelling predicts, to obtain a negative Vm in 5mM $[Cl^-]_o$ that there would need to be a positive ion conductance leaving the adipocyte or a –ve ion conductance entering the cell, as such, the presence of another ion permeability was suggested. In the adipocytes that did not depolarise to 0mV it is possible that there is a very small background permeability to K^+ with a P_k/P_{Cl} of 0.23, however this is so small that very little change in Vm would occur in $[Na^+]_o$ substitution with $[K^+]_o$.

4.6 Discussion

To date, adipocyte electrophysiology has not been comprehensively studied. There are few reports describing ion channels present on the adipocyte plasma membrane or their roles in adipocyte physiology. The majority of electrophysiological studies have been conducted in primary tissue explants or in differentiated adipocytes from pre-adipocytes. This could be due to the difficulty in applying electrophysiological methods to the adipocyte. Primary adipocytes are composed predominantly of lipid with only a thin cytoplasm. Seal formation within the giga ohm range is difficult because of persistent clogging of the pipette tip with lipid. Often due to the fragility of the cells, it is difficult to maintain seals upon the adipocyte cytoplasm in an experimental perifusion system. Previously, adipocytes were considered to be somewhat inert and not a focus of intense study. It is only in recent years that the complex role and functions of adipocytes in energy homeostasis have become apparent. See Chapter 1, Section 1.3.

Differentiated 3T3-L1 adipocytes were used for the cell-attached investigations due to the observation that the likelihood of seal formation was improved with differentiated 3T3-L1 adipocytes. In chapter 2, the two adipocyte models exhibited similar electrophysiological responses, as such we can assume in this case that the experimental outcomes are transferrable between the differentiated 3T3-L1 adipocytes and the primary adipocytes.

K^+ is believed to be the predominant ion that controls Vm for many cell types, however it is uncertain as to whether it regulates Vm in adipocytes. The Vm of primary and 3T3-L1 adipocytes were measured in this study to be -34.4±1.5mV (n=68) and -28.5±1.2mV (n=88), respectively. The Vm values obtained were similar to the Vm observations of others. See Chapter 2, Table 2.3. 50mM

extracellular K^+ failed to depolarise the plasma membrane of primary rat adipocytes prompting investigation into the ion species involved in adipocyte Vm. Extracellular Cl^- removal was shown to depolarise both cell types, indicative of Cl^- channels on the plasma membrane.

Single-channel currents were observed in all pipette solutions used, however they were not the standard box shape of single channel currents or resembling of single-channel traces observed for NSCC or Cl^- in brown adipocytes (Sabanov and Nedergaard, 1995). The sharp transient openings, originally suspected to be caused by HEPES blockade of the channel were not altered upon buffer substitution to TES.

The conductance of the currents observed with NaCl as the pipette solution was 20.6±4.6pS. This was reduced when Cl^- was substituted with aspartate 10.3±4pS however this was not a significant reduction in conductance, possibly as a result of the low number of repeats. Channel events were still occurring with a conductance of 10pS, likely to be due to Na^+ conductance through NSCC channels. The conductances observed when either NaCl or KCl were used were similar (Table 4.4). It was suspected that both Cl^- and NSCC channel types were responsible for the events observed. Open probability was not calculated due to the difficulties in discerning the single-channel events between these. Due to the large number of replicates needed to compile single-channel data and the difficulties in discerning between events of Cl^- and NSCC, the perforated patch clamp technique was re-visited to investigate the presence of NSCC on white fat adipocytes and 3T3-L1 adipocytes. These data are presented in Chapter 2.

With regard to Cl^- channels, there is only one published report of Cl^- channels in white adipocytes (Inoue et al., 2010), although the recording of Cl^- channels in these cells have been observed previously within this laboratory (Pulbutr, 2009).

An outwardly-rectifying chloride current was identified in mouse adipocytes with the whole-cell patch clamp technique. Current was induced following adipocyte exposure to a hypotonic challenge, with diminution following return to isotonic solution. The Cl^- channel was identified as a volume-sensitive outwardly rectifying Cl^- channel, the basis of the response to hypotonic challenge and the significant inhibition of current at positive potentials by glibenclamide. It is unlikely that this channel is the same as observed in this study as the 3T3-L1 adipocytes used here were bathed in isotonic solution. Metabolic changes also induce changes in intracellular osmolytes which could lead to regulatory volume decrease (RVD) in adipocytes, again it is unlikely this is the case in our adipocytes as they were patched in their basal state.

Anion channels have been more frequently observed in brown adipocytes. Initially, ion efflux studies utilising radio-labelled Cl^- demonstrated an α-adrenoceptor induced (stimulated by 1μM noradrenaline) efflux of Cl^- ions (Dasso et al., 1990). The characteristics of the channel responsible for this efflux were not characterised as it is not possible to ascertain this information with ion flux studies. Later, perforated patch clamp investigations by Pappone and Lee (1995) identified an α-adrenoceptor stimulated Ca^{2+} activated Cl^- current in rat brown adipocytes. It is well documented that stimulation of brown adipocytes with noradrenaline results in a triphasic membrane potential response, the first phase being an α-adrenoceptor stimulated rapid depolarisation. All authors to date who report anion channels in brown adipose tissue agree that Cl^- efflux is a candidate for the mediation of the α adrenergic induced depolarisation observed (Sabanov and Nedergaard, 1995, Pappone and Lee, 1995, Bae et al., 1999). The observation that an increased outward Cl^- permeability induces membrane depolarisation suggests that Cl^- is not passively distributed across the membrane and is in fact maintained at elevated $[Cl^-]_i$

concentrations. Equilibrium potential calculations by Dasso (1990), and Pappone (1995) indicate that brown adipocytes are capable of maintaining elevated $[Cl^-]_i$ concentrations (Dasso et al., 1990, Pappone and Lee, 1995).

In addition to the Ca^{2+} activated Cl^- current, a separate volume activated chloride current was detected in the same brown adipocytes. It is unlikely that either of the channels reported in brown adipocytes are representative of the Cl^- currents observed in this study as adipocytes were bathed in isotonic solution, and the currents observed were spontaneously active whilst the Cl^- current commonly reported in brown adipocytes required α-adrenoceptor stimulation.

Non-selective cation channels have been reported in both brown and white adipocytes (Koivisto et al., 1993, Siemen and Reuhl, 1987). Later studies by Sherwin identified an ATP activated non-selective cation conductance in white primary white fat adipocytes by whole-cell and perforated-patch methods. It was suggested that the NSCC conductance would result in cellular depolarisation (Lee and Pappone, 1997). This is in agreement with the observations of Ringer *et al* (2000). Ringer *et al* (2000) reported a β-adrenoceptor activated inward Na^+ current carried by the NSCC in brown fat, this NSCC is reported to be responsible for the 3rd phase depolarisation in the tri-phasic response to adrenoceptor stimulation. The inward Na^+ current was potentiated in the presence of β-adrenoceptor agonists BRL 37344 and BRL 35135A (100nM) and as expected was inhibited by insulin (100nM) (Ringer et al., 2000).

NSCC conductances reported to date in white adipose tissue are ~21pS-28pS (Sabanov and Nedergaard, 1995). This is double the suggested putative NSCC conductance reported here at 10pS. Ringer *et al* (2000) suggested that NSCC were similar between brown and white adipose cell types, with the physiological knowledge of one being transferrable to the other. The NSCC current presented

in this chapter appears to be different to those previously reported in brown and white adipocytes as channel events were spontaneously active, frequently detectable in the cell-attached configuration, and did not require adrenergic stimulation.

It is possible that the currents observed were due to the presence of glutamate receptors in adipocytes, these are ligand gated cation channels that pass Na^+ and K^+ in equal proportions giving rise to an equilibrium potential of ~0mV. Glutamate receptors are predominantly expressed in the synapse, however their presence has been demonstrated in BAT and epididymal WAT by immunohistochemistry (Nicolaysen et al., 2007). In addition to its role as an excitory neurotransmitter glutamate has also been reported to have an important role in cellular energy metabolism, as such the presence of glutamate does not necessarily represent a neurotransmitter function. As adipocytes have an important role in energy metabolism it is possible that these channels do indeed exist in adipocytes. The slope conductance of synaptic non NMDA (N-methyl-D-aspartate) glutamate receptor channels has been reported to be ~15pS, additionally these channels have been reported to exhibit a linear current-voltage relationship (Traynelis et al., 1993). These characteristics match those of the channels observed within this study, as such it is possible that non NMDA glutamate receptor channels are present in adipocytes.

4.7 Summary

To summarise, ion channels are present and active on the plasma membrane surface of 3T3-L1 adipocytes. The presence of Cl^- channels has been shown on the basis of the membrane potential effects of Cl^- observed in Chapter 2 in conjunction with the observed multiple substates when Cl^- was present in the pipette solution (Figure 4.3). The identities of the Cl^- channel (s) present on the membrane surface of the 3T3-L1 adipocytes remains unidentified. For CIC channel activation there is a requirement for Cl^-, as such in the absence of Cl^- we would expect not to observe Cl^- channel conductance. Furthermore VRAC is an unlikely candidate for the regulation of membrane potential. VRAC's are inhibited by Verapamil. In this study verapamil (20μM) did not cause a membrane potential response in our perforated patch clamp experiments in Cl^- rich solution. See Chapter 2, Figure 2.10. Of the Cl^- channels reviewed, we suggest CFTR as a candidate for the Cl^- conductances observed within this study. Both adipose and epithelial cells are derived from the mesoderm. Mesenchymal stem cells can be differentiated into either adipocytes (Billon et al., 2008) or endothelial cells (Oswald et al., 2004). As the two cell types share the same embryological origin, it is possible that CFTR may also be expressed in our differentiated 3T3-L1 cells.

In our cell-attached patch clamp, ion substitution of Cl^- for gluconate still gave channel activity. The channel type active in NaGlu is unlikely to be a member of the CIC channels. There was a reduction in conductance when Cl^- was substituted for Glu^-. Statistics identified this as being not significant, however this could be attributed to the low n number. As channel events were still occurring when $NaGlu^-$ was used as the pipette solution we suggest the presence of NSCC on the adipocyte plasma membrane. Extracellular substitution of bath

Na^+ for NMG^- had a significant hyperpolarising effect on membrane potential (see Figure 2.19). As the channel observed within this thesis had a reversal potential of 0 and a slope conductance of 16pS it is possible that this channel is a non NMDA glutamate receptor channel.

Additionally Nernst estimates of $[Cl^-]_i$ of ~100mM were 10x in excess of that which were predicted by the GHK equation (~10mM). 100mM $[Cl^-]_i$ is also excessively high under the given experimental conditions when compared to that which has been reported for any other cell type.

Further pharmacological and molecular characterisation are required to clarify the identity of the Cl^- and NSCC channels responsible for the events observed in this study.

Chapter 5

General Discussion

5.1 Summary of Findings

Currently, Ca^{2+} influx pathways in adipocytes have not yet been fully characterised. An increase in cellular Ca^{2+} influx by dihydropyridine-sensitive $Ca_v1.2$/ $Ca_v1.3$ VGCCs on the plasma membrane of the adipocyte is suggested as being one potential mechanism underlying the induction of the insulin resistant state in adipocytes (Draznin et al., 1987b). Adipocytes have a prominent role in the maintenance of whole-body energy homeostasis, as such disruption of the ability of the adipocyte to maintain energy homeostasis is implicated in the onset of peripheral insulin resistance and type II diabetes (Antuna-Puente et al., 2008). Ca^{2+} is an essential and ubiquitous second messenger, as discussed in Sections 1.3.1 to 1.3.2, Ca^{2+} is essential for lipolysis, lipogenesis and insulin stimulated glucose uptake, as such it is likely that dysregulated $[Ca^{2+}]_i$ can have detrimental effects on adipocyte function.

Additionally, very little is known about adipocyte Vm and the ion conductance's that regulate this. $Ca_v1.2$ /$Ca_v1.3$ channels are reported to activate upon membrane depolarisation, and are reported to deactivate under conditions of prolonged depolarisation (Hille, 2001). Other physiological regulators of adipocyte function such as adrenoceptor agonists/ antagonists are also suggested to regulate adipocyte function via alterations in membrane potential (van Mil et al., 1995, Xue et al., 2001), as such it is possible that Vm does play an important role in adipocyte function, and possibly influence adipocyte Ca^{2+} homeostasis. Perforated-patch investigations revealed the resting membrane potential of white fat adipocytes and differentiated 3T3-L1 adipocytes to be ~-30mV, a similar value to that already reported by others but using different techniques (Perry and Hales, 1969, Ramirez-Ponce et al., 1990, Beigelman and Shu, 1972). Elevation of $[K^+]_o$ did not have a significant effect on adipocyte Vm.

In Chapter 2, the ion species involved in the control of adipocyte Vm were found to be Cl^- and Na^+. The identity of the underlying Cl^- conductances observed remains unknown despite the single-channel investigations presented in Chapter 4.

In Chapter 3, $[Ca^{2+}]_i$ imaging investigations are suggestive of functional Ca^{2+} influx pathways on the plasma membrane of adipocytes. Utilisation of known voltage-gated calcium channel (VGCC) antagonists nifedipine and verapamil were indicative of $Ca_v1.3$ having a role in basal Ca^{2+} influx. Western blot investigations confirmed the presence of the α subunit of $Ca_v1.3$ in primary white fat adipocytes. However, it is unlikely that VGCCs have a role in the maintenance of basal $[Ca^{2+}]_i$, as, at stable Vm's of ~-30mV VGCCs are likely to reside in an inactivated state. Contrary to the observations of others, conditions of elevated $[K^+]_o$ cannot be used in conjunction with known VGCC inhibitors to determine the presence of VGCCs on the plasma membrane of adipocytes, since these conditions do not have a significant effect on adipocyte Vm. Depolarising conditions of Cl^- also did not cause any significant elevation in $[Ca^{2+}]_i$. VGCCs can activate, with resultant Ca^{2+} influx at depolarisations up to 0mV. If however VGCCs reside in an inactivated state, it is required that the inactivation is removed prior to reactivation. Since no further increase in $[Ca^{2+}]_i$ was observed on decreasing $[Cl^-]_o$ to 5mM, a condition known to depolarise adipocyte Vm to ~-7mV, suggests that the $Ca_v1.3$ channels are either absent or inactive.

The reverse mode of the NCX has been previously reported in primary adipocytes, especially at the depolarised Vm's of ~-30mV that were measured. In support of this idea, the $[Ca^{2+}]_i$ imaging data in Chapter 3, Figure 3.16 show a small increase in $[Ca^{2+}]_i$ following substitution of $[Na^+]_o$ for $[K^+]_o$. As such, the involvement of the NCX as means of Ca^{2+} entry was further investigated. $[Ca^{2+}]_i$ imaging data in conjunction with known pharmacological NCX inhibitors SN-6

and KBR-7943 was indicative of the presence of the reverse mode of the NCX as a Ca^{2+} entry pathway. Modelling of $[ion]_i$ also suggests that at a $[Ca^{2+}]_i$ of ~100nM, and an RMP of -30mV that the exchanger would operate in the forward mode. The reverse mode would occur as a Ca^{2+} re-entry pathway following $[Ca^{2+}]_o$ removal and the subsequent re-addition of $[Ca^{2+}]_o$. Western blotting was carried out to further investigate protein expression of the NCX in adipocytes, however this was unable to confirm the presence of the NCX. Due to the reported non-specific effects of NCX inhibitors upon other channel types, the presence and role of the reverse mode of the NCX in adipocytes remains uncertain. To confirm that the elevation of $[Ca^{2+}]_i$ observed upon buffer substitution for low $[Na^+]_o$ was due to the activity of the reverse mode of the NCX (see Figure 3.16), this protocol should have been repeated with NCX inhibitors SN-6 and KBR-7943, however due to time constraints and the consistent issues surrounding retention of the Fluo-4 AM dye in adipocytes, this could not be repeated.

Utilising animal knockout modes and molecular techniques, such as SiRNA (small interfering RNA) knockdown to inactivate the gene for the NCX, are other molecular techniques which may aid the determination of the role of the reverse mode of the NCX as a pathway of Ca^{2+} entry in adipocytes (Jackson and Linsley, 2010).

Insulin did not cause a significant affect on $[Ca^{2+}]_i$ following 30 minutes of acute exposure. It is possible that insulin does not give rise to dysregulated Ca^{2+} influx under the conditions used within this investigation. To further investigate the effect of the insulin resistant state upon $[Ca^{2+}]_{i,}$ it would be valuable to conduct $[Ca^{2+}]_i$ imaging experiments in adipose tissue sourced from insulin resistant rats/ human subjects. Within this investigation, re-addition of $[Ca^{2+}]_o$, the inhibitory effect of verapamil and KBR-7943 on Ca^{2+} influx were lost in acute

insulin conditions, suggestive of insulin promoting Ca^{2+} influx via another pathway.

Additionally, investigations within this thesis are suggestive of the presence of non-selective cation channels (NSCCs) on the plasma membrane of the adipocyte. Substitution of $[K^+]_o$ for $[Na^+]_o$ did not affect adipocyte membrane potential, however when $[Na^+]_o$ was subject to equimolar substitution by NMG-Cl (a compound which does not permeate NSCCs), membrane hyperpolarisation resulted. Addition of 2-APB, a known inhibitor of TRPC and TRPM NSCCs (see Table 2.6) (Chapter 2, Figure 2.20) did not have an effect on membrane potential, which lessens the likelihood of this channel type being a cation influx pathway in adipocytes. NSCCs as a Na^+ entry pathway have previously been reported in primary white adipocytes (Ringer et al., 2000). Additionally, cellular Ca^{2+} entry via NSCCs have been reported in other cell types (Magoski et al., 2000), so it is also likely that the NSCCs present in the adipocyte plasma membrane are also a source of Ca^{2+} influx in the white fat adipocyte. Cell attached investigations in Chapter 4 revealed channel characteristics that were in support of the presence of a NSCC in adipocytes. There was no significant difference in channel conductance between pipette solutions containing either Na^+ or K^+. Single channel slope conductances reported within this investigation of 16pS are similar to that reported for the non NMDA glutamate receptor channel (~15pS). Additionally this channel type passes Na^+ and K^+ equally, has a linear current voltage relationship and a reversal potential of 0. Expression of non NMDA glutamate receptor channels is predominantly within the central nervous system, however, non NMDA glutamate receptor channels have been reported in BAT, and various WAT adipose tissue depots (Nicolaysen, 2007). Further pharmacological investigations are required to confirm the identity of the NSCCs present on the plasma membrane surface of the white fat adipocyte.

Due to the plethora of reported NSCCs and the promiscuous effects of NSCC antagonists on other channel types (Pena and Ordaz, 2008), pharmacological investigations need to be performed in conjunction with molecular and patch-clamp methods. Overall as $[Ca^{2+}]_i$ has an important role in adipocytes; $[Ca^{2+}]_i$ measurements in conjunction with functional measurements of glucose uptake or lipolysis are required to study this hypothesis. Due to time constraints, functional assays were not performed within this investigation.

5.2 Does another second messenger act to regulate adipocyte function?

It is possible that another intracellular messenger acts in conjunction with $[Ca^{2+}]_i$ to regulate adipocyte function. PIP_2 is a possible candidate. It is also possible that the altered adipocyte calcium homeostasis occurs secondary or tertiary to the effects of insulin. As shown in Chapter 3, there was a reduced expression of $Ca_v1.3$ on the plasma membrane of adipocytes sourced from Zucker obese rats. In insulin resistance, IRS-1 levels and activity are decreased (Dresner et al., 1999). IRS-1 is associated with PI3K, which generates the complex phosphorylation cascade involving PIP_2 and PKC. Additionally, PIP_2 is present in lower concentrations in animal models of type 2 diabetes (Thore et al., 2007), with insulin-induced insulin resistant adipocytes exhibiting a decrease in plasma membrane PIP_2 (Horvath et al., 2008). Cellular levels of PIP_2 are decreased in insulin resistance induced by chronic insulin-stimulation in 3T3-L1 cells (Ryan and Hinchcliffee, 2011). The mechanism by which insulin resistance decreases PIP_2 is yet to be elucidated, although consequences of PIP_2 depletion have been reported. Depleted PIP_2 levels cause partial inhibition of $Ca_v1.2$ and $Ca_v1.3$ channel activity (Roberts-Crowley et al., 2009), and reduced vesicle trafficking in exocytotic processes (Thore et al., 2007). It is therefore possible that insulin resistance induced reductions in PIP_2 leading to reduced trafficking

and activity of VGCCs, resulting in reduced VGCC expression in the adipocyte plasma membrane and subsequently, reduced Ca^{2+} influx. Currently, the role of PIP_2 in Ca^{2+} channel trafficking has not fully been clarified. It is known, however, that association of VGCC α-subunits with different β-subunits does affect the sensitivity of VGCCs to levels of PIP_2 (Roberts-Crowley et al., 2009). PIP_2 is also implicated in adipokine secretion, with a requirement for PIP_2 in the trafficking of adiponectin containing secretory vesicles (Bedi et al., 2006). Both PIP_2 and Ca^{2+} are required for GLUT4 trafficking, reductions in either or both would give rise to reduced insulin-stimulated glucose uptake. Diacylglycerol (DAG) is a second product of PIP_2 hydrolysis, which together with Ca^{2+} activate PKC, and certain TRP channel isoforms (Hardie and Muallem, 2009). As PKC is also involved in insulin-stimulated glucose uptake (Kahn et al., 2006), it is possible that insulin-induced reductions in PIP_2 and subsequently lowered $[Ca^{2+}]_i$ levels, also act at the level of PKC to reduce insulin-stimulated glucose uptake. PIP_2 is the precursor to IP3, which regulates store-operated calcium release. It seems plausible to suggest that low PIP_2 levels would not sufficiently activate store-operated calcium release, potentially ameliorating insulin-induced stimulation of store-operated Ca^{2+} release as a source of elevated $[Ca^{2+}]_i$, although it has been suggested that low levels of cellular PIP_2 are sufficient for IP_3-induced calcium release (Loew, 2007). The role and identities of store-operated Ca^{2+} channels in adipocyte Ca^{2+} homeostasis requires further investigation. Conversely, elevated $[Ca^{2+}]_i$ is also associated with a loss of PIP_2 (Thore et al., 2007). Thus, it is possible that there is a complex interplay between cellular $[Ca^{2+}]_i$ and PIP_2, with alterations in either having the capacity to affect the level of other.

5.3 Membrane potential, $[Ca^{2+}]_i$ and PIP_2

Secretory cell types, such as pancreatic islet beta cells, conduct their secretory processes at positive membrane potentials in response to plasma membrane depolarisation. Adipocytes, by comparison, have a relatively-depolarised membrane potential and as such it is likely that adipokine secretion from adipocytes is constitutive, with the alterations in adipokine secretion following insulin resistance attributed to altered cellular levels of PIP_2 rather than membrane potential. PIP_2 is required for adiponectin secretion. Insulin resistance results in reduced cellular PIP_2 levels, and reduced adiponectin secretion, which would result in elevated circulating levels of the insulin resistance inducing cytokines TNF-α and IL6. Elevated levels of TNF-α and IL-6 can further contribute to the development of insulin resistance by stimulation of adipocyte lipolysis. Exogenous lipids have been shown to inhibit Ca^{2+} currents of both native and recombinant VGCCs from all three families of α_1-subunits ($Ca_v1.x$ – $Ca_v3.x$)(Roberts-Crowley et al., 2009), potentially causing further inhibition of Ca^{2+} influx.

PIP_2 is known to protect against Na^+ dependent inactivation of the NCX when it is operating in the forward mode (Ca^{2+} efflux), although the effects of PIP_2 upon the reverse mode of the exchanger are unknown. It is likely that the NCX has a role in maintaining Ca^{2+} influx in the white fat adipocyte, although further investigation, possibly by way of NCX knockouts or patch-clamping are required to confirm this hypothesis.

5.4 Critique of adipocyte models used within this investigation

Experiments within this thesis were performed using rat primary adipocytes and differentiated 3T3-L1 adipocytes. Primary rat white adipocytes are commonly used for biochemical and electrophysiological studies as they are widely

available, in comparison to primary human adipose sources. However, species variations have been reported between adipocytes of rat and human origin, with differences in adipokine secretion and lipolysis. The role of adipocyte-derived TNF-α in the pathogenesis of insulin resistance in rodents has been established, however this has not been clarified in adipocyte-derived TNF-α (Ruan et al., 2002). Also the expression of adipocyte β-adrenoceptors varies between rodents and humans, with expression of the β_1-adrenoceptor being prominent in humans, and the β_3-adrenoceptor predominating in rodents. This is an important consideration for functional studies as the affinity of the β-adrenoceptor agonist isoprenaline is 100 times higher for the β_1-adrenoceptor over the β_3-adrenoceptor; such differences in β-adrenoceptor expression would affect the cellular responses of adipocytes to β-adrenoceptor agonists. As differences between human and rodent adipocytes have been noted, it may be more appropriate to conduct experiments in human adipocytes (*in vitro*) or in a clinical setting (*in vivo*), to ensure that findings in rodent adipocyte samples are truly transferrable to human adipocytes. However, technical and experimental manipulations of primary adipocytes are difficult due to the elevated cellular lipid content and thin cytoplasm, particularly in the instance of adipocytes sourced from animal models of obesity, or obese/ insulin resistant humans. In these instances, adipocytes tend to be enlarged further and are more difficult to handle.

Differentiated 3T3-L1s were also used within this study, their advantages have been discussed in Chapter 3. However, there are reported differences in cellular physiology between isolated primary adipocytes and clonal cell lines. This was not an issue for the perforated patch investigations presented in Chapter 3, as electrophysiological responses to experimental manipulations were similar between the primary and differentiated 3T3-L1 adipocytes (Yorek et al., 1999),

suggestive of a similar mechanism underlying membrane potential for both cell types. Another consideration is the use of primary adipocyte cultures (pre-adipocytes differentiated into mature adipocytes in culture). The advantage of primary culture of pre-adipocytes is that it reduces the risk of collagenase treatment removing surface proteins. Thus, primary cell culture of adipocytes may aid detection of channel proteins expressed at the adipocyte cell membrane particularly in Western blot and in patch clamp experiments. Additionally, the $[Ca^{2+}]_i$ measurements made within this thesis represent the total $[Ca^{2+}]_i$ of the adipocyte cytoplasm. If intracellular Ca^{2+} signal transduction is localised, the methods used within this thesis would be unable to detect this in adipocytes. If adipocytes were flattened in morphology, then $[Ca^{2+}]_i$ imaging techniques would be more likely to detect localised $[Ca^{2+}]_i$ events. However, confocal $[Ca^{2+}]_i$ imaging has been employed in adipocytes and no regional $[Ca^{2+}]_i$ hotspots were identified (personal communication with Dr P.A Smith).

In summary, results from the $[Ca^{2+}]_i$ measurement studies have revealed the presence of VGCCs and the reverse mode of the Na^+/Ca^{2+} exchanger in white rat adipocytes, a visual overview is presented in Figure 5.1 .The presence of VGCCs in white adipocytes was confirmed in this study, however their physiological functions have not been fully elucidated. Further experiments are needed to advance the knowledge about the molecular and biophysical characteristics of these channel types in white fat adipocytes. The physiological roles of these Ca^{2+} influx pathways in other adipocyte functions, such as insulin-stimulated glucose uptake and adipokine secretion and lipolysis, require further investigation. Furthermore, K^+ was found not to affect adipocyte resting membrane potential. Although Cl^- and Na^+ were found to be the ion species regulating adipocyte resting membrane potential, the identity of the channel types underlying these conductances is also yet to be determined.

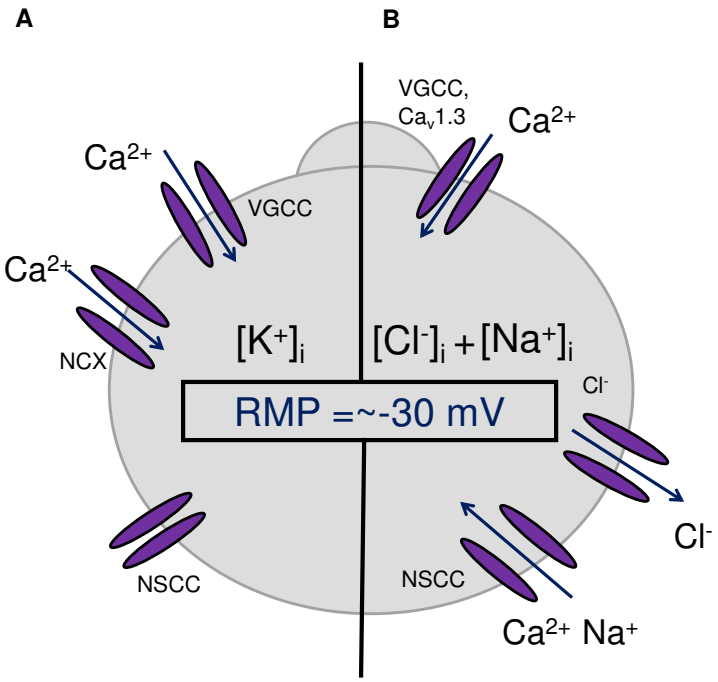

Figure 5.1. Overview of ion channels present on the adipocyte plasma membrane. A, ion channels reported by others in adipocytes (Pershadsingh et al., 1989, Ramirez-Ponce et al., 1990, Beigelman and Shu, 1972). B, ion channels identified within this thesis.

Bibliography

ABRAMOWITZ, J. & BIRNBAUMER, L. 2009. Physiology and pathophysiology of canonical transient receptor potential channels. *The FASEB Journal,* 23**,** 297-328.

AHMADIAN, M., DUNCAN, R. E. & SUL, H. S. 2009. The skinny on fat: lipolysis and fatty acid utilization in adipocytes. *Trends in Endocrinology & Metabolism,* 20**,** 424-428.

AILHAUD, G. (ed.) 2001. *Adipose Tissue Protocols*: Humana Press.

AITA, Y., KUREBAYASHI, N., HIROSE, S. & MATURANA, A. D. 2011. Protein kinase D regulates the human cardiac L-type voltage-gated calcium channel through serine 1884. *FEBS Lett,* 585**,** 3903-6.

AKIYAMA, Y., KAMEI, C. & TASAKA, K. 1990. Histamine lipolysis II: effects of histamine and related compounds on membrane potentials of rat adipocytes. *Methods Find Exp Clin Pharmacol,* 12**,** 457-65.

AL-HILLI, S. & WILLANDER, M. 2009. Membrane potential measurements across a human fat cell using ZnO nanorods. *Nanotechnology,* 20**,** 175103.

ALESSANDRI-HABER, N., DINA, O. A., CHEN, X. & LEVINE, J. D. 2009. TRPC1 and TRPC6 channels cooperate with TRPV4 to mediate mechanical hyperalgesia and nociceptor sensitization. *J Neurosci,* 29**,** 6217-28.

ALLEN, D. O. & BECK, R. R. 1986. Role of calcium ion in hormone-stimulated lipolysis. *Biochem Pharmacol,* 35**,** 767-72.

ALLEN, T. L. & FEBBRAIO, M. A. IL6 as a mediator of insulin resistance: fat or fiction? *Diabetologia,* 53**,** 399-402.

ALTIMIMI, H. F. & SCHNETKAMP, P. P. 2007. Na+/Ca2+-K+ exchangers (NCKX): functional properties and physiological roles. *Channels (Austin),* 1**,** 62-9.

ALVAREZ DE LA ROSA, D., CANESSA, C. M., FYFE, G. K. & ZHANG, P. 2000. Structure and regulation of amiloride-sensitive sodium channels. *Annu Rev Physiol,* 62**,** 573-94.

ANDERSON, M. P., GREGORY, R. J., THOMPSON, S., SOUZA, D. W., PAUL, S., MULLIGAN, R. C., SMITH, A. E. & WELSH, M. J. 1991. Demonstration that CFTR is a chloride channel by alteration of its anion selectivity. *Science,* 253**,** 202-5.

ANKORINA-STARK, I., AMSTRUP, J. & NOVAK, I. 2002. Regulation of the Na+/Ca2+ exchanger in rat pancreatic ducts. *J Membr Biol,* 186**,** 43-53.

ANNUNZIATO, L., PIGNATARO, G. & DI RENZO, G. F. 2004. Pharmacology of brain Na+/Ca2+ exchanger: from molecular biology to therapeutic perspectives. *Pharmacol Rev,* 56**,** 633-54.

ANTIGNY, F., NOREZ, C., BECQ, F. & VANDEBROUCK, C. CFTR and Ca Signaling in Cystic Fibrosis. *Front Pharmacol,* 2**,** 67.

ANTUNA-PUENTE, B., FEVE, B., FELLAHI, S. & BASTARD, J. P. 2008. Adipokines: the missing link between insulin resistance and obesity. *Diabetes Metab,* 34**,** 2-11.

ANTUNES, C. M., SALGADO, A. P., ROSARIO, L. M. & SANTOS, R. M. 2000. Differential patterns of glucose-induced electrical activity and intracellular calcium responses in single mouse and rat pancreatic islets. *Diabetes,* 49**,** 2028-38.

AOSAKI, T. & KASAI, H. 1989. Characterization of two kinds of high-voltage-activated Ca-channel currents in chick sensory neurons. Differential sensitivity to dihydropyridines and omega-conotoxin GVIA. *Pflugers Arch,* 414**,** 150-6.

ARIKKATH, J. & CAMPBELL, K. P. 2003. Auxiliary subunits: essential components of the voltage-gated calcium channel complex. *Curr Opin Neurobiol,* 13**,** 298-307.

ARMSTRONG, C. M. & BEZANILLA, F. 1973. Currents related to movement of the gating particles of the sodium channels. *Nature,* 242**,** 459-61.

ARMSTRONG, C. M. & HILLE, B. 1998. Voltage-gated ion channels and electrical excitability. *Neuron,* 20**,** 371-80.

ARMSTRONG, D. L. 1989. Calcium channel regulation by calcineurin, a Ca2+-activated phosphatase in mammalian brain. *Trends Neurosci,* 12**,** 117-22.

ARNER, P. 2003. The adipocyte in insulin resistance: key molecules and the impact of the thiazolidinediones. *Trends in Endocrinology & Metabolism,* 14**,** 137-145.

ARNER, P. 2005a. Human fat cell lipolysis: biochemistry, regulation and clinical role. *Best Pract Res Clin Endocrinol Metab,* 19**,** 471-82.

ARNER, P. 2005b. Insulin resistance in type 2 diabetes -- role of the adipokines. *Curr Mol Med,* 5**,** 333-9.

ARNON, A., HAMLYN, J. M. & BLAUSTEIN, M. P. 2000. Na(+) entry via store-operated channels modulates Ca(2+) signaling in arterial myocytes. *Am J Physiol Cell Physiol,* 278**,** C163-73.

AULCHENKO, Y. S., PULLEN, J., KLOOSTERMAN, W. P., YAZDANPANAH, M., HOFMAN, A., VAESSEN, N., SNIJDERS, P. J., ZUBAKOV, D., MACKAY, I., OLAVESEN, M., SIDHU, B., SMITH, V. E., CAREY, A., BEREZIKOV, E., UITTERLINDEN, A. G., PLASTERK, R. H., OOSTRA, B. A. & VAN DUIJN, C. M. 2007. LPIN2 is associated with type 2 diabetes, glucose metabolism, and body composition. *Diabetes,* 56**,** 3020-6.

BADOU, A., JHA, M. K., MATZA, D., MEHAL, W. Z., FREICHEL, M., FLOCKERZI, V. & FLAVELL, R. A. 2006. Critical role for the beta regulatory subunits of Cav channels in T lymphocyte function. *Proc Natl Acad Sci U S A,* 103**,** 15529-34.

BAE, Y. M., PARK, M. K., LEE, S. H., HO, W.-K. & EARM, Y. E. 1999. Contribution of Ca2+-activated K+ channels and non-selective cation channels to membrane potential of pulmonary arterial smooth muscle cells of the rabbit. *The Journal of Physiology,* 514**,** 747-758.

BALLARD, C. & SCHAFFER, S. 1996. Stimulation of the Na+/Ca2+ exchanger by phenylephrine, angiotensin II and endothelin 1. *J Mol Cell Cardiol,* 28**,** 11-7.

BANERJEE, R. R., RANGWALA, S. M., SHAPIRO, J. S., RICH, A. S., RHOADES, B., QI, Y., WANG, J., RAJALA, M. W., POCAI, A., SCHERER, P. E., STEPPAN, C. M., AHIMA, R. S., OBICI, S., ROSSETTI, L. & LAZAR, M. A. 2004. Regulation of fasted blood glucose by resistin. *Science,* 303**,** 1195-8.

BANGA, A., BODLES, A. M., RASOULI, N., RANGANATHAN, G., KERN, P. A. & OWENS, R. J. 2008. Calcium is involved in formation of high molecular weight adiponectin. *Metabolic syndrome and related disorders,* 6**,** 103-111.

BARRITT, G. J. 1999. Receptor-activated Ca2+ inflow in animal cells: a variety of pathways tailored to meet different intracellular Ca2+ signalling requirements. *Biochem J,* 337 (Pt 2)**,** 153-69.

BAYS, H., MANDARINO, L. & DEFRONZO, R. A. 2004. Role of the Adipocyte, Free Fatty Acids, and Ectopic Fat in Pathogenesis of Type 2 Diabetes Mellitus: Peroxisomal Proliferator-Activated Receptor Agonists Provide a Rational Therapeutic Approach. *Journal of Clinical Endocrinology & Metabolism,* 89**,** 463-478.

BEDI, D., CLARKE, K. J., DENNIS, J. C., ZHONG, Q., BRUNSON, B. L., MORRISON, E. E. & JUDD, R. L. 2006. Endothelin-1 inhibits adiponectin secretion through a phosphatidylinositol 4,5-bisphosphate/actin-dependent mechanism. *Biochemical and Biophysical Research Communications,* 345**,** 332-339.

BEER, N. A., JAKUBOWICZ, D. J., BEER, R. M., AROCHA, I. R. & NESTLER, J. E. 1993. Effects of nitrendipine on glucose tolerance and serum insulin and dehydroepiandrosterone

sulfate levels in insulin-resistant obese and hypertensive men. *J Clin Endocrinol Metab,* 76**,** 178-83.

BEGUM, N., LEITNER, W., REUSCH, J. E., SUSSMAN, K. E. & DRAZNIN, B. 1993. GLUT-4 phosphorylation and its intrinsic activity. Mechanism of Ca(2+)-induced inhibition of insulin-stimulated glucose transport. *J Biol Chem,* 268**,** 3352-6.

BEGUM, N., SUSSMAN, K. E. & DRAZNIN, B. 1992. Calcium-induced inhibition of phosphoserine phosphatase in insulin target cells is mediated by the phosphorylation and activation of inhibitor 1. *J Biol Chem,* 267**,** 5959-63.

BEIGELMAN, P. M. & HOLLANDER, P. B. 1962. Effect of insulin upon resting electrical potential of adipose tissue. *Proc Soc Exp Biol Med,* 110**,** 590-5.

BEIGELMAN, P. M. & HOLLANDER, P. B. 1963. Effect of insulin and rat weight upon rat adipose tissue membrane resting electrical potential (REP). *Diabetes,* 12**,** 262-7.

BEIGELMAN, P. M. & HOLLANDER, P. B. 1964. EFFECTS OF ELECTROLYTES UPON ADIPOSE TISSUE MEMBRANE ELECTRICAL POTENTIALS. *Proc Soc Exp Biol Med,* 115**,** 14-6.

BEIGELMAN, P. M. & SHU, M. J. 1972. Adipose resting membrane potential: in vitro responses to C1 - and K+. *Proc Soc Exp Biol Med,* 141**,** 618-21.

BERNATCHEZ, G., TALWAR, D. & PARENT, L. 1998. Mutations in the EF-hand motif impair the inactivation of barium currents of the cardiac alpha1C channel. *Biophys J,* 75**,** 1727-39.

BERRIDGE, M. J., BOOTMAN, M. D. & RODERICK, H. L. 2003. Calcium signalling: dynamics, homeostasis and remodelling. *Nat Rev Mol Cell Biol,* 4**,** 517-29.

BERRIDGE, M. J., LIPP, P. & BOOTMAN, M. D. 2000. The versatility and universality of calcium signalling. *Nat Rev Mol Cell Biol,* 1**,** 11-21.

BEZPROZVANNY, I., WATRAS, J. & EHRLICH, B. E. 1991. Bell-shaped calcium-response curves of Ins(1,4,5)P3- and calcium-gated channels from endoplasmic reticulum of cerebellum. *Nature,* 351**,** 751-4.

BILLON, N., MONTEIRO, M. C. & DANI, C. 2008. Developmental origin of adipocytes: new insights into a pending question. *Biol Cell,* 100**,** 563-75.

BLACKMORE, P. F. & AUGERT, G. 1989. Effect of hormones on cytosolic free calcium in adipocytes. *Cell Calcium,* 10**,** 561-567.

BLAUSTEIN, M. P. & LEDERER, W. J. 1999. Sodium/Calcium Exchange: Its Physiological Implications. *Physiol. Rev.,* 79**,** 763-854.

BODEN, G. & CHEN, X. 1995. Effects of fat on glucose uptake and utilization in patients with non-insulin-dependent diabetes. *J Clin Invest,* 96**,** 1261-8.

BODEN, G., CHEN, X., RUIZ, J., WHITE, J. V. & ROSSETTI, L. 1994. Mechanisms of fatty acid-induced inhibition of glucose uptake. *J Clin Invest,* 93**,** 2438-46.

BODEN, G. & SHULMAN, G. I. 2002. Free fatty acids in obesity and type 2 diabetes: defining their role in the development of insulin resistance and beta-cell dysfunction. *Eur J Clin Invest,* 32 Suppl 3**,** 14-23.

BORMANN, J. 1988. Electrophysiology of GABAA and GABAB receptor subtypes. *Trends Neurosci,* 11**,** 112-6.

BOULAY, G., BROWN, D. M., QIN, N., JIANG, M., DIETRICH, A., ZHU, M. X., CHEN, Z., BIRNBAUMER, M., MIKOSHIBA, K. & BIRNBAUMER, L. 1999. Modulation of Ca(2+) entry by polypeptides of the inositol 1,4, 5-trisphosphate receptor (IP3R) that bind transient receptor potential (TRP): evidence for roles of TRP and IP3R in store depletion-activated Ca(2+) entry. *Proc Natl Acad Sci U S A,* 96**,** 14955-60.

BREHM, P. & ECKERT, R. 1978. Calcium entry leads to inactivation of calcium channel in Paramecium. *Science,* 202**,** 1203-1206.

BROWN, M. S. & GOLDSTEIN, J. L. 1997. The SREBP Pathway: Regulation of Cholesterol Metabolism by Proteolysis of a Membrane-Bound Transcription Factor. *Cell,* 89**,** 331-340.

BRUNING, J. C., WINNAY, J., CHEATHAM, B. & KAHN, C. R. 1997. Differential signaling by insulin receptor substrate 1 (IRS-1) and IRS-2 in IRS-1-deficient cells. *Mol Cell Biol,* 17**,** 1513-21.

BUSSELBERG, D., PLATT, B., MICHAEL, D., CARPENTER, D. O. & HAAS, H. L. 1994. Mammalian voltage-activated calcium channel currents are blocked by Pb2+, Zn2+, and Al3+. *J Neurophysiol,* 71**,** 1491-7.

BYYNY, R. L., LOVERDE, M., LLOYD, S., MITCHELL, W. & DRAZNIN, B. 1992. Cytosolic calcium and insulin resistance in elderly patients with essential hypertension. *Am J Hypertens,* 5**,** 459-64.

CARMEN, G. Y. & VICTOR, S. M. 2006. Signalling mechanisms regulating lipolysis. *Cell Signal,* 18**,** 401-8.

CARRIER, G. O. 1995. Whole-cell and perforated patch recordings of four distinct K+ currents in acutely dispersed coeliac-superior mesenteric ganglia neurons of adult rats. *Brain Research,* 701**,** 1-12.

CARROLL, L., VOISEY, J. & VAN DAAL, A. 2004. Mouse models of obesity. *Clinics in Dermatology,* 22**,** 345-349.

CATTERALL, W. A. 2000. Structure and regulation of voltage-gated Ca2+ channels. *Annu Rev Cell Dev Biol,* 16**,** 521-55.

CATTERALL, W. A., CHANDY, K. G., CLAPHAM, D. E., GUTMAN, G. A., HOFMANN, F., HARMAR, A. J., ABERNETHY, D. R. & SPEDDING, M. 2003a. International Union of Pharmacology: Approaches to the nomenclature of voltage-gated ion channels. *Pharmacological Reviews,* 55**,** 573-574.

CATTERALL, W. A., PEREZ-REYES, E., SNUTCH, T. P. & STRIESSNIG, J. 2005. International Union of Pharmacology. XLVIII. Nomenclature and structure-function relationships of voltage-gated calcium channels. *Pharmacol Rev,* 57**,** 411-25.

CATTERALL, W. A., STRIESSNIG, J., SNUTCH, T. P. & PEREZ-REYES, E. 2003b. International Union of Pharmacology. XL. Compendium of voltage-gated ion channels: calcium channels. *Pharmacol Rev,* 55**,** 579-81.

CENA, B. S. V. 1998. *Ion Channel Pharmacology*.

CENS, T., ROUSSET, M., LEYRIS, J. P., FESQUET, P. & CHARNET, P. 2006. Voltage- and calcium-dependent inactivation in high voltage-gated Ca(2+) channels. *Prog Biophys Mol Biol,* 90**,** 104-17.

CHAMBERLIN, M. E. & STRANGE, K. 1989. Anisosmotic cell volume regulation: a comparative view. *Am J Physiol,* 257**,** C159-73.

CHAVES, V. E., FRASSON, D. & KAWASHITA, N. H. 2011. Several agents and pathways regulate lipolysis in adipocytes. *Biochimie,* 93**,** 1631-40.

CHENG, K., HASPEL, H. C., VALLANO, M. L., OSOTIMEHIN, B. & SONENBERG, M. 1980. Measurement of membrane potentials (psi) of erythrocytes and white adipocytes by the accumulation of triphenylmethylphosphonium cation. *J Membr Biol,* 56**,** 191-201.

CHERNYSH, O., CONDRESCU, M. & REEVES, J. P. 2008. Sodium-dependent inactivation of sodium/calcium exchange in transfected Chinese hamster ovary cells. *Am J Physiol Cell Physiol,* 295**,** C872-82.

CHERRINGTON, A. D., MOORE, M. C., SINDELAR, D. K. & EDGERTON, D. S. 2007. Insulin action on the liver in vivo. *Biochem Soc Trans,* 35**,** 1171-4.

CHILTON, L., OHYA, S., FREED, D., GEORGE, E., DROBIC, V., SHIBUKAWA, Y., MACCANNELL, K. A., IMAIZUMI, Y., CLARK, R. B., DIXON, I. M. C. & GILES, W. R. 2005. K+ currents regulate the resting membrane potential, proliferation, and contractile responses in ventricular fibroblasts and myofibroblasts. *American Journal of Physiology - Heart and Circulatory Physiology,* 288**,** H2931-H2939.

CHINI, B. & PARENTI, M. 2004. G-protein coupled receptors in lipid rafts and caveolae: how, when and why do they go there? *Journal of Molecular Endocrinology,* 32**,** 325-338.

CHUNG, S. & KACZMAREK, L. K. 1995. Modulation of the inactivation of voltage-dependent potassium channels by cAMP. *J Neurosci,* 15**,** 3927-35.

CLARK, S., JORDT, S. E., JENTSCH, T. J. & MATHIE, A. 1998. Characterization of the hyperpolarization-activated chloride current in dissociated rat sympathetic neurons. *J Physiol,* 506 (Pt 3)**,** 665-78.

CLAUSEN, T. 1996. The Na+, K+ pump in skeletal muscle: quantification, regulation and functional significance. *Acta Physiol Scand,* 156**,** 227-35.

CLEMENT, Y. 1996. Structural and pharmacological aspects of the GABAA receptor: involvement in behavioral pathogenesis. *J Physiol Paris,* 90**,** 1-13.

CLIFFORD, E. E., PARKER, K., HUMPHREYS, B. D., KERTESY, S. B. & DUBYAK, G. R. 1998. The P2X1 Receptor, an Adenosine Triphosphateâ€"Gated Cation Channel, Is Expressed in Human Platelets but not in Human Blood Leukocytes. *Blood,* 91**,** 3172-3181.

COBURN, C. T., HAJRI, T., IBRAHIMI, A. & ABUMRAD, N. A. 2001. Role of CD36 in membrane transport and utilization of long-chain fatty acids by different tissues. *J Mol Neurosci,* 16**,** 117-21; discussion 151-7.

COETZEE, W. A., AMARILLO, Y., CHIU, J., CHOW, A., LAU, D., MCCORMACK, T., MORENO, H., NADAL, M. S., OZAITA, A., POUNTNEY, D., SAGANICH, M., VEGA-SAENZ DE MIERA, E. & RUDY, B. 1999. Molecular diversity of K+ channels. *Ann N Y Acad Sci,* 868**,** 233-85.

COLLINS, T. J., LIPP, P., BERRIDGE, M. J. & BOOTMAN, M. D. 2001. Mitochondrial Ca(2+) uptake depends on the spatial and temporal profile of cytosolic Ca(2+) signals. *J Biol Chem,* 276**,** 26411-20.

COMBS, T. P., BERG, A. H., OBICI, S., SCHERER, P. E. & ROSSETTI, L. 2001. Endogenous glucose production is inhibited by the adipose-derived protein Acrp30. *J Clin Invest,* 108**,** 1875-81.

CORRY, B., O'MARA, M. & CHUNG, S. H. 2004. Conduction mechanisms of chloride ions in ClC-type channels. *Biophys J,* 86**,** 846-60.

CZECH, M. P. 2002. Fat Targets for Insulin Signaling. *Molecular Cell,* 9**,** 695-696.

D'ANGLEMONT DE TASSIGNY, A., SOUKTANI, R., GHALEH, B., HENRY, P. & BERDEAUX, A. 2003. Structure and pharmacology of swelling-sensitive chloride channels, I(Cl,swell). *Fundam Clin Pharmacol,* 17**,** 539-53.

DACQUET, C., LOIRAND, G., RAKOTOARISOA, L., MIRONNEAU, C. & MIRONNEAU, J. 1989. (+)-[3H]-PN 200-110 binding to cell membranes and intact strips of portal vein smooth muscle: characterization and modulation by membrane potential and divalent cations. *Br J Pharmacol,* 97**,** 256-62.

DAI, S., HALL, D. D. & HELL, J. W. 2009. Supramolecular Assemblies and Localized Regulation of Voltage-Gated Ion Channels. *Physiological Reviews,* 89**,** 411-452.

DALTON, S., TAKAHASHI, S. X., MIRIYALA, J. & COLECRAFT, H. M. 2005. A single CaVbeta can reconstitute both trafficking and macroscopic conductance of voltage-dependent calcium channels. *J Physiol,* 567**,** 757-69.

DASSO, L., CONNOLLY, E. & NEDERGAARD, J. 1990. [alpha]1-Adrenergic stimulation of Cl- efflux in isolated brown adipocytes. *FEBS Letters,* 262**,** 25-28.

DAVIS, R. J., BRAND, M. D. & MARTIN, B. R. 1981. The effect of insulin on plasma-membrane and mitochondrial-membrane potentials in isolated fat-cells. *Biochem J,* 196**,** 133-47.

DE GREEF, C., VAN DER HEYDEN, S., VIANA, F., EGGERMONT, J., DE BRUIJN, E. A., RAEYMAEKERS, L., DROOGMANS, G. & NILIUS, B. 1995. Lack of correlation between mdr-1 expression and volume-activation of cloride-currents in rat colon cancer cells. *Pflugers Arch,* 430**,** 296-8.

DE LEON, M., WANG, Y., JONES, L., PEREZ-REYES, E., WEI, X., SOONG, T. W., SNUTCH, T. P. & YUE, D. T. 1995. Essential Ca(2+)-binding motif for Ca(2+)-sensitive inactivation of L-type Ca2+ channels. *Science,* 270**,** 1502-6.

DELLA ROCCA, G. J., VAN BIESEN, T., DAAKA, Y., LUTTRELL, D. K., LUTTRELL, L. M. & LEFKOWITZ, R. J. 1997. Ras-dependent mitogen-activated protein kinase activation by G protein-coupled receptors. Convergence of Gi- and Gq-mediated pathways on calcium/calmodulin, Pyk2, and Src kinase. *J Biol Chem,* 272**,** 19125-32.

DEMAUREX, N., POBURKO, D. & FRIEDEN, M. 2009. Regulation of plasma membrane calcium fluxes by mitochondria. *Biochim Biophys Acta,* 1787**,** 1383-94.

DIEZ, J. J. & IGLESIAS, P. 2003. The role of the novel adipocyte-derived hormone adiponectin in human disease. *Eur J Endocrinol,* 148**,** 293-300.

DILMAC, N., HILLIARD, N. & HOCKERMAN, G. H. 2004. Molecular determinants of frequency dependence and Ca2+ potentiation of verapamil block in the pore region of Cav1.2. *Mol Pharmacol,* 66**,** 1236-47.

DING, V. D., QURESHI, S. A., SZALKOWSKI, D., LI, Z., BIAZZO-ASHNAULT, D. E., XIE, D., LIU, K., JONES, A. B., MOLLER, D. E. & ZHANG, B. B. 2002. Regulation of insulin signal transduction pathway by a small-molecule insulin receptor activator. *Biochem J,* 367**,** 301-6.

DIOCHOT, S., RICHARD, S., BALDY-MOULINIER, M., NARGEOT, J. & VALMIER, J. 1995. Dihydropyridines, phenylalkylamines and benzothiazepines block N-, P/Q- and R-type calcium currents. *Pflugers Arch,* 431**,** 10-9.

DIRAISON, F., YANKAH, V., LETEXIER, D., DUSSERRE, E., JONES, P. & BEYLOT, M. 2003. Differences in the regulation of adipose tissue and liver lipogenesis by carbohydrates in humans. *J Lipid Res,* 44**,** 846-53.

DOAN, T. N. & KUNZE, D. L. 1999. Contribution of the hyperpolarization-activated current to the resting membrane potential of rat nodose sensory neurons. *The Journal of Physiology,* 514**,** 125-138.

DONG, H., DUNN, J. & LYTTON, J. 2002. Stoichiometry of the cardiac Na+/Ca2+ exchanger NCX1.1 measured in transfected HEK cells. *Biophys. J.,* 82**,** 1943-1952.

DRAZNIN, B. 1988. Intracellular calcium, insulin secretion, and action. *The American Journal of Medicine,* 85**,** 44-58.

DRAZNIN, B., KAO, M. & SUSSMAN, K. E. 1987a. Insulin and glyburide increase cytosolic free-Ca2+ concentration in isolated rat adipocytes. *Diabetes,* 36**,** 174-8.

DRAZNIN, B., LEWIS, D., HOULDER, N., SHERMAN, N., ADAMO, M., GARVEY, W. T., LEROITH, D. & SUSSMAN, K. 1989. Mechanism of insulin resistance induced by sustained levels of cytosolic free calcium in rat adipocytes. *Endocrinology,* 125**,** 2341-9.

DRAZNIN, B., SUSSMAN, K., KAO, M., LEWIS, D. & SHERMAN, N. 1987b. The existence of an optimal range of cytosolic free calcium for insulin-stimulated glucose transport in rat adipocytes. *J Biol Chem,* 262**,** 14385-8.

DRAZNIN, B., SUSSMAN, K. E., ECKEL, R. H., KAO, M., YOST, T. & SHERMAN, N. A. 1988. Possible role of cytosolic free calcium concentrations in mediating insulin resistance of obesity and hyperinsulinemia. *J Clin Invest,* 82**,** 1848-52.

DRESNER, A., LAURENT, D., MARCUCCI, M., GRIFFIN, M. E., DUFOUR, S., CLINE, G. W., SLEZAK, L. A., ANDERSEN, D. K., HUNDAL, R. S., ROTHMAN, D. L., PETERSEN, K. F. & SHULMAN, G. I. 1999. Effects of free fatty acids on glucose transport and IRS-1-associated phosphatidylinositol 3-kinase activity. *J Clin Invest,* 103**,** 253-9.

DUTZLER, R. 2004. The structural basis of ClC chloride channel function. *Trends Neurosci,* 27**,** 315-20.

DUTZLER, R., CAMPBELL, E. B., CADENE, M., CHAIT, B. T. & MACKINNON, R. 2002. X-ray structure of a ClC chloride channel at 3.0 A reveals the molecular basis of anion selectivity. *Nature,* 415**,** 287-94.

EGGERMONT, J. 2004. Calcium-activated chloride channels: (un)known, (un)loved? *Proc Am Thorac Soc,* 1**,** 22-7.

ELDEFRAWI, A. T. & ELDEFRAWI, M. E. 1987. Receptors for gamma-aminobutyric acid and voltage-dependent chloride channels as targets for drugs and toxicants. *FASEB J,* 1**,** 262-71.

ELG, S., MARMIGERE, F., MATTSSON, J. P. & ERNFORS, P. 2007. Cellular subtype distribution and developmental regulation of TRPC channel members in the mouse dorsal root ganglion. *J Comp Neurol,* 503**,** 35-46.

ELLINOR, P. T., ZHANG, J. F., RANDALL, A. D., ZHOU, M., SCHWARZ, T. L., TSIEN, R. W. & HORNE, W. A. 1993. Functional expression of a rapidly inactivating neuronal calcium channel. *Nature,* 363**,** 455-8.

ENGFELDT, P., HELLMER, J., WAHRENBERG, H. & ARNER, P. 1988. Effects of insulin on adrenoceptor binding and the rate of catecholamine-induced lipolysis in isolated human fat cells. *J Biol Chem,* 263**,** 15553-60.

ERTEL, E. A., CAMPBELL, K. P., HARPOLD, M. M., HOFMANN, F., MORI, Y., PEREZ-REYES, E., SCHWARTZ, A., SNUTCH, T. P., TANABE, T., BIRNBAUMER, L., TSIEN, R. W. & CATTERALL, W. A. 2000. Nomenclature of Voltage-Gated Calcium Channels. *Neuron,* 25**,** 533-535.

ESTEVEZ, R., BOETTGER, T., STEIN, V., BIRKENHAGER, R., OTTO, E., HILDEBRANDT, F. & JENTSCH, T. J. 2001. Barttin is a Cl- channel beta-subunit crucial for renal Cl- reabsorption and inner ear K+ secretion. *Nature,* 414**,** 558-61.

EVANS, M. G. & MARTY, A. 1986. Calcium-dependent chloride currents in isolated cells from rat lacrimal glands. *J Physiol,* 378**,** 437-60.

FAHLKE, C., RHODES, T. H., DESAI, R. R. & GEORGE, A. L., JR. 1998. Pore stoichiometry of a voltage-gated chloride channel. *Nature,* 394**,** 687-90.

FAHLKE, C., RUDEL, R., MITROVIC, N., ZHOU, M. & GEORGE, A. L., JR. 1995. An aspartic acid residue important for voltage-dependent gating of human muscle chloride channels. *Neuron,* 15**,** 463-72.

FAIN, J. N., MADAN, A. K., HILER, M. L., CHEEMA, P. & BAHOUTH, S. W. 2004. Comparison of the release of adipokines by adipose tissue, adipose tissue matrix, and adipocytes from visceral and subcutaneous abdominal adipose tissues of obese humans. *Endocrinology,* 145**,** 2273-82.

FANTUZZI, G. 2005. Adipose tissue, adipokines, and inflammation. *J Allergy Clin Immunol,* 115**,** 911-9; quiz 920.

FARRAR, S. J., WHITING, P. J., BONNERT, T. P. & MCKERNAN, R. M. 1999. Stoichiometry of a ligand-gated ion channel determined by fluorescence energy transfer. *J Biol Chem,* 274**,** 10100-4.

FELIX, R., GURNETT, C. A., DE WAARD, M. & CAMPBELL, K. P. 1997. Dissection of functional domains of the voltage-dependent Ca2+ channel alpha2delta subunit. *J Neurosci,* 17**,** 6884-91.

FENG, N. C., SATOH, H., URUSHIDA, T., KATOH, H., TERADA, H., WATANABE, Y. & HAYASHI, H. 2006. A selective inhibitor of Na+/Ca2+ exchanger, SEA0400, preserves cardiac function and high-energy phosphates against ischemia/reperfusion injury. *J Cardiovasc Pharmacol,* 47**,** 263-70.

FISHER, R. M., ERIKSSON, P., HOFFSTEDT, J., HOTAMISLIGIL, G. S., THORNE, A., RYDEN, M., HAMSTEN, A. & ARNER, P. 2001. Fatty acid binding protein expression in different adipose tissue depots from lean and obese individuals. *Diabetologia,* 44**,** 1268-73.

FISHER, R. M., THORNE, A., HAMSTEN, A. & ARNER, P. 2002. Fatty acid binding protein expression in different human adipose tissue depots in relation to rates of lipolysis and insulin concentration in obese individuals. *Mol Cell Biochem,* 239**,** 95-100.

FLEISCHMANN, B. K., MURRAY, R. K. & KOTLIKOFF, M. I. 1994. Voltage window for sustained elevation of cytosolic calcium in smooth muscle cells. *Proc Natl Acad Sci U S A,* 91**,** 11914-8.

FOX, A. P., NOWYCKY, M. C. & TSIEN, R. W. 1987. Single-channel recordings of three types of calcium channels in chick sensory neurones. *J Physiol,* 394**,** 173-200.

FRAYN, K. N. 2001. Adipose tissue and the insulin resistance syndrome. *Proc Nutr Soc,* 60**,** 375-80.

FRAYN, K. N. 2003. *Metabolic regulation. A human perspective*, Blackwell.

FRUHBECK, G., GOMEZ-AMBROSI, J., MURUZABAL, F. J. & BURRELL, M. A. 2001. The adipocyte: a model for integration of endocrine and metabolic signaling in energy metabolism regulation. *Am J Physiol Endocrinol Metab,* 280**,** E827-47.

FUCHTENBUSCH, M., STANDL, E. & SCHATZ, H. 2000. Clinical efficacy of new thiazolidinediones and glinides in the treatment of type 2 diabetes mellitus. *Exp Clin Endocrinol Diabetes,* 108**,** 151-63.

FULLER, C. M. & BENOS, D. J. 1992. CFTR! *Am J Physiol,* 263**,** C267-86.

FURUKAWA, T., OGURA, T., KATAYAMA, Y. & HIRAOKA, M. 1998. Characteristics of rabbit ClC-2 current expressed in Xenopus oocytes and its contribution to volume regulation. *Am J Physiol,* 274**,** C500-12.

GABRIELY, I., MA, X. H., YANG, X. M., ATZMON, G., RAJALA, M. W., BERG, A. H., SCHERER, P., ROSSETTI, L. & BARZILAI, N. 2002. Removal of visceral fat prevents insulin resistance and glucose intolerance of aging: an adipokine-mediated process? *Diabetes,* 51**,** 2951-8.

GALIC, S., OAKHILL, J. S. & STEINBERG, G. R. 2010. Adipose tissue as an endocrine organ. *Mol Cell Endocrinol,* 316**,** 129-39.

GAMMELTOFT, S. & VAN OBBERGHEN, E. 1986. Protein kinase activity of the insulin receptor. *Biochem J,* 235**,** 1-11.

GAO, T., YATANI, A., DELL'ACQUA, M. L., SAKO, H., GREEN, S. A., DASCAL, N., SCOTT, J. D. & HOSEY, M. M. 1997. cAMP-Dependent Regulation of Cardiac L-Type Ca2+ Channels Requires Membrane Targeting of PKA and Phosphorylation of Channel Subunits. *Neuron,* 19**,** 185-196.

GARBER, S. S., HOSHI, T. & ALDRICH, R. W. 1990. Interaction of forskolin with voltage-gated K+ channels in PC12 cells. *J Neurosci,* 10**,** 3361-8.

GARCIA-BARRADO, M. J., SANCHO, C., IGLESIAS-OSMA, M. C. & MORATINOS, J. 2001. Effects of verapamil and elgodipine on isoprenaline-induced metabolic responses in rabbits. *Eur J Pharmacol,* 415**,** 105-15.

GAUR, S., MORTON, M. E., FRICK, G. P. & GOODMAN, H. M. 1998a. Growth hormone regulates the distribution of L-type calcium channels in rat adipocyte membranes. *Am J Physiol,* 275**,** C505-14.

GAUR, S., SCHWARTZ, Y., TAI, L. R., FRICK, G. P. & GOODMAN, H. M. 1998b. Insulin produces a growth hormone-like increase in intracellular free calcium concentration in okadaic acid-treated adipocytes. *Endocrinology,* 139**,** 4953-61.

GAUR, S., YAMAGUCHI, H. & GOODMAN, H. M. 1996a. Growth hormone increases calcium uptake in rat fat cells by a mechanism dependent on protein kinase C. *Am J Physiol,* 270**,** C1485-92.

GAUR, S., YAMAGUCHI, H. & GOODMAN, H. M. 1996b. Growth hormone regulates cytosolic free calcium in rat fat cells by maintaining L-type calcium channels. *Am J Physiol,* 270**,** C1478-84.

GEE, K. R., BROWN, K. A., CHEN, W. N. U., BISHOP-STEWART, J., GRAY, D. & JOHNSON, I. 2000. Chemical and physiological characterization of fluo-4 Ca2+-indicator dyes. *Cell Calcium,* 27**,** 97-106.

GINSBURG, K. S. & BERS, D. M. 2005. Isoproterenol does not enhance Ca-dependent Na/Ca exchange current in intact rabbit ventricular myocytes. *J Mol Cell Cardiol,* 39**,** 972-81.

GIORGINO, F., LAVIOLA, L. & ERIKSSON, J. W. 2005. Regional differences of insulin action in adipose tissue: insights from in vivo and in vitro studies. *Acta Physiol Scand,* 183**,** 13-30.

GIRARDIER, L., SEYDOUX, J. & CLAUSEN, T. 1968. Membrane potential of brown adipose tissue. A suggested mechanism for the regulation of thermogenesis. *J Gen Physiol,* 52**,** 925-40.

GLATZ, J. F. C., LUIKEN, J. J. F. P. & BONEN, A. 2010. Membrane Fatty Acid Transporters as Regulators of Lipid Metabolism: Implications for Metabolic Disease. *Physiological Reviews,* 90**,** 367-417.

GLAVINAS, H., KRAJCSI, P., CSEREPES, J. & SARKADI, B. 2004. The role of ABC transporters in drug resistance, metabolism and toxicity. *Curr Drug Deliv,* 1**,** 27-42.

GOTO, K., FUJII, K., ABE, I. & FUJISHIMA, M. 2000. Sympathetic Control of Arterial Membrane Potential by ATP-Sensitive K+-Channels. *Hypertension,* 35**,** 379-384.

GREEN, H. & KEHINDE, O. 1975. An established preadipose cell line and its differentiation in culture II. Factors affecting the adipose conversion. *Cell,* 5**,** 19-27.

GREEN, H. & MEUTH, M. 1974. An established pre-adipose cell line and its differentiation in culture. *Cell,* 3**,** 127-133.

GUERRE-MILLO, M. 2004. Adipose tissue and adipokines: for better or worse. *Diabetes Metab,* 30**,** 13-9.

GUNTHER, W., PIWON, N. & JENTSCH, T. J. 2003. The ClC-5 chloride channel knock-out mouse - an animal model for Dent's disease. *Pflugers Arch,* 445**,** 456-62.

GUO, X. & LIAO, K. 2000. Analysis of gene expression profile during 3T3-L1 preadipocyte differentiation. *Gene,* 251**,** 45-53.

GUO, Z. K., CELLA, L. K., BAUM, C., RAVUSSIN, E. & SCHOELLER, D. A. 2000. De novo lipogenesis in adipose tissue of lean and obese women: application of deuterated water and isotope ratio mass spectrometry. *Int J Obes Relat Metab Disord,* 24**,** 932-7.

HALL, D. A., CARMINES, P. K. & SANSOM, S. C. 2000. Dihydropyridine-sensitive Ca(2+) channels in human glomerular mesangial cells. *Am J Physiol Renal Physiol,* 278**,** F97-F103.

HALONEN, J. & NEDERGAARD, J. 2002. Adenosine 5'-monophosphate is a selective inhibitor of the brown adipocyte nonselective cation channel. *J Membr Biol,* 188**,** 183-97.

HAMIDA, Z. H., COMTOIS, A. S., PORTMANN, M., BOUCHER, J. P. & SAVARD, R. 2011. Effect of electrical stimulation on lipolysis of human white adipocytes. *Applied Physiology*

Nutrition and Metabolism-Physiologie Appliquee Nutrition Et Metabolisme, 36**,** 271-275.

HANLON, M. R., BERROW, N. S., DOLPHIN, A. C. & WALLACE, B. A. 1999. Modelling of a voltage-dependent Ca2+ channel Î² subunit as a basis for understanding its functional properties. *FEBS Letters,* 445**,** 366-370.

HANRAHAN, J. W. & TABCHARANI, J. A. 1990. Inhibition of an outwardly rectifying anion channel by HEPES and related buffers. *J Membr Biol,* 116**,** 65-77.

HAO, H., MU-LAN, H., RONG, T., HAI-YING, S., RUI, H., WEI-JIN, Z., BING-XIANG, Y., CHU-PAK, L., HUNG-FAT, T. & GUI-RONG, L. 2009. Characterization of ion channels in human preadipocytes. *Journal of Cellular Physiology,* 218**,** 427-435.

HARA-CHIKUMA, M., YANG, B., SONAWANE, N. D., SASAKI, S., UCHIDA, S. & VERKMAN, A. S. 2005. ClC-3 chloride channels facilitate endosomal acidification and chloride accumulation. *J Biol Chem,* 280**,** 1241-7.

HARANO, Y., KAGEYAMA, A., HIROSE, J., ASAKURA, Y., YOKOTA, T., IKEBUCHI, M., SUZUKI, M. & OMAE, T. 1995. Improvement of insulin sensitivity for glucose metabolism with the long-acting Ca-channel blocker amlodipine in essential hypertensive subjects. *Metabolism,* 44**,** 315-9.

HARDIE, R. C. & MUALLEM, S. 2009. Lipids in Ca2+ signalling--an introduction. *Cell Calcium,* 45**,** 517-20.

HARRIS, A. 1992. Cystic fibrosis gene. *Br Med Bull,* 48**,** 738-53.

HARTZELL, C., PUTZIER, I. & ARREOLA, J. 2005. Calcium-activated chloride channels. *Annu Rev Physiol,* 67**,** 719-58.

HASPEL, D., KRIPPEIT-DREWS, P., AGUILAR-BRYAN, L., BRYAN, J., DREWS, G. & DUFER, M. 2005. Crosstalk between membrane potential and cytosolic Ca2+ concentration in beta cells from Sur1-/- mice. *Diabetologia,* 48**,** 913-21.

HATA, T., MAKINO, N., NAKANISHI, H. & YANAGA, T. 1988. Modulation of Na+-Ca2+ exchange in cardiac sarcolemmal vesicles by Ca2+ antagonists. *Mol Cell Biochem,* 84**,** 65-76.

HE, Z., FENG, S., TONG, Q., HILGEMANN, D. W. & PHILIPSON, K. D. 2000. Interaction of PIP(2) with the XIP region of the cardiac Na/Ca exchanger. *Am J Physiol Cell Physiol,* 278**,** C661-6.

HERD, P. A., HAMMOND, R. P. & HAMOLSKY, M. W. 1973. Sodium pump activity during norepinephrine-stimulated respiration in brown adipocytes. *Am J Physiol,* 224**,** 1300-4.

HERING, S., ACZEL, S., KRAUS, R. L., BERJUKOW, S., STRIESSNIG, J. & TIMIN, E. N. 1997. Molecular mechanism of use-dependent calcium channel block by phenylalkylamines: role of inactivation. *Proc Natl Acad Sci U S A,* 94**,** 13323-8.

HERING, S., BERJUKOW, S., SOKOLOV, S., MARKSTEINER, R., WEISS, R. G., KRAUS, R. & TIMIN, E. N. 2000. Molecular determinants of inactivation in voltage-gated Ca2+ channels. *J Physiol,* 528 Pt 2**,** 237-49.

HERING, S., BEYL, S., STARY, A., KUDRNAC, M., HOHAUS, A., GUY, H. R. & TIMIN, E. 2008. Pore stability and gating in voltage-activated calcium channels. *Channels (Austin),* 2.

HERLITZE, S., XIE, M., HAN, J., HUMMER, A., MELNIK-MARTINEZ, K. V., MORENO, R. L. & MARK, M. D. 2003. Targeting mechanisms of high voltage-activated Ca2+ channels. *J Bioenerg Biomembr,* 35**,** 621-37.

HILGEMANN, D. W. & BALL, R. 1996. Regulation of cardiac Na+,Ca2+ exchange and KATP potassium channels by PIP2. *Science,* 273**,** 956-9.

HILLE, B. 2001. *Ion channels of excitable membranes*, Sinauer Associates.

HIRAKAWA, Y., KUGA, T., KANAIDE, H. & TAKESHITA, A. 1994. Actions of a new Ca2+ channel antagonist, CD832, on two types of Ca2+ channels in smooth muscle. *Eur J Pharmacol,* 252**,** 267-74.

HOCKERMAN, G. H., PETERSON, B. Z., JOHNSON, B. D. & CATTERALL, W. A. 1997. Molecular determinants of drug binding and action on L-type calcium channels. *Annu Rev Pharmacol Toxicol,* 37**,** 361-96.

HOFER, G. F., HOHENTHANNER, K., BAUMGARTNER, W., GROSCHNER, K., KLUGBAUER, N., HOFMANN, F. & ROMANIN, C. 1997. Intracellular Ca2+ inactivates L-type Ca2+ channels with a Hill coefficient of approximately 1 and an inhibition constant of approximately 4 microM by reducing channel's open probability. *Biophys J,* 73**,** 1857-65.

HOFMANN, T., OBUKHOV, A. G., SCHAEFER, M., HARTENECK, C., GUDERMANN, T. & SCHULTZ, G. 1999. Direct activation of human TRPC6 and TRPC3 channels by diacylglycerol. *Nature,* 397**,** 259-263.

HORVATH, E. M., TACKETT, L., MCCARTHY, A. M., RAMAN, P., BROZINICK, J. T. & ELMENDORF, J. S. 2008. Antidiabetogenic effects of chromium mitigate hyperinsulinemia-induced cellular insulin resistance via correction of plasma membrane cholesterol imbalance. *Mol Endocrinol,* 22**,** 937-50.

HORWITZ, B. A., HOROWITZ, J. M., JR. & SMITH, R. E. 1969. Norepinephrine-induced depolarization of brown fat cells. *Proc Natl Acad Sci U S A,* 64**,** 113-20.

HOTTA, K., FUNAHASHI, T., BODKIN, N. L., ORTMEYER, H. K., ARITA, Y., HANSEN, B. C. & MATSUZAWA, Y. 2001. Circulating concentrations of the adipocyte protein adiponectin are decreased in parallel with reduced insulin sensitivity during the progression to type 2 diabetes in rhesus monkeys. *Diabetes,* 50**,** 1126-33.

HOUSE, S. J., POTIER, M., BISAILLON, J., SINGER, H. A. & TREBAK, M. 2008. The non-excitable smooth muscle: calcium signaling and phenotypic switching during vascular disease. *Pflugers Arch,* 456**,** 769-85.

HU, E., LIANG, P. & SPIEGELMAN, B. M. 1996. AdipoQ is a novel adipose-specific gene dysregulated in obesity. *J Biol Chem,* 271**,** 10697-703.

HUANG, L., BHATTACHARJEE, A., TAYLOR, J. T., ZHANG, M., KEYSER, B. M., MARRERO, L. & LI, M. 2004. [Ca2+]i regulates trafficking of Cav1.3 (alpha1D Ca2+ channel) in insulin-secreting cells. *Am J Physiol Cell Physiol,* 286**,** C213-21.

HUI, A., ELLINOR, P. T., KRIZANOVA, O., WANG, J.-D., DIEBOLD, R. J. & SCHWARTZ, A. 1991. Molecular cloning of multiple subtypes of a novel rat brain isoform of the Î±1 subunit of the voltage-dependent calcium channel. *Neuron,* 7**,** 35-44.

HULME, J. T., KONOKI, K., LIN, T. W., GRITSENKO, M. A., CAMP, D. G., 2ND, BIGELOW, D. J. & CATTERALL, W. A. 2005. Sites of proteolytic processing and noncovalent association of the distal C-terminal domain of CaV1.1 channels in skeletal muscle. *Proc Natl Acad Sci U S A,* 102**,** 5274-9.

INOUE, H., TAKAHASHI, N., OKADA, Y. & KONISHI, M. 2010. Volume-sensitive outwardly rectifying chloride channel in white adipocytes from normal and diabetic mice. *Am J Physiol Cell Physiol,* 298**,** C900-9.

IWAMOTO, T. 2004. Forefront of Na+/Ca2+ exchanger studies: molecular pharmacology of Na+/Ca2+ exchange inhibitors. *J Pharmacol Sci,* 96**,** 27-32.

IWAMOTO, T., INOUE, Y., ITO, K., SAKAUE, T., KITA, S. & KATSURAGI, T. 2004a. The exchanger inhibitory peptide region-dependent inhibition of Na+/Ca2+ exchange by SN-6 [2-[4-(4-nitrobenzyloxy)benzyl]thiazolidine-4-carboxylic acid ethyl ester], a novel benzyloxyphenyl derivative. *Mol Pharmacol,* 66**,** 45-55.

IWAMOTO, T. & KITA, S. 2004. Development and application of Na+/Ca2+ exchange inhibitors. *Mol Cell Biochem,* 259**,** 157-61.

IWAMOTO, T. & KITA, S. 2006. YM-244769, a novel Na+/Ca2+ exchange inhibitor that preferentially inhibits NCX3, efficiently protects against hypoxia/reoxygenation-induced SH-SY5Y neuronal cell damage. *Mol Pharmacol,* 70**,** 2075-83.

IWAMOTO, T., KITA, S., UEHARA, A., IMANAGA, I., MATSUDA, T., BABA, A. & KATSURAGI, T. 2004b. Molecular determinants of Na+/Ca2+ exchange (NCX1) inhibition by SEA0400. *J Biol Chem,* 279**,** 7544-53.

IWAMOTO, T., PAN, Y., NAKAMURA, T. Y., WAKABAYASHI, S. & SHIGEKAWA, M. 1998. Protein kinase C-dependent regulation of Na+/Ca2+ exchanger isoforms NCX1 and NCX3 does not require their direct phosphorylation. *Biochemistry,* 37**,** 17230-8.

IWAMOTO, T., PAN, Y., WAKABAYASHI, S., IMAGAWA, T., YAMANAKA, H. I. & SHIGEKAWA, M. 1996a. Phosphorylation-dependent regulation of cardiac Na+/Ca2+ exchanger via protein kinase C. *J Biol Chem,* 271**,** 13609-15.

IWAMOTO, T., WATANO, T. & SHIGEKAWA, M. 1996b. A novel isothiourea derivative selectively inhibits the reverse mode of Na+/Ca2+ exchange in cells expressing NCX1. *J Biol Chem,* 271**,** 22391-7.

IZAWA, T. & KOMABAYASHI, T. 1994. Ca2+ and lipolysis in adipocytes from exercise-trained rats. *J Appl Physiol,* 77**,** 2618-24.

JACKSON, A. L. & LINSLEY, P. S. 2010. Recognizing and avoiding siRNA off-target effects for target identification and therapeutic application. *Nat Rev Drug Discov,* 9**,** 57-67.

JACOBSSON, B. & SMITH, U. 1972. Effect of cell size on lipolysis and antilipolytic action of insulin in human fat cells. *J Lipid Res,* 13**,** 651-6.

JARVIS, S. E. & ZAMPONI, G. W. 2007. Trafficking and regulation of neuronal voltage-gated calcium channels. *Curr Opin Cell Biol,* 19**,** 474-82.

JAY, A. W. & BURTON, A. C. 1969. Direct measurement of potential difference across the human red blood cell membrane. *Biophys J,* 9**,** 115-21.

JENSEN, B., FARACH-CARSON, M. C., KENALEY, E. & AKANBI, K. A. 2004. High extracellular calcium attenuates adipogenesis in 3T3-L1 preadipocytes. *Experimental Cell Research,* 301**,** 280-292.

JENTSCH, T. J. 1996. Chloride channels: a molecular perspective. *Curr Opin Neurobiol,* 6**,** 303-10.

JENTSCH, T. J., NEAGOE, I. & SCHEEL, O. 2005. CLC chloride channels and transporters. *Curr Opin Neurobiol,* 15**,** 319-25.

JENTSCH, T. J., STEIN, V., WEINREICH, F. & ZDEBIK, A. A. 2002. Molecular structure and physiological function of chloride channels. *Physiol Rev,* 82**,** 503-68.

JEONG, H.-J., HONG, S.-H., LEE, D.-J., PARK, J.-H., KIM, K.-S. & KIM, H.-M. 2002. Role of Ca2+ on TNF-Î± and IL-6 secretion from RBL-2H3 mast cells. *Cellular Signalling,* 14**,** 633-639.

JONES, S. W. 1998. Overview of voltage-dependent calcium channels. *J Bioenerg Biomembr,* 30**,** 299-312.

JUNG, S.-R., REED, B. J. & SWEET, I. R. 2009. A highly energetic process couples calcium influx through L-type calcium channels to insulin secretion in pancreatic Î²-cells. *American Journal of Physiology - Endocrinology And Metabolism,* 297**,** E717-E727.

KAHN, S. E., HULL, R. L. & UTZSCHNEIDER, K. M. 2006. Mechanisms linking obesity to insulin resistance and type 2 diabetes. *Nature,* 444**,** 840-846.

KAMEI, C., MUKAI, T. & TASAKA, K. 1992. Histamine-induced depolarization and the cyclic AMP--protein kinase A system in isolated guinea pig adipocytes. *Jpn J Pharmacol,* 60**,** 179-86.

KAMIGAKI, M., SAKAUE, S., TSUJINO, I., OHIRA, H., IKEDA, D., ITOH, N., ISHIMARU, S., OHTSUKA, Y. & NISHIMURA, M. 2006. Oxidative stress provokes atherogenic changes in adipokine gene expression in 3T3-L1 adipocytes. *Biochemical and Biophysical Research Communications,* 339**,** 624-632.

KAMP, T. J. & HELL, J. W. 2000. Regulation of cardiac L-type calcium channels by protein kinase A and protein kinase C. *Circ Res,* 87**,** 1095-102.

KARLSSON, E. A. & BECK, M. A. The burden of obesity on infectious disease. *Exp Biol Med (Maywood),* 235**,** 1412-24.

KARSCHIN, A. 1999. G Protein Regulation of Inwardly Rectifying K+ Channels. *Physiology,* 14**,** 215-220.

KARUNASEKARA, Y., DULHUNTY, A. F. & CASAROTTO, M. G. 2009. The voltage-gated calcium-channel beta subunit: more than just an accessory. *Eur Biophys J,* 39**,** 75-81.

KASS, R. S. 2004. Sodium Channel Inactivation Goes with the Flow. *The Journal of General Physiology,* 124**,** 7-8.

KATOCS, A. S., JR., LARGIS, E. E. & ALLEN, D. O. 1974. Role of Ca2+ in adrenocorticotropic hormone-stimulated lipolysis in the perfused fat cell system. *J Biol Chem,* 249**,** 2000-4.

KAWAI, A. 1985. The role of calmodulin in hormone-stimulated lipolysis. *Metabolism,* 34**,** 303-8.

KAWANO, T., ZOGA, V., MCCALLUM, J. B., WU, H. E., GEMES, G., LIANG, M. Y., ABRAM, S., KWOK, W. M., HOGAN, Q. H. & SARANTOPOULOS, C. D. 2009. ATP-sensitive potassium currents in rat primary afferent neurons: biophysical, pharmacological properties, and alterations by painful nerve injury. *Neuroscience,* 162**,** 431-443.

KELLY, K. L., DEENEY, J. T. & CORKEY, B. E. 1989. Cytosolic free calcium in adipocytes. Distinct mechanisms of regulation and effects on insulin action. *J Biol Chem,* 264**,** 12754-7.

KERSHAW, E. E. & FLIER, J. S. 2004. Adipose Tissue as an Endocrine Organ. *Journal of Clinical Endocrinology & Metabolism,* 89**,** 2548-2556.

KERSTEN, S. 2001. Mechanisms of nutritional and hormonal regulation of lipogenesis. *EMBO Rep,* 2**,** 282-6.

KIM, J. B. & SPIEGELMAN, B. M. 1996. ADD1/SREBP1 promotes adipocyte differentiation and gene expression linked to fatty acid metabolism. *Genes Dev,* 10**,** 1096-107.

KIM, J. H., KIEFER, L. L., WOYCHIK, R. P., WILKISON, W. O., TRUESDALE, A., ITTOOP, O., WILLARD, D., NICHOLS, J. & ZEMEL, M. B. 1997. Agouti regulation of intracellular calcium: role of melanocortin receptors. *Am J Physiol,* 272**,** E379-84.

KIM, J. H., MYNATT, R. L., MOORE, J. W., WOYCHIK, R. P., MOUSTAID, N. & ZEMEL, M. B. 1996. The effects of calcium channel blockade on agouti-induced obesity. *FASEB J,* 10**,** 1646-52.

KLIP, A. & RAMLAL, T. 1987. Cytoplasmic Ca2+ during differentiation of 3T3-L1 adipocytes. Effect of insulin and relation to glucose transport. *J Biol Chem,* 262**,** 9141-6.

KLOCKNER, U. & ISENBERG, G. 1985. Action potentials and net membrane currents of isolated smooth muscle cells (urinary bladder of the guinea-pig). *Pflugers Arch,* 405**,** 329-39.

KOHN, A. D., SUMMERS, S. A., BIRNBAUM, M. J. & ROTH, R. A. 1996. Expression of a Constitutively Active Akt Ser/Thr Kinase in 3T3-L1 Adipocytes Stimulates Glucose Uptake and Glucose Transporter 4 Translocation. *Journal of Biological Chemistry,* 271**,** 31372-31378.

KOIVISTO, A., DOTZLER, E., RUSS, U., NEDERGAARD, J. & SIEMEN, D. 1993. Nonselective cation channels in brown and white fat cells. *EXS,* 66**,** 201-11.

KONDO, K., KOZAWA, O., TAKATSUKI, K. & OISO, Y. 1989. Ca2+ influx stimulated by vasopressin is mediated by phosphoinositide hydrolysis in rat smooth muscle cells. *Biochem Biophys Res Commun,* 161**,** 677-82.

KORNAK, U., KASPER, D., BOSL, M. R., KAISER, E., SCHWEIZER, M., SCHULZ, A., FRIEDRICH, W., DELLING, G. & JENTSCH, T. J. 2001. Loss of the ClC-7 chloride channel leads to osteopetrosis in mice and man. *Cell,* 104**,** 205-15.

KOSCHAK, A., REIMER, D., HUBER, I., GRABNER, M., GLOSSMANN, H., ENGEL, J. & STRIESSNIG, J. 2001. alpha 1D (Cav1.3) Subunits Can Form L-type Ca2+ Channels Activating at Negative Voltages. *J. Biol. Chem.,* 276**,** 22100-22106.

KOUMI, S., SATO, R. & ARAMAKI, T. 1994. Characterization of the calcium-activated chloride channel in isolated guinea-pig hepatocytes. *J Gen Physiol,* 104**,** 357-73.

KRANIAS, E. G. & BERS, D. M. 2007. Calcium and cardiomyopathies. *Subcell Biochem,* 45**,** 523-37.

KRAPIVINSKY, G. B., ACKERMAN, M. J., GORDON, E. A., KRAPIVINSKY, L. D. & CLAPHAM, D. E. 1994. Molecular characterization of a swelling-induced chloride conductance regulatory protein, pICln. *Cell,* 76**,** 439-48.

LACINOVÁ, L. & HOFMANN, F. 2005. Ca2+- and voltage-dependent inactivation of the expressed L-type Cav1.2 calcium channel. *Archives of Biochemistry and Biophysics,* 437**,** 42-50.

LAFONTAN, M. & LANGIN, D. 2009. Lipolysis and lipid mobilization in human adipose tissue. *Prog Lipid Res,* 48**,** 275-97.

LAGO, F., GOMEZ, R., GOMEZ-REINO, J. J., DIEGUEZ, C. & GUALILLO, O. 2009. Adipokines as novel modulators of lipid metabolism. *Trends Biochem Sci,* 34**,** 500-10.

LANGIN, D., DICKER, A., TAVERNIER, G., HOFFSTEDT, J., MAIRAL, A., RYDEN, M., ARNER, E., SICARD, A., JENKINS, C. M., VIGUERIE, N., VAN HARMELEN, V., GROSS, R. W., HOLM, C. & ARNER, P. 2005. Adipocyte lipases and defect of lipolysis in human obesity. *Diabetes,* 54**,** 3190-7.

LAPENSEE, C. R., HUGO, E. R. & BEN-JONATHAN, N. 2008. Insulin Stimulates Interleukin-6 Expression and Release in LS14 Human Adipocytes through Multiple Signaling Pathways. *Endocrinology,* 149**,** 5415-5422.

LARGE, V., PERONI, O., LETEXIER, D., RAY, H. & BEYLOT, M. 2004. Metabolism of lipids in human white adipocyte. *Diabetes Metab,* 30**,** 294-309.

LARGE, V., REYNISDOTTIR, S., LANGIN, D., FREDBY, K., KLANNEMARK, M., HOLM, C. & ARNER, P. 1999. Decreased expression and function of adipocyte hormone-sensitive lipase in subcutaneous fat cells of obese subjects. *J Lipid Res,* 40**,** 2059-66.

LEBLANC, N. & HUME, J. R. 1990. Sodium current-induced release of calcium from cardiac sarcoplasmic reticulum. *Science,* 248**,** 372-6.

LEE, S. C. & PAPPONE, P. A. 1997. Membrane responses to extracellular ATP in rat isolated white adipocytes. *Pflugers Arch,* 434**,** 422-8.

LI, W. C., SOFFE, S. R. & ROBERTS, A. 2004. A direct comparison of whole cell patch and sharp electrodes by simultaneous recording from single spinal neurons in frog tadpoles. *J Neurophysiol,* 92**,** 380-6.

LI, Y., WOO, V. & BOSE, R. 2001. Platelet hyperactivity and abnormal Ca(2+) homeostasis in diabetes mellitus. *Am J Physiol Heart Circ Physiol,* 280**,** H1480-9.

LI, Z., MATSUOKA, S., HRYSHKO, L. V., NICOLL, D. A., BERSOHN, M. M., BURKE, E. P., LIFTON, R. P. & PHILIPSON, K. D. 1994. Cloning of the NCX2 isoform of the plasma membrane Na(+)-Ca2+ exchanger. *J Biol Chem,* 269**,** 17434-9.

LI, Z., NICOLL, D. A., COLLINS, A., HILGEMANN, D. W., FILOTEO, A. G., PENNISTON, J. T., WEISS, J. N., TOMICH, J. M. & PHILIPSON, K. D. 1991. Identification of a peptide inhibitor of the cardiac sarcolemmal Na(+)-Ca2+ exchanger. *J Biol Chem,* 266**,** 1014-20.

LIANG, H., DEMARIA, C. D., ERICKSON, M. G., MORI, M. X., ALSEIKHAN, B. A. & YUE, D. T. 2003. Unified mechanisms of Ca2+ regulation across the Ca2+ channel family. *Neuron,* 39**,** 951-60.

LIN, K. H., ERAZO-FISCHER, E. & TASCHENBERGER, H. 2012. Similar intracellular Ca2+ requirements for inactivation and facilitation of voltage-gated Ca2+ channels in a glutamatergic mammalian nerve terminal. *J Neurosci,* 32**,** 1261-72.

LIN, X., JO, H., SAKAKIBARA, Y., TAMBARA, K., KIM, B., KOMEDA, M. & MATSUOKA, S. 2006. Beta-adrenergic stimulation does not activate Na+/Ca2+ exchange current in guinea pig, mouse, and rat ventricular myocytes. *Am J Physiol Cell Physiol,* 290**,** C601-8.

LINCK, B. 1998. Functional comparison of the three isoforms of the Na+/Ca2+ exchanger (NCX1, NCX2, NCX3). *Am. J. Physiol.,* 274**,** C415-C423.

LIPSCOMBE, D., HELTON, T. D. & XU, W. 2004. L-type calcium channels: the low down. *J Neurophysiol,* 92**,** 2633-41.

LISHKO, P. V., KIRICHOK, Y., REN, D., NAVARRO, B., CHUNG, J. J. & CLAPHAM, D. E. 2012. The control of male fertility by spermatozoan ion channels. *Annu Rev Physiol,* 74**,** 453-75.

LOEW, L. M. 2007. Where does all the PIP2 come from? *J Physiol,* 582**,** 945-51.

LONN, M., MEHLIG, K., BENGTSSON, C. & LISSNER, L. 2010. Adipocyte size predicts incidence of type 2 diabetes in women. *FASEB J,* 24**,** 326-31.

LONNQVIST, F., WAHRENBERG, H., HELLSTROM, L., REYNISDOTTIR, S. & ARNER, P. 1992. Lipolytic catecholamine resistance due to decreased beta 2-adrenoceptor expression in fat cells. *J Clin Invest,* 90**,** 2175-86.

LORENZON, N. M. & FOEHRING, R. C. 1995. Characterization of pharmacologically identified voltage-gated calcium channel currents in acutely isolated rat neocortical neurons. I. Adult neurons. *J Neurophysiol,* 73**,** 1430-42.

LORY, P., RASSENDREN, F. A., RICHARD, S., TIAHO, F. & NARGEOT, J. 1990. Characterization of voltage-dependent calcium channels expressed in Xenopus oocytes injected with mRNA from rat heart. *J Physiol,* 429**,** 95-112.

LUCERO, M. T. & PAPPONE, P. A. 1989. Voltage-gated potassium channels in brown fat cells. *J Gen Physiol,* 93**,** 451-72.

LUCERO, M. T. & PAPPONE, P. A. 1990. Membrane responses to norepinephrine in cultured brown fat cells. *J Gen Physiol,* 95**,** 523-44.

LUNDGREN, M., BUREN, J., RUGE, T., MYRNAS, T. & ERIKSSON, J. W. 2004. Glucocorticoids down-regulate glucose uptake capacity and insulin-signaling proteins in omental but not subcutaneous human adipocytes. *J Clin Endocrinol Metab,* 89**,** 2989-97.

LUYCKX, V. A., LECLERCQ, B., DOWLAND, L. K. & YU, A. S. 1999. Diet-dependent hypercalciuria in transgenic mice with reduced CLC5 chloride channel expression. *Proc Natl Acad Sci U S A,* 96**,** 12174-9.

LYTTON, J. 2007. Na+/Ca2+ exchangers: three mammalian gene families control Ca2+ transport. *Biochem J,* 406**,** 365-82.

MAACK, C., GANESAN, A., SIDOR, A. & O'ROURKE, B. 2005. Cardiac sodium-calcium exchanger is regulated by allosteric calcium and exchanger inhibitory peptide at distinct sites. *Circ Res,* 96**,** 91-9.

MACLENNAN, D. H. 2000. Ca2+ signalling and muscle disease. *Eur J Biochem,* 267**,** 5291-7.

MAEDA, N., SHIMOMURA, I., KISHIDA, K., NISHIZAWA, H., MATSUDA, M., NAGARETANI, H., FURUYAMA, N., KONDO, H., TAKAHASHI, M., ARITA, Y., KOMURO, R., OUCHI, N., KIHARA, S., TOCHINO, Y., OKUTOMI, K., HORIE, M., TAKEDA, S., AOYAMA, T., FUNAHASHI, T. & MATSUZAWA, Y. 2002. Diet-induced insulin resistance in mice lacking adiponectin/ACRP30. *Nat Med,* 8**,** 731-7.

MAGEE, W. P., DESHMUKH, G., DENINNO, M. P., SUTT, J. C., CHAPMAN, J. G. & TRACEY, W. R. 2003. Differing cardioprotective efficacy of the Na+/Ca2+ exchanger inhibitors SEA0400 and KB-R7943. *Am J Physiol Heart Circ Physiol,* 284**,** H903-10.

MAGOSKI, N. S., KNOX, R. J. & KACZMAREK, L. K. 2000. Activation of a Ca2+-permeable cation channel produces a prolonged attenuation of intracellular Ca2+ release in Aplysia bag cell neurones. *J Physiol,* 522 Pt 2**,** 271-83.

MAIN, M. J., GRANTHAM, C. J. & CANNELL, M. B. 1997. Changes in subsarcolemmal sodium concentration measured by Na-Ca exchanger activity during Na-pump inhibition and beta-adrenergic stimulation in guinea-pig ventricular myocytes. *Pflugers Arch,* 435**,** 112-8.

MANNING FOX, J. E., GYULKHANDANYAN, A. V., SATIN, L. S. & WHEELER, M. B. 2006. Oscillatory Membrane Potential Response to Glucose in Islet Î²-Cells: A Comparison of Islet-Cell Electrical Activity in Mouse and Rat. *Endocrinology,* 147**,** 4655-4663.

MARSHALL, S. & OLEFSKY, J. M. 1980. Effects of insulin incubation on insulin binding, glucose transport, and insulin degradation by isolated rat adipocytes. Evidence for hormone-induced desensitization at the receptor and postreceptor level. *J Clin Invest,* 66**,** 763-72.

MATSUDA, T., ARAKAWA, N., TAKUMA, K., KISHIDA, Y., KAWASAKI, Y., SAKAUE, M., TAKAHASHI, K., TAKAHASHI, T., SUZUKI, T., OTA, T., HAMANO-TAKAHASHI, A., ONISHI, M., TANAKA, Y., KAMEO, K. & BABA, A. 2001. SEA0400, a novel and selective inhibitor of the Na+-Ca2+ exchanger, attenuates reperfusion injury in the in vitro and in vivo cerebral ischemic models. *J Pharmacol Exp Ther,* 298**,** 249-56.

MATSUDA, T., KOYAMA, Y. & BABA, A. 2005. Functional proteins involved in regulation of intracellular Ca(2+) for drug development: pharmacology of SEA0400, a specific inhibitor of the Na(+)-Ca(2+) exchanger. *J Pharmacol Sci,* 97**,** 339-43.

MATSUOKA, S., NICOLL, D. A., HE, Z. & PHILIPSON, K. D. 1997. Regulation of cardiac Na(+)-Ca2+ exchanger by the endogenous XIP region. *J Gen Physiol,* 109**,** 273-86.

MCCARTY, M. F. 2006. PKC-mediated modulation of L-type calcium channels may contribute to fat-induced insulin resistance. *Medical Hypotheses,* 66**,** 824-831.

MCDONALD, T. F., PELZER, S., TRAUTWEIN, W. & PELZER, D. J. 1994. Regulation and modulation of calcium channels in cardiac, skeletal, and smooth muscle cells. *Physiol Rev,* 74**,** 365-507.

MCHUGH, D., SHARP, E. M., SCHEUER, T. & CATTERALL, W. A. 2000. Inhibition of cardiac L-type calcium channels by protein kinase C phosphorylation of two sites in the N-terminal domain. *Proc Natl Acad Sci U S A,* 97**,** 12334-8.

MCKHANN, G. M., 2ND, D'AMBROSIO, R. & JANIGRO, D. 1997. Heterogeneity of astrocyte resting membrane potentials and intercellular coupling revealed by whole-cell and gramicidin-perforated patch recordings from cultured neocortical and hippocampal slice astrocytes. *J Neurosci,* 17**,** 6850-63.

MEHRA, A., MACDONALD, I. & PILLAY, T. S. 2007. Variability in 3T3-L1 adipocyte differentiation depending on cell culture dish. *Anal Biochem,* 362**,** 281-3.

MILLER, C. 2000. An overview of the potassium channel family. *Genome Biol,* 1**,** REVIEWS0004.

MINDELL, J. A., MADUKE, M., MILLER, C. & GRIGORIEFF, N. 2001. Projection structure of a ClC-type chloride channel at 6.5 A resolution. *Nature,* 409**,** 219-23.

MOHAMMAD-PANAH, R., HARRISON, R., DHANI, S., ACKERLEY, C., HUAN, L. J., WANG, Y. & BEAR, C. E. 2003. The chloride channel ClC-4 contributes to endosomal acidification and trafficking. *J Biol Chem,* 278**,** 29267-77.

MOHAN, C. G. & GANDHI, T. 2008. Therapeutic potential of Voltage gated Calcium channels. *Mini Rev Med Chem,* 8**,** 1285-90.

MOLLEMAN, A. 2003. *Patch Clamping. An introductory guide to patch clamp electrophysiology*.

MOORMAN, J. R., PALMER, C. J., JOHN, J. E., 3RD, DURIEUX, M. E. & JONES, L. R. 1992. Phospholemman expression induces a hyperpolarization-activated chloride current in Xenopus oocytes. *J Biol Chem,* 267**,** 14551-4.

MORAGA-CID, G., YEVENES, G. E., SCHMALZING, G., PEOPLES, R. W. & AGUAYO, L. G. A Single phenylalanine residue in the main intracellular loop of alpha1 gamma-aminobutyric acid type A and glycine receptors influences their sensitivity to propofol. *Anesthesiology,* 115**,** 464-73.

MURRELL-LAGNADO, R. D. & ALDRICH, R. W. 1993. Interactions of amino terminal domains of Shaker K channels with a pore blocking site studied with synthetic peptides. *J Gen Physiol,* 102**,** 949-75.

MYNLIEFF, M. & BEAM, K. G. 1992. Characterization of voltage-dependent calcium currents in mouse motoneurons. *J Neurophysiol,* 68**,** 85-92.

NAHUM-LEVY, R., LIPINSKI, D., SHAVIT, S. & BENVENISTE, M. 2001. Desensitization of NMDA receptor channels is modulated by glutamate agonists. *Biophys J,* 80**,** 2152-66.

NAKAMURA, T., LASSER-ROSS, N., NAKAMURA, K. & ROSS, W. N. 2002. Spatial segregation and interaction of calcium signalling mechanisms in rat hippocampal CA1 pyramidal neurons. *J Physiol,* 543**,** 465-80.

NAKATA, M., NAGASAKA, S., KUSAKA, I., MATSUOKA, H., ISHIBASHI, S. & YADA, T. 2006. Effects of statins on the adipocyte maturation and expression of glucose transporter 4 (SLC2A4): implications in glycaemic control. *Diabetologia,* 49**,** 1881-92.

NEDERGAARD, J. 1981. Effects of cations on brown adipose tissue in relation to possible metabolic consequences of membrane depolarisation. *Eur J Biochem,* 114**,** 159-67.

NEELY, A., OLCESE, R., WEI, X., BIRNBAUMER, L. & STEFANI, E. 1994. Ca(2+)-dependent inactivation of a cloned cardiac Ca2+ channel alpha 1 subunit (alpha 1C) expressed in Xenopus oocytes. *Biophys J,* 66**,** 1895-903.

NICOLAYSEN, A., GAMMELSAETER, R., STORM-MATHISEN, J., GUNDERSEN, V. & IVERSEN, P. O. 2007. The components required for amino acid neurotransmitter signaling are present in adipose tissues. *J Lipid Res,* 48**,** 2123-32.

NILIUS, B. & DROOGMANS, G. 2003. Amazing chloride channels: an overview. *Acta Physiol Scand,* 177**,** 119-47.

NILIUS, B., EGGERMONT, J., VOETS, T. & DROOGMANS, G. 1996. Volume-activated Cl-channels. *Gen Pharmacol,* 27**,** 1131-40.

NILIUS, B. & VOETS, T. 2005. TRP channels: a TR(I)P through a world of multifunctional cation channels. *Pflugers Arch,* 451**,** 1-10.

NISHIMURA, S., TAKESHIMA, H., HOFMANN, F., FLOCKERZI, V. & IMOTO, K. 1993. Requirement of the calcium channel Î² subunit for functional conformation. *FEBS Letters,* 324**,** 283-286.

NISHIZUKA, Y. 1995. Protein kinase C and lipid signaling for sustained cellular responses. *The FASEB Journal,* 9**,** 484-96.

NONOGAKI, K., FULLER, G. M., FUENTES, N. L., MOSER, A. H., STAPRANS, I., GRUNFELD, C. & FEINGOLD, K. R. 1995. Interleukin-6 stimulates hepatic triglyceride secretion in rats. *Endocrinology,* 136**,** 2143-9.

NTAMBI, J. M. & YOUNG-CHEUL, K. 2000. Adipocyte Differentiation and Gene Expression. *The Journal of Nutrition,* 130**,** 3122S-3126S.

OGATA, M., IWAMOTO, T., TAZAWA, N., NISHIKAWA, M., YAMASHITA, J., TAKAOKA, M. & MATSUMURA, Y. 2003. A novel and selective Na+/Ca2+ exchange inhibitor, SEA0400, improves ischemia/reperfusion-induced renal injury. *Eur J Pharmacol,* 478**,** 187-98.

OLCESE, R., QIN, N., SCHNEIDER, T., NEELY, A., WEI, X., STEFANI, E. & BIRNBAUMER, L. 1994. The amino terminus of a calcium channel beta subunit sets rates of channel inactivation independently of the subunit's effect on activation. *Neuron,* 13**,** 1433-8.

OPATOWSKY, Y., CHEN, C. C., CAMPBELL, K. P. & HIRSCH, J. A. 2004. Structural analysis of the voltage-dependent calcium channel beta subunit functional core and its complex with the alpha 1 interaction domain. *Neuron,* 42**,** 387-99.

OSWALD, J., BOXBERGER, S., JORGENSEN, B., FELDMANN, S., EHNINGER, G., BORNHAUSER, M. & WERNER, C. 2004. Mesenchymal stem cells can be differentiated into endothelial cells in vitro. *Stem Cells,* 22**,** 377-84.

OUCHI, N., PARKER, J. L., LUGUS, J. J. & WALSH, K. Adipokines in inflammation and metabolic disease. *Nat Rev Immunol,* 11**,** 85-97.

PAPPONE, P. A. & LEE, S. C. 1995. Alpha-adrenergic stimulation activates a calcium-sensitive chloride current in brown fat cells. *J Gen Physiol,* 106**,** 231-58.

PAREDES, R. M., ETZLER, J. C., WATTS, L. T., ZHENG, W. & LECHLEITER, J. D. 2008. Chemical calcium indicators. *Methods,* 46**,** 143-151.

PAREKH, A. B. & PUTNEY, J. W., JR. 2005. Store-operated calcium channels. *Physiol Rev,* 85**,** 757-810.

PATH, G., BORNSTEIN, S. R., GURNIAK, M., CHROUSOS, G. P., SCHERBAUM, W. A. & HAUNER, H. 2001. Human breast adipocytes express interleukin-6 (IL-6) and its receptor system: increased IL-6 production by beta-adrenergic activation and effects of IL-6 on adipocyte function. *J Clin Endocrinol Metab,* 86**,** 2281-8.

PAULMICHL, M., LI, Y., WICKMAN, K., ACKERMAN, M., PERALTA, E. & CLAPHAM, D. 1992. New mammalian chloride channel identified by expression cloning. *Nature,* 356**,** 238-41.

PEARSON, E. R., FLECHTNER, I., NJÃ¸LSTAD, P. L. R., MALECKI, M. T., FLANAGAN, S. E., LARKIN, B., ASHCROFT, F. M., KLIMES, I., CODNER, E., IOTOVA, V., SLINGERLAND, A. S., SHIELD, J., ROBERT, J.-J., HOLST, J. J., CLARK, P. M., ELLARD, S., SÃ¸VIK, O., POLAK, M. & HATTERSLEY, A. T. 2006. Switching from Insulin to Oral Sulfonylureas in Patients with Diabetes Due to Kir6.2 Mutations. *New England Journal of Medicine,* 355**,** 467-477.

PENA, F. & ORDAZ, B. 2008. Non-selective cation channel blockers: potential use in nervous system basic research and therapeutics. *Mini Rev Med Chem,* 8**,** 812-9.

PEREZ-ARMENDARIZ, M., ROY, C., SPRAY, D. C. & BENNETT, M. V. 1991. Biophysical properties of gap junctions between freshly dispersed pairs of mouse pancreatic beta cells. *Biophys J,* 59**,** 76-92.

PERRY, M. C. & HALES, C. N. 1969. Rates of effux and intracellular concentrations of potassium, sodium and chloride ions in isolated fat-cells from the rat. *Biochem J,* 115**,** 865-71.

PERSHADSINGH, H. A., LEE, L. Y. & SNOWDOWNE, K. W. 1989. Evidence for a sodium/calcium exchanger and voltage-dependent calcium channels in adipocytes. *FEBS Lett,* 244**,** 89-92.

PESIRIDIS, G. S., DIAMOND, E. & VAN DUYNE, G. D. 2009. Role of pICLn in methylation of Sm proteins by PRMT5. *J Biol Chem,* 284**,** 21347-59.

PHILIPSON, K. D. & NICOLL, D. A. 2000. Sodium-calcium exchange: a molecular perspective. *Annu. Rev. Physiol.,* 62**,** 111-133.

PIWON, N., GUNTHER, W., SCHWAKE, M., BOSL, M. R. & JENTSCH, T. J. 2000. ClC-5 Cl- -channel disruption impairs endocytosis in a mouse model for Dent's disease. *Nature,* 408**,** 369-73.

PIXLEY, S. K. & PUN, R. Y. 1990. Cultured rat olfactory neurons are excitable and respond to odors. *Brain Res Dev Brain Res,* 53**,** 125-30.

PLANELLS-CASES, R. & JENTSCH, T. J. 2009. Chloride channelopathies. *Biochim Biophys Acta,* 1792**,** 173-89.

POULOS, S. P., DODSON, M. V. & HAUSMAN, G. J. Cell line models for differentiation: preadipocytes and adipocytes. *Exp Biol Med (Maywood),* 235**,** 1185-93.

PRAGNELL, M., DE WAARD, M., MORI, Y., TANABE, T., SNUTCH, T. P. & CAMPBELL, K. P. 1994. Calcium channel [beta]-subunit binds to a conserved motif in the I-II cytoplasmic linker of the [alpha]1-subunit. *Nature,* 368**,** 67-70.

PULBUTR, C., SMITH 2009. Roles of Calcium in Adipocyte Cell Function. *School of Biomedical Sciences,* Doctor of Philosophy.

PURCELL, S. H., CHI, M. M. & MOLEY, K. H. Insulin-Stimulated Glucose Uptake Occurs in Specialized Cells within the Cumulus Oocyte Complex. *Endocrinology,* 153**,** 2444-2454.

PUTNEY, J. W., JR., BROAD, L. M., BRAUN, F. J., LIEVREMONT, J. P. & BIRD, G. S. 2001. Mechanisms of capacitative calcium entry. *J Cell Sci,* 114**,** 2223-9.

QUEDNAU, B. D., NICOLL, D. A. & PHILIPSON, K. D. 1997. Tissue specificity and alternative splicing of the Na+/Ca2+ exchanger isoforms NCX1, NCX2, and NCX3 in rat. *Am J Physiol,* 272**,** C1250-61.

QUINTON, P. M. 1990. Cystic fibrosis: a disease in electrolyte transport. *FASEB J,* 4**,** 2709-17.

RABE, K., LEHRKE, M., PARHOFER, K. G. & BROEDL, U. C. 2008. Adipokines and insulin resistance. *Mol Med,* 14**,** 741-51.

RAMIREZ-PONCE, M. P., ACOSTA, J. & BELLIDO, J. 1991. Effects of noradrenaline and insulin on electrical activity in white adipose tissue of rat. *Rev Esp Fisiol,* 47**,** 217-21.

RAMIREZ-PONCE, M. P., ACOSTA, J. & BELLIDO, J. A. 1990. Electrical activity in white adipose tissue of rat. *Rev Esp Fisiol,* 46**,** 133-8.

RAMIREZ-PONCE, M. P., ACOSTA, J., BELLIDO, J. A. & MATEOS, J. C. 1998. Noradrenaline modulates the electrical activity of white adipocytes by a cAMP-dependent mechanism. *J Endocrinol,* 159**,** 397-402.

RAMIREZ-PONCE, M. P., MATEOS, J. C. & BELLIDO, J. A. 2002. Insulin increases the density of potassium channels in white adipocytes: possible role in adipogenesis. *J Endocrinol,* 174**,** 299-307.

RAMIREZ-PONCE, M. P., MATEOS, J. C. & BELLIDO, J. A. 2003. Human adipose cells have voltage-dependent potassium currents. *J Membr Biol,* 196**,** 129-34.

RAMIREZ-PONCE, M. P., MATEOS, J. C., CARRION, N. & BELLIDO, J. A. 1996. Voltage-dependent potassium channels in white adipocytes. *Biochem Biophys Res Commun,* 223**,** 250-6.

RAMIREZ-ZACARIAS, J. L., CASTRO-MUNOZLEDO, F. & KURI-HARCUCH, W. 1992. Quantitation of adipose conversion and triglycerides by staining intracytoplasmic lipids with Oil red O. *Histochemistry,* 97**,** 493-7.

RAN, I., MATHERS, D. A. & PUIL, E. 2004. Pentobarbital induces thalamic oscillations in brain slices, modulated by GABA and glycine receptors. *Neuropharmacology,* 47**,** 985-93.

RANDLE, P. J., GARLAND, P. B., HALES, C. N. & NEWSHOLME, E. A. 1963. The glucose fatty-acid cycle. Its role in insulin sensitivity and the metabolic disturbances of diabetes mellitus. *Lancet,* 1**,** 785-9.

RANGANATHAN, G., UNAL, R., POKROVSKAYA, I., YAO-BORENGASSER, A., PHANAVANH, B., LECKA-CZERNIK, B., RASOULI, N. & KERN, P. A. 2006. The lipogenic enzymes DGAT1, FAS, and LPL in adipose tissue: effects of obesity, insulin resistance, and TZD treatment. *J Lipid Res,* 47**,** 2444-50.

RANKOVIC, V., LANDGRAF, P., KANYSHKOVA, T., EHLING, P., MEUTH, S. G., KREUTZ, M. R., BUDDE, T. & MUNSCH, T. 2011. Modulation of calcium-dependent inactivation of L-type Ca2+ channels via beta-adrenergic signaling in thalamocortical relay neurons. *PLoS One,* 6**,** e27474.

RATHI, S. S., SAINI, H. K., XU, Y. J. & DHALLA, N. S. 2004. Mechanisms of low Na+-induced increase in intracellular calcium in KCl-depolarized rat cardiomyocytes. *Mol Cell Biochem,* 263**,** 151-62.

REUSCH, J. E., BEGUM, N., SUSSMAN, K. E. & DRAZNIN, B. 1991. Regulation of GLUT-4 phosphorylation by intracellular calcium in adipocytes. *Endocrinology,* 129**,** 3269-73.

REUSCH, J. E., SUSSMAN, K. E. & DRAZNIN, B. 1993. Inverse relationship between GLUT-4 phosphorylation and its intrinsic activity. *J Biol Chem,* 268**,** 3348-51.

REUTER, H., HENDERSON, S. A., HAN, T., MATSUDA, T., BABA, A., ROSS, R. S., GOLDHABER, J. I. & PHILIPSON, K. D. 2002. Knockout mice for pharmacological screening: testing the specificity of Na+-Ca2+ exchange inhibitors. *Circ Res,* 91**,** 90-2.

REUTER, H., POTT, C., GOLDHABER, J. I., HENDERSON, S. A., PHILIPSON, K. D. & SCHWINGER, R. H. 2005. Na(+)--Ca2+ exchange in the regulation of cardiac excitation-contraction coupling. *Cardiovasc Res,* 67**,** 198-207.

RIGO, J. M., HANS, G., NGUYEN, L., ROCHER, V., BELACHEW, S., MALGRANGE, B., LEPRINCE, P., MOONEN, G., SELAK, I., MATAGNE, A. & KLITGAARD, H. 2002. The anti-epileptic drug levetiracetam reverses the inhibition by negative allosteric modulators of neuronal GABA- and glycine-gated currents. *Br J Pharmacol,* 136**,** 659-72.

RINGER, E., RUSS, U. & SIEMEN, D. 2000. [beta]3-Adrenergic stimulation and insulin inhibition of non-selective cation channels in white adipocytes of the rat. *Biochimica et Biophysica Acta (BBA) - Biomembranes,* 1463**,** 241-253.

ROBERTS-CROWLEY, M. L., MITRA-GANGULI, T., LIU, L. & RITTENHOUSE, A. R. 2009. Regulation of voltage-gated Ca2+ channels by lipids. *Cell Calcium,* 45**,** 589-601.

ROBERTS, R., HODSON, L., DENNIS, A. L., NEVILLE, M. J., HUMPHREYS, S. M., HARNDEN, K. E., MICKLEM, K. J. & FRAYN, K. N. 2009. Markers of de novo lipogenesis in adipose tissue: associations with small adipocytes and insulin sensitivity in humans. *Diabetologia,* 52**,** 882-90.

ROBINSON, P., ETHERIDGE, S., SONG, L., ARMENISE, P., JONES, O. T. & FITZGERALD, E. M. 2010. Formation of N-type (Cav2.2) voltage-gated calcium channel membrane microdomains: Lipid raft association and clustering. *Cell Calcium,* 48**,** 183-94.

RODBELL, M. 1964. METABOLISM OF ISOLATED FAT CELLS .I. EFFECTS OF HORMONES ON GLUCOSE METABOLISM + LIPOLYSIS. *Journal of Biological Chemistry,* 239**,** 375-&.

RODEN, M., PRICE, T. B., PERSEGHIN, G., PETERSEN, K. F., ROTHMAN, D. L., CLINE, G. W. & SHULMAN, G. I. 1996. Mechanism of free fatty acid-induced insulin resistance in humans. *J Clin Invest,* 97**,** 2859-65.

RODERICK, H. L. & COOK, S. J. 2008. Ca2+ signalling checkpoints in cancer: remodelling Ca2+ for cancer cell proliferation and survival. *Nat Rev Cancer,* 8**,** 361-375.

ROTH, J., QIANG, X., MARBAN, S. L., REDELT, H. & LOWELL, B. C. 2004. The Obesity Pandemic: Where Have We Been and Where Are We Going? *Obesity,* 12**,** 88S-101S.

RUAN, H., MILES, P. D., LADD, C. M., ROSS, K., GOLUB, T. R., OLEFSKY, J. M. & LODISH, H. F. 2002. Profiling gene transcription in vivo reveals adipose tissue as an immediate target of tumor necrosis factor-alpha: implications for insulin resistance. *Diabetes,* 51**,** 3176-88.

RUSS, U., RINGER, T. & SIEMEN, D. 1993. A voltage-dependent and a voltage-independent potassium channel in brown adipocytes of the rat. *Biochimica et Biophysica Acta - Biomembranes,* 1153**,** 249-256.

SABANOV, V. & NEDERGAARD, J. 1995. Chloride Channels in Brown Adipocyte Plasma Membranes: Candidates for Mediation of [alpha]1-Adrenergic Depolarization? *Biochemical and Biophysical Research Communications,* 211**,** 639-647.

SAKMANN, N. 2009. *Single-Channel Recording*, Springer.

SANGUINETTI, M. C. & KASS, R. S. 1984. Voltage-dependent block of calcium channel current in the calf cardiac Purkinje fiber by dihydropyridine calcium channel antagonists. *Circulation Research,* 55**,** 336-348.

SANGUINETTI, M. C. & SPECTOR, P. S. 1997. Potassium channelopathies. *Neuropharmacology,* 36**,** 755-62.

SATIN, L. S., TAVALIN, S. J., KINARD, T. A. & TEAGUE, J. 1995. Contribution of L- and non-L-type calcium channels to voltage-gated calcium current and glucose-dependent insulin secretion in HIT-T15 cells. *Endocrinology,* 136**,** 4589-601.

SAVAGE, D. B., SEWTER, C. P., KLENK, E. S., SEGAL, D. G., VIDAL-PUIG, A., CONSIDINE, R. V. & O'RAHILLY, S. 2001. Resistin / Fizz3 expression in relation to obesity and peroxisome proliferator-activated receptor-gamma action in humans. *Diabetes,* 50**,** 2199-202.

SAVIANE, C., CONTI, F. & PUSCH, M. 1999. The muscle chloride channel ClC-1 has a double-barreled appearance that is differentially affected in dominant and recessive myotonia. *J Gen Physiol,* 113**,** 457-68.

SCHIMMEL, R. J. 1973. The influence of extracellular calcium ion on hormone-activated lipolysis. *Biochimica et Biophysica Acta (BBA) - Lipids and Lipid Metabolism,* 326**,** 272-278.

SCHMIDT-ROSE, T. & JENTSCH, T. J. 1997. Transmembrane topology of a CLC chloride channel. *Proc Natl Acad Sci U S A,* 94**,** 7633-8.

SCHNEIDER-PICARD, G., COLES, J. A. & GIRARDIER, L. 1985. Alpha- and beta-adrenergic mediation of changes in metabolism and Na/K exchange in rat brown fat. *J Gen Physiol,* 86**,** 169-88.

SCHULTZ, B. D., SINGH, A. K., DEVOR, D. C. & BRIDGES, R. J. 1999. Pharmacology of CFTR chloride channel activity. *Physiol Rev,* 79**,** S109-44.

SCHULTZ, B. D., VENGLARIK, C. J., BRIDGES, R. J. & FRIZZELL, R. A. 1995. Regulation of CFTR Cl- channel gating by ADP and ATP analogues. *J Gen Physiol,* 105**,** 329-61.

SCHWALLER, B. Cytosolic Ca2+ buffers. *Cold Spring Harb Perspect Biol,* 2**,** a004051.

SCHWARTZ, Y., GOODMAN, H. M. & YAMAGUCHI, H. 1991. Refractoriness to growth hormone is associated with increased intracellular calcium in rat adipocytes. *Proc Natl Acad Sci U S A,* 88**,** 6790-4.

SEABRA, V., STACHLEWITZ, R. F. & THURMAN, R. G. 1998. Taurine blunts LPS-induced increases in intracellular calcium and TNF-alpha production by Kupffer cells. *Journal of Leukocyte Biology,* 64**,** 615-21.

SEIBERT, F. S., CHANG, X. B., ALEKSANDROV, A. A., CLARKE, D. M., HANRAHAN, J. W. & RIORDAN, J. R. 1999. Influence of phosphorylation by protein kinase A on CFTR at the cell surface and endoplasmic reticulum. *Biochim Biophys Acta,* 1461**,** 275-83.

SHANIK, M. H., XU, Y., Å KRHA, J., DANKNER, R., ZICK, Y. & ROTH, J. 2008. Insulin Resistance and Hyperinsulinemia. *Diabetes Care,* 31**,** S262-S268.

SHEPPARD, D. N. 2004. CFTR channel pharmacology: novel pore blockers identified by high-throughput screening. *J Gen Physiol,* 124**,** 109-13.

SHERMAN, A., KEIZER, J. & RINZEL, J. 1990. Domain model for Ca2(+)-inactivation of Ca2+ channels at low channel density. *Biophys J,* 58**,** 985-95.

SHI, H., HALVORSEN, Y.-D., ELLIS, P. N., WILKISON, W. O. & ZEMEL, M. B. 2000. Role of intracellular calcium in human adipocyte differentiation. *Physiol. Genomics,* 3**,** 75-82.

SIEMEN, D. & REUHL, T. 1987. Non-selective cationic channel in primary cultured cells of brown adipose tissue. *Pflugers Arch,* 408**,** 534-6.

SKOMEDAL, T., AASS, H. & OSNES, J. B. 1984. Specific binding of [3H]prazosin to myocardial cells isolated from adult rats. *Biochem Pharmacol,* 33**,** 1897-906.

SMALL, D. 2009. Dysregulation of Calcium Homeostasis in Alzheimer's Disease. 1824-1829.

SMITH, P. A., BOKVIST, K., ARKHAMMAR, P., BERGGREN, P. O. & RORSMAN, P. 1990. Delayed rectifying and calcium-activated K+ channels and their significance for action potential repolarization in mouse pancreatic beta-cells. *J Gen Physiol,* 95**,** 1041-59.

SMITH, U. 1971. Effect of cell size on lipid synthesis by human adipose tissue in vitro. *J Lipid Res,* 12**,** 65-70.

SMITH, U. 2002. Impaired ('diabetic') insulin signaling and action occur in fat cells long before glucose intolerance--is insulin resistance initiated in the adipose tissue? *Int J Obes Relat Metab Disord,* 26**,** 897-904.

SOARES, A. F., GUICHARDANT, M., COZZONE, D., BERNOUD-HUBAC, N., BOUZAIDI-TIALI, N., LAGARDE, M. & GELOEN, A. 2005. Effects of oxidative stress on adiponectin secretion and lactate production in 3T3-L1 adipocytes. *Free Radic Biol Med,* 38**,** 882-9.

STARK, R. J., READ, P. D. & O'DOHERTY, J. 1980. Insulin does not act by causing a change in membrane potential or intracellular free sodium and potassium concentration of adipocytes. *Diabetes,* 29**,** 1040-3.

STEFANOVICH, V. 1979. Influence of theophylline on concentrations of cyclic 3′,5′-adenosine monophosphate and cyclic 3′,5′-guanosine monophosphate of rat brain. 587-594.

STEPPAN, C. M., BAILEY, S. T., BHAT, S., BROWN, E. J., BANERJEE, R. R., WRIGHT, C. M., PATEL, H. R., AHIMA, R. S. & LAZAR, M. A. 2001. The hormone resistin links obesity to diabetes. *Nature,* 409**,** 307-12.

STOTZ, S. C., HAMID, J., SPAETGENS, R. L., JARVIS, S. E. & ZAMPONI, G. W. 2000. Fast inactivation of voltage-dependent calcium channels. A hinged-lid mechanism? *J Biol Chem,* 275**,** 24575-82.

STOUTHARD, J. M., ROMIJN, J. A., VAN DER POLL, T., ENDERT, E., KLEIN, S., BAKKER, P. J., VEENHOF, C. H. & SAUERWEIN, H. P. 1995. Endocrinologic and metabolic effects of interleukin-6 in humans. *Am J Physiol,* 268**,** E813-9.

STRAUB, S. V., PEREZ, S. M., TAN, B., COUGHLAN, K. A., TREBINO, C. E., COSGROVE, P., BUXTON, J. M., KREEGER, J. M. & JACKSON, V. M. 2011. Pharmacological inhibition of Kv1.3 fails to modulate insulin sensitivity in diabetic mice or human insulin-sensitive tissues. *American Journal of Physiology - Endocrinology And Metabolism,* 301**,** E380-E390.

STUTZMANN, G. E., CACCAMO, A., LAFERLA, F. M. & PARKER, I. 2004. Dysregulated IP3 signaling in cortical neurons of knock-in mice expressing an Alzheimer's-linked mutation in presenilin1 results in exaggerated Ca2+ signals and altered membrane excitability. *J Neurosci,* 24**,** 508-13.

STYS, P. K., WAXMAN, S. G. & RANSOM, B. R. 1992. Ionic mechanisms of anoxic injury in mammalian CNS white matter: role of Na+ channels and Na(+)-Ca2+ exchanger. *J Neurosci,* 12**,** 430-9.

SUNG, H.-Y., KANG, S.-W., KIM, J.-L., LI, J., LEE, E.-S., GONG, J.-H., HAN, S. J. & KANG, Y.-H. Oleanolic acid reduces markers of differentiation in 3T3-L1 adipocytes. *Nutrition Research,* 30**,** 831-839.

SUZUKI, M., MORITA, T. & IWAMOTO, T. 2006. Diversity of Cl(-) channels. *Cell Mol Life Sci,* 63**,** 12-24.

SZENT-GYORGYI, A. G. 1975. Calcium regulation of muscle contraction. *Biophys J,* 15**,** 707-23.

TABCHARANI, J. A., LOW, W., ELIE, D. & HANRAHAN, J. W. 1990. Low-conductance chloride channel activated by cAMP in the epithelial cell line T84. *FEBS Lett,* 270**,** 157-64.

TAFTI, B. A. & HANTASH, B. M. 2008. Dual regulation of the cardiac L-type calcium channel in L6 cells by protein kinase C. *Cell Calcium,* 44**,** 545-53.

TAHA, C. & KLIP, A. 1999. The insulin signaling pathway. *J Membr Biol,* 169**,** 1-12.

TAKAHASHI, A., CAMACHO, P., LECHLEITER, J. D. & HERMAN, B. 1999. Measurement of intracellular calcium. *Physiol Rev,* 79**,** 1089-125.

TAKAHASHI, K., TAKAHASHI, T., SUZUKI, T., ONISHI, M., TANAKA, Y., HAMANO-TAKAHASHI, A., OTA, T., KAMEO, K., MATSUDA, T. & BABA, A. 2003. Protective effects of SEA0400, a novel and selective inhibitor of the Na+/Ca2+ exchanger, on myocardial ischemia-reperfusion injuries. *Eur J Pharmacol,* 458**,** 155-62.

TAKEO, S., ELIMBAN, V. & DHALLA, N. S. 1985. Modification of cardiac sarcolemmal Na+-Ca2+ exchange by diltiazem and verapamil. *Can J Cardiol,* 1**,** 131-8.

TEBAR, F., RAMIREZ, I. & SOLEY, M. 1993. Epidermal growth factor modulates the lipolytic action of catecholamines in rat adipocytes. Involvement of a Gi protein. *J Biol Chem,* 268**,** 17199-204.

TERZIC, A., JAHANGIR, A. & KURACHI, Y. 1995. Cardiac ATP-sensitive K+ channels: regulation by intracellular nucleotides and K+ channel-opening drugs. *American Journal of Physiology - Cell Physiology,* 269**,** C525-C545.

TEUBER, L., WATJENS, F. & JENSEN, L. H. 1999. Ligands for the benzodiazepine binding site--a survey. *Curr Pharm Des,* 5**,** 317-43.

THORE, S., WUTTKE, A. & TENGHOLM, A. 2007. Rapid turnover of phosphatidylinositol-4,5-bisphosphate in insulin-secreting cells mediated by Ca2+ and the ATP-to-ADP ratio. *Diabetes,* 56**,** 818-26.

TOGASHI, K., INADA, H. & TOMINAGA, M. 2008. Inhibition of the transient receptor potential cation channel TRPM2 by 2-aminoethoxydiphenyl borate (2-APB). *Br J Pharmacol,* 153**,** 1324-30.

TOROK, T. L. 2007. Electrogenic Na+/Ca2+-exchange of nerve and muscle cells. *Prog Neurobiol,* 82**,** 287-347.

TOTH, A., KISS, L., VARRO, A. & NANASI, P. P. 2009. Potential therapeutic effects of Na+/Ca2+ exchanger inhibition in cardiac diseases. *Curr Med Chem,* 16**,** 3294-321.

TRAYNELIS, S. F., ANGUS SILVER, R. & CULL-CANDY, S. G. 1993. Estimated conductance of glutamate receptor channels activated during EPSCs at the cerebellar mossy fiber-granule cell synapse. *Neuron,* 11**,** 279-289.

TSIEN, R. W., ELLINOR, P. T. & HORNE, W. A. 1991. Molecular diversity of voltage-dependent Ca2+ channels. *Trends in pharmacological sciences,* 12**,** 349-354.

TSUGA, K., TOHSE, N., YOSHINO, M., SUGIMOTO, T., YAMASHITA, T., ISHII, S. & YABU, H. 2002. Chloride conductance determining membrane potential of rabbit articular chondrocytes. *J Membr Biol,* 185**,** 75-81.

TSURU, M., KATAGIRI, H., ASANO, T., YAMADA, T., OHNO, S., OGIHARA, T. & OKA, Y. 2002. Role of PKC isoforms in glucose transport in 3T3-L1 adipocytes: insignificance of atypical PKC. *American Journal of Physiology - Endocrinology And Metabolism,* 283**,** E338-E345.

TU, P., KUNERT-KEIL, C., LUCKE, S., BRINKMEIER, H. & BOURON, A. 2009. Diacylglycerol analogues activate second messenger-operated calcium channels exhibiting TRPC-like properties in cortical neurons. *J Neurochem,* 108**,** 126-38.

TUOMILEHTO, J., RASTENYTE, D., BIRKENHÃ¤GER, W. H., THIJS, L., ANTIKAINEN, R., BULPITT, C. J., FLETCHER, A. E., FORETTE, F. O., GOLDHABER, A., PALATINI, P., SARTI, C., STAESSEN, J. A. & FAGARD, R. 1999. Effects of Calcium-Channel Blockade in Older Patients with Diabetes and Systolic Hypertension. *New England Journal of Medicine,* 340**,** 677-684.

VALVERDE, M. A., DIAZ, M., SEPULVEDA, F. V., GILL, D. R., HYDE, S. C. & HIGGINS, C. F. 1992. Volume-regulated chloride channels associated with the human multidrug-resistance P-glycoprotein. *Nature,* 355**,** 830-3.

VAN MIL, H. G., KERKHOF, C. J. & SIEGENBEEK VAN HEUKELOM, J. 1995. Modulation of the isoprenaline-induced membrane hyperpolarization of mouse skeletal muscle cells. *Br J Pharmacol,* 116**,** 2881-8.

VAN PETEGEM, F., CLARK, K. A., CHATELAIN, F. C. & MINOR, D. L., JR. 2004. Structure of a complex between a voltage-gated calcium channel beta-subunit and an alpha-subunit domain. *Nature,* 429**,** 671-5.

VAN RENTERGHEM, C. & LAZDUNSKI, M. 1993. Endothelin and vasopressin activate low conductance chloride channels in aortic smooth muscle cells. *Pflugers Arch,* 425**,** 156-63.

VAZQUEZ-VELA, M. E. F., TORRES, N. & TOVAR, A. R. 2008. White Adipose Tissue as Endocrine Organ and Its Role in Obesity.

VAZQUEZ, G., WEDEL, B. J., TREBAK, M., ST. JOHN BIRD, G. & PUTNEY, J. W. 2003. Expression Level of the Canonical Transient Receptor Potential 3 (TRPC3) Channel Determines Its Mechanism of Activation. *Journal of Biological Chemistry,* 278**,** 21649-21654.

VENKATACHALAM, K. & MONTELL, C. 2007. TRP channels. *Annu Rev Biochem,* 76**,** 387-417.

VOETS, T., DROOGMANS, G. & NILIUS, B. 1996. Membrane currents and the resting membrane potential in cultured bovine pulmonary artery endothelial cells. *J Physiol,* 497 (Pt 1)**,** 95-107.

WAGNER, J. A., COZENS, A. L., SCHULMAN, H., GRUENERT, D. C., STRYER, L. & GARDNER, P. 1991. Activation of chloride channels in normal and cystic fibrosis airway epithelial cells by multifunctional calcium/calmodulin-dependent protein kinase. *Nature,* 349**,** 793-6.

WAHLI, W. & MICHALIK, L. PPARs at the crossroads of lipid signaling and inflammation. *Trends Endocrinol Metab,* 23**,** 351-63.

WALKER, D., BICHET, D., CAMPBELL, K. P. & DE WAARD, M. 1998. A beta 4 isoform-specific interaction site in the carboxyl-terminal region of the voltage-dependent Ca2+ channel alpha 1A subunit. *J Biol Chem,* 273**,** 2361-7.

WANG, H. & ECKEL, R. H. 2009. Lipoprotein lipase: from gene to obesity. *Am J Physiol Endocrinol Metab,* 297**,** E271-88.

WANG, M. C., COLLINS, R. F., FORD, R. C., BERROW, N. S., DOLPHIN, A. C. & KITMITTO, A. 2004. The three-dimensional structure of the cardiac L-type voltage-gated calcium channel: comparison with the skeletal muscle form reveals a common architectural motif. *J Biol Chem,* 279**,** 7159-68.

WATANO, T., KIMURA, J., MORITA, T. & NAKANISHI, H. 1996. A novel antagonist, No. 7943, of the Na+/Ca2+ exchange current in guinea-pig cardiac ventricular cells. *Br J Pharmacol,* 119**,** 555-63.

WEBER, A. & SIEMEN, D. 1989. Permeability of the non-selective channel in brown adipocytes to small cations. *Pflugers Arch,* 414**,** 564-70.

WEBSTER, J. I. & CARLSTEDT-DUKE, J. 2002. Involvement of multidrug resistance proteins (MDR) in the modulation of glucocorticoid response. *J Steroid Biochem Mol Biol,* 82**,** 277-88.

WEINREICH, F. & JENTSCH, T. J. 2001. Pores formed by single subunits in mixed dimers of different CLC chloride channels. *J Biol Chem,* 276**,** 2347-53.

WHITEHEAD, J. P., MOLERO, J. C., CLARK, S., MARTIN, S., MENEILLY, G. & JAMES, D. E. 2001. The role of Ca2+ in insulin-stimulated glucose transport in 3T3-L1 cells. *J Biol Chem,* 276**,** 27816-24.

WILDE, D. W. & LEE, K. S. 1989. Outward potassium currents in freshly isolated smooth muscle cell of dog coronary arteries. *Circ Res,* 65**,** 1718-34.

WRIGHT, S. H. 2004. Generation of resting membrane potential. *Adv Physiol Educ,* 28**,** 139-42.

WRONG, O. M., NORDEN, A. G. & FEEST, T. G. 1994. Dent's disease; a familial proximal renal tubular syndrome with low-molecular-weight proteinuria, hypercalciuria, nephrocalcinosis, metabolic bone disease, progressive renal failure and a marked male predominance. *QJM,* 87**,** 473-93.

XIAO, Y. F., GOMEZ, A. M., MORGAN, J. P., LEDERER, W. J. & LEAF, A. 1997. Suppression of voltage-gated L-type Ca2+ currents by polyunsaturated fatty acids in adult and neonatal rat ventricular myocytes. *Proc Natl Acad Sci U S A,* 94**,** 4182-7.

XU, W. & LIPSCOMBE, D. 2001. Neuronal CaV1.3{alpha}1 L-Type Channels Activate at Relatively Hyperpolarized Membrane Potentials and Are Incompletely Inhibited by Dihydropyridines. *J. Neurosci.,* 21**,** 5944-5951.

XUE, B., GREENBERG, A. G., KRAEMER, F. B. & ZEMEL, M. B. 2001. Mechanism of intracellular calcium ([Ca2+]i) inhibition of lipolysis in human adipocytes. *The FASEB Journal,* 15**,** 2527-2529.

XUE, B., MOUSTAID, N., WILKISON, W. O. & ZEMEL, M. B. 1998. The agouti gene product inhibits lipolysis in human adipocytes via a Ca2+-dependent mechanism. *FASEB J,* 12**,** 1391-6.

YAGUCHI, T. & NISHIZAKI, T. 2010. Extracellular high K(+) stimulates vesicular glutamate release from astrocytes by activating voltage-dependent calcium channels. *J Cell Physiol*.

YAHAGI, N., SHIMANO, H., HASTY, A. H., MATSUZAKA, T., IDE, T., YOSHIKAWA, T., AMEMIYA-KUDO, M., TOMITA, S., OKAZAKI, H., TAMURA, Y., IIZUKA, Y., OHASHI, K.,

OSUGA, J.-I., HARADA, K., GOTODA, T., NAGAI, R., ISHIBASHI, S. & YAMADA, N. 2002. Absence of Sterol Regulatory Element-binding Protein-1 (SREBP-1) Ameliorates Fatty Livers but Not Obesity or Insulin Resistance inLep ob /Lep ob Mice. *Journal of Biological Chemistry,* 277**,** 19353-19357.

YAMADA, K., NAKATA, M., HORIMOTO, N., SAITO, M., MATSUOKA, H. & INAGAKI, N. 2000. Measurement of glucose uptake and intracellular calcium concentration in single, living pancreatic beta-cells. *J Biol Chem,* 275**,** 22278-83.

YAMADA, M., INANOBE, A. & KURACHI, Y. 1998. G protein regulation of potassium ion channels. *Pharmacol Rev,* 50**,** 723-60.

YAMAMOTO, D. & SUZUKI, N. 1987. Blockage of chloride channels by HEPES buffer. *Proc R Soc Lond B Biol Sci,* 230**,** 93-100.

YAMAUCHI, T., KAMON, J., MINOKOSHI, Y., ITO, Y., WAKI, H., UCHIDA, S., YAMASHITA, S., NODA, M., KITA, S., UEKI, K., ETO, K., AKANUMA, Y., FROGUEL, P., FOUFELLE, F., FERRE, P., CARLING, D., KIMURA, S., NAGAI, R., KAHN, B. B. & KADOWAKI, T. 2002. Adiponectin stimulates glucose utilization and fatty-acid oxidation by activating AMP-activated protein kinase. *Nat Med,* 8**,** 1288-95.

YAVUZ, D. G., TUGLULAR, S., KOÇAK, H., ATAKAN, A., OZENER, C., AKOGLU, E. & AKALIN, S. 2004. Angiotension converting enzyme inhibition and calcium channel blockage improves cyclosporine induced glucose intolerance in rats. *Transplantation Proceedings,* 36**,** 171-174.

YOKOYAMA, C., WANG, X., BRIGGS, M. R., ADMON, A., WU, J., HUA, X., GOLDSTEIN, J. L. & BROWN, M. S. 1993. SREBP-1, a basic-helix-loop-helix-leucine zipper protein that controls transcription of the low density lipoprotein receptor gene. *Cell,* 75**,** 187-97.

YOREK, M., JAIPAUL, N., DUNLAP, J. & BIELEFELDT, K. 1999. Endothelin-stimulated Ca2+ mobilization by 3T3-L1 adipocytes is suppressed by tumor necrosis factor-alpha. *Arch Biochem Biophys,* 361**,** 241-51.

YOUNG, A. B., ZUKIN, S. R. & SNYDER, S. H. 1974. Interaction of benzodiazepines with central nervous glycine receptors: possible mechanism of action. *Proc Natl Acad Sci U S A,* 71**,** 2246-50.

ZEMEL, M. B., KIM, J. H., WOYCHIK, R. P., MICHAUD, E. J., KADWELL, S. H., PATEL, I. R. & WILKISON, W. O. 1995. Agouti regulation of intracellular calcium: role in the insulin resistance of viable yellow mice. *Proceedings of the National Academy of Sciences,* 92**,** 4733-4737.

ZEMKOVA, H., SVOBODA, P., TEISINGER, J. & VYSKOCIL, F. 1985. On the mechanism of catecholamine-induced hyperpolarization of skeletal muscle cells. *Naunyn Schmiedebergs Arch Pharmacol,* 329**,** 18-23.

ZHANG, X. Q., AHLERS, B. A., TUCKER, A. L., SONG, J., WANG, J., MOORMAN, J. R., MOUNSEY, J. P., CARL, L. L., ROTHBLUM, L. I. & CHEUNG, J. Y. 2006. Phospholemman inhibition of the cardiac Na+/Ca2+ exchanger. Role of phosphorylation. *J Biol Chem,* 281**,** 7784-92.

ZHANG, Y., LIN, J. X. & VILCEK, J. 1988. Synthesis of interleukin 6 (interferon-beta 2/B cell stimulatory factor 2) in human fibroblasts is triggered by an increase in intracellular cyclic AMP. *J Biol Chem,* 263**,** 6177-82.

ZHANG, Y. H. & HANCOX, J. C. 2009. Regulation of cardiac Na+-Ca2+ exchanger activity by protein kinase phosphorylation--still a paradox? *Cell Calcium,* 45**,** 1-10.

ZHOU, L., WANG, X., YANG, Y., WU, L., LI, F., ZHANG, R., YUAN, G., WANG, N., CHEN, M. & NING, G. 2011. Berberine attenuates cAMP-induced lipolysis via reducing the inhibition of phosphodiesterase in 3T3-L1 adipocytes. *Biochimica et Biophysica Acta (BBA) - Molecular Basis of Disease,* 1812**,** 527-535.

ZIERLER, K. L. 1966. Possible mechanisms of insulin action on membrane potential and ion fluxes. *Am J Med,* 40**,** 735-9.

Appendices

Macros

The calibrate Macro

```
//calibrate 22Apr2009//
worksheet -d B%[%h,>'A'];
%n=C%h;
%A=%h;
ncs=wks.ncols;
nrs=wks.nrows;
type %h %n $(i) $(ncs);
//check cells//

 for(i=ncs;i>1;i--){
  window -t plot calibrate1 %n;
  layer -w %A i 1 i nrs 200;
  getyesno KEEP Y;
  layer -d;
  if (y==0){
   del wcol(i);
  };
 };
//now form average//
ncs=wks.ncols;
nct=ncs+1;
worksheet -c average;
col(average)[nrs]=0;
wcol(nct)=0;
for(i=2;i<=ncs;i++){
wcol(nct)=wcol(nct)+wcol(i);
};
//calculate average and plot//
wcol(nct)=wcol(nct)/(ncs-2);
wks.col$(nct).label$=$(ncs-1);

%n=%h;
window -t plot calibrate2 G%nAverage;
layer -w %n nct 1 nct nrs 200;

k=0;
getnumber
(Start) xst
(End) xen
(Linear regression) k:2s
(Regress start) xre
(Calibration times);
 layer -d
```

The data macro

```
//calibrate 24Apr2009//
worksheet -d B%[%h,>'A'];
```

```
%n=C%h;
%A=%h;
ncs=wks.ncols;
nrs=wks.nrows;
//type %h %n $(i) $(ncs);//

//check cells//
 for(i=ncs;i>1;i--){
  window -t plot calibrate1 %n;
  layer -w %A i 1 i nrs 200;
  getyesno (Use record) Y;
  layer -d;
  if (y==0){
   del wcol(i);
  };
 };

//now form average//
ncs=wks.ncols;
nct=ncs+1;
tot=ncs-1;
worksheet -c average;
col(average)[nrs]=0;
wcol(nct)=0;
for(i=2;i<=ncs;i++){
wcol(nct)=wcol(nct)+wcol(i);
};
//calculate average and plot//
wcol(nct)=wcol(nct)/(ncs-2);
wks.col$(nct).label$=$(ncs-1);

%n=%h;
window -t plot calibrate2 G%nAverage;
layer -w %n nct 1 nct nrs 200;

//get calibration timings//
k=0;kd=350;
getnumber
(Kd Fluo4 in nm) kd
(Calib Start) xmid
(Calib End) xen
(Linear regression) k:2s
(Regress start) xst
(Calibration times);
//type $(xre) $(xst) $(xen);//
layer-d;

//find min fluo and correct//;
 loop (n,2,ncs){
  limit %(%h,n) -b xmid -e xen;
  wcol(n)=wcol(n)-limit.ymin;
 };

//linear regression and normalization//
 if (k==1){
  loop (n,2,ncs){
   lr %(%h,n) -b xst -e xmid;
```

```
   wcol(nct)=lr.b*wcol(1)+lr.a;
   wcol(n)=wcol(n)*100/wcol(nct);
  };
 };

//find max and calculate cal//;
 xen=xen-120;
 loop (n,2,ncs){
  limit %(%h,n) -b xmid -e xen;
  ymax=limit.ymax;
  wcol(nct)=wcol(n)/(ymax-wcol(n));
  limit %(%h,n) -b xmst -e xmid;
  wcol(n)=kd*wcol(nct);
  ymin=limit.ymin;
  //type $(n) $(ymax) $(ymin) $(350*ymin/(ymax-ymin));//
 };
//worksheet -s 2 1 ncs nrs;//
//worksheet -p 200 calibrate1;//

 ncs=wks.ncols-1;
 nrs=wks.nrows;
 for(i=ncs;i>1;i--){
  worksheet -s i 1 i xmid;
  worksheet -p 200 calcium1;
  getyesno KEEP Y;
  layer -d;
   if (y==0){
    del wcol(i);
   };
  };

//now form average//
ncs=wks.ncols-1;
nct=ncs+1;
col(average)[nrs]=0;
wcol(nct)=0;
for(i=2;i<=ncs;i++){
wcol(nct)=wcol(nct)+wcol(i);
};
//calculate average and plot//
wcol(nct)=wcol(nct)/(ncs-2);
wks.col$(nct).label$=$(ncs-2);

%n=%h;
worksheet -s 2 1 ncs xmid;
worksheet -p 200 calcium1;
window -r %h G%n;
```

Sources of the chemicals

Chemicals obtained from Alomone labs, Israel: Anti-$Ca_v1.2$ rabbit primary antibody (ACC-003A), Anti-$Ca_v1.3$ rabbit primary antibody (ACC-005A).

Chemicals obtained from BDH Lab supplies, UK: Glycine, $NaCO_3$, NaH_2PO_4

Chemicals obtained from Bio-Rad™ Precision Plus Protein Dual Colour Standards (161-0374).

Chemicals obtained from Fisher Scientific, UK: NaCl, NaOH, Sucrose

Chemicals obtained from Invitrogen Molecular Probes, USA: Fluo-4 acetoxymethyl ester (AM) (F14201).

Chemicals obtained from LI-COR Biosciences Odyssey, USA: Goat anti-rabbit (680nM red) secondary 962-68021, Donkey anti-mouse (680nM red) 926-68072, Donkey anti-goat (680nM red) 926-68074.

Chemicals obtained from Sigma, UK: Ammonium persulfate (APS), Amphortericin B, Anti-β-actin mouse primary antibody, Bay K 8644, BSA, Collagenase type II (C6885), EGTA, Folin reagent, HEPES, Isoprenaline, $MgCl_2$, Nifedipne, Poly-D-lysine, Ponceau S solution, Sodium dodecyl sulphate, Tris-base, Tween® 20, Verapamil

Chemicals obtained from Tocris, UK: KBR-R7943

DMSO was used as a diluent for: 2-APB, BayK8644, Fluo-4 AM, KB-R7943, nifedipine, verapamil.

Acetic acid was used as the diluent for insulin stock solution.

Hanks solution

Hanks physiological solution containing (in mM): 5.6KCl, 138 NaCl, 1.2 NaH_2PO_4, 10 HEPES (N-2-Hydroxyethylpiperazine-N'-2-ethansulfonic acid), 2.6$CaCl_2$, 1$MgCl_2$, 4.3$NaHCO_{3.,}$ pH 7.4 (NaOH).

Fresh Hank's solution was made daily, and supplemented with 5mM glucose and 0.01% (w/w) bovine serum albumin (BSA, Sigma catalogue number A3803). Hank's/BSA solution was used for the isolation of primary adipocytes, the maintence of cell suspensions and as the perifusion medium for the Fluo-4 AM $[Ca^{2+}]_i$ imaging experiments. For the Ca^{2+}-free solutions $CaCl_2$ was replaced by equimolar substitution with $MgCl_2$ to maintain the concentration of divalent cation salts in the Hank's solution.

	Chemical composition of the Hanks solutions (mM)						
	KCL	NaCl	$MgCl_2$	$CaCl_2$	HEPES	$NaHCO_3$	$NaHPO_4$
Hank's solution	5.6	138	1.2	2.6	10	4.3	1.2
Isotonic high K^+ solution	50	92.6	1.2	2.6	10	4.3	1.2
Isotonic low Na^+ solution	5.6	97.6	1.2	2.6	10	4.3	1.2

Solutions used in western blotting experiments

5 x TBE buffer contains:

27g Tris-base

13.75g Boric acid

10ml 0.5 M EDTA (pH 8.0)

Dissolve all in 500 ml double distilled H_2O

Lysis buffer contains:

20mM Tris

1 mM EGTA

320 mM Sucrose

0.1% Triton X100

1mM NaF

10mM Beta glycerolphosphate

Dissolve in dH_2O, pH7.6

Lowery A solution 500ml contains:

2g NaOH

1g SDS

10g $NaCO_3$

Lowery B solution contains:

1% $CuSO_4$

2% NaK Tartate

2X Solubilisation buffer contains:

2.5ml 0.5M Tris

2.0ml Glycerol

2.0ml 10% SDS

2.5ml dH_2O

1.0ml Beta mercaptoethanol

40µl 2.5% Bromophenol blue

Electrophoresis buffer (1 Litre) contains:

30.3g Tris

144g Tris

10g SDS

Transfer buffer (2.5 Litres) contains:

7.58

36g Glycine

2.0L dH_2O

0.5L Methanol

Keep in cold room

TBST (0.1% Tween)(10 Litres) contains:

30.29g Tris

73.12g NaCl

Dissolve in 1 Litre dH_2O

Adjust to pH 7.6

Make up to 10 litres, add 10ml Tween 20 to a final concentration of 0.1%

Investigation into the presence of non selective cation channels in DRG neurons

To source a positive control and confirm the actions of 2-APB, DRG's from male wistar rats were isolated. Cellular isolation and patch clamp methods were performed as described by (Sagar et al., 2004). We failed to successfully patch DRG neurons, with the predominant difficulty being an inability to successfully form seals. Instead calcium imaging with Fluo4-AM was utilised.

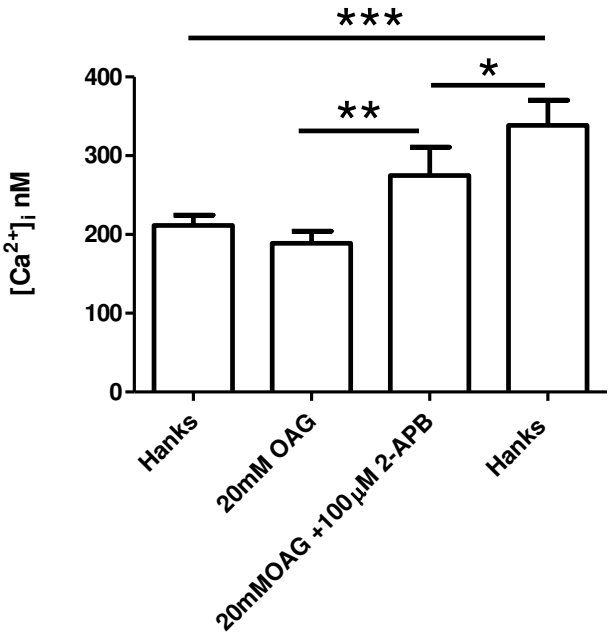

Figure 1. Investigation into the presence of non selective cation channels in DRG neurons by measurement of $[Ca^{2+}]_i$ with Fluo 4-AM. Perifusion of 20mM OAG did not cause any significant increase in $[Ca^{2+}]_i$ OAG in the presence of 100µM 2-APB did significantly increase $[Ca^{2+}]_i$, with $[Ca^{2+}]_i$ significantly increasing further following washout of both OAG and 2-APB *P<0.05, **P<0.01, ***P<0.001) (Bonferroni's multiple comparison test) (n=13).

OAG was used as an activator of non selective cation channels (Grimaldi et al., 2003), and 2-APB as an inhibitor of non selective cation channels (Togashi et al., 2008). Figure 1 shows that perifusion of 20mM (1-oleoyl-2-acetyl-sn-glycerol) OAG did not significantly increase $[Ca^{2+}]_i$. Perifusion of 20mM OAG with 100µM 2-APB caused a significant increase in $[Ca^{2+}]_i$ P<0.05 (Bonferroni's multiple comparison test) which was not reversed following removal of OAG and APB. Subanalysis showed that 23% of DRG's had an increase in $[Ca^{2+}]_i$ following perifusion of 20mM OAG (n=3 out of 13), however this was not significant. Of these cells, 2-APB did not reverse the increase in $[Ca^{2+}]_i$. 2-APB caused a further increase in $[Ca^{2+}]_i$ in 92% of all DRG's tested (12 out of 13) regardless of the nature of response to OAG.

It was hypothesised that the synthetic diacylglycerol analog, 1-oleoyl-2-acetyle-sn-glyverol (OAG) would activate TRP channels, this effect being manifest by an increase in $[Ca^{2+}]_i$. It was expected this effect would be ameliorated upon perifusion of 2-APB in the presence of OAG, with $[Ca^{2+}]_i$ levels returning to basal following washout of all agents. The observation that 20mM OAG does not cause an increase in $[Ca^{2+}]_i$ indicates that OAG is not activating TRPC's as expected

(Grimaldi et al., 2003), Fig 1. This could be because that there is not a strong expression of OAG responsive TRPC's in the DRG's within our preparation, or that the channels are inactive.

Inside out patch clamp and calcium imaging in CHO-K1 cells expressing either TRPC3. 4, 5 and 6 revealed that 100μM OAG activated and stimulated Mn^{2+} influx in cells expressing either TRPC3 or TRPC6 only (Hofmann et al., 1999) but not in TRPC1/4/5 expressing cells. Inhibition of TRPC5 channels by OAG has also been reported (Okada et al., 1999).

DRG's are reported to express TRPC5 and TRPC6, it is possible that the inhibitory effect of OAG on TRP5 is masking any Ca^{2+} influx potentiating that may be occurring through TRPC6. Without knowledge of the channel expression and function on the membrane surface of the DRGs used in this investigation it is only possible to speculate on potential rational for the discrepant OAG effect seen.

With regard to 2-APB, the results presented here are contradictory to the original hypothesis. 2-APB is activating Ca^{2+} influx, possibly by activating another channel type, or that there is a strong expression of another channel type within our preparation with opposite responses to both agents used here, masking any effects that would be apparent in an expression system only containing TRPC channels.

Discrepant effects of 2-APB have previously been reported the suspected accountability for which is due to the ability of 2-APB to form dimmers (Dobrydneva and Blackmore, 2001) affecting drug binding to the receptor site on the channel. The discrepant effects were on the basis of varied levels of inhibition between different cell/channel types and experimental models and location of drug binding site, as opposed to potentiating a calcium influx signal or interaction with other agonists/antagonists. It is possible that 2-APB is causing Ca^{2+} release from stores. 2-APB is reported to inhibit $InsP_3$ induced Ca^{2+} release (Maruyama et al., 1997), however blockade of Ca^{2+} release through $InsP_3$ by 2-APB is also considered to be inconsistent (Bootman et al., 2002). 2-APB is not equally potent at inhibiting $InsP_3$-inducd Ca^{2+} release within different cell types. One suggestion is that $InsP_3$ receptors exist as different isoforms ($InsP_3$ 1-3), with 2-APB exhibiting varying selectivity for each isoform. Increasing $InsP_3$ concentration can eradicate the inhibitory effect of 2-APB, the

presence of 1μM of Ins(1,4,5)P3 completely reversed the inhibitory effects of 2-APB on Ca^{2+} efflux in rat cerebellar microsomes (Maruyama et al., 1997). As such different cell types with differing basal, or capacities to generate Ins(1,4,5)P3 are likely to require differing concentrations of 2-APB to observe an inhibitory effect on Ca^{2+} release (Bootman et al., 2002).